KEELE UNIVERSITY: Research Institute for the Environment, Physical Sciences and Applied Mathematics

Design of novel porous melamine-formaldehyde materials for molecular recognition

A thesis submitted to Keele University in partial fulfilment of the requirements for the degree of Doctor of Philosophy.

By Lina Meghani
July 2011

Do not go where the path may lead, go instead where there is no path and leave a trail.

-Ralph Waldo Emerson

Contents

Acknowledgements

I would like to take this opportunity to thank all those who have supported me through this tough yet fulfilling journey…

I firstly wish to express my gratitude to my supervisors Chrystelle Egger and Daniel Kaesmayr for accepting me to work on this project, as well as offering me invaluable assistance, support and guidance throughout my time at Keele. Their advice, words of wisdom and encouragement provided motivation and inspired me to persevere even under conditions of extreme frustration!

I am deeply grateful to Vladimir Zholobenko for his help and advice during the times when Chrystelle was unavailable. I would also like to say a special thank you to Falko Drijfhout for allowing me to use his HPLC equipment as well as helping me with all the complex technical issues that went with it! I wish to express my appreciation to Karen Walker and Dave Furness in the Electron Microscopy Unit who were extremely patient and dedicated much of their time in helping me produce the SEM micrographs that are included here. I would also like to thank all the technical and administrative staff within the research institute for helping me with issues regarding equipment, computers and all the official procedures involved in the process of completing a PhD.

This project would not have been complete without the EPSRC analytical facilities (mass spectrometry and solid-state NMR services) and also BASF for running the mercury porosimetry measurements and welcoming me to their facilities as well as funding this project. I would also like to thank Richard Ansell in Leeds University for his help in packing the HPLC columns with the materials I produced in this work.

I would also like to thank all the members, past and present, in the office of L.J. 004A for providing a friendly atmosphere, making each day enjoyable, even when moral was at an all time low! I would also like to express my sincerest gratitude to all the friends I made at Keele. Their encouragement, advice and general good nature made being far away from home much easier to cope with. I wish them all good luck and I will miss them whilst I am embracing new opportunities in the big wide world…

Finally, I would like to express my gratitude to my beloved family for their support, understanding and endless love, throughout the duration of my studies. Without their influences I would not have achieved all that I have nor be the person I am today. I cannot thank them enough for standing by me through all the good and challenging times.

Abstract

Porous materials have played a pivotal role in the hosting of guest species. They provide a good diffusion medium, display high surface area and often the pores are size specific and bear the correct functionality to enhance retention of analytes. This work shows how such materials, based on melamine-formaldehyde (MF) chemistry are designed.

The melamine motif has been known to form supramolecular aggregates in *solution* with other triazine-containing molecules. It was, thus, anticipated that cross-linked MF networks would carry over the same recognition properties into *solid* matrices. Also, recognition was thought to be enhanced significantly if different chemical functions were brought into the material.

With this in mind, the successful introduction of different chemical groups onto the melamine motif was shown. These new derivatives were then converted into resins, using formaldehyde, and further cross-linked to produce porous materials. Thorough structural characterisation was carried out at this stage and a clear level of understanding/control has been gained on how to tune the porosity within such matrices.

Analysis of functionality was carried out using various spectroscopic techniques, the most important one being infrared studies. This revealed that two characteristic peaks in *all* cross-linked systems (with and without incorporated derivatives) appear at 1350cm^{-1} and 1150 cm^{-1}, although the nature of these is yet to be elucidated. When different functional groups were incorporated into MF networks, the infrared spectra varied slightly. Additionally, determining cross-linking density within materials using spectroscopic techniques was investigated but has not yet been fully accomplished.

Finally the extent of molecular retention of certain analytes within porous MF materials was evaluated. The pre-ground materials were successfully used as stationary phases in HPLC columns, behaving extremely well under the high pressure conditions. Out of the various analytes injected, certain amino acids displayed variation in retention and elution depending on the composition of the stationary phase.

Table of Abbreviations:

ATR: Attenuated Total Reflectance

BET: Brunauer-Emmett-Teller

CP MAS NMR: Cross-Polarised Magic Angle Spinning Nuclear Magnetic Resonance

CDTA: (1,2-Cyclohexylenedi nitrilo)-tetraacetic Acid

DEPT: Distortionless Enhancement by Polarisation Transfer

DIPEA: Di-isopropylethylamine

DMF: *N,N*-Dimethylformamide

DMSO: Dimethylsulfoxide

DTPA: Diethylene Triamine Pentaacetic Acid

EDTA: Ethylenediaminetetraacetic acid

EGDMA: Ethylene glycol dimethacrylate

F: Formaldehyde

FA: Formic acid

HPLC: High Performance Liquid Chromatography

IR: Infrared spectroscopy

LC-MS: Liquid Chromatography-Mass Spectrometry

MF: Melamine-formaldehyde

MIP: Molecular Imprinted Polymer

MMA: Methylmethacrylic acid

NTA: Nitrilotriacetic acid

SEM: Scanning Electron Microscopy

TGA/DSC: Thermal Gravimetric Analysis- Differential Scanning Calorimetry

Table of chemical structures:

1 melamine

2 cyanuric acid

3 4-amino-6-butylamino-2-(R)-1-phenylethylamino-1,3,5-triazine

4 4-amino-6-butylamino-2-(S)-1-phenylethylamino-1,3,5-triazine

5 4-amino-6-butylamino-2-[(R)-1-(1-naphthyl)ethylamino]-1,3,5-triazine

6 4-amino-6-butylamino-2-[(S)-1-(1-naphthyl)ethylamino]-1,3,5-triazine

7 cyanuric chloride

8 L-alanine

9 L-alanine-n-octadecyl ester-4-toluenesulfonate

10 2-amino-4,6-dichloro-1,3,5-triazine

11 2-amino-4,6-bis(S-1-n-octadecyloxycarbonyl-1-ethylamino)-1,3,5-triazine

12 2,4-diamino-6-chloro-1,3,5-triazine

13 4,6-amino-2-[(R)-1-phenylethyl]-1,3,5-triazine

14 4,6-amino-2-isopropyl-1,3,5-triazine

15 hexadecyl-(2S)-2-[(4,6-diamino-1,3,5-triazin-2-yl)amino]propanoate

16 4-amino-2-[(1S)-1-phenylethylamino]-6-chloro-1,3,5-triazine

17 2- [(1S)-1-phenylethylamino]-4-[(1R)-1-phenylethylamino]- 6-chloro-1,3,5-triazine

18 2-isopropylamino-4-amino-6-chloro-1,3,5-triazine

19 2- [(1S)-isopropylamino]-4-[(1R)-isoproylamino]- 6-chloro-1,3,5-triazine

20 (R)-1-phenylethylamine

21 4,6-diamino-2-allylamino-1,3,5-triazine

22 5-[(4,6-diamino-1,3,5-triazin-2-yl)amino]pentan-1-ol

23 acetoguanamine

Overview

Melamine has had extensive usage in chemical research and in industrial applications over the last century. It is a nitrogen-rich chemical consisting of a triazine ring substituted with 3 amino groups. This means that it contains both proton acceptors and donors and this has allowed it to be used in building supramolecular structures by forming complexes through complementary binding (binding that occurs ubiquitously in nature). Also, it has played an important role in the production of materials with exceptional properties. These materials are formed by reacting melamine with a cross-linker, formaldehyde, to form precursors (resins). Subsequently, these resins polymerise to form robust, thermally stable networks with well known applications (wood coating for finishing, fire retardant coatings, dinnerware, *etc*).

Recently however, through the process of sol-gel chemistry, melamine-formaldehyde (MF) precursors have been demonstrated to undergo polymerisation reactions in aqueous solutions to produce materials with high porosities. This sol-gel process offers many advantages in terms of designing materials. Firstly, it allows the synthesis of networks to take place at lower temperatures than conventional solid-state techniques, therefore being perfectly adapted to temperatures at which organic monomers can polymerise without denaturing them. Also, if the precursors used are water soluble, as are MF resins, this allows reactions to occur in an inexpensive, non-toxic solvent. Finally, the slow evolution of sol to gel facilitates shaping and the incorporation of other chemical entities (filler, dyes, metal salts, biological compounds, *etc*) that can modify the final

physical properties of a material, without having to be chemically modified under the given reaction conditions.

In this project, an attempt is made to connect the concept of porous MF materials formed under aqueous conditions with the ability of melamine to bind to other triazine-type compounds through weak intermolecular interactions. The aim of this work is therefore to produce nano-porous materials capable of molecular recognition, primarily in water. Such materials would offer potential advances in applications where "trapped" molecules play a significant role i.e. biosensors, membrane separators and catalysis. A class of materials, molecularly imprinted polymers (MIPs) are already capable of molecular uptake and extensive research has gone into adapting silicate based sol-gel systems for these applications. However, the use of other organic sol-gel precursors such as MF resins has not been widely reported, despite the potential melamine, as a single molecule, has shown for weak molecular binding. Furthermore, in this work, the intention is to broaden the potential of MF networks for recognition by introducing other functional groups to enhance and extend the retention of biological-type compounds.

In this work we firstly explain how three melamine derivatives were prepared. Secondly, we show how novel MF materials were synthesised by incorporating these new derivatives into MF networks. In addition to this, we describe methods used to maximise pore retention by a method called post-treatment. This was carried out with two different aqueous solutions: one containing n-butanol and another containing glutaraldehyde which react at hydroxyl and amino positions respectively within the cross-linked networks.

After drying the different systems, the structural properties and pore structures were thoroughly characterised. TGA/DSC was used to assess the thermal stability of different systems. The surface area of porous systems was quantified by the nitrogen sorption technique. Mercury porosimetry measurements gave pore size distributions. Finally, scanning electron microscopy was used to view the texture, grain and pore sizes of successfully prepared materials. Many trends were identified between the incorporated monomers and the observed material structures, leading to a certain extent of control in the synthesis.

Thirdly, functional group characterisation within the materials is reported using, primarily, IR spectroscopy adapted to solids (ATR-IR) which was used in conjunction with Raman spectroscopy and, at times, solid-state NMR to consolidate the previous spectroscopic findings.

The final stage of this work focussed on investigating the potential the synthesised materials had in retaining specific analytes (cyanuric acid, phenol and different amino acids) through weak interactions. This work was carried out by packing materials into HPLC columns and evaluating the retention of the analytes mentioned by chromatography. The various findings from this study are also reported here.
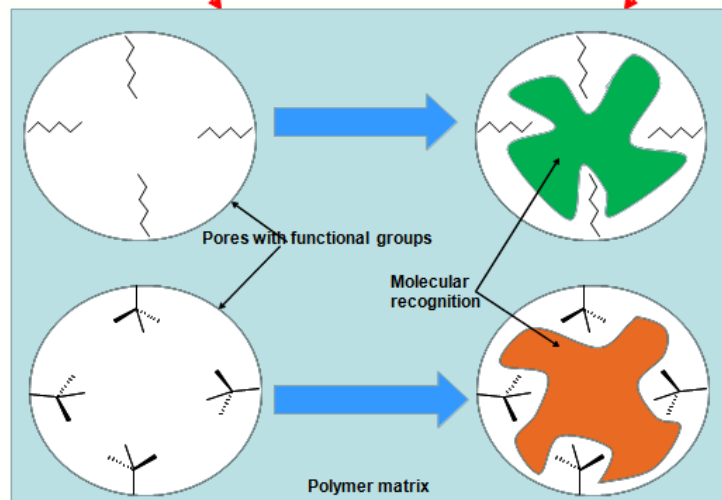
The following figure schematically represents the aims of this work.

Molecular recognition within melamine-formaldehyde materials

CHAPTER 1: Synthesis of Melamine Derivatives

Contents

1. Introduction

Melamine **1** was first prepared by Liebig in 1834. He discovered that, by heating potassium thiocyanate with ammonium chloride, a stable heterocyclic structure formed. In fact melamine is often the principal final product of high temperature reactions between ammonia and carbon dioxide which emphasises how stable the molecule really is.[1] Over the years it has had many uses in industrial applications such as coatings and in the thermoplastics industry. When melamine reacts with formaldehyde it forms resins, the precursors used in producing polymers with exceptional properties.[2]

However the use of melamine is not limited exclusively to industrial applications. The melamine motif as a single molecule has, in recent years, become of academic interest. It belongs to a group of compounds called 1,3,5-triazines, six-membered aromatic cycles consisting of alternating carbon and nitrogen atoms and is additionally substituted with three amino groups.

1
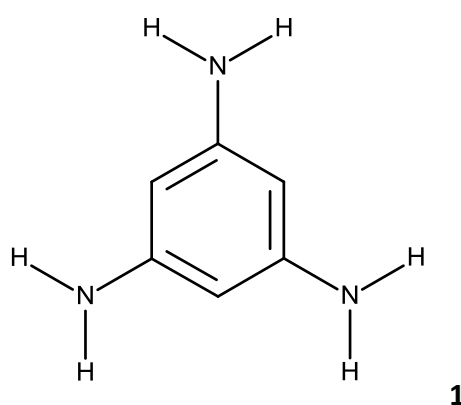
This molecule is very nitrogen rich, and due to the special arrangement of the different atoms, it contains both proton acceptors and donors, making it very easy to

form hydrogen bonds with other molecules.[3] Figure 1.1 shows, for instance, how melamine can interact with an organic molecule riboflavin (vitamin B2).[4]
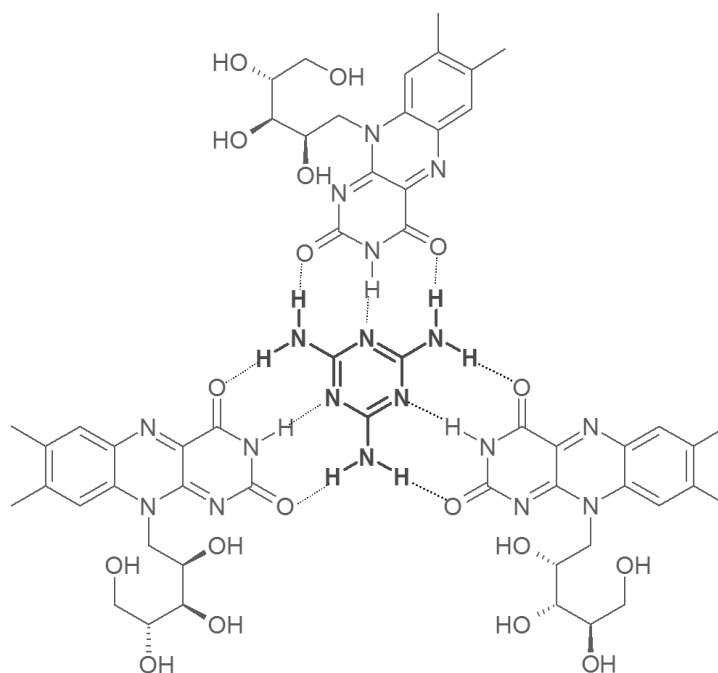
Figure 1.1: Melamine binding to riboflavin through intermolecular bonding. The dashed lines represent the intermolecular bonds between the compounds.

Many molecules in nature have the ability to bind through these types of interactions (enzyme-substrate binding, joining of the two strands of DNA in a double helix structure, antigen-antibody complexes, *etc*). Scientists, with the aim of mimicking this property, have therefore used melamine extensively in building supramolecular structures, with appropriate molecules.

1.1   Supramolecular Chemistry

Melamine and melamine derivatives have played an important role in a very active area of chemistry called supramolecular chemistry. Jean-Marie Lehn, the 1987 Nobel Prize winner of Chemistry, coined this term.[5] He used it to describe complex entities created from the association of two or more chemical species held together by intermolecular forces.[6] The weak bonds could later be tweaked through change of solvent or pH, for example, to break and separate the two molecules again. It is often referred to as Molecular Recognition and, despite it being a relatively young field, the principles, perspectives, and recent developments in supramolecular chemistry has grown exponentially in the last few decades.

1.1.1. Intermolecular Interactions[7]

Intermolecular forces are attractive forces that arise due to the interactions between molecular species. They can be attributed to association between functional groups and can, therefore, favour certain geometries. They are also known as "weak" forces as opposed to stronger covalent and ionic bonding. Intermolecular forces fall into different categories; the main ones along with the energy associated are listed in Table 1.1.

Table 1.1: Different types of non covalent interaction alongside their estimated energies.[7]

Bond Type	Bond energy (kJ/mol)
London Dispersion	2
Hydrophobic effects	1-3
Hydrogen bond	<12 (weak) 16-60 (moderate) 60+(strong)
π- π	0-50
π -cation	5-80
Dipole-dipole	5-50
Dipole-ion	50-200

The three main interactions of interest in this work are hydrogen bonding, π-π interactions and the hydrophobic effect.

Hydrogen bonds are the most crucial and favoured of secondary interactions to construct supramolecular architectures due to their selectivity, tuneable strength and directionality. Chemists often refer to hydrogen bonding as a special type of dipole-dipole interaction in which hydrogen atoms attached to electronegative atoms are attracted to the dipole of adjacent molecules or functional groups. Not all hydrogen bonds, however, can be defined as such. In some hydrogen bonds the hydrogen is not covalently bonded to either of the electronegative atoms, it is equally attracted to both.[8] This is why in Table

1.1 this particular intermolecular bond can be divided into 3 different subcategories of variable strength:

i.   Strong hydrogen bonds include linear complexes formed with the hydrogen atom approximately equidistant between the two electronegative atoms *e.g.* HF complexes.

ii.   Moderate hydrogen bonds arise from molecules having a slightly bent geometry as is the case in alcohol and water.

iii.   Finally, weak hydrogen bonds arise due to interactions with donors that possess C-H bonds in which the attached proton has a low pKa.

In 1988 Levitt et *al.*[9] interestingly reported that there exists a significant interaction (of approximately 12kJ/mol) between a hydrogen bond donor such as >NH and the centre of a benzene ring, which acts as a hydrogen bond acceptor, however this more commonly comes under the term of π-π stacking.

Aromatic π-π interactions can also often occur between two aromatic rings when one is electron rich and the other is electron deficient. There are two types of π interactions: face-to-face or face-to-edge as shown in Figure 1.2.[10]
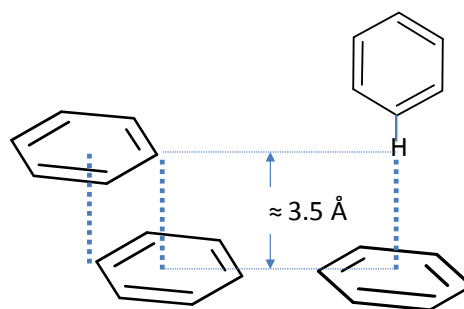
Figure 1.2: π stacking in aromatic systems. Two types of π-stacking can occur: face-to-face (left) or face-to-edge (right). The intermolecular distance between the two entities is approximately 3.5Å.

The face-to-face stacking involves the overlap of p orbitals in π conjugated systems as opposed to face-to-edge stacking which involves interactions between π conjugated systems and hydrogen atoms with a partial positive charge.

The hydrophobic effect, usually categorised as a weak interaction which arises from the association of non-polar species, may be described as the exclusion of non-polar molecules from polar solvents, water for example, since the non-polar species are not easily solvated.[7]

Even though non covalent interactions are weak, the cooperative effect of several such interactions may lead to the formation, under a variety of conditions, of reversible, thermodynamically or kinetically stable supramolecular assemblies such as sheets, rosettes or ribbon motifs.[11] The particular hydrophobic effect for amphiphiles can promote molecular assembly to form polymolecular systems of many different forms

such as layers, membranes, vesicles, micelles, *etc via* the different assembling structures the molecules take, for example see Figure 1.3.
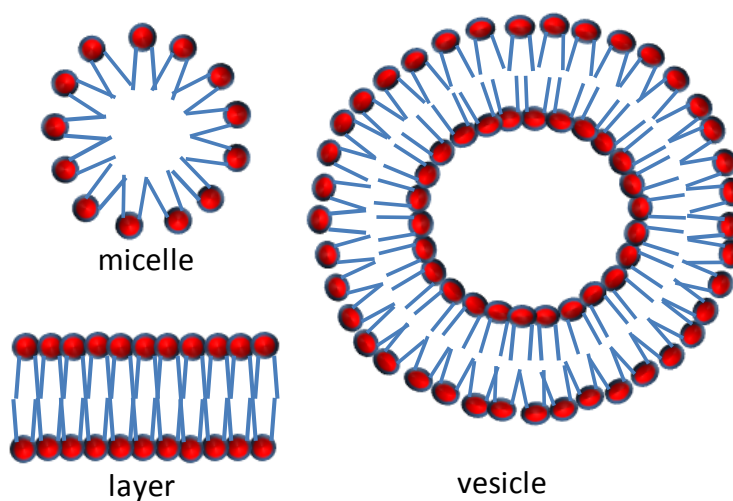
Figure 1.1: Different structures formed by the self-assembly of amphiphilic molecules due to hydrophobic effects.

As melamine already has the required properties to allow the assembling of molecules through intermolecular hydrogen bonding, it seems that incorporating other functional groups susceptible to interactions such as π stacking and/or hydrophobic effects can further extend the potential of recognition.[3] Some work has previously been carried out in synthesising melamine derivatives and using them for this purpose.

1.1.2. Melamine and Melamine Derivatives in Supramolecular Chemistry

Many research groups have identified the potential of melamine in building supramolecular structures in solution (Lehn,[12,13,14] Reinhoudt,[15] Whitesides,[16,17,18,19,20]). Indeed, melamine self-assembles in non-polar solvents with itself or other similar molecules such as cyanuric acid or barbituric acid to build very stable structures, through hydrogen bonding (Figure 1.4).
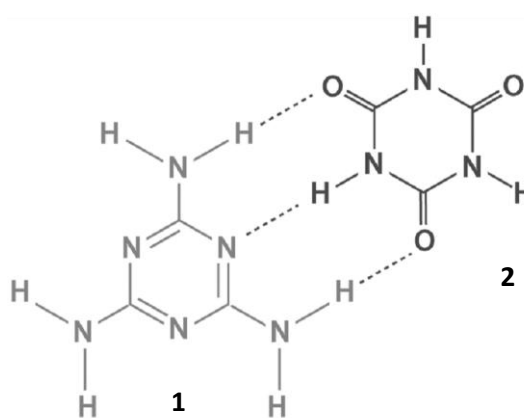
Figure 1.4: Intermolecular bonding (represented with dashed lines) between melamine **1** and cyanuric acid **2**.

As this bonding can occur every 120° or so in a plane, and in turn, the additional cyanuric acid molecules can bind to three other melamine molecules, it produces sheet-like structures as shown in Figure 1.5.
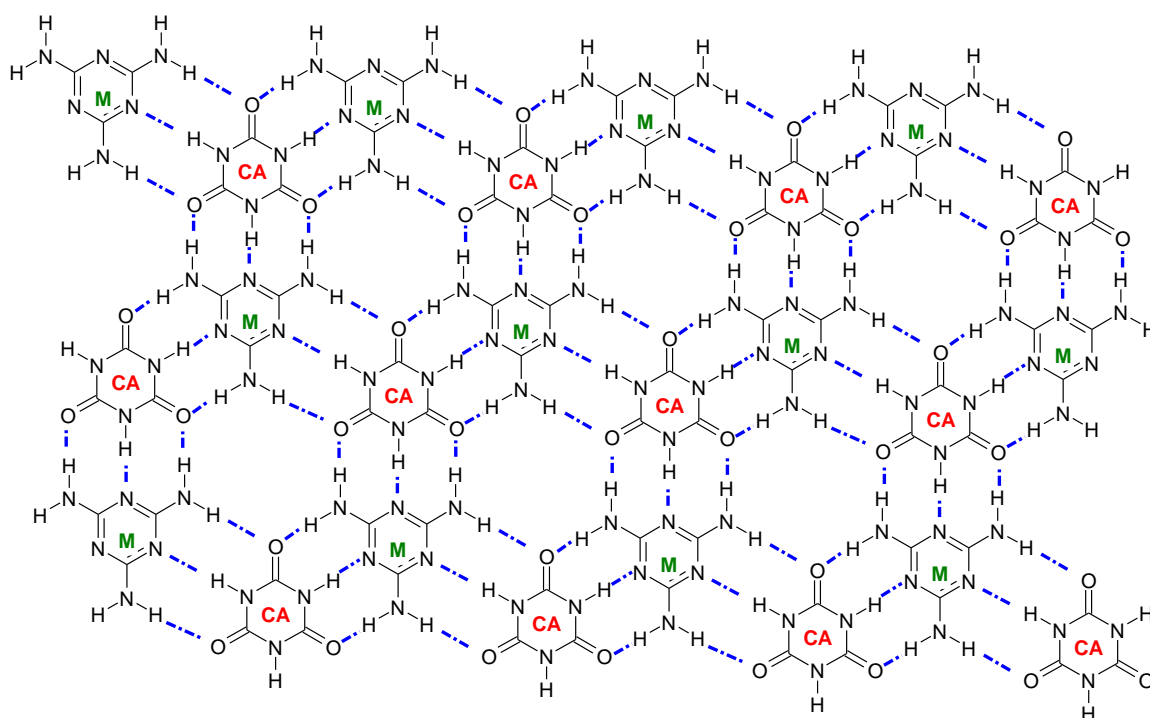
Figure 1.5: Extensive melamine-cyanuric acid intermolecular bonding which produced

sheet-like structures (M=melamine, CA=cyanuric acid, and the blue lines represent the

intermolecular bonds).

The Whitesides group extensively investigated this cyanuric acid-melamine

crystal packing. They recognised that these molecules could form three different sub-

motifs in the solid state: linear tapes, crinkled tapes and a cyclic rosette motif, as shown

in Figure 1.6.
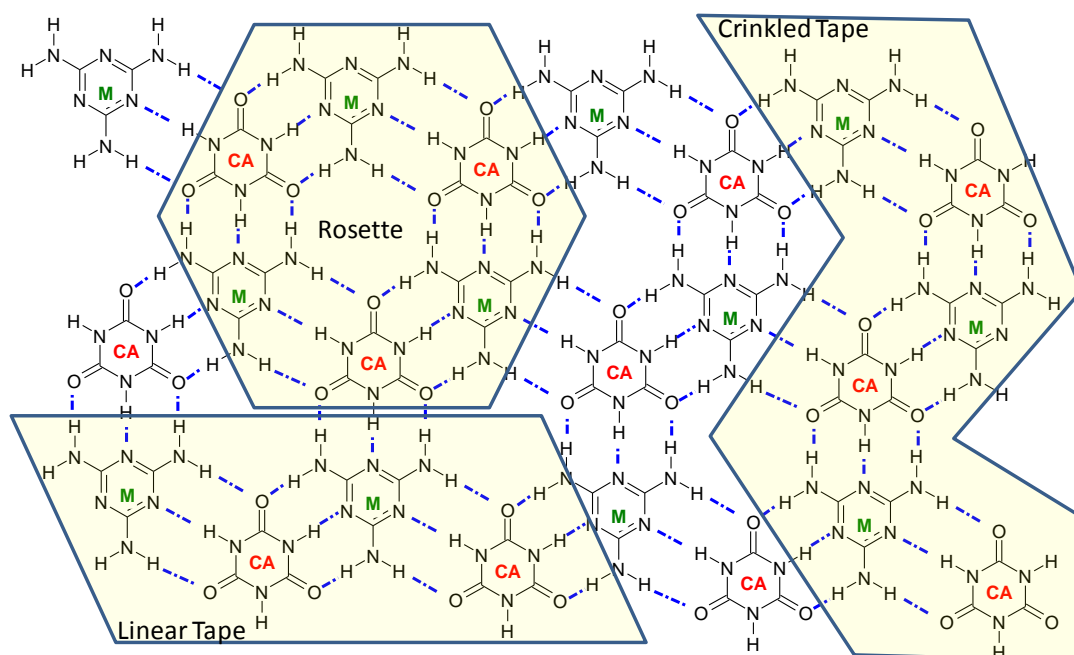
Figure 1.6: Proposed sub-structures for melamine-cyanuric acid complexes.

They reported that the introduction of structural changes to either cyanuric acid or the melamine motif favours the formation of one structural architecture over another. For instance, one of their strategies to promote the rosette formation was to use peripheral crowding where steric bulk was introduced onto melamine. On the other hand, small substituents were found to promote linear tape type structures.

One major drawback of supramolecular architectures based on hydrogen bonding is essentially their lack of stability in polar solvents.[21] In 1997, Ariga *et al.*[22,23,24] noticed the need to adapt molecular recognition, by multiple hydrogen bonding, to aqueous solutions. They noted that artificial receptor molecules are only effective in non aqueous media because if their recognition was to be carried out in water, strong hydrogen bonding with water would perturb the recognition effect. The group suggested that, along with electrostatic interactions, there are several approaches for including

effective hydrogen bonding in molecular systems constantly in contact with bulk water. To enhance the effectiveness of hydrogen bonding, cooperative interactions or the creation of proper hydrophobic micro-environments can be enhanced. The group therefore extended the size of the substituents used previously in studying the crystal packing of melamine (with cyanuric acid), to include melamine derivatives bearing long alkyl chains that produce molecules with amphiphilic properties.

In 2005, Liu *et al.*[3] also reported work of great interest involving the chiral recognition of 19 natural α-amino acids in methanol-water systems. Firstly the group synthesised a series of melamine derivatives bearing various chiral functional substituents. Using mass spectrometry (MS), they then evaluated the ability of the derivatives to bind with the amino acids. They confirmed that the enantioselectivities were encouraging and that four particular derivatives **3**, **4**, **5** and **6** could provide excellent chiral discrimination for 17 of the 19 amino acids.

3   **4**   **5**   **6**
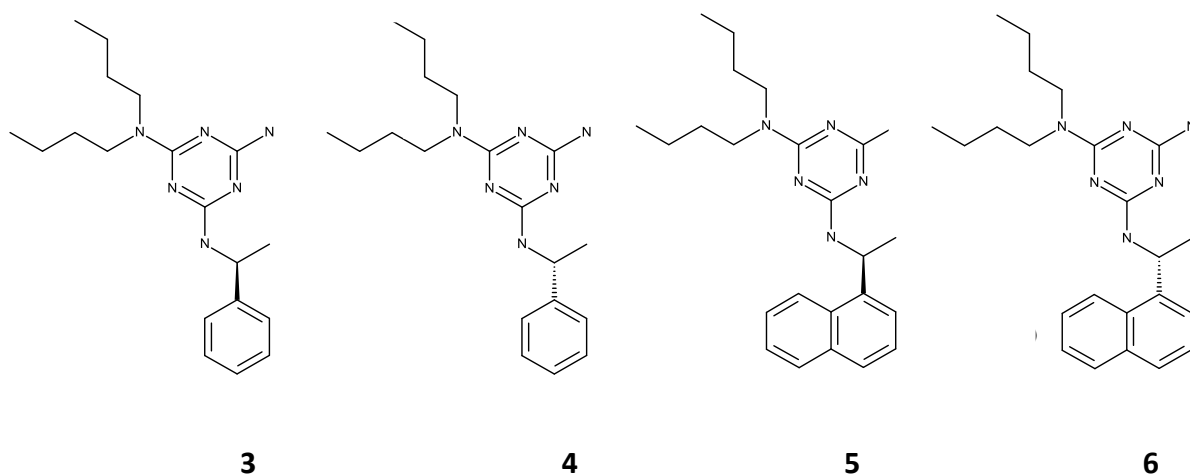
Melamine has also been used to synthesise dendrimers that can be tethered onto ordered inorganic components as shown in Figure 1.7.[25,27,28] The dendritic core, which is often highly porous, can display interesting host behaviour. The dense outer layer shields the interior region from the surrounding medium thus mimicking the hydrophobic pocket regions in enzymes. They offer a high degree of surface functionality and versatility. Dendrimers therefore tend to be used for drug delivery and for creating functional materials.[7]
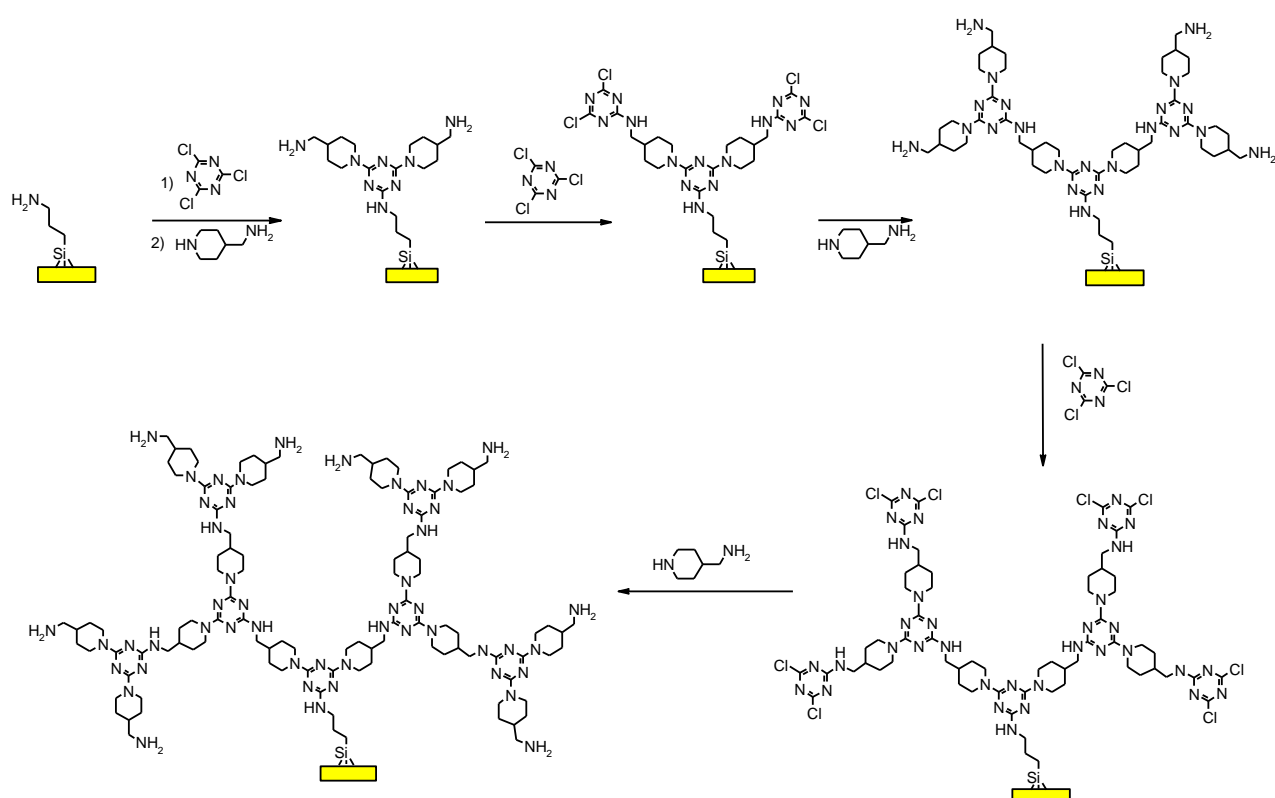
Figure 2: Synthesis of melamine dendrimers attached to a silica backbone. The dendrimer attached to a silica backbone is created firstly by reacting cyanuric chloride to available amine groups on the silica surface. Then diamines are attached to the the triazine, forming the first generation. These steps are continued until the required number of generations is created.

Melamine dendrimers were first developed by Zhang *et al.*[26] in 2000. The main reasons for incorporating cyanuric acid were to exploit the diverse reactivity of triazines and to prepare dendrimers of significant structural diversity, based both on the number of diamines available and the ability to manipulate their placement within the structure. Additionally, triazines also create domains for molecular recognition.[24] They suggested that these triazine-based dendrimers can be used in the preparation of supramolecular assemblies in solution and solid states leading to applications in medicine (drug delivery), advanced materials (heterogeneous catalysts, sensing materials) and separations (membranes, chromatography columns) when anchored to solid supports.

There are, however, limitations involved with the synthesis and application of dendrimers. Most importantly the synthesis of these materials involves many steps, whereby numerous reactions are performed on the same molecule.[27] This usually means very low end yields due to the numerous purification steps to produce the integral non-defected structure. Also the stability of dendrimers, depending on the number of generations, can be an issue.[28]

In this work the aim is to investigate if novel functions can successfully be incorporated into cross-linked networks and because melamine-formaldehyde resins and materials form in water, this adds potential for later recognition of given analytes in water. Cross-linked and porous networks offer high surface area and, therefore, high reactivity and good diffusion through materials.

1.2   Synthesis of melamine derivatives

1.2.1 From cyanuric chloride

Due to the features seen previously, there is no shortage of procedures for the synthesis of monomer derivatives. Most mono-, di- and trisubstituted derivatives are synthesised from cyanuric chloride **7**,[29,30,31] the structure of which is revealed in Figure 1.8.

7
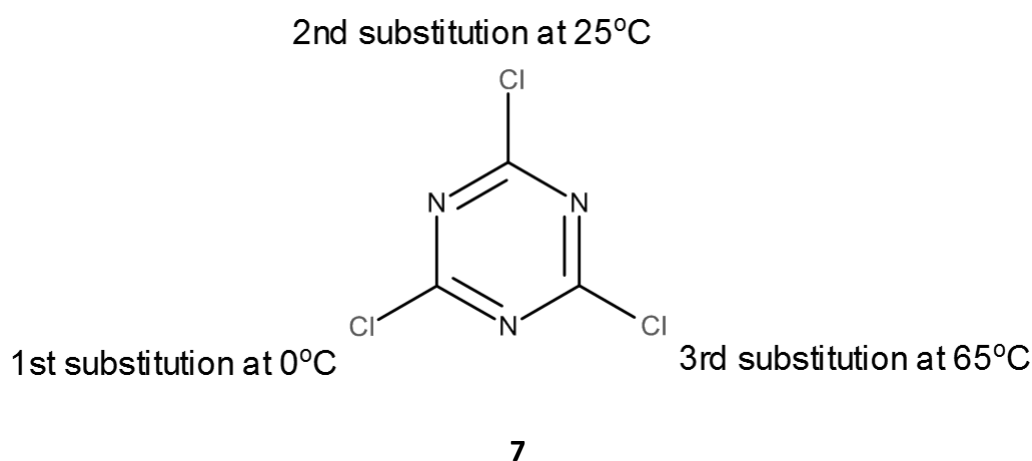
Figure 1.8: Empirical rule for substituting cyanuric chloride in order to obtain melamine derivatives.

The chloride groups can easily be displaced by various nucleophiles under certain conditions. Usually, a base is required such as sodium carbonate or a tertiary amine. As Figure 1.8 shows, the substitution of the first chloride substituent can be carried out at low temperatures. Room temperature is usually sufficient for the second substitution and the third can generally be carried out above 60°C. These temperatures, however, are only an empirical rule and they are of course greatly affected by the nature of the nucleophile

(basic strength and steric factors) and the substituents already present on the triazine ring.

The synthesis procedure used by Lehn involved reacting cyanuric chloride with ammonia in DMF at 0°C for the first substitution, 45°C for the second substitution and then 120°C for the final substitution with a functional amine. [13] The reaction mixture was then purified by column chromatography to obtain the final derivative in adequate yields.

The procedures reported by Whitesides[17-21] differed from the above by adding the first functional amine at 0°C in THF with the base DIPEA (diisopropylethylamine). After an hour the reaction mixture was heated to 30°C and the second functional amine was added and left to react for a further 2 hours. Finally the reaction was concentrated and partitioned between ethyl acetate and brine and then dissolved in a 1,4-dioxane- 30% aqueous NH_4OH (3:1) solution and heated under pressure for 5-8 hours. Again the crude mixture required purification by column chromatography.[19,20,21]

Another group (Würthner *et al.*[32,33,34]) synthesised hydrogen bonded superstructures to form supramolecular dyes. They aimed to synthesise long chain chiral melamine derivatives for self assembly with perylene bisimide in aliphatic solvents. One of their derivatives included two chiral long chain esters onto the triazine ring. For this purpose, they firstly synthesised a chiral amino acid ester salt, as shown in Scheme 1.1. The attachment of the latter to the triazine ring was carried out by using DIPEA as a solvent and reacting that with the commercially available 2-amino-4,6-dichlorotriazine, thus eliminating the need to monosubstitute cyanuric chloride with ammonia.
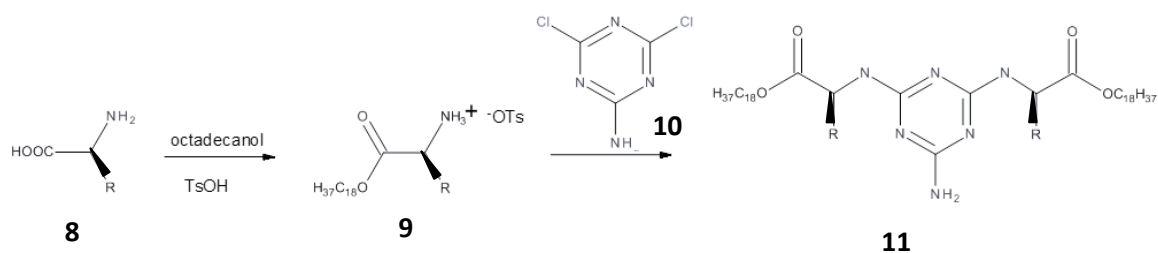
Scheme 1.1: synthesis of chiral melamine derivatives.

Other examples of melamine derivatives prepared from cyanuric chloride include chiral melamine derivatives synthesised by Liu et *al.*[3] whereby chirality was introduced to the triazine ring by substitution of commercially available chiral amines, using a similar procedure to Lehn and Whitesides (reaction in THF with DIPEA at 0°C for the first substitution followed by bubbling of ammonia through the solution at room temperature and finally the third substitution at 40°C for 30 hours).

All the above procedures refer to the di- and trisubstitution of cyanuric chloride with two or three different functional amines (amines other than ammonia). In order to retain two amine functions on the triazine ring for further reaction with formaldehyde, so as to cross-link the network (described in Chapter 2), one and only one functional amine must be incorporated per triazine motif. However, it seems more uncommon to synthesise derivatives of this type. Only one report has been found on this topic. Mahler et al.[35] reported that their synthesis was simply the dissolution of cyanuric chloride in ice-cooled acetone with drop-wise addition of the functional amine (also dissolved in cold acetone). After 30 minutes the reaction mixture was added to distilled water and the precipitate obtained was dried, dissolved in 1,4-dioxane and refluxed with constant bubbling of gaseous ammonia into the mixture for 5 hours.

1.2.2 From 2 -chloro-4,6-diamino-1,3,5-triazine

In 2009, Wong Chi Man's research group reported an even more simplified route to the synthesis of mono-functional melamine derivatives.[22] 2 -chloro-4,6-diamino-1,3,5-triazine **12** is a commercial compound. It was reacted with a functional amine, allylamine, by heating in a mixture of ethanol/water. This procedure required no purification steps as there was only one possible substitution on the triazine ring and a high yield (85%) was obtained.

12
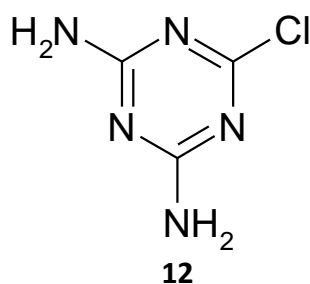
1.2.3 Direct synthesis from melamine

Bann et *al.*[1] reported in 1958 that melamine derivatives can be synthesised from melamine and amines reacted together at very high temperatures (300-500°C) in solvents such as ethylene glycol, though reaction times were very long which suggests this process is more industrial however. Table 1.2 summarises the different procedures discussed above.

Table 1.2: Summary of the different procedures discussed for the various methods employed by leading research groups in synthesising melamine derivatives.

Procedure	Solvents	HCl acceptor	Purification	Yield (%)
from cyanuric chloride				
Lehn[13-15]	DMF	Excess NH_3	Column chromatography	76
Whitesides[17-21]	THF then NH_4OH/H_2O mixture	DIPEA	Column chromatography	85
Liu[3]	THF	DIPEA	Column chromatography	62
Mahler[37]	Acetone and dioxane	Excess NH_3	-	71
from 2-amino-4,6-dichloro-1,3,5-triazine				
Würthner[34]	DIPEA	Excess DIPEA	Recrystallisation from hot ethanol	73-99
from 2-chloro-4,6-diamino-1,3,5-triazine				
Wong Chi Man[22]	$EtOH/H_2O$	$NaHCO_3$	-	85
from melamine				
Bann[1]	Ethylene or propylene glycol	-	unknown	unknown

2. Results and Discussion

The three different monomers chosen for this work **13** (later referred to as monomer 1)**, 14** (monomer 2) and **15** (monomer 3) are shown below. The decision on the choice of functional groups to incorporate was based on the fact that melamine derivatives acetoguanamine **23**, benzoguanamine **24** and caprinoguanamine **25** are commercially available and can be used for comparison. However, here the attachment is on the amino groups as opposed to a direct substitution of an alkyl or aromatic group. Also the inspiration of using melamine derivatives to carry out chiral recognition came from the findings of Liu *et al.*[3]
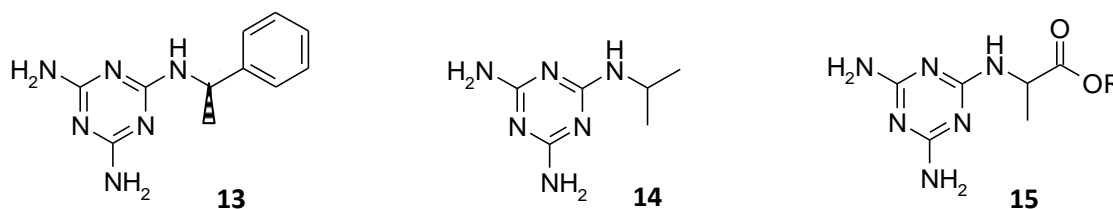
These chosen monomers have varied structural diversity. The first monomer carries a 1-phenylethyl amino group which is a bulky substituent with a chiral centre (in this work, the R version was synthesised). The second monomer contains an isopropylamine function and the third one has an ester function with a chiral centre which could then potentially be converted into an amino acid function (however, in this

work the racemate was synthesised, as explained in paragraph 2.1). Broad types of interactions are covered by these monomers (π interactions, hydrophobic effect) and the property of chirality. In each case, the substitution of the amino group with a more complex amino group will quite likely reduce the number of cross-linker molecules (formaldehyde) that can react with the monomer in the resin synthesis step described later in Chapter 2. In fact, further substitutions with hydrophobic compounds could also lead to difficulties in dissolving these monomers under aqueous conditions, conditions in which the subsequent material synthesis is carried out. Therefore, unlike the monomers produced by Liu *et al.*[3], only one amino group was chosen to be substituted and later in material synthesis, only 10% of the derivative is incorporated.

Many of the different procedures discussed in the introduction were repeated and readapted to the target molecules, on a small scale. Notably, the syntheses of Liu *et al.*[3] and the well established procedures from Lehn *et al.*[15] were initially used (the need for a Paar vessel for the reaction of Whitesides *et al.*[17-20] meant this synthesis procedure was not tried in this work). The problem however for these procedures was that the analyses of the ^{1}H and ^{13}C NMR spectra of the crude products were complex (residual solvent and DIPEA remained). A further purification would therefore be essential by column chromatography. These procedures would be more complicated and time consuming when synthesising on a large scale. Therefore the need of a relatively clean procedure with no purification step was preferred so that the desired product could easily be isolated and characterised by ^{1}H and ^{13}C NMR. For this reason the synthesis by Mahler *et al.*[37] was pursued. The results obtained are discussed in the section below.

2.1 Synthesis of the alanine ester toluene sulfonate salt (towards Monomer 3)

Monomer 3 required "activation" of the amine function in L-alanine before attachment to the triazine ring could be carried out (described by Würthner *et al.*[34]). The preliminary reaction involves converting L-alanine into the toluene sulfonate salt. Although the aim was to have an enantiomerically pure monomer, trials were carried out on the cheaper D,L-alanine until the reaction procedure was optimised. Only after, would it be viable to synthesise the monomer with solely the L-alanine substitution.

Figure 1.9 shows the ^{1}H and ^{13}C NMR of this salt (peaks in ^{1}H NMR spectrum at 2.0 ppm are due to residual acetone, peaks at 2.3 ppm due to DMSO and at 3.3 ppm due to water. This also applies to all spectra that follow). The ^{13}C NMR DEPT (Distortionless Enhancement by Polarization Transfer) spectrum helps to differentiate which peaks are due to CH_2. There is a slight discrepancy in the integration ratio in ^{1}H NMR spectrum. However the synthesis of monomer 3 with the crude product obtained from this reaction was pursued, as discussed later.
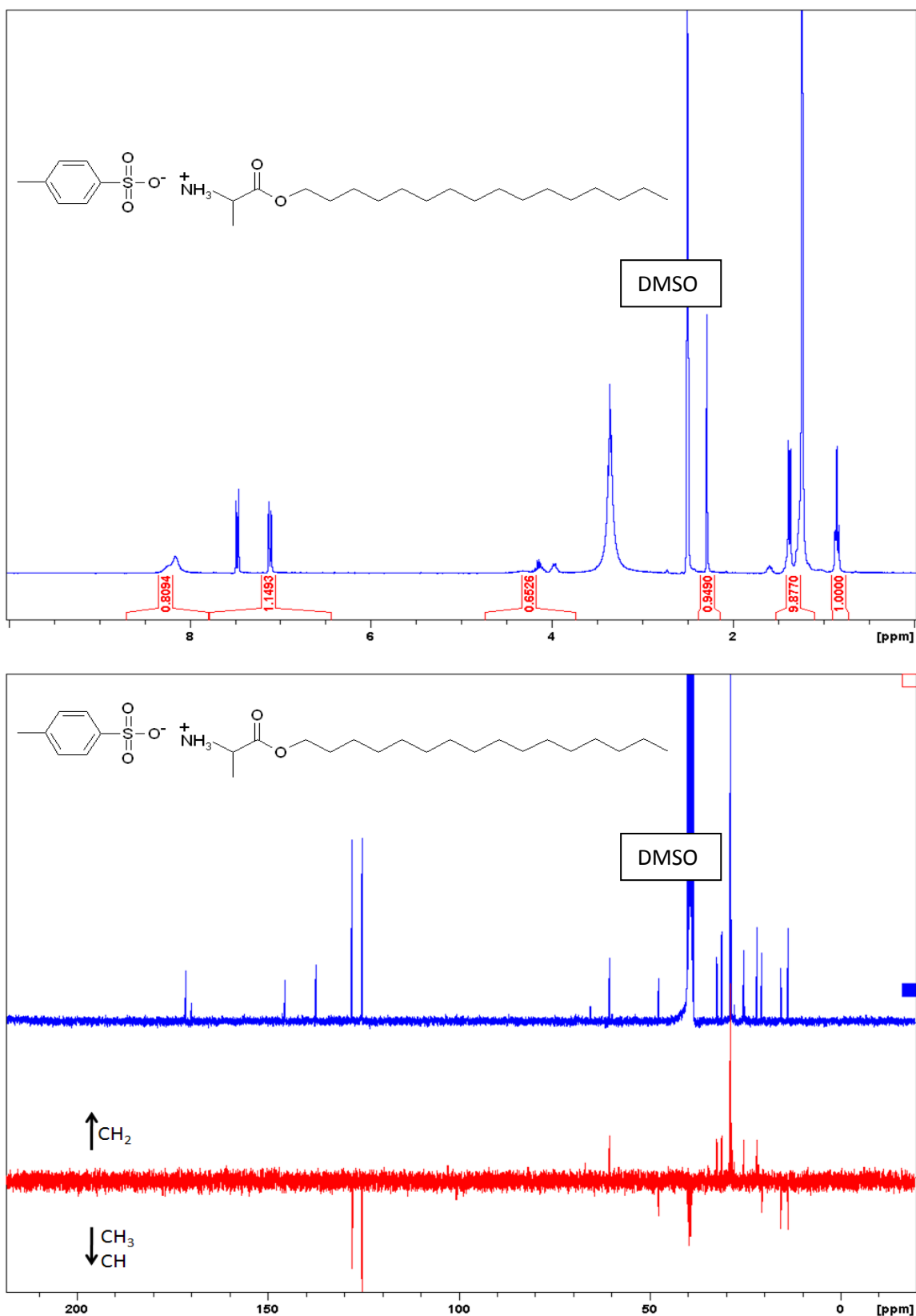
Figure 1.9: NMR spectra of alanine ester toluene sulfonate salt carried out in [D$_6$] DMSO. Top ^{1}H NMR. Bottom- ^{13}C NMR (blue) with DEPT spectrum (red) to help differentiate the CH$_2$ signals.

2.2 Synthesis of monomers using the procedure outlined by Mahler *et al.*

General Scheme

The syntheses of the first two monomers took place in two steps: firstly, the attachment of the functional amine followed by substitution with ammonia. The final ester compound (monomer 3) was synthesised in three steps as discussed previously starting from L-alanine, converting it to the amino-acid ester tolsyl ester (Scheme 1.2), which was then substituted onto the triazine ring in the same way as for monomers 1 and 2. Further substitution of chloride groups with ammonia was then carried out in a final step. Scheme 1.2 outlines these different steps.
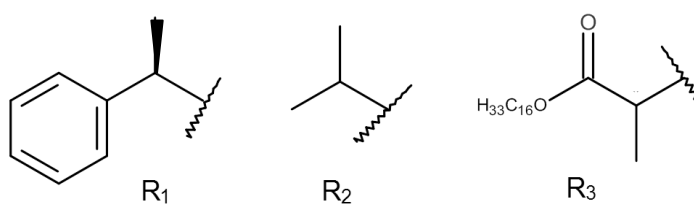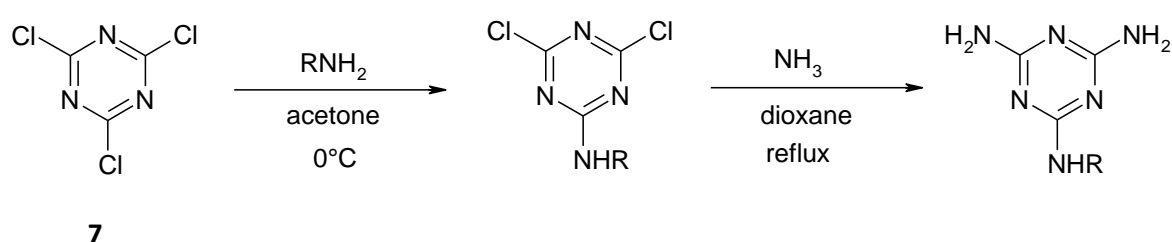
Scheme 1.2: Synthetic route for monomers. The first step outlines how the functional amine was potentially substituted and the second step outlines how the remaining chlorides would be substituted with ammonia.

Results for monomer 1

Figure 1.10 shows the ^{1}H and ^{13}C NMR spectra for monomer 1. The ^{1}H NMR spectrum shows that there is a significant shift of signals between starting material and product, especially the quartet for CH which has shifted from 4.0 ppm to 5.0 ppm. This quartet is where the biggest shift should occur as it is the closest group to the amine function that attaches itself to the triazine ring during the course of the reaction, thus these protons are the only ones to be in a very different chemical environment. This type of shift is, however, observed to a lesser extent with the ^{13}C NMR spectrum signals. The reaction was repeated and different batches of the same monomer produced identical spectra each time.

Although the reaction was carried out in a 1:1 stoichiometric ratio, a small quartet can be observed at 4.8 ppm in ^{1}H NMR and a small signal at 52 ppm in the ^{13}C NMR spectrum or so can also be observed, suggesting that there is formation of a side product in small amounts, perhaps due to di-substitutions. [Note that the peaks at 2.5 ppm (^{1}H) and 40 ppm (^{13}C) are due to DMSO, the peak at 3.0-4.0 ppm (^{1}H) is due to water and 3.6 ppm (^{1}H) and 66 ppm (^{13}C) are due to residual dioxane].
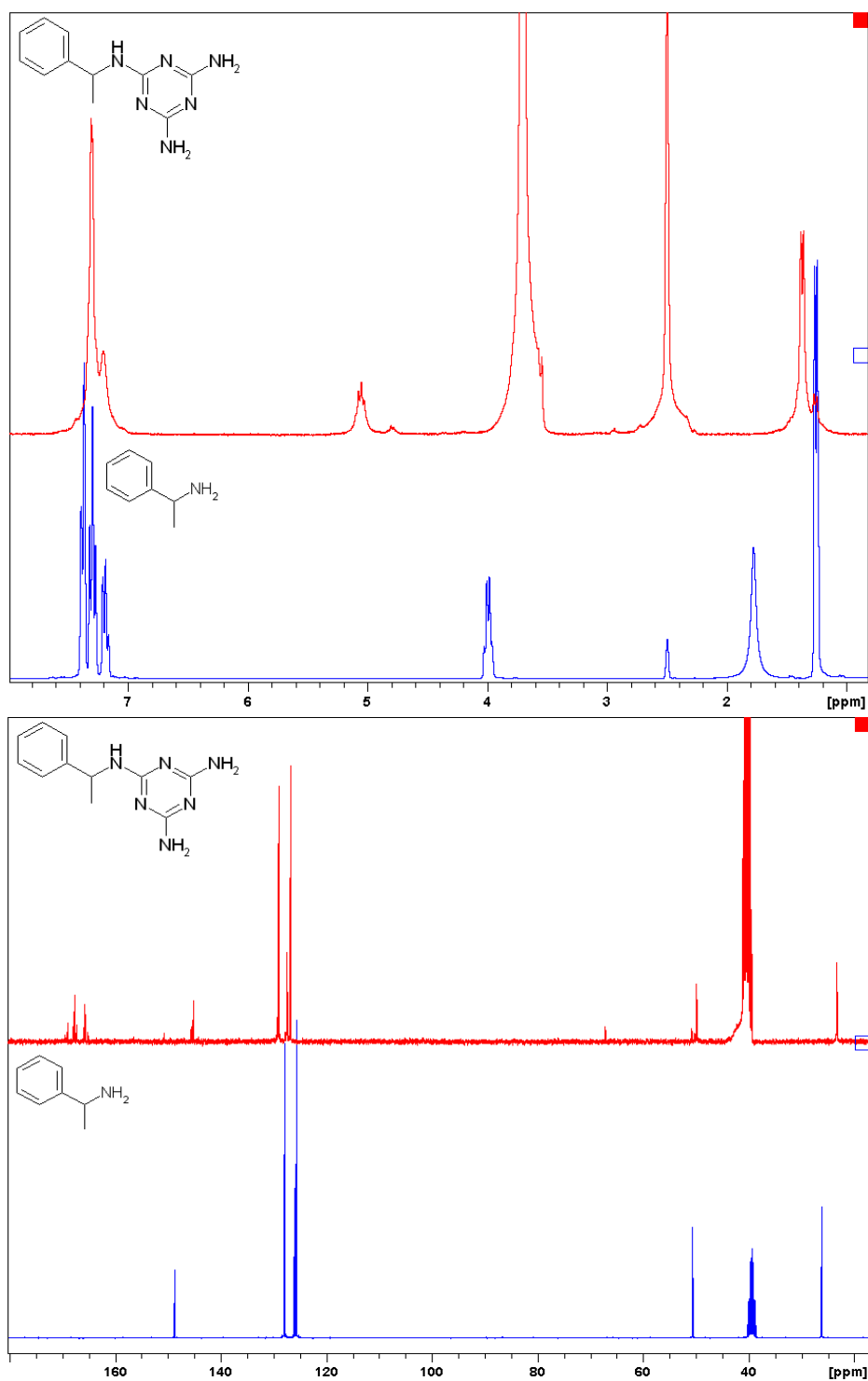
Figure 1.10: ^{1}H NMR (top) and ^{13}C NMR (bottom) spectra carried out in [D$_6$] DMSO of the crude product obtained for the synthesis of monomer 1 using the procedure by Mahler *et al* (crude product spectra in red, initial amine spectra in blue).

To verify if disubstitution was occurring, further product characterisation was carried out with LC-MS and this actually confirmed that although the desired product was present, the diphenylethyl substituted compound **17** and also the mono-chloro mono-phenylethyl substituted triazine compound **16** were also present, as shown in Figure 1.11 (the mass spectra can be found in Appendix A page III).
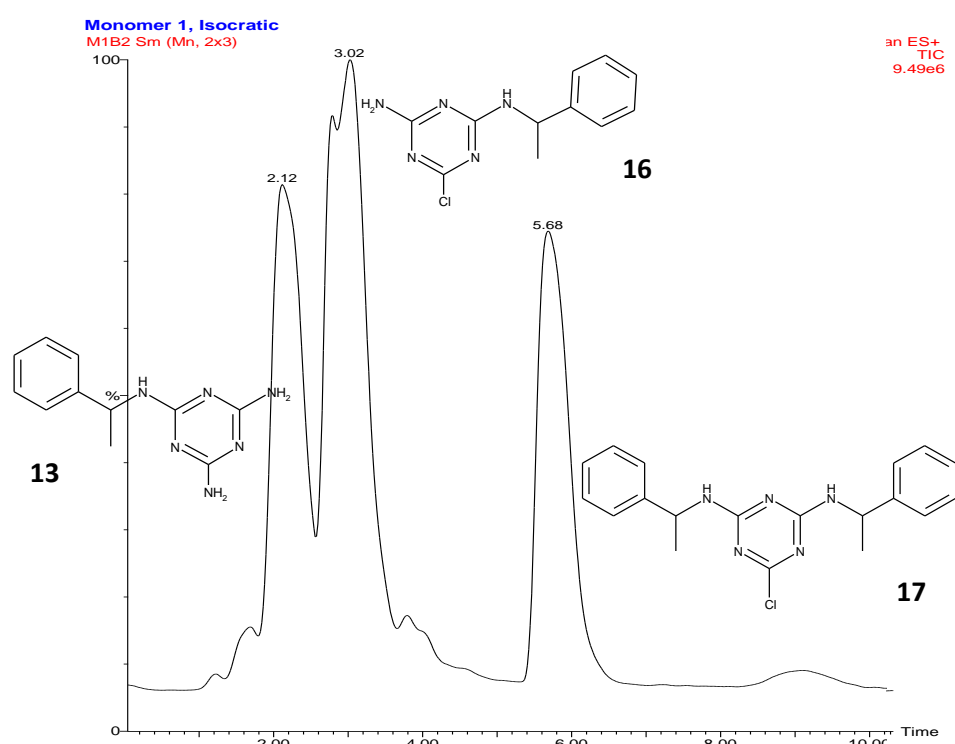
Figure 1.11: Liquid chromatogram of the crude mixture obtained for the synthesis of monomer 1 using the procedure by Mahler *et al.* The chromatogram shows a mixture of compounds.

The chromatogram suggests that the desired compound only makes up ~30% of the crude mixture with approximately ~35% of the di-substituted compound with a remaining chloride group and ~35% of the mono substituted compound still with a remaining chloride group (see Appendix 1). At first the reaction was left to react longer with

ammonia but this made very little difference. The difficulty in substituting the final chloride with ammonia may be due to the bubbling of ammonia gas taking place at high temperatures, i.e. the gas does not stay in solution and escapes, therefore is unlikely to react. With the results shown above, it was also not worth pursuing a purification step as the yield recovered would be low and also the chromatogram shows that separation of the desired product and the mono substituted compound with a remaining chloride group would most likely be difficult as Figure 1.11 shows a bad resolution between the peaks at 2.12 minutes and 3.02 minutes.

Results for monomer 2

The reaction steps to produce monomer 2 were slightly modified from the previous reaction described for monomer 1. Firstly the reaction time of the first step was increased as, after an hour of reaction, ^{1}H and ^{13}C NMR analysis showed that the starting materials were still present. Secondly, the extraction procedure after the second step was also altered. The solid residue after concentration was simply washed with a base due to its very low solubility in other organic solvents. Figure 1.12 shows the ^{1}H and ^{13}C NMR spectra of the starting amine and the crude product.
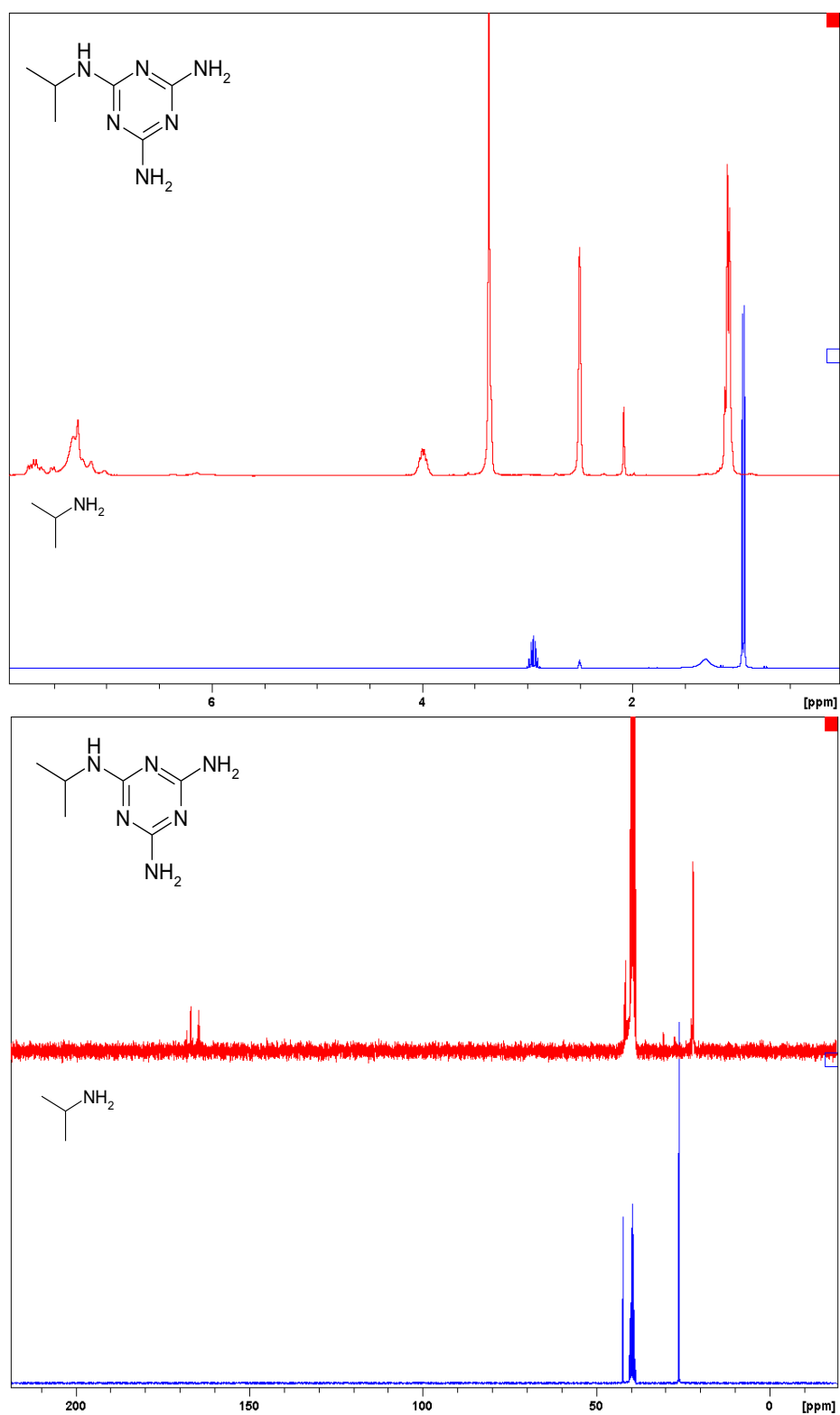
Figure 1.12: ^{1}H NMR (top) and ^{13}C NMR spectra (bottom) carried out in [D$_6$] DMSO of the crude product obtained for the synthesis of monomer 2 using the procedure by Mahler *et al.* (crude product spectra in red, initial amine spectra in blue).

In the ^{1}H NMR spectrum, a very significant shift for the CH septuplet is observed. It has shifted from 3.0 ppm in the starting material to 4.0 ppm in the monomer. Again, this CH group is where the largest shift should occur upon attachment to the triazine ring. The rest of the spectrum shows very slight differences. Again, the ^{13}C NMR spectrum on the other hand shows very little shift of the alkyl signal from starting material to product. This is due to the low sensitivity of ^{13}C NMR in detecting the change from >CH-NH$_2$ to >CH-NH-.

The LC-MS (Figure 1.13) does not confirm the presence of one sole structure but instead that three different compounds were present: (i) 2,4-diamino-6-chloro-1,3,5-triazine **12** (~25%), (ii) the mono-isopropyl mono-amino compound with a remaining chloride group **18** (~30%) and (iii) the di-isopropyl substituted compound with a remaining chloride group **19** (~35%). There were no mass ions present for the desired product.
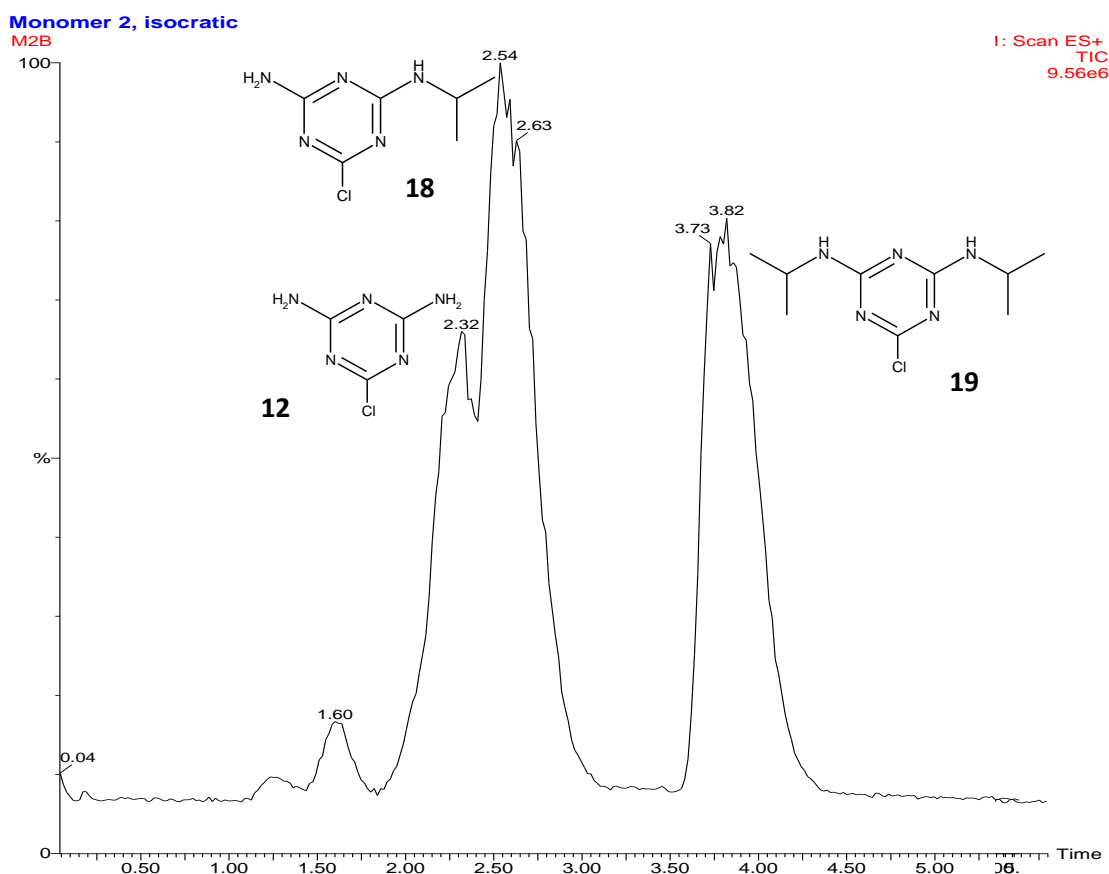
Figure 1.13: Liquid chromatogram carried out in acetonitrile/water of the crude mixture obtained for monomer 2 after 5 hours of bubbling under ammonia. It shows no evidence of the desired compound but instead a mixture of 2-chloro-4,6-diamino1,3,5 triazine, the mono- isopropyl mono- amino compound with a remaining chloride group and the di-isopropyl substituted compound with a remaining chloride group.

Due to the large amounts of the mono-chloro-substituted compounds left after 5 hours of refluxing in the presence of ammonia, an attempt was made to further increase the reaction time to 12 hours. This, once again, did not lead to a significant increase in the amount of fully aminated triazine due most likely to ammonia gas not staying in solution at high temperatures.

This synthetic route was as a consequence abandoned and instead a new modified path was followed, as shown in Scheme 1.3, whereby the addition of the functional amine was carried out in the final step (in DMF) and before that di-subustitution of cyanuric chloride with ammonia gas was carried out first (i.e. the steps were swapped around). This way the substitution of ammonia was carried out at lower temperatures.
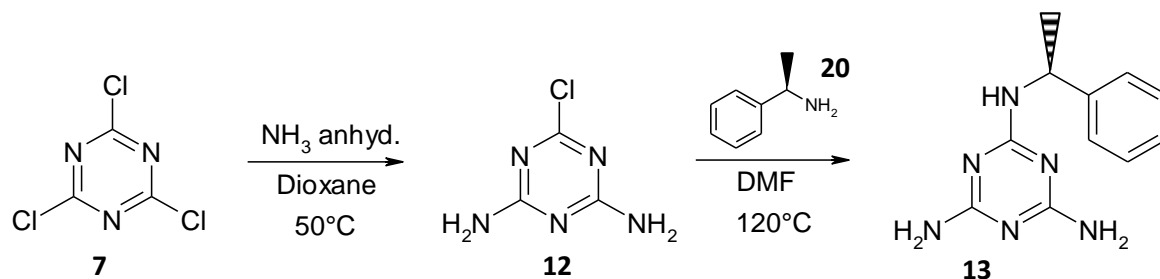
Scheme 1.3: Adapted synthesis route to optimise conversion of monomer 1 whereby the controlled substitution of two chloride groups by ammonia is carried out first so that the functional amine can then substitute the remaining chloride group.

Ammonia was bubbled into a mixture of cyanuric acid at 50°C to form the di-amino substituted triazine ring (^{1}H and ^{13}C NMR and LC-MS analysis confirmed that this step was successful). This, in turn, was dissolved in DMF and refluxed at high temperatures with L-(α)-methylbenzylamine to substitute the final chloride group. The problem here was that recrystallisation of the product from the crude mixture was very difficult, plus DMF is difficult to remove by evaporation (column chromatography was not attempted). This also discarded the feasibility of large scale synthesis.

The yields obtained for the crude product of monomers 1 and 2 synthesis described here differ by 10 % (higher yield for crude monomer 1) and the results from LC-MS data show that the synthesis of monomer 2 is more difficult to achieve and this may be due to

the structure of the functional amine. The aromaticity of L-1-phenylethylamine (L-(α)-methylbenzylamine) may be responsible for this as it is a more electron rich system which is able to donate electrons to the electron withdrawing triazine group or simply π interactions between the systems.

2.3   Using the procedure outlined by Wong Chi Man *et al.*

General Scheme

In 2009, a paper by Wong Chi Man *et al.*[22] on a reaction procedure to synthesise mono substituted melamine derivatives was published. The interesting point in this procedure is its apparent ease.
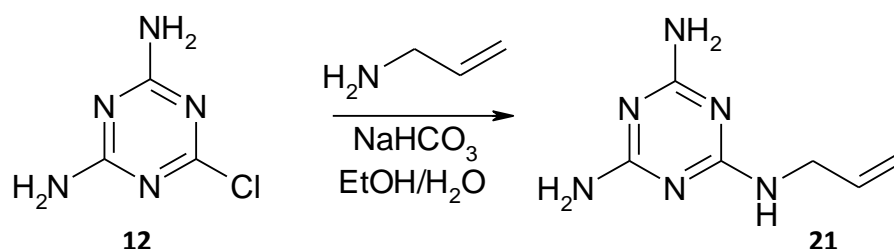
Scheme 1.4: Scheme describing to route to synthesise melamine derivatives according to Wong Chi Man et *al.*

The starting product, 2-chloro-4,6-diamino-1,3,5-triazine was commercially available, therefore removing the initial step outlined previously (step 1, Figure 1.17). Apparently, solvents with high boiling point temperatures such as DMF were not required and refluxing at a temperature reached by a solvent mixture of ethanol and water (1:1) sufficed.

All the monomers were then re-synthesised using this procedure.

Results from monomer 1

For monomer 1 a thick yellow crude product was obtained. The ^{1}H and ^{13}C NMR spectra are shown in Figure 1.13. The ^{1}H NMR spectrum shows a substantial shift of the quartet circled in orange (from 4.0 ppm to 5.0 ppm) and the appearance of new peaks at 6.0 ppm.
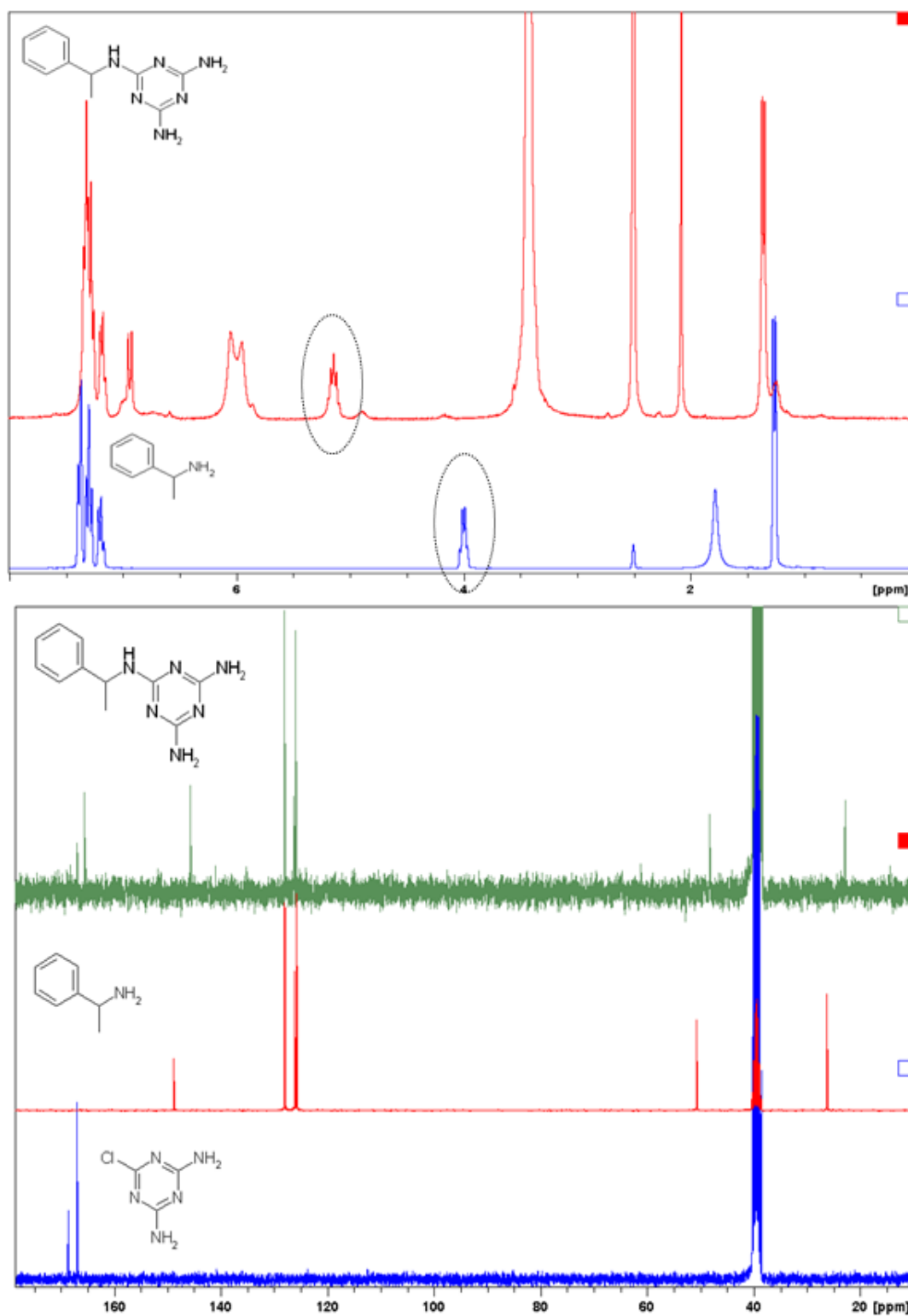
Figure 1.13 ^{1}H NMR (top) and ^{13}C NMR (bottom)carried out in [D$_6$] DMSO of the crude product obtained for the synthesis of monomer 1 (red in top and green in bottom) using the procedure by Wong Chi Man *et al.* The starting products are also shown (blue in top spectrum and red and blue in bottom spectrum).

Figure 1.14 shows the MS of this product in which the desired mass ion is present at m/z=231. The peak at m/z=335 is due to the di-substituted compound, however further confirmation on purity is required by a chromatographic technique.

Despite this, however, the crude product obtained here was used further for material synthesis as it did not contain any chloride groups.
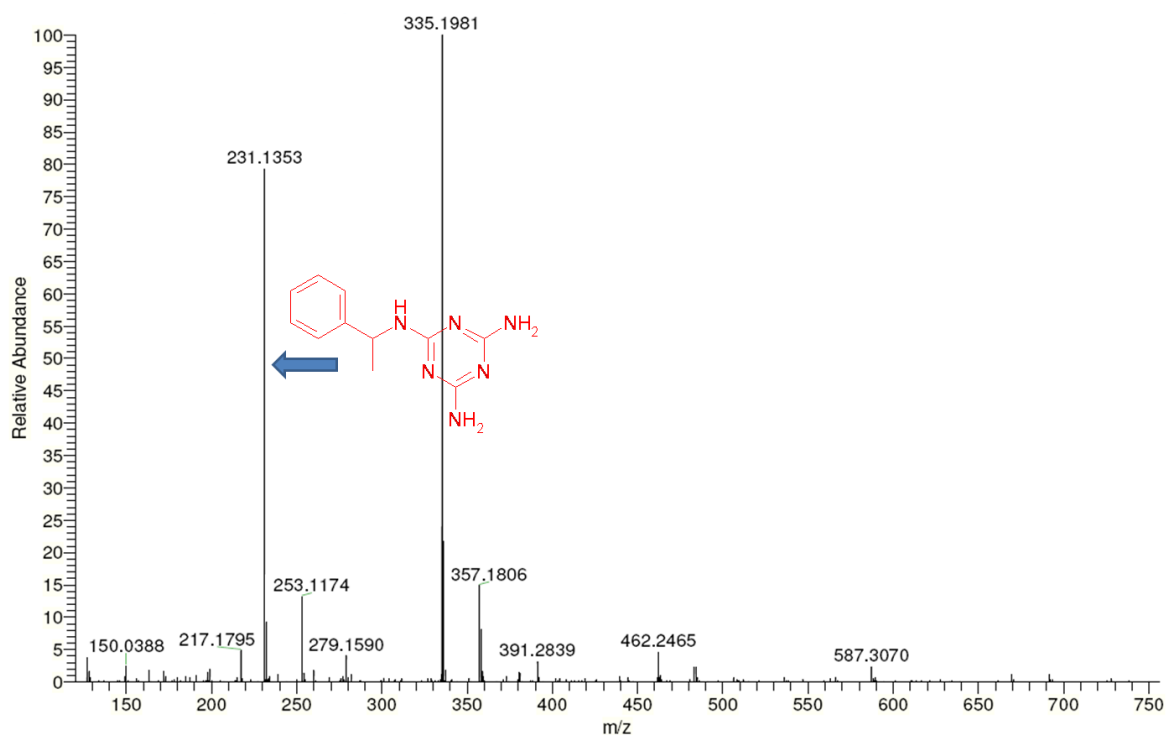
Figure 1.14: Mass spectrum of monomer 1 synthesised using the procedure by Wong Chi Man *et al*. It shows that the mass ion (m/z=231) of the desired product is present but also the mass ion of the di-substituted compound is also present.

__Results from monomer 2__

For monomer 2 similar remarks are made. There are shifts in the ^{1}H and ^{13}C NMR spectra (Figure 1.15). The MS data confirmed that the target compound is present (Figure 1.16).
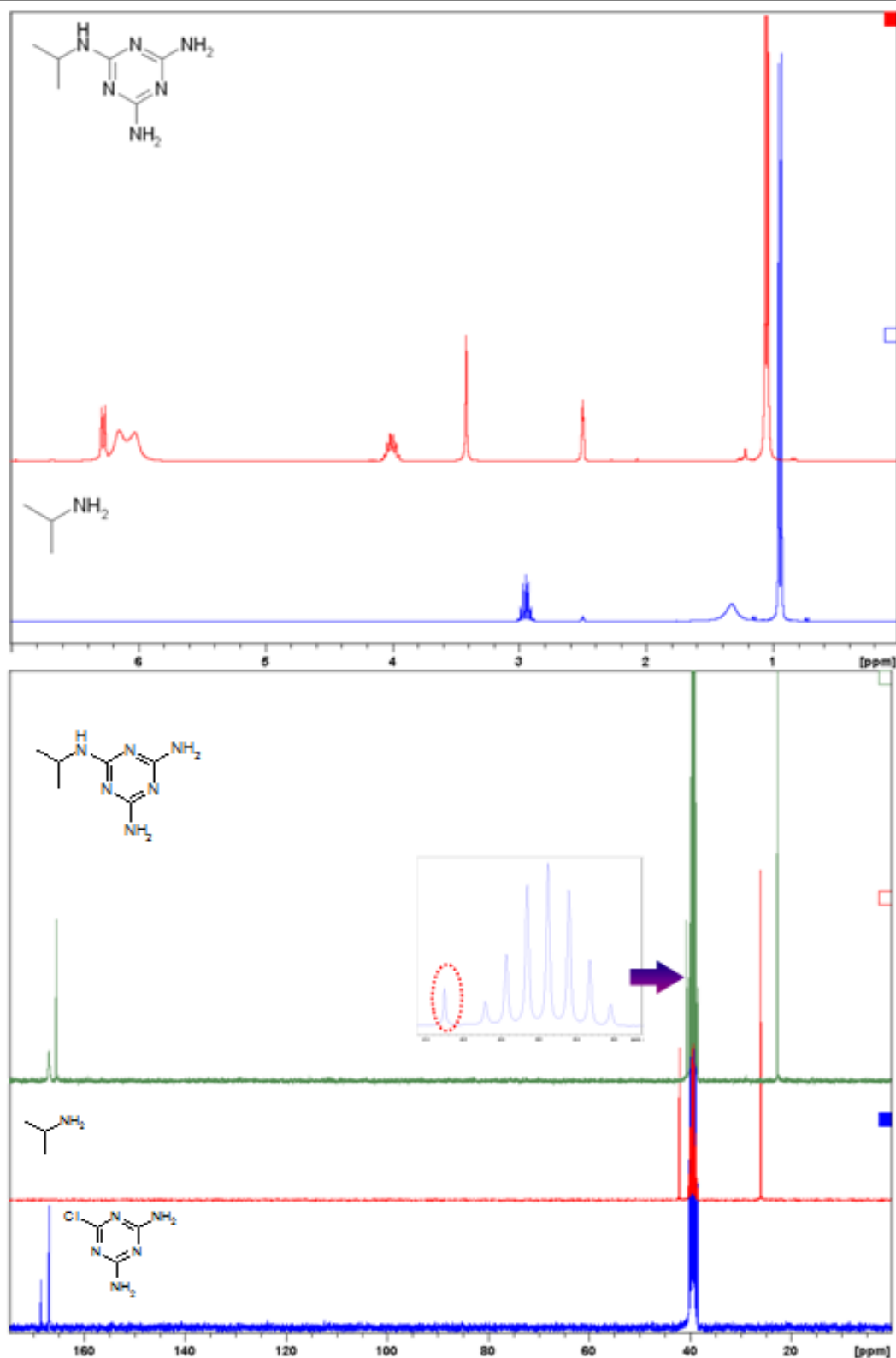
Figure 1.15: ^{1}H NMR (top) and ^{13}C NMR (bottom) carried out in [D$_6$] DMSO of the crude product obtained for the synthesis of monomer 2 (in red) using the procedure by Wong Chi Man *et al.* The spectra in blue represent the starting amine. In the top spectrum, the inset shows the zoom-in of the region from 38 to 41 ppm where the CH signal can be better distinguished from the DMSO signals.
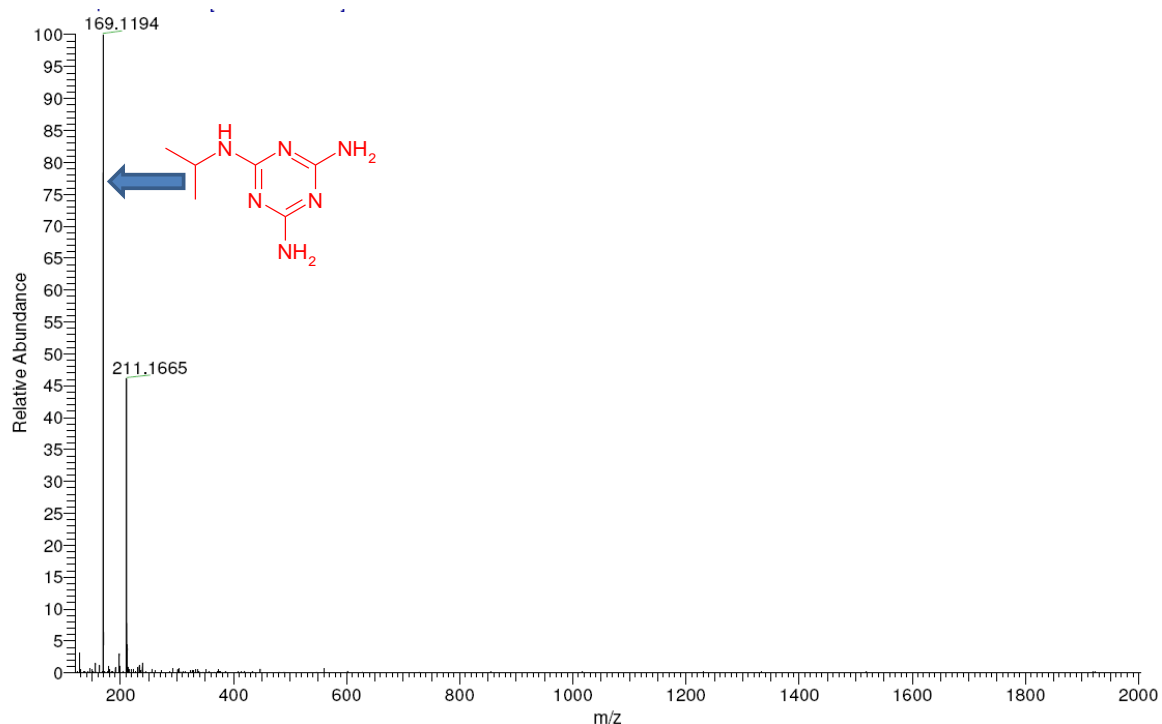
Figure 1.16: Mass spectrum of monomer 2 synthesised using the procedure by Wong Chi Man *et al*. It shows that the mass ion (m/z=169) of the desired product is present but also that the mass ion of the di-substituted compound is also present but is not the most intense peak.

Like monomer 1, both the mono-substituted product (for which the molecular ion is at m/z=169) and the di-substituted product (for which the molecular ion is at m/z=211) are present. Contrary to the mass spectrum of monomer 1 produced by this route (Figure 1.14), the mass ion for the desired product is the most intense. However, confirmation is required by a chromatographic technique. Material synthesis was however pursued with this crude mixture.

__Results from monomer 3__

As monomers 1 and 2 showed positive results, the amine "activated" amino acid ester synthesised previously was also reacted with 2-chloro-4,6-diamino-1,3,5-triazine. The ^{1}H and ^{13}C NMR spectra and mass spectra are shown in Figure 1.17 and Figure 1.18 respectively.
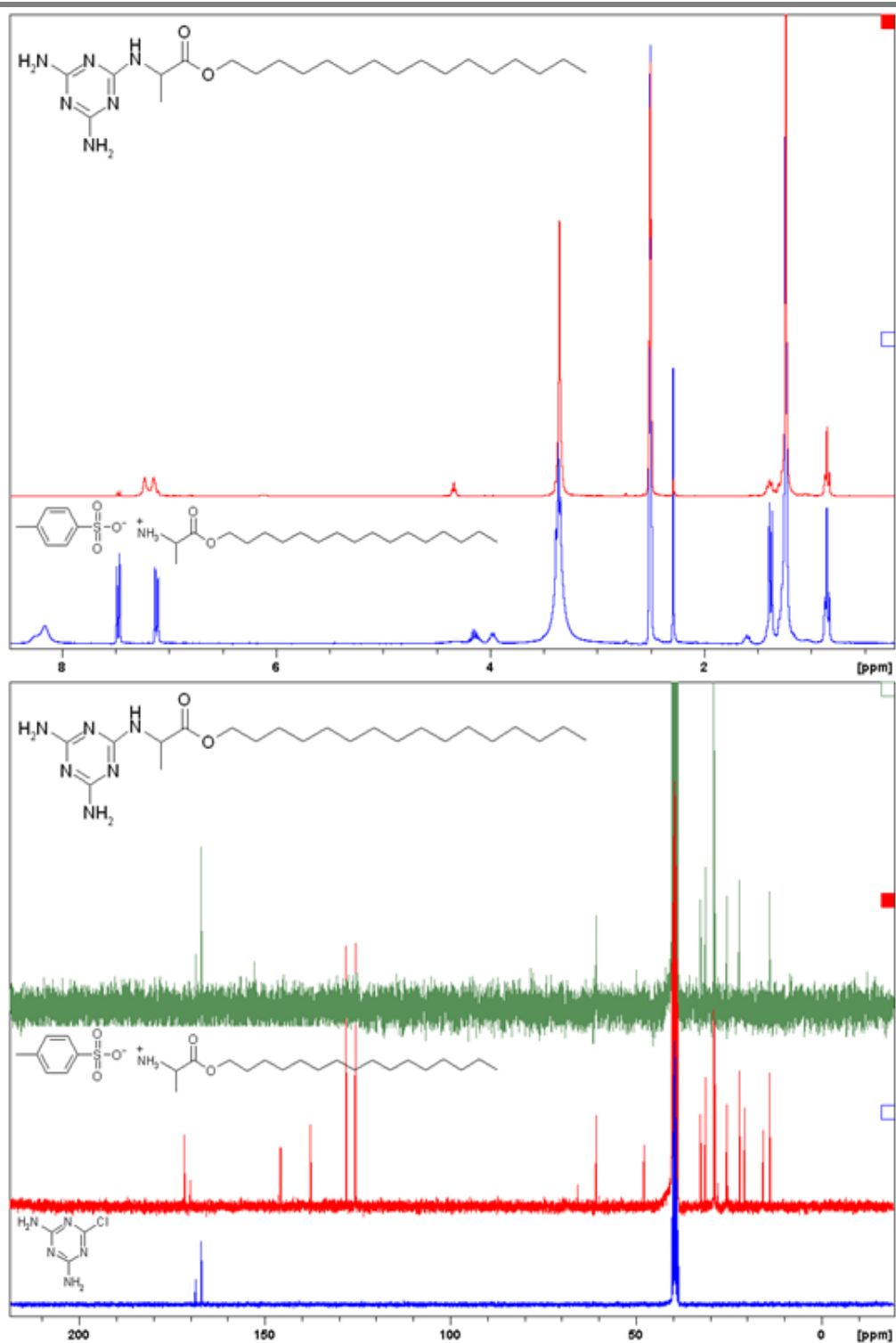
Figure 1.17: ^{1}H NMR (top) and ^{13}C NMR (bottom) spectra carried out in [D$_6$] DMSO of the crude product obtained for the synthesis of monomer 3 (in red on top spectrum and in green on bottom spectrum) using the procedure by Wong Chi Man *et al.* The starting products are also shown in blue in the ^{1}H NMR spectrum and in blue and red on the ^{13}C NMR spectrum.
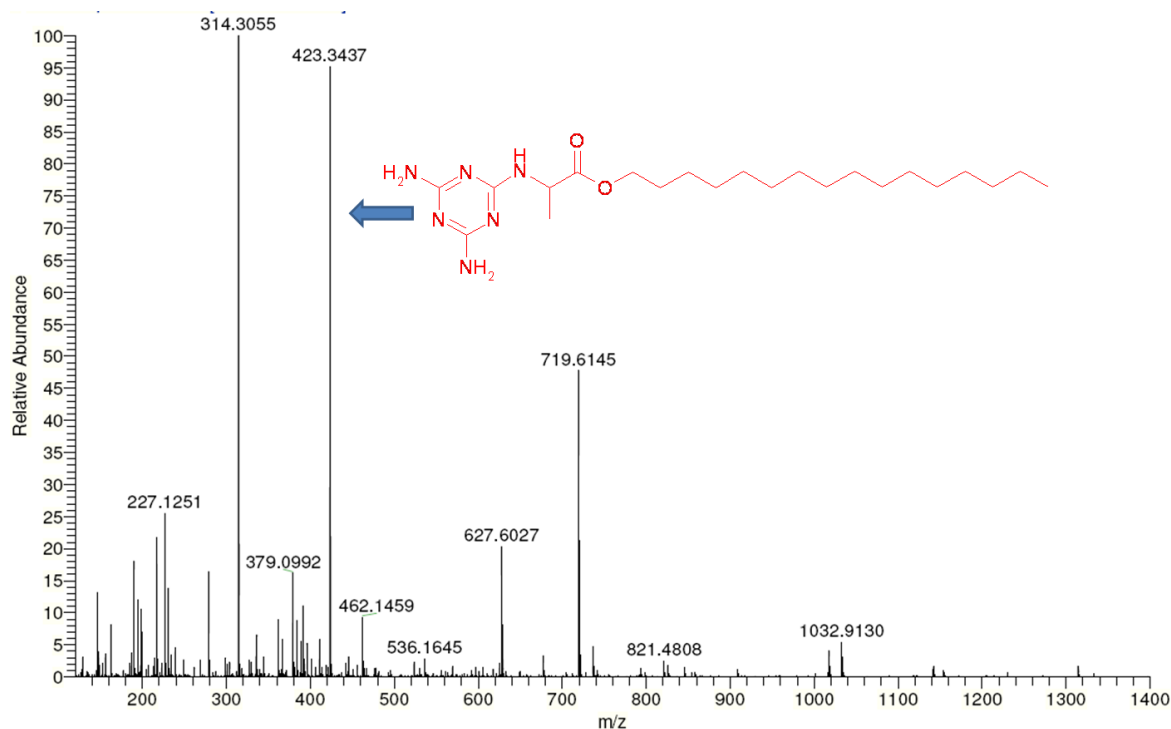
Figure 1.18: Mass spectrum of monomer 3. The mass ion of the desired compound is at m/z=423 and the mass ion of the di-substituted compound is at m/z=719. The chemical structure of the mass ion at m/z=314 (the base peak) is unknown.

The ^{1}H NMR spectrum shows a very slight shift of the quartet due to CH (from 4.20 to 4.44 ppm). Again the shifts are less noticeable in the ^{13}C NMR spectrum as it is not as sensitive as ^{1}H NMR. The mass spectrum confirms that the desired compound is present as is the di-substituted compound and perhaps a few other small impurities. Chromatographic data is also required as with the other monomers to quantify the purity of the crude mixture.

2.4 Using the procedure outlined by Bann *et al.*
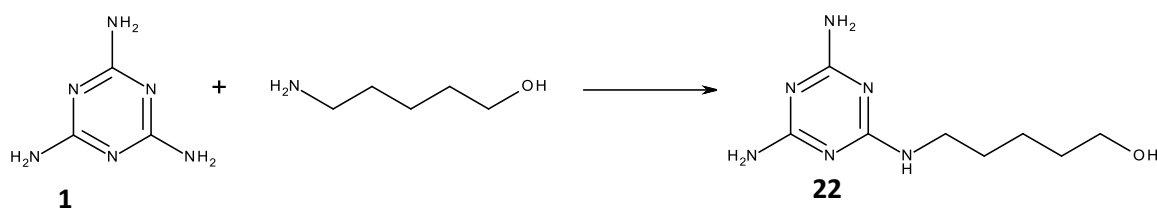
Scheme: 1.4: Synthesis of melamine derivatives directly from melamine and the functional amine

As the facilities at BASF are adapted to large scale and higher temperature reactions, the procedure by Bann *et al.*[1] was attempted with melamine and 5-aminopentanol. The conditions were much harsher than the previous synthesis routes followed and much more adaptable to industrial facilities. The reaction was attempted on a 400 g scale, which is a far larger amount than what is required in the material synthesis section and any similar synthesis route would have to be scaled down to approximately 10 g at Keele University. Nevertheless, proof of concept of large scale synthesis could benefit future industrial applications for the types of materials produced in this work.

The ^{13}C NMR spectrum of the product obtained from the resulting procedure is presented below (Figure 1.19). The presence of a double peak at 176-178 ppm suggests that substitution on the melamine has occurred (two different amine attachments on triazine carbon atoms). However, as discussed previously, this synthesis was not pursued for the purpose of this work (very high temperatures and long reaction times) but demonstrated that this procedure could be a viable industrial alternative.
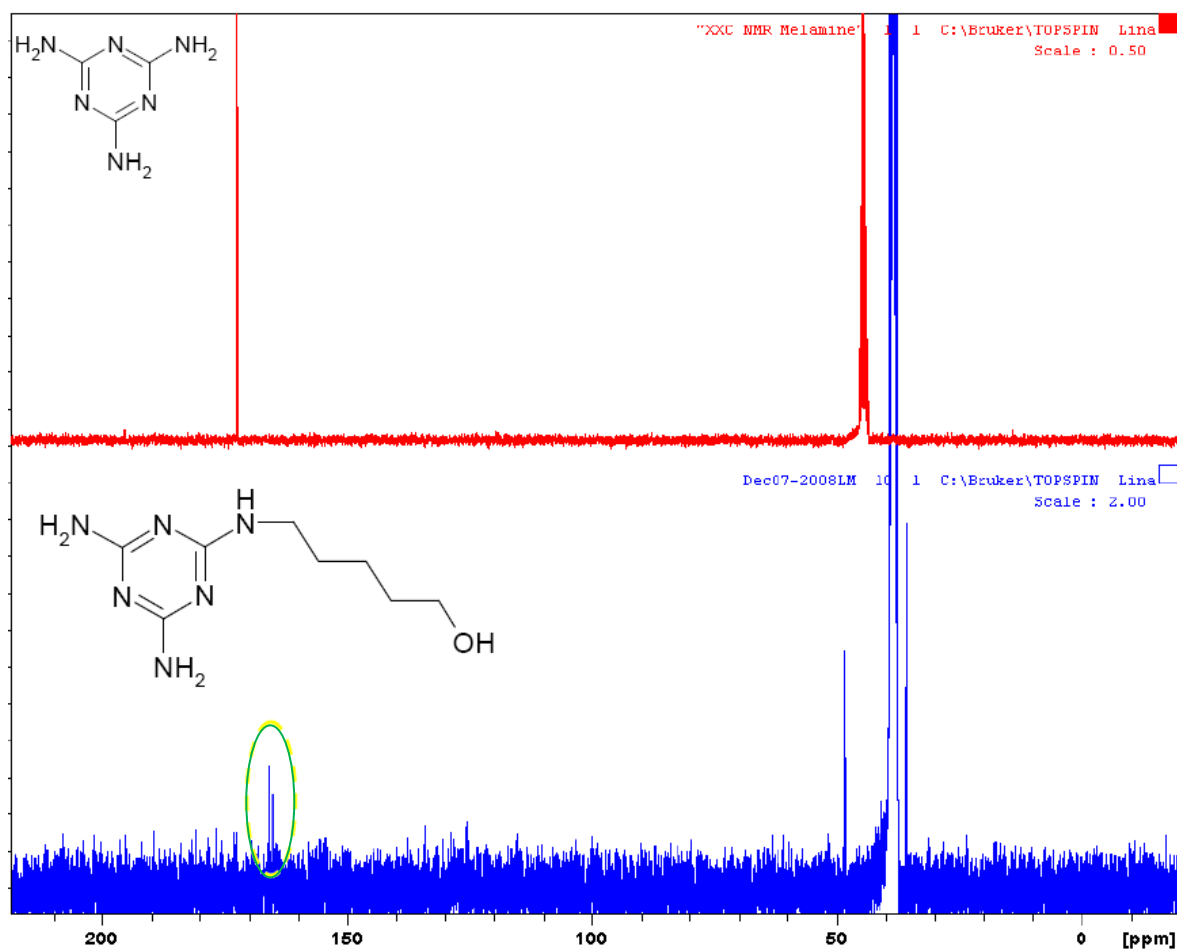
Figure 1.19: ^{13}C NMR spectrum carried out in [D$_6$] DMSO of a melamine derivative produced directly from melamine (blue) and melamine (red) as suggested by Bann *et al[1]*. The signal/noise ratio is very high and a higher number of scan would have perhaps produced a better quality spectrum.

More analysis is required to conclude on the confirmation of the presence of desired product. However, as this route was not fully pursued, further analyses were not carried out.

3. Conclusions

The procedure by Wong Chi Man *et al.* was therefore used to scale up the synthesis of derivatives and produce 5 g of monomer derivatives. Although the mass spectra of all monomer (1,2 and 3) suggested the presence of the di-substituted monomers as well as the desired monomers, material synthesis with the crude mixture was pursued. The table below (Table 1.3) sums up the various results and conclusions that were obtained here.

Table 1.3: Summary of the various results and conclusions that can be drawn for the different syntheses discussed in this chapter.

Procedure	Desired compound obtained	Crude Yield (%)	Comments
Mahler *et al.*[37]	Monomer 1: yes but not pure	82	LC-MS showed only 30% was desired product
	Monomer 2: no	61	-
	Monomer 3: not attempted	-	-
"Modified" Mahler	Crude product not recoverable from solution in DMSO	-	-
Wong Chi Man *et al.*[22]	Monomer 1: yes but potentially with a large amount of di-substituted triazine	98	Chromatographic analysis required to determine purity. Material synthesis continued with these crude mixtures
	Monomer 2: yes with small amount of di-substituted compound	100	
	Monomer 3: yes with small amount of di-substituted compound and potentially other impurities	100	

4. Experimental

All chemicals were bought from major suppliers and used as received with no further purification. The ^{1}H and ^{13}C NMR spectra were recorded on a Bruker spectrometer, 300MHz, at room temperature in [D$_6$] DMSO. LC-MS measurements were carried out with an Alliance 2690, interfaced to a quadrupole mass spectrometer: Quattro II, Micromass, ESI. The LC separation was performed using a Restek C18 5 µm column, 150 mmx2 mm internal diameter at a flow rate of 50 µL/min. The mobile phase used was a water/0.5mM TFA/methanol gradient where the percentage of methanol was changed linearly as follows: 0 min, 5%,; 3 min, 5%; 6 min, 50%; 7 mins, 50%; 8 min, 95%; 12 min, 5%. However, as the in-house LC-MS equipment failed to work during the course of this project, mass spectrometry had to be carried out externally at EPSRC MS service (Swansea University). The instrumentation used was Thermofisher LTQ Orbitrap XL.

4.1 Synthesis of the alanine ester salt (n-hexadecanol para-toluenesulfonic acid monohydrate)

Para-Toluene sulfonic acid monohydrate was purchased from Aldrich. Hexadecanol (97% pure) and D,L alanine (99% pure) were purchased from Acros.

One equivalent of L-alanine (0.89 g, 10 mmol), 1.1 equivalents of 4-toluenesulfonic acid monohydrate (2.07 g, 11 mmol) and 1.1 equivalents of hexadecanol (2.67 g, 11 mmol) were suspended in toluene (50 mL) and refluxed for 20 hours with a Dean-stark trap. The resulting mixture was concentrated *in vacuo* and the colourless solid residue was recrystallised from acetone. Yield: 98%. 100% purity from NMR spectra.

^{1}H ([D$_6$] DMSO, 300 MHz) δ= 0.85 (m, 3H **CH$_3$**-(CH$_2$)$_{15}$), 1.24 (s, 30H, 15CH$_2$), 1.38 (d, 3H, **CH$_3$**-(CH)J=7.5), 2.29 (s, 3H, **CH$_3$**-Ph), 4.11 (m, 1H, **CH**-(CH$_3$)), 7.11 (d, 2H, 2x **CH**$_{ar}$,J=8.3), 7.47 (d, 2H, 2x **CH** $_{ar,}$ J=7.9), 8.10 (br, 3H, **NH$_3$$^+$**).

^{13}C ([D$_6$] DMSO, 75 MHz) δ= 13.9 (**CH$_3$**-(CH$_2$)$_{15}$), 15.9 (**CH$_3$**-Ph), 20.7 (**CH$_3$**-CH), 22(CH$_2$), 25.5 (CH$_2$), 28.9 (n CH$_2$), 31.3 (CH$_2$), 32.5 (CH$_2$), 48 (**CH**-CH$_3$), 61 (CH$_2$), 66 (CH$_2$), 125.4 (2xC$_{ar}$), 128.0 (2xC$_{ar}$), 137.0-145.5 (C$_{ar}$), 170.0 (C-O), 171.4 (C=O).

4.2 Synthesis from cyanuric chloride

Cyanuric chloride (99% purity), L-(α)-methylbenzylamine (99% purity) and isopropylamine (99% purity) were purchased from Acros.

Monomer 1

Cyanuric chloride (2 g, 11 mmol) was dissolved in 100 mL ice-cooled acetone (2°C). While vigorously stirring, a solution of L-(α)-methylbenzylamine (1.20 g, 10 mmol) in acetone (50 mL) was added drop-wise so that the temperature did not exceed 3°C (over ~50 mins). The complete reaction mixture was stirred a further hour at 2-5 °C by continuously changing the ice bath over this period. The reaction mixture was then concentrated to leave a sticky white solid. The white solid was then dissolved in dioxane (100 mL) in a large 3-neck flask and refluxed while bubbling with ammonia for 5 hours. The reaction mixture was then concentrated *in vacuo* to remove as much dioxane as possible. The contents of the flask was then dissolved in dichloromethane (100 mL) and washed 3 times with water (3x100 mL). The organic phase was dried and concentrated *in vacuo*. Yield: 82%.

^{1}H ([D$_6$] DMSO, 300 MHz) δ=1.38 (d, 3H, CH$_3$, J-6.4), 5.14 (m, 1H, CH), 7.23-7.44 (m, CH$_{ar}$).

^{13}C ([D$_6$] DMSO, 75 MHz) δ=23.1 (CH$_3$), 48.8 (CH), 127.8-144.6 (aromatic C), 165.2-168.1 (triazine C).

Monomer 2

Cyanuric chloride (2 g, 11 mmol) was dissolved in 100mL ice-cooled acetone (2°C). While vigorously stirring, a solution of isopropylamine (0.57 g, 10 mmol) in acetone (50 mL) was added drop wise so that the temperature did not exceed 3°C (over 50 mins). The complete reaction mixture was stirred a further 5 hours at 2-5°C by continuously changing the ice bath over this period. The reaction mixture was then concentrated to leave a sticky white solid. The white solid was then dissolved in dioxane (100 mL) in a large 3-neck flask and refluxed while bubbling with ammonia for 5 hrs. The reaction mixture was then concentrated *in vacuo* to remove as much dioxane as possible. The white solid residue was washed with dilute NaOH (100 mL). The remaining solid was filtered off and dried. Yield 61%.

^{1}H ([D$_6$] DMSO, 300 MHz) δ= 1.10 (d, 6H, 2CH$_3$, J=6.7), 3.99 (sextuplet, 1H, **CH**-(2xCH$_3$), J=6.8), 7.02-7.80 (br, 5H, NH$_2$).

^{13}C ([D$_6$] DMSO, 75 MHz) δ= 17.5 (CH$_3$), 37.0 (CH), 160.1-163.4 (C$_{triazine}$).

4.3 **Synthesis from 2 -chloro-4,6-diamino-1,3,5-triazine**

Monomer 1

L-(α)-methylbenzylamine (3g, 25.0 mmol) was added to a mixture of 2-chloro-4,6-diamino-1,3,5-triazine (3g, 20.6 mmol) and NaHCO$_3$ (1.7g, 20.6 mmol) in EtOH/water (350 mL, 1:1). After 4 hours the solution went clear. The reaction mixture was heated to 90°C for 40 hours and then concentrated *in vacuo*. Yield: 98%. Estimated purity from mass spectrum: 44%.

^{1}H ([D$_6$] DMSO, 300 MHz) δ=1.36 (d, 3H, CH$_3$, J=6.8), 5.15 (m, 1H, CH), 5.96 (m, broad, NH$_2$+NH), 6.92 (d, 2H, NH$_2$), 7.18-7.35 (m, 5H, 5xCH$_{ar}$).

^{13}C ([D$_6$] DMSO, 75 MHz) δ= 22.9 (CH$_3$), 48.2 (CH), 126.1-128.0 (C$_{ar}$), 165.7-167.1 (triazine C)

Elemental Analysis: C$_{11}$H$_{15}$N$_6$

Mass spectrometry: 231 (M1+H$^+$)

Monomer 2

Isopropylamine (1.46 g, 25.0 mmol) was added to a mixture of 2-chloro-4,6-diamino-1,3,5-triazine (3g, 20.6 mmol) and NaHCO$_3$ (1.7g, 20.6 mmol) in EtOH/water (350 mL, 1:1). After 4 hours the solution went clear. The reaction mixture was heated to 90°C for 40 hours and then concentrated *in vacuo*. Yield: 100%. 69% estimated porosity from mass spectrum.

^{1}H ([D$_6$] DMSO, 300 MHz) δ=1.11 (d, 6H, 2CH$_3$, J=6.4), 4.01 (m, 1H, CH, J=8.1), 6.03-6.24 (m, broad, 2xNH$_2$+NH).

^{13}C ([D$_6$] DMSO, 75 MHz) δ= 22.7 (CH$_3$), 40.3 (CH), 165.5-166.9 (triazine C)

Elemental Analysis: C$_6$H$_{13}$N$_6$

Mass spectrometry: 169 (M2+H$^+$)

Monomer 3

The previously synthesised alanine ester salt (2.46 g, 25.0 mmol) was added to a mixture of 2-chloro-4,6-diamino-1,3,5-triazine (3g, 20.6 mmol) and NaHCO$_3$ (1.7 g, 20.6 mmol) in EtOH/water (350 mL, 1:1). After 4 hours the solution went clear. The reaction mixture was heated to 90°C for 40 hours and then concentrated _in vacuo_. Yield: 100%. Estimated porosity from mass spectrum: 30%.

^{1}H (DMSO, 300 MHz) δ=0.85 (m, 3H, **CH$_3$**-(CH$_2$)$_{15}$), 1.23 (s, 30H, 15xCH$_2$), 1.44 (m, 3H, **CH$_3$**-CH), 4.44 (m, 1H, CH), 7.18-7.47 (m, broad,2xNH$_2$+NH).

^{13}C ([D$_6$] DMSO, 75 MHz) δ= 13.7 (**CH$_3$**-(CH$_2$)$_{15}$), 22.1(CH$_2$), 25.4 (CH$_2$), 29.0 (n CH$_2$), 31.3 (CH$_2$), 33.6 (CH$_2$), 60.6 (CH$_2$), 167.1-169.4 (C$_{triazine}$).

Elemental Analysis: C$_{22}$H$_{46}$O$_2$N$_6$

Mass spectrometry: 423 (M3+H$^+$)

4.4   **Synthesis from melamine**

5-aminopentanol (319 g, 3.1 mol) was poured into a 3-neck flask equipped with a mechanical stirrer, a cooler, a nitrogen gas inlet and a waste gas washer filled with sulphuric acid (w~30%.). At room temperature, ethylene glycol was added drop wise to the 5-aminopentanol (500 mL). When the reaction mixture was at 40°C, half of the initial quantity of melamine (190 g, 1.5 mol) was added slowly forming a white suspension. After 30 minutes, 75 mL of phosphoric acid (85 mL) was added drop wise to the reaction mixture. Release of NH_3 was observed (presence of salt formation in the gas washer). The suspension to turned a yellow colour. The temperature was not allowed to go above 180°C. After 10 hours the second half of the melamine (190 g, 1.5 mol) was added and stirred for another 6 hours. After the reaction mixture had cooled, the mixture was extracted with ethyl acetate and concentrated in *vacuo*.

^{13}C ([D$_6$] DMSO, 75 MHz) δ=36 (CH$_2$x2), 49 (CH$_2$-N and CH$_2$-O), 165-166 (C$_{triazine}$)

5. References

[1] Bann, B. and Miller, S. A. (1958). "Melamine And Derivatives Of Melamine." *Chem. Rev.* **58**(1): 131-172.

[2] Stoye, D., Freitag W., Beuschel, G., (1996). *Resins for coatings: chemistry, properties, and applications*, Hanser (pg 109).

[3] Liu, Q., Zhang, S., Wu, B., Guo, J., Xie, J., Gu, M., Zhao, Y., Yun, L., Liu, K., (2005). "Chiral Melamine Derivatives: Design, Synthesis, and Application to Mass Spectrometry-Based Chiral Analysis." *Anal.Chem.* **77**(16): 5302-5310.

[4] Roy, B., Saha, A., Nandi, A. K. (2011). "Melamine sensing through riboflavin stabilized gold nanoparticles." *Analyst* **136**(1): 67-70.

[5] Ariga, K. and Kunitake T. (2006). *Supramolecular chemistry: fundamentals and applications: advanced textbook,* Springer.

[6] Lehn, J.-M. (1988). "Supramolecular Chemistry—Scope and Perspectives Molecules, Supermolecules, and Molecular Devices (Nobel Lecture)." *Angew*. *Chem*. *Int. Ed*. *(English)* **27**(1): 89-112.

[7] Steed, J. W. and Atwood, J. L. (2009). *Supramolecular chemistry,* Wiley.

[8] Emsley J. (1980). "Very strong hydrogen bonding." *Chem. Soc. Rev.* **9**(1): 91-124.

[9] Levitt, M. and Perutz, M. F. (1988). "Aromatic rings act as hydrogen bond acceptors."
J. Mol. Biol. **201**(4): 751-754.

[10] Hunter, C. A., Lawson, K. R., Perkins, J., Urch, C. J. (2001). "Aromatic interactions."   *J.
Chem. Soc. Perkin Trans. 2*(5): 651-669.

[11] Shao, X.-B., Jiang, X.-K., Zhu, S-Z., Li, Z-T. (2004). "Strapped porphyrin rosettes based
on the melamine-cyanuric acid motif. Self-assembly and supramolecular recognition."
Tetrahedron **60**(41): 9155-9162.

[12] Cao, Y. W., Chai, X. D., Chen, S. G., Jiang, Y. S., Yang, W. S., Lu, R., Ren, Y. Z.,
Blanchard-Desce, M., Li, T. J., Lehn, J. M. (1995). "A new series of nonlinear optical organic
materials with molecular receptor: design and synthesis." *Syn. Metals* **71**(1-3): 1733-1734

[13] Yang, W. S., Chen, S. G., Chai, X. D., Cao, Y. W., Lu, R., Chai, W. P., Jiang, Y. S., Li, T. J.,
Lehn, J. M. (1995). "Formation of Mesophase by Hydrogen-Bond Directed Self-Assembly
between Barbituric-Acid and Melamine Derivatives." *Syn. Metals* **71**(1-3): 2107-2108.

[14] Russell, K. C., Lehn, J. M., Kyritsakas, N., DeCian, A., Fischer, J. (1998). "Self-assembly
of hydrogen-bonded supramolecular strands from complementary melamine and
barbiturate components with chiral selection." *NJC* **22**(2): 123-128.

[15] Arduini, M., Crego-Calama, M., Timmerman, P., Reinhoudt, D. N. (2003). "Novel type of hydrogen-bonded assemblies based on the melamine-cyanuric acid motif." *J. Org. Chem.* **68**(3): 1097-1106.

[16] Mathias, J. P., Simanek, E. E., Zerkowski, J. A., Seto, C. T., Whitesides, G. M. (1994). "Structural Preferences of Hydrogen-Bonded Networks in Organic Solution - the Cyclic CA3.M3 "Rosette". *J. Am. Chem. Soc.* **116**(10): 4316-4325.

[17] Seto, C. T. and Whitesides G. M. (1990). "Self-assembly based on the cyanuric acid-melamine lattice." *J. Am. Chem. Soc.* **112**(17): 6409-6411.

[18] Mathias, J. P., Simanek , E. E., Whitesides, G. M. (1994). "Self-Assembly through Hydrogen Bonding: Peripheral Crowding - A New Strategy for the Preparation of Stable Supramolecular Aggregates Based on Parallel, Connected CA3.M3 Rosettes." *J. Am. Chem. Soc.* **116**(10): 4326-4340.

[19] Zerkowski, J. A., MacDonald, J. C., Seto, C. T., Wierda, D. A., Whitesides, G. M. (1994). "Design of Organic Structures in the Solid State: Molecular Tapes Based on the Network of Hydrogen Bonds Present in the Cyanuric Acid. Melamine Complex." *J. Am. Chem. Soc.* **116**(6): 2382-2391.

[20] Li, X., Chin, D. N., Whitesides, G. M. (1996). "Synthesis and Evaluation of Thioether-Based Tris-Melamines as Components of Self-Assembled Aggregates Based on the CA·M Lattice." *J.Org. Chem* **61**(5): 1779-1786.

[21] Arrachart, G., Carcel, C., Trens, P., Moreau, J. J. E., Man, M. W. C. (2009). "Silylated Melamine and Cyanuric Acid as Precursors for Imprinted and Hybrid Silica Materials with Molecular Recognition Properties." *Chem.–Eur. J.* **15**(25): 6279-6288.

[22] Ariga, K. and Kunitake, T. (1998). "Molecular Recognition at Air-Water and Related Interfaces: Complementary Hydrogen Bonding and Multisite Interaction." *Acc. Chem. Res.* **31**(6): 371-378.

[23] Kimizuka, N., Kawasaki, T., Hirata, K., Kunitake, T. (1998). "Supramolecular membranes. Spontaneous assembly of aqueous bilayer membrane *via* formation of hydrogen bonded pairs of melamine and cyanuric acid derivatives. *J. Am. Chem. Soc.* **120**(17): 4094-4104.

[24] Kawasaki, T., Tokuhiro, M., Kimizuka, N., Kunitake, T. (2001). "Hierarchical self-assembly of chiral complementary hydrogen-bond networks in water: Reconstitution of supramolecular membranes." *J. Am. Chem. Soc.* **123**(28): 6792-6800.

[25] Steffensen, M. B., Hollink, E., Kuschel, F., Bauer, M., Simanek, E.E . (2006). "Dendrimers based on [1,3,5]-triazines." *J. Polym. Sci. A Polym. Chem.* **44**(11): 3411-3433.

[26] Zhang, W. and. Simanek , E. E (2000). "Dendrimers Based on Melamine. Divergent and Orthogonal, Convergent Syntheses of a G3 Dendrimer." *Org. Lett.* **2**(6): 843-845.

[27] Bosman, A. W., Janssen, H. M., Meijer, E. W. (1999). "About Dendrimers: Structure, Physical Properties, and Applications." *Chem. Rev.* **99**(7): 1665-1688.

[28] Zimmerman, S. C., Zeng, F., Reichert, D.E.C., Kolotuchin, S. V. (1996). "Self-Assembling Dendrimers." *Science* **271**(5252): 1095-1098.

[29] Blotny, G. (2006). "Recent applications of 2,4,6-trichloro-1,3,5-triazine and its derivatives in organic synthesis." *Tetrahedron* **62**(41): 9507-9522.

[30] Montalbetti, C., Coulter, T. S., Uddin, M. K., Reigniera, S. G., Magaraci, F., Granas, C., Krog-Jensen, C., Felding, J. (2006). "Synthetic strategies to prepare 2-alkyl, 2-aryl and 2-acetylenyl substituted 4,6-diamino-1,3,5-triazines." *Tet. Lett*. **47**(33): 5973-5975.

[31] Menicagli, R., Samaritani, S., Gori, S. (1999). "2-(alk-1 '-ynyl)-4,6-dimethoxy-1,3,5-triazines *via* Pd-mediated alkynylation of 2-chloro-4,6-dimethoxy-1,3,5-triazine." *Tet. Lett*. **40**(48): 8419-8422.

[32] Thalacker, C. and Würthner, F. (2002). "Chiral Perylene Bisimide–Melamine Assemblies: Hydrogen Bond-Directed Growth of Helically Stacked Dyes with Chiroptical Properties." *Adv. Funct. Mater.* **12**(3): 209-218.

[33] Thalacker, C., Miura, A., De Feyter, S., De Schryver, F. C., Wurthner, F. (2005). "Hydrogen bond directed self-assembly of core-substituted naphthalene bisimides with melamines in solution and at the graphite interface." *Org. Biomol. Chem*. **3**(3): 414-422.

[34] Wurthner, F. and Yao, S. (2003). "Merocyanine dyes containing imide functional groups: Synthesis and studies on hydrogen bonding to melamine receptors." *J. Org. Chem.* **68**(23): 8943-8949.

[35] Mahler, J. and Rafler, G. (1999). "Modified melamine resins for optical applications." *Opt. Mater.* **12**(2-3): 363-368.

CHAPTER 2:
Synthesis of Novel Porous Melamine-Formaldehyde Materials

Contents

1. Introduction

1.1.   Porous materials

Porous materials are a well-investigated field in scientific research,[1] as they have applications in many areas of chemistry,[2,3] physics[4,5] and biology[6,7,8]. Introducing porosity into a material changes or brings new properties such as low density, low thermal conductivity, high optical translucency and high permeability which have important applications in thermal and electrical insulation for example. Plus, pores within "nanoporous" type materials can also allow for the hosting of guest species by size and shape selectivity,[9] which can prove to be very useful for chemical separations *e.g.* membranes, catalysts and chemical sensors.[10]

Synthesis of porous materials varies greatly depending on the pore sizes required. These different synthesis strategies are depicted in Figure 2.1. IUPAC determined a nomenclature (based on nitrogen sorption isotherms) for porous materials such that materials with pores below 2 nm are termed microporous, materials with pores between 2-50 nm are termed mesoporous and materials with larger pores than 50 nm are termed macroporous.[11]
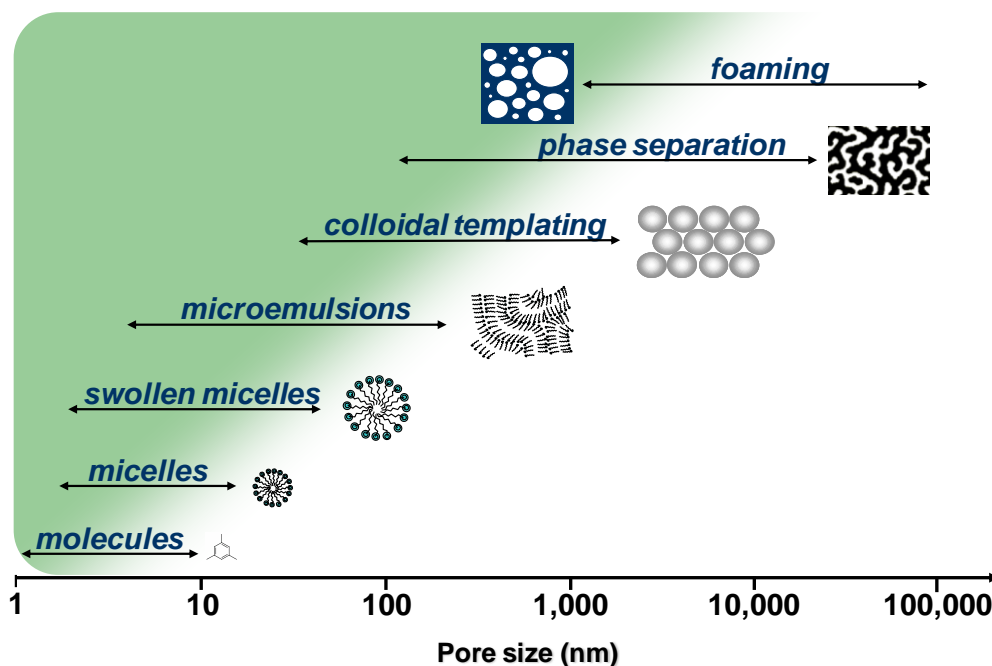
Figure 2.1: Schematic representation of the different techniques employable to tune the size of pores within materials. Templating methods tend to be used for pores sizes on the lower end of the scale (below 1000nm). Pores of 1000 nm and above tend to be synthesised by biphasic systems such as phase separation processes and foaming techniques.

Microporous materials, usually crystalline structured, are essentially designed by the regular assemblies of molecular units.[12] Materials in the mesporous range are designed by using templating methods,[13] such as mesophase imprinting as shown in Figure 2.2, whereby the pores are generated when polymerisation "locks" the template in place and then the latter is removed. Evidently, the size of the pore is determined by the size of the template and this approach can even be extended to form macroporous materials.[14]
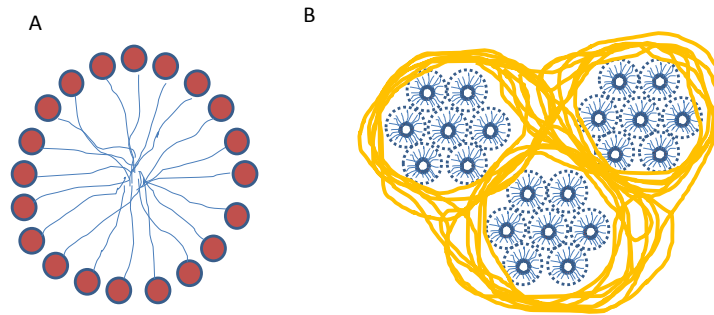
Figure 2.2: (A) Micelle formation of surfactants.[15] Surfactants are schematised above with hydrophilic head (red) and lipophilic tail. Therefore in a polar solvent, surfactants tend to assemble as micelles. (B): Formation of mesoporous materials by surfactant templating: A continuous network is formed around micellar arrangements of surfactants therefore locking them in place. Upon removal of the latter, uniform pores are left behind.

Templating methods are often referred to as the "bottom-up" approach by which pores formed in macroscopic objects are constructed from the molecular level upwards. It offers more versatility in tailoring pore structures especially in the case of hosting guest species. The cavities are generated by a template, therefore offering endless possibilities in shape, size and chemical properties, so long as the matrix "locking" the template is compatible with the latter, and its removal does not cause any damage.

However, an alternative technique is to incorporate gas into a liquid medium and then subsequently set the liquid to keep the structure of the gas bubbles. This is called direct foaming,[16] as shown in Figure 2.1. It is an example of the "top-down" approach, whereby pores are introduced into a pre-formed material. Lithography is another common technique for producing pores in an existing bulk materials and the principle of this is

displayed in Figure 2.3. This top-down approach offers arbitrary geometrical designs and increasing precision at the nanometer-level.
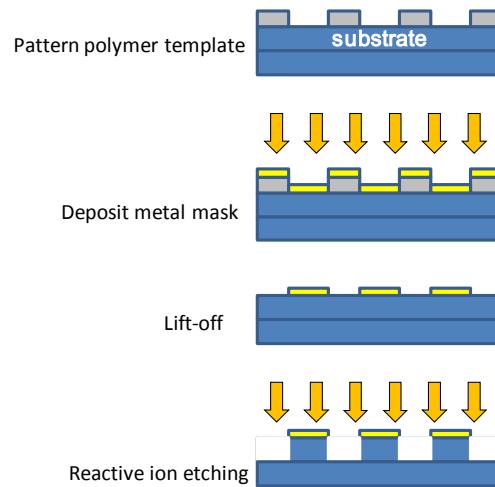
Figure 2.3: Lithography lift-off technique[17]: A photo-resist pattern layer is placed onto the surface of a polymer. The surface is illuminated with UV light. The pattern is then removed and the unexposed parts selectively etched to leave behind pores.

Additionally, there exist systems for which the growing (polymeric) network is intertwined with its original solvent so that a true three dimensional biphasic medium results. Such systems originate from the sol-gel process and can lead to porous frameworks if the solvent is removed successfully without altering the newly formed material.

1.2   Sol-gel chemistry as a means to create porous materials

Sol-gel chemistry started in the mid 19th century, with the fabrication of ceramics at lower temperatures than that of conventional solid-state processes[18]. Since then, the process has been improved, diversified and extended to the production of a wide range of materials, including aerogels (a class of highly porous materials with low densities and high surface areas)[19,20,21]. It involves the assembly, at ambient temperatures, of precursors in a solution which eventually form a solid network. The sol-gel process is schematically represented in Figure 2.4.

Firstly, chemical precursors are dissolved in a solvent. Upon addition of a catalyst, they begin to react on a nanometric scale producing what is called a "sol" (colloidal solution). This "sol" then undergoes a gelation step where further polycondensation of the precursors results in the formation of a biphasic system: a solid network which entraps the solvent phase. The control of pore sizes within this gel comes from a delicate balance between thermodynamics and kinetics of the reaction mixture in the gelation step[22].

Porous materials are thus truly formed once removal of the solvent from the wet gel occurs. This final process, in order to successfully leave pores intact, requires treatment in specific conditions (*e.g.* supercritical drying). If, however, the material is dried in ambient conditions, the pores tend to collapse and the material shrinks into a dense material known as a xerogel (Figure 2.4).
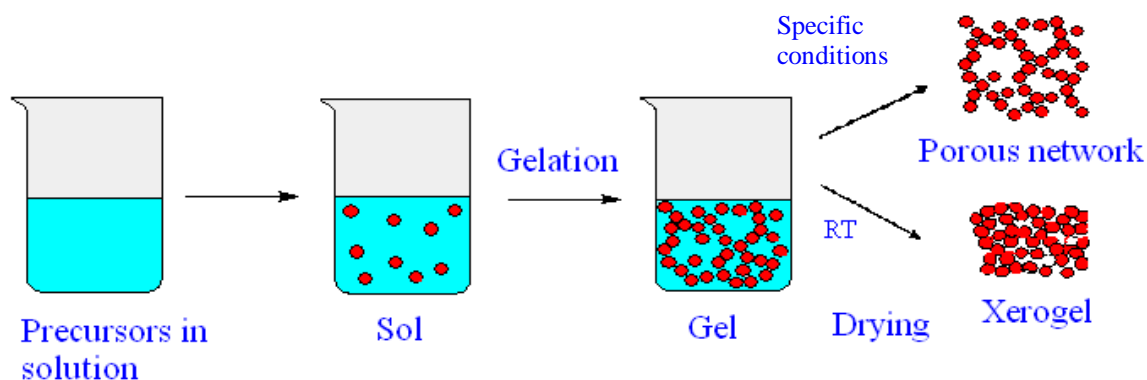
Figure 2.4: Scheme illustrating the principal steps of sol-gel chemistry to form porous materials emphasising the importance of the drying process[23].

The sol-gel process is very versatile and therefore capable of producing a wide range of materials, depending on the nature, for instance, of the precursors used (metal oxides for catalysts,[24] silicates for thermal applications,[25] *etc.*). Furthermore, the slow evolution of sol to gel facilitates the shaping and moulding of the final material for specific applications (fibres, films and monoliths)[26]. Also, it allows the incorporation of additional compounds that would modify the final properties of the material: for instance, dyes that change the final colour, or metal salts for use as catalysts, biomolecules for medical applications or fillers which have an impact on the elasticity, strength and textures of the material.[27,28,29] To date, sol-gel processing has been reported for producing new materials in catalysis,[18] chemical and biochemical sensors,[30] membranes,[31] fibres,[21] optical media,[32] electrochemical devices,[33] HPLC stationary phases[34,35,36] and in many engineering industries such as ceramics, nuclear and electronic industries.[19]

1.2.1 The drying process

Generating solvent cavities of given size and connectivity within sol-gel materials is not always easy to control synthetically and requires careful control over the nature and amounts of precursors, reaction solvents and catalysts during gel synthesis. As mentioned previously, pores are essentially generated within gels, once the solvent is removed. The majority of the overall volume in these gels is occupied by the liquid phase and its removal has important consequences on the network sustainability. The solvent, initially inundating the pores, when exposed to air starts evaporating and consequently forming menisci inside the pores at the liquid-vapor interface, as depicted in Figure 2.5. These menisci indicate that the evaporating solvent is creating pressure on the pore walls. This pressure can eventually lead to the collapse of the whole porous structure.
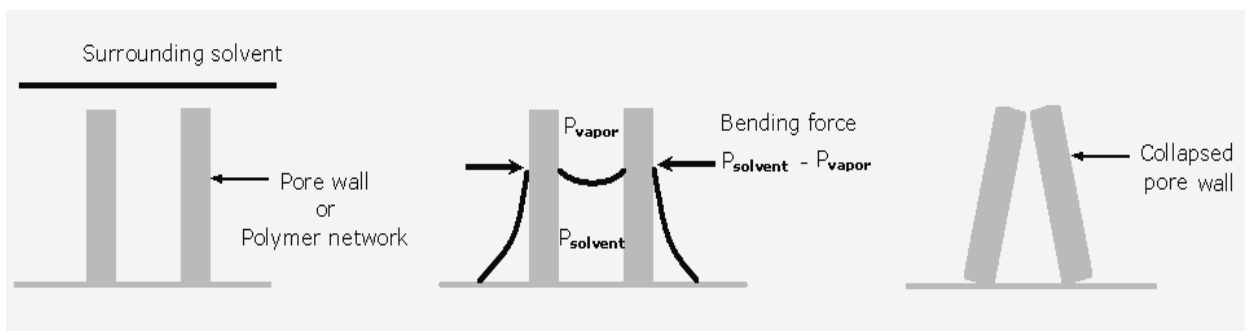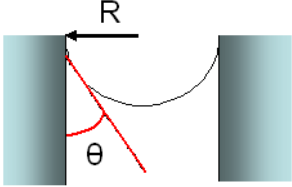
Figure 2.5: Capillary pressures leading to pore destruction. Vapour and liquid pressures caused by the surface tension of the evaporating solvent, exerts pressure on the pore walls. This pressure can gravely affect pore retention as it eventually leads to it collapsing.[37]

If the pore is modeled as an ideal cylinder, the meniscus formed inside it is a hemisphere. It is the curvature that indicates that there is a certain affinity between the

pore walls and the solvent. This is strongly influenced by the surface tension and polarity of the liquid in that particular environment. It creates what is referred to as capillary pressures, *i.e.* pressure created by a solvent in a capillary structure. This pressure follows the Young-Laplace equation: [38]

$$P_C = \frac{2\gamma \cos \theta}{R}$$

- P_c: capillary pressure (Pa)
- γ: surface tension of solvent in pore (Nm^{-1})
  - (γ_{water}=0.073 Nm^{-1})
  - ($\gamma_{ethanol}$=0.022 Nm^{-1})
  - ($\gamma_{pentane}$=0.015 Nm^{-1})
- θ: wetting angle (rad)
- R: radius of capillary (m)

Figure 2.6: Young-Laplace equation used to model the pressure exerted by the solvent in a cylindrical pore. The equation proves that the pressure exerted is directly proportional to the surface tension of a solvent and the contact angle it creates with the pore walls, but is inversely proportional to the radius of the pore.

The magnitude of affinity for a specific surface by a solvent is given by the contact angle θ, which is the wetting angle of a specific liquid on a specific surface (see Figure 2.6). If the affinity is very strong, the wetting is very good, and most of the meniscus is in contact with the surface (θ close to 0°). On the contrary, if the wetting is poor (*e.g.* water in Teflon), the contact between the meniscus and the pore wall is minimal ($\theta \geq$ than 90°), as illustrated in Figure 2.7.

good wetting
$0 < \cos\theta < 1$
$P \rightarrow P_{max}$

bad wetting
$-1 < \cos\theta \leq 0$
$P \rightarrow P_{min}$
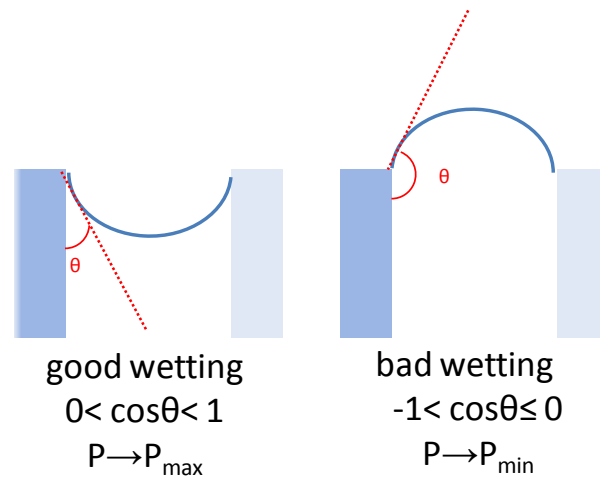
Figure 2.7: Different types of contact angles that various solvents can form with a given surface. Solvents with a high affinity for the pore network display good wetting whereas solvents with a low affinity display bad wetting.

One drying process which was successfully used to create aerogels is supercritical drying, by which the solvent (typically CO_2) is used under supercritical conditions of temperature and pressure and no longer truly behaves as a liquid. Therefore it has no surface tension and no wetting properties and upon removal, it causes minimal damage to the pore structure. However this method is technically demanding and cannot be applied routinely to the drying of all porous materials.

According to the Young-Laplace equation (in Figure 2.6), methods to reduce the capillary pressures generated in liquid-air systems upon solvent removal are either to (i) minimise the surface tension of solvents or (ii) tune the pore on the larger scale so as to help minimise the magnitude of the capillary pressures during the drying process.[39, 40]

Creating pores of large diameters can however hinder the intention of producing porous materials with high surface areas. Varying the solvent can also be difficult to control since the precursors have to initially be soluble in the solvent for the sol-gel process to start, thus limiting the choice. A means to overcome this is to progressively displace the solvent (often water) from wet gels for less hydrophilic solvents such as ethanol or pentane (referred to as solvent exchange).[41] Alternatively, the surface of the pores can be chemically modified so as to switch the overall polarity of the walls and decrease the solvent-network affinity (favouring non-wetting) so that the solvent can be removed without causing too much destruction to the pores. This method is referred to as post-treatment. Figure 2.8 shows how this method can help to enhance pore retention in bulk materials.
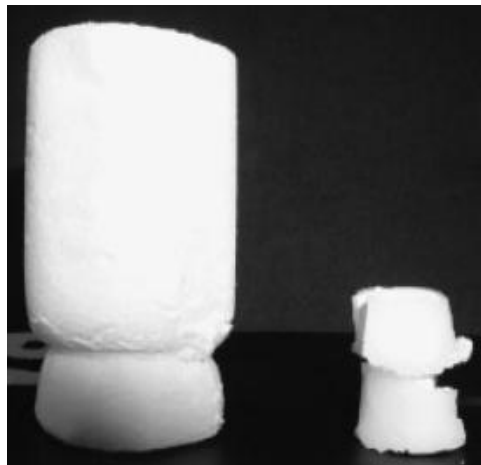
Figure 2.8: Enhanced pore retention with the post-treatment method. The sample on the left is the result of a gel which has been post treated prior to drying whereas the sample on the right is the same gel with no post treatment applied, dried at ambient temperature.[42]

Organic precursors can make organic polymers relying on the strong C-C covalent bonds, which are much stronger than the Si-Si bonds in silica aerogels.[21] Researchers have reported producing such materials from organic precursors, such as urea-formaldehyde,[43] resorcinol-formaldehyde[44,45] and melamine-formaldehyde.[46,47] Melamine-formaldehyde as a precursor presents interesting features such as a high variability of cross-linking and outstanding chemical and thermal resistances for the resulting materials.[51]

1.2.2   Melamine-formaldehyde chemistry

Melamine-formaldehyde (MF) resin solutions have been used as industrial adhesives and coatings for over a large part of the last century.[48,49,50] They are impressively cheap resins and consequently have a number of everyday applications such as paper laminates, wood agglomerates, decorative laminates or as moulding compounds in dinnerware.

Generally, to manufacture the materials described above, MF resins are produced with a high solid content in water as the reaction medium. Melamine-formaldehyde aerogels, on the other hand, are produced when the resin solid content in water is kept at 10-30% and the solvent plays the role of the porogen. The resin formation takes place by the addition of formaldehyde onto the amino positions on melamine in acidic or basic conditions forming hydroxymethylated (methylol) melamines.[51,52] These species are commonly called MF resins and the addition of formaldehyde is known as methylolation (see Scheme 2.2, first step).

Studies have shown that a mixture of compounds is formed at this stage, varying from one methylol group up to six, since there are six N-H bonds (by IR[53]and Raman Spectroscopy,[54] LC/MS[55,56] and ^{1}H and ^{13}C NMR[57,58]). During the synthesis of MF resins, the addition of formaldehyde is reversible and eventually leads to an equilibrium which is influenced by the molar ratio of melamine to formaldehyde (M:F), so if the M:F is 1:6 then the formation of hexamethylol (fully substituted) melamines is favoured. As a total of six substitutions is potentially possible on the melamine ring, this can lead to up to 9 possible species co-existing, which are only sparingly soluble in water. Moreover, the basicity of the resin precursor decreases with increased substitutions. This is because the addition of the oxygen atom lowers the electron density of the triazine ring thus explaining why the pKa of melamine is 5,[59] whereas hexamethylol melamine is a hundred times more acidic[60] (pKa=3).
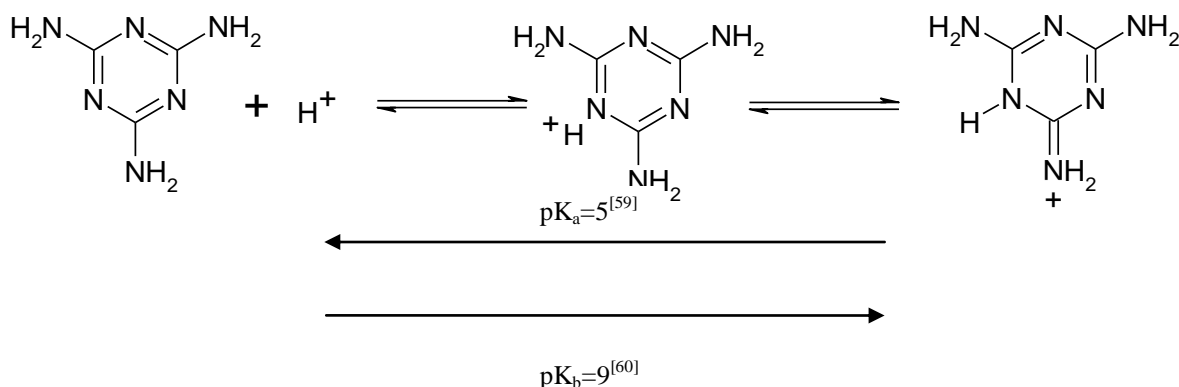
Scheme 2.1: The reaction equilibrium and species present upon acidification/basification of melamine.[64]

Highly methylolated resins tend to react further by self-condensation (the precursors react with each other to form larger aggregates and eventually precipitate out of

solution). In order to prevent this and to be able to enhance the storage of resins for later use, alcohols can be added in this step to alkylate resins (transetherification). All commercial resins are transetherified.

Subsequently if transetherification is not carried out and the reaction is "one-pot", these methylol species that are in aqueous solution, condense upon acidification to form two types of bridges, as shown in the second step of Scheme 2.2. This eventually results in a fully cross-linked MF network.
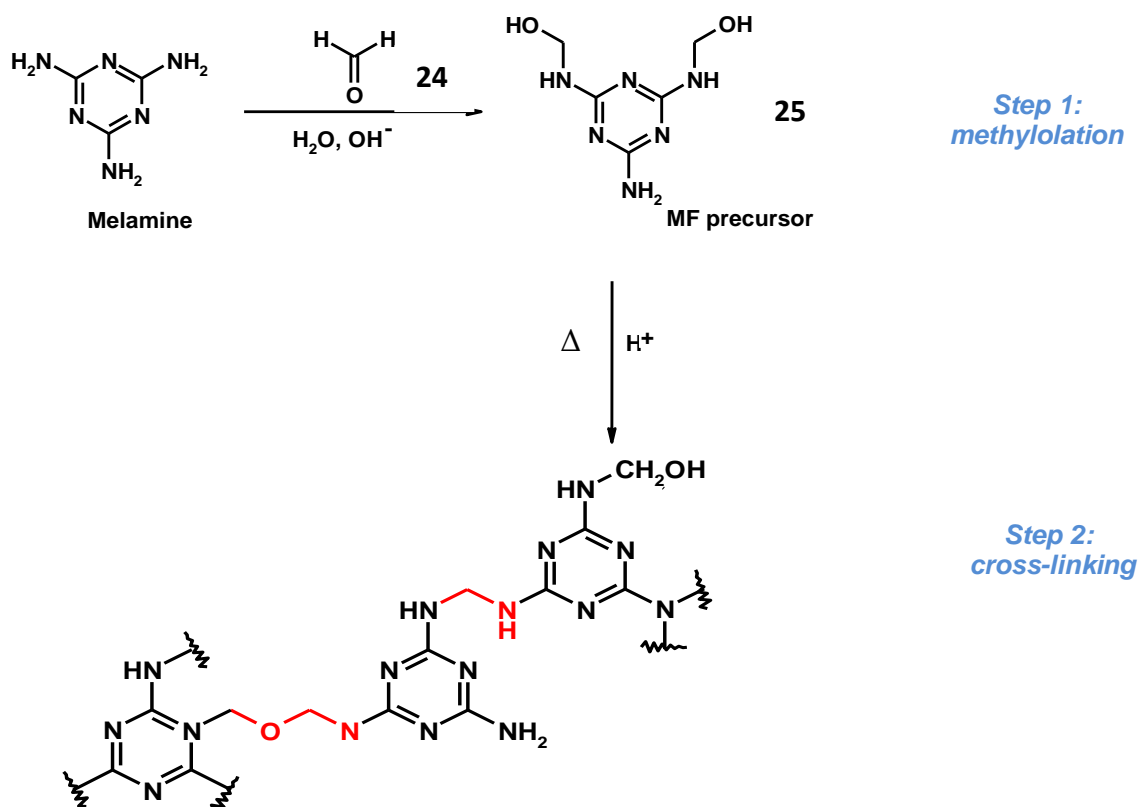
Scheme 2.2: Reaction scheme for synthesising melamine-formaldehyde networks. The first step, referred to as methylolation, involves the addition of formaldehyde onto melamine to produce MF precursors. The second step is when the precursors are cross-linked upon addition of an acid catalyst. In this step two types of bridging can occur: methylene (N-C-N) and methylene ether (O-C-N) bridges.[39]

The condensation can occur in two ways (Scheme 2.3): firstly the methylol group reacts with unreacted amine, to give the methylene bridge ($-CH_2-$) with the loss of a molecule of water; secondly, it is possible for two methylol groups to condense with each other to give an ether bridge ($-CH_2-O-CH_2-$) with the loss water. There is also the possibility of converting the ether bridge to a methylene bridge with the loss of formaldehyde by heating the network. This is of importance to industries, as formaldehyde is a suspected carcinogen and this curing step allows for zero formaldehyde emission[61].
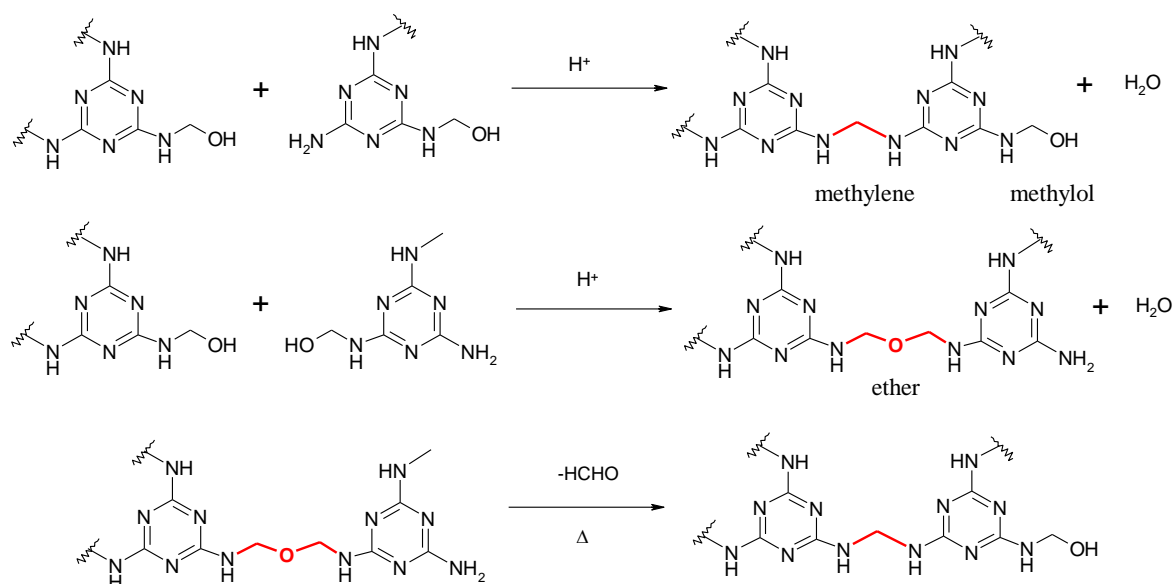
Scheme 2.3: The different types of bridging possible between melamine-formaldehyde species. Firstly the methylol group of one precursor can react with the free amine of another precursor to form methylene bridging. Alternatively, two methylol groups can react to form methylene ether bridging. Methylene ether bridges can however transform into a methylene bridges upon heating, with release of formaldehyde.

The majority of the previous work reported on MF has been with strong acids (generally HCl or H_3PO_4) but Blank mentioned that strong acids tend to be more effective with fully alkylated MF resins whereas weak acids are more suitable for amine rich melamines (resins which are non or partially alcoholated)[62]. The polymerisation with weak acids undergoes general acid catalysis, depicted in Scheme 2.4, as opposed to specific acid catalysis (Scheme 2.5, for strong acids) and both methods have different ways of stabilising the intermediate MF species.
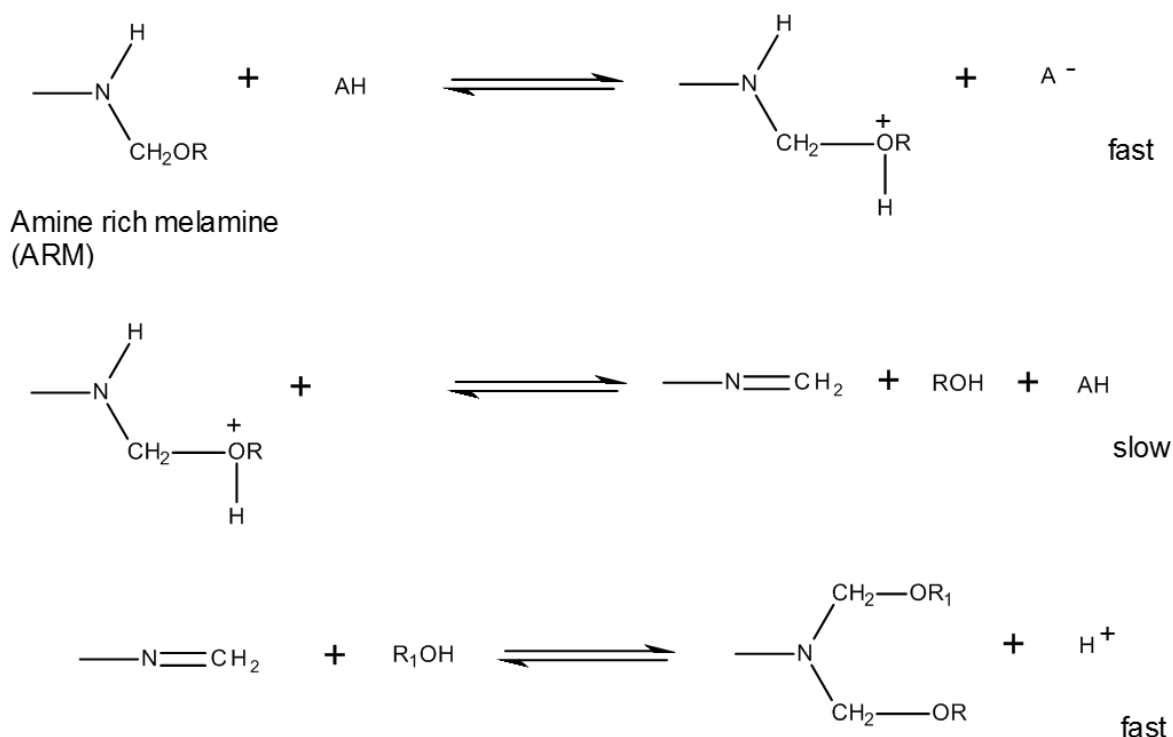
Scheme 2.4: Amine rich melamine resins are catalysed by general acid catalysis (with weak acids).[63] This leads to the stabilisation of intermediate species with the counterion (slow).

Fully alkylated melamine (ARM)
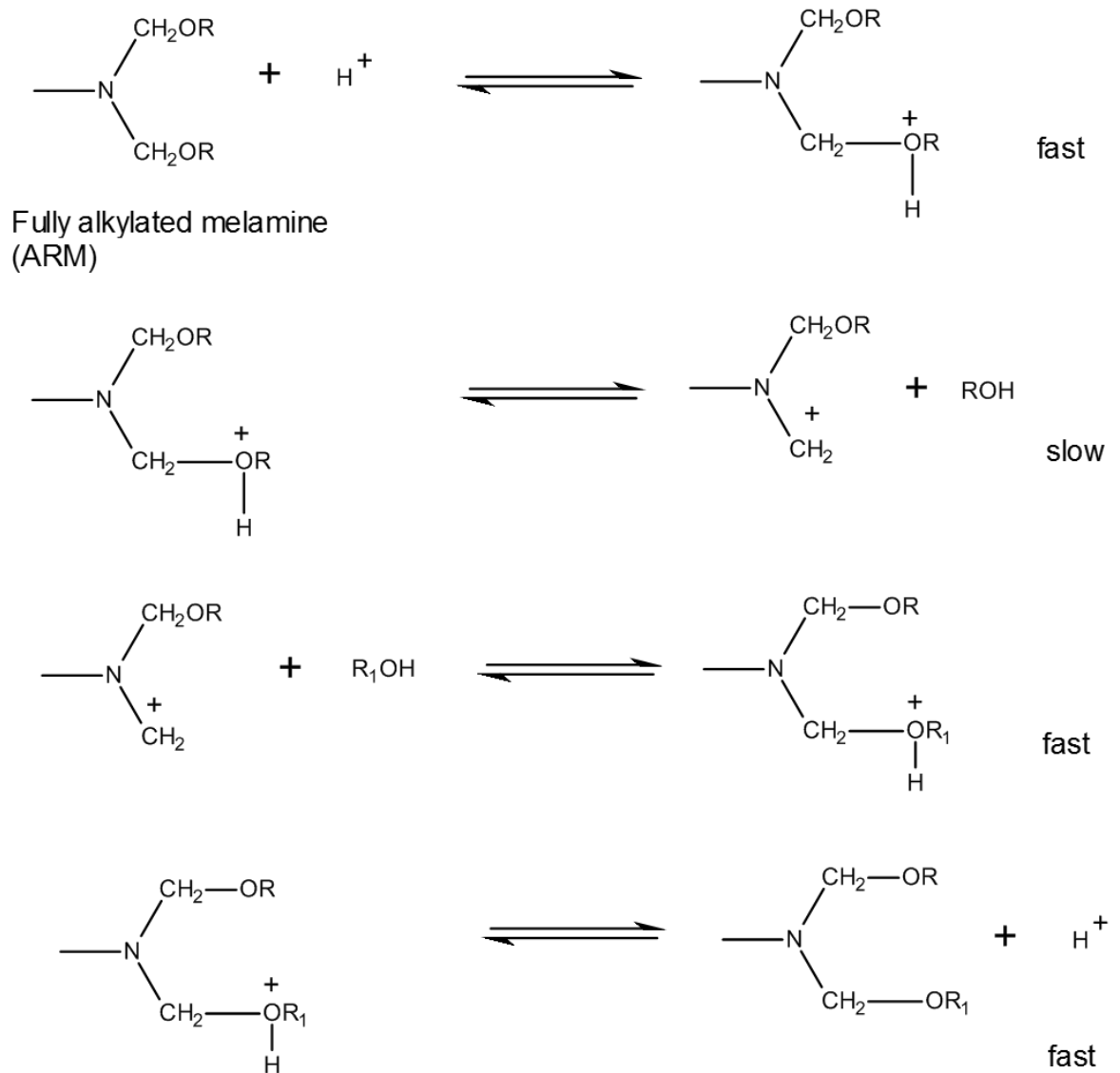
Scheme 2.5: Fully alkylated melamine resins are catalysed by specific acid catalysis (with strong acids).[63] This leads to the formation of a carbocation (slow) which is stabilised by the neighbouring nitrogen.

Strong acids are less effective at promoting cross-linking because they can also protonate the triazine ring and not the hydroxyl groups (which is where cross-linking occurs) thus neutralising portions of the catalyst.[64] It has also been reported that formic

acid (a weak acid, pK_A=3.75[65]) tends to produce MF aerogel type materials with higher porosities and surface areas than the materials produced from gels catalysed by H_2SO_4, with given MF resins.[66]

The interesting feature of MF materials is the chemical diversity present in the material. Functional groups such as hydroxyl, amino, ether and alkyl groups are scattered within the matrix. The concentration of these functional groups in MF gels is strongly influenced by the formaldehyde content, (more methylene ether bridges are present in gels with higher formaldehyde content), the amount of acid catalyst (less free amino groups) and the amount of resins present in solution (the solid content).[42, 66]

The presence of hydroxyl and primary amine groups allows for further reactions of etherification and amination (post-treatment) which, as a result, decreases the hydrophilicity within the network and favours pore retention as described previously. Within MF gels, etherification occurs with the addition of alcohols and amination can occur between aldehydes and the free primary amine groups within the matrix. Using commercially available dialdehydes may also bridge pore walls together to potentially make the pores more robust to capillary pressures. Figure 2.9 better illustrates the post-treatment strategies described here for MF matrices.
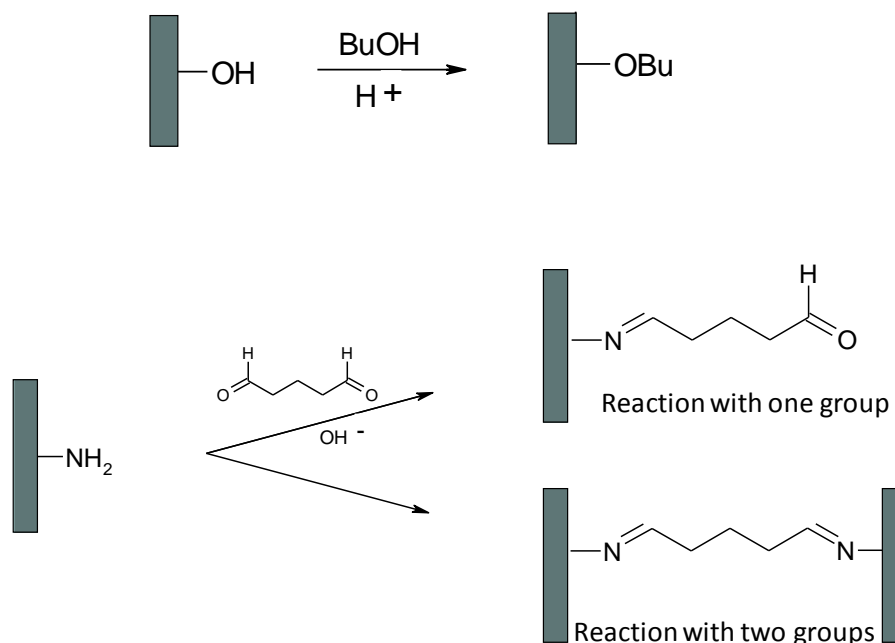
Figure 2.9: Chemical reactions that occur with alcohol and aldehyde post-treatments.

Top: post-treatment with butanol to modify hydroxyl groups into butoxy functions.

Bottom: post treatment with glutaraldehyde to transform free amino groups into imine

type functions and also to potentially bridge pore walls together to make the pores more

robust.

One aim in this work is to enhance and extend functionality in MF materials by

incorporating different melamine-based monomers (slightly less polar than melamine),

notably those synthesised in Chapter 1. Therefore the introduction of these new

functionalities may also enhance the porosity retention by decreasing the overall network

polarity.

Although the retention of porosity can be estimated for samples (if the density of

the samples is calculated, it can be compared to the density of a non-porous sample),

more accurate measurements are required to quantify pore sizes and surface areas. However, structural characterisation of porous networks can be challenging. The specific case of characterising porous MF is described next.

1.3   Characterisation of porous melamine-formaldehyde materials

The main techniques for characterising porous MF materials are (i) nitrogen sorption (for the surface area of materials), (ii) mercury porosimetry (to quantify the pore size distribution) and (iii) Scanning Electron Microscopy, SEM (to probe the material textures).

a) Nitrogen sorption

Goworek *et al.*[67] carried out adsorption measurements on porous MF materials. Their adsorption/desorption isotherms seem to be of type IV (see appendix, page xiv) and give a BET surface area of around 200 m^2g^{-1}, as shown in Figure 2.10. Similarly, Baraka *et al*[68] also carried out BET characterisation on MF resins (although these contained other chelating functional groups). They described the shape of the isotherms, which were also of type IV, as resulting from materials with open pores arising mainly from non-crystalline intra-aggregation. Both groups concluded that their materials can be classified as mesoporous. It is important to note here though that, for both cases, the synthesis conditions are different to the ones used in this work.

.

The isotherm for the MF material produced by Goworek *et al.* showed that although there is some form of levelling off that occurs at relative pressures of $p_0/p=1$ (the maximum relative pressure obtained by this technique), it is difficult to say if all the pores within the sample are entirely filled. Nitrogen sorption therefore has limitations in fully characterising materials in the mesoporous-macroporous range and alternative techniques are require to determine pore sizes in this region. The plateau formed at low relative pressure (*e.g.* in the $p_0/p=0.1-0.8$ region) is where the BET surface area is calculated, and the lower the gradient of this slope the more accurate the value of this surface area obtained.

b) Mercury intrusion measurements

Egger *et al.*[69] used mercury porosimetry to define the pore size distribution in given MF porous materials, synthesised *via* a bicontinuous micro-emulsion templating strategy. This technique enabled the group to see that their materials had a bimodal pores size distribution and that a well defined pore size distribution was achieved within a certain range, as shown in Figure 2.10.
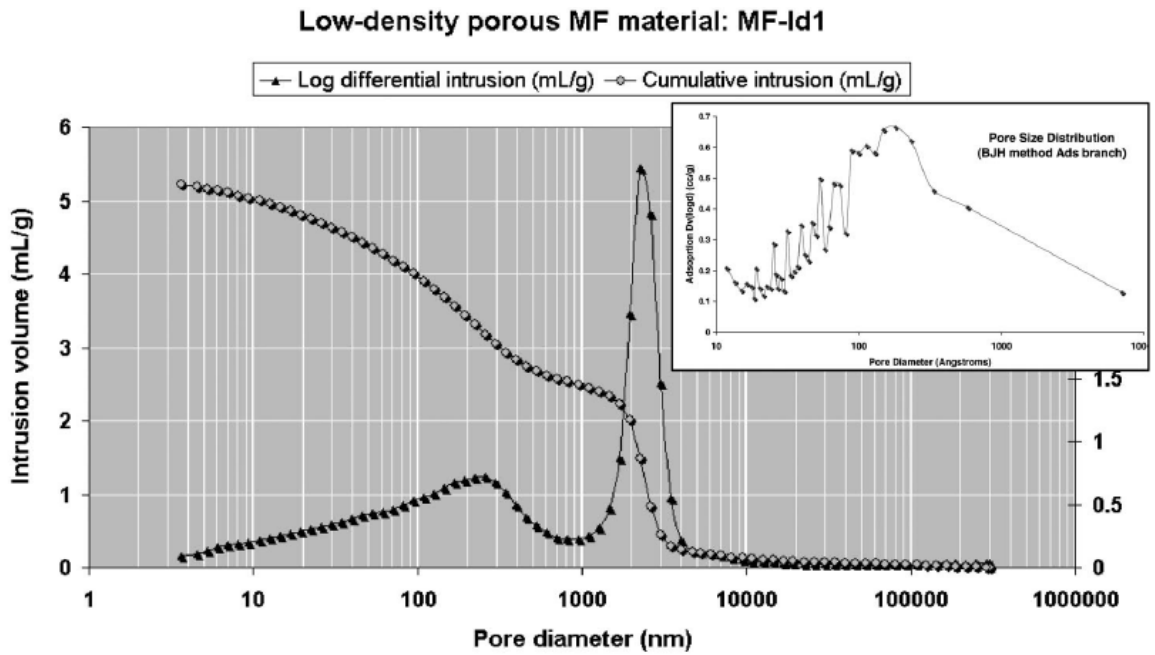
Figure 2.10: The mercury intrusion plot of a porous MF material obtained by Egger *et al.*[69] shows that the materials studied have a bimodal pore size distribution (reading from right to left). The intrusion measurements show a narrow pore size distribution from 1000-5000 nm. After this however, when higher pressures are applied to the material, the second rather broad pore size distribution from 5 nm to 1000 nm suggests that the sample was damaged by crushing of material upon mercury loading.

On the other hand, when high pressures are applied to intrude mercury into the narrower pore ranges, the sample is crushed and this can lead to a very broad pore size distribution, lacking in precision. Mercury intrusion therefore has limitations for very narrow pores and alternative techniques need to be used such as x-ray scattering.

c) SEM imaging

In the paper by Egger *et al.*[69] quoted above for the mercury data, the group related their findings to electron micrographs of material samples to visualise the structure of their bimodal systems. They found that their material, when cross-linked with a strong acid H_2SO_4, produced threadlike materials. Although these materials had high pore volumes, the BET surface area was very low.

Intrusion Volume mL/g	1.6
Surface Area m²/g	1.4
Porosity %volume	73
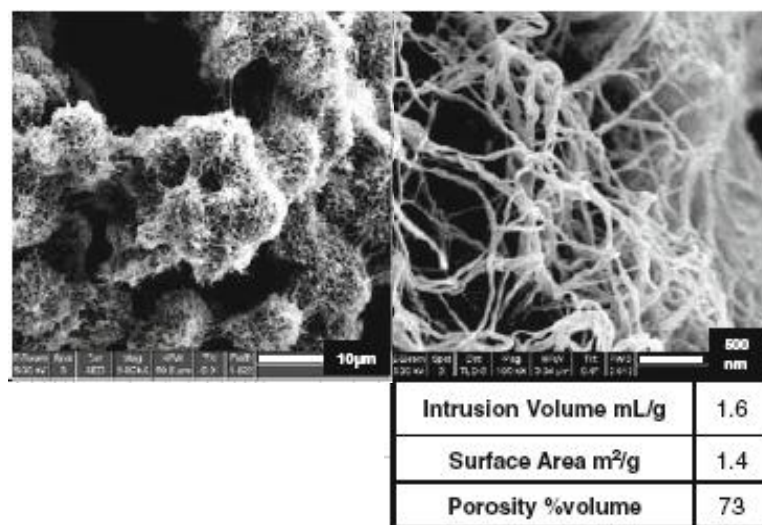
Figure 2.11: Scanning electron micrographs of a material synthesised with aqueous MF cross-linked with H_2SO_4. The SEM reveals that the material is very fibre like explaining why it has a good porous volume but a low surface area.[69]

Du Fresne von Hohenesche *et al.*[70] incorporated commercially available melamine type derivatives into similar materials as those produced above by Egger *et al.* (by micro-emulsion templating). The SEM showed that the incorporation of caprinoguanamine (in 10% molar amounts) led to the pore walls having a significant amount of porosity, which pure MF materials did not display.

The limitation of this technique, however, is that it is not quantitative and that although very different pore size distributions may be accounted for, the technique only screens a small surface area, producing a 2D micrograph of a 3D network, which may not be statistically reliable. Also, a common problem with taking these micrographs is that they undergo the phenomenon of charging which prevents the emission of secondary electrons and therefore blurs the micrographs. Gold coating can help to form an even layer over the sample; however this modifies the pore size hence the micrographs produced distorted information on the latter.

d) Thermal Analysis

Although thermal analysis does not help characterise porosity in a material, it does provide useful information on the thermal stability of the skeletal network (especially since MF resins are well known for their thermal stability). Such measurements will probe the effect of the post-treatment of materials and/or the incorporation of different monomers on the thermal stability of MF networks.

Hong *et al.*[71] and Hwang *et al.*[72] characterised MF resin capsules and found that there was a great weight loss for MF at 420°C therefore leading to the conclusion that the melting point of the materials is in this region. Devallencourt *et al.*[73] also carried out the analysis of methylated MF resins with 20% solid content using TGA coupled to an FTIR source. They observed four successive mass losses on the thermogravimetric trace: one at 78°C corresponding to the evaporation of water, another at 185°C which, according to IR, was due to loss of methanol, formaldehyde and amines (due to the sublimation of melamine). At 407°C, more formaldehyde, methanol and amine were detected, as well as

CO_2 and NH_3 (indicating the materials had already started to combust). A different study shows that ammonia is eliminated at 440°C, thus indicating full thermal condensation of melamine[74].

2. Experimental

2.1   Synthesis of MF materials:

NaOH (0.4 g) was dissolved in water in a three-necked flask equipped with a hot-plate stirrer and thermometer. Melamine (0.4 mol, 20 g) and formaldehyde solution (37% w/w) (44 mL) ⌂were added to the base solution and instantaneously lowered into a pre-heated oil-bath set at 130°C. The temperature of the solution was checked regularly to make sure it did not rise too much above 80°C. The appearance of the mixture was also monitored which should go clear within 20 minutes. At the point where the solution goes clear, the mixture was reacted further for 10 minutes at 70°C. It was then cooled and filtered off to remove any remaining solid.

The weight percentage solid content was measured and recorded using Mettler LP16 moisture analyser at 120°C.

Approximately 20 g of the resin solution was then transferred to 30 mL plastic vials and formic acid (ranging from 1 g-3 g, according to the required MF/FA ratio) was added to each vial. The set of vials were placed in a hot water bath at 60°C for 2 hours. The vials were then left standing for a further 12 hours to allow the gels to fully set.

Each set gel was removed from the plastic vial and then divided into three equal parts. One part was left to dry at room temperature for 24 hours. The other one was put into ~30 mL (or until all of the gel was surrounded by solvent) of a 10% acidified (with HCl to pH 1) butanol-water solution and the final part was place into ~30 mL of a 10% basified (with NaOH to pH 9) glutaraldehyde-water solution. Each sample immersed in butanol

---

⌂For the 1:5 M:F resin solution, 0.4 mol of melamine and 145mL formalin solution were used

and glutaraldehyde solutions were placed in an oven at 70°C for 2 hours. They were then removed from the oven and left to cool to room temperature. Materials were then extracted from the solutions and left to dry at room temperature for 24 hours.

Estimation of Porosity

Measurements were taken (mass, diameter and height of sample) to obtain an estimated porosity based on geometrical considerations using the following calculation:

$$Total\ Volume\ (V_T) = Volume\ of\ pores\ (V_P) + Volume\ of\ material\ network\ (V_{MF})$$

$$Porosity = \frac{volume\ of\ pores}{total\ volume} = \frac{V_P}{V_T} = \frac{V_T - V_{MF}}{V_T}$$

$$\therefore as\ \rho\ (density) = \frac{mass}{volume} \qquad (samples\ were\ cylindrical\ \therefore V = \frac{\pi d^2}{4} l)$$
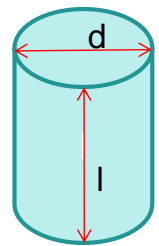
$$Porosity = \frac{\rho_{MF} - \rho_T}{\rho_{MF}} = 1 - \frac{\rho_T}{\rho_{MF}} \qquad \rho_{MF}\ (Porosity\ of\ dense\ MF) = 1.68 g/dm^3 \quad [70]$$

The error that can be expected on this calculation is ±10% due to errors associated with the balance and the measuring ruler.

2.2 Synthesis of materials containing different monomers

The same experimental procedure as above was applied to the samples containing different monomers. The monomers were mixed in with melamine in the resin process using the quantities indicated in the table below.

Table 2.1: Molar quantities of additional monomers incorporated into MF networks.

Resin	Moles of Melamine	Moles of Additional Monomer
Pure MF	0.40	-
MF with 10% aecetoguanamine	0.34	0.03
MF with 10% benzoguanamine	0.34	0.03
MF with 10% caprinoguanamine	0.33	0.03
MF with 20% acetoguanamine	0.31	0.06
MF with 10% monomer 1	0.34	0.03
MF with 10% monomer 2	0.34	0.03
MF containing amine 1 in resin synthesis	0.36	0.04

2.3   Instrumentation used for the characterisation work

a) Nitrogen Sorption

Nitrogen sorption measurements were carried out using a Quantachrome Autosorb 1. The adsorbate used was nitrogen, the vacuum pressure was 10^4-10^5 Torr, the equilibrium time was 1 minute and the tolerance was 3. The samples were cut into large chunks and placed into sample cells of 9 or 12 mm diameter. Prior to analysis, the samples were outgassed at 50°C for 12 hours. Porosity analysis comprises adsorption and desorption of nitrogen at 77K into the sample pores and the working range was p/p_0=0 to 1. The software used to view the isotherms produced was Autosorb version 1.50.

b) Mercury Porosimetry

Mercury Intrusion was carried out by BASF-SE. Approximately 200 mg of a bulk sample was necessary for each measurement. The instrumentation used was Autopore IV Micromeritics, Software-Version V1.09. The range of pore sizes checked was from 0.0037μm to 200μm.

c) Scanning Electron Microscopy

Fragments of the sample were carefully chipped off and mounted on a carbon pad stuck onto a 2.5 cm metal stub. This was then coated in gold using a gold sputterer: Emscope FD500, using argon, at 25 mA for 2.5 minutes. A coating of 10 nm thickness was estimated. The samples were then imaged using a Hitachi S4500 Field Emission Scanning

Electron Microscope (FE-SEM) with an electron beam of 3 eV or 5 eV (indicated with the micrograph).

d) Thermal Analysis

The instrument used for the TGA/DSC measurements is a simultaneous thermal analyser: STA1500. The samples were analysed with a nitrogen (carrier gas) flow and a heat rate of 20°C/min from room temperature to 800°C. A mass of 5-10 mg was placed as a crushed solid in a metal crucible so that there was good contact with the material and the bottom of the crucible. This was placed onto the balance with a reference crucible and lowered into the furnace prior to carrying out measurements. The software used was Infinity Pro Version V.4.2.140.

3. Results and discussion

3.1 Effect of the synthesis parameters on calculated porosity

In order to optimise the porosity and surface area within MF based materials, the parameters that were varied were (i) the amount of formic acid (ii) the type of drying methods and (iii) the type of monomers incorporated.

Table 2.2 gather the synthesis parameters used for all samples synthesised. For each sample the solid content of the resin solution (MF w/w%) is shown alongside MF to formic acid ratio (MF/FA), the formaldehyde to formic acid ratio (F/FA) and the calculated porosities of all samples dried at room temperature, post-treated with butanol and those post-treated with glutaraldehyde.

3.1.1 Role of formic acid as a catalyst for material formation

The key reagent in the material formation based on melamine and melamine-type resins is, as discussed in the introduction, the acid. Although the majority of previous MF material synthesis with given MF resins was carried out with strong acids, the only acid used in this work was formic acid as the systems are non alkoxylated and also they produce materials of higher surface areas to those synthesised with strong acids[69].

An interesting observation that was made during the addition of formic acid to MF resin solutions was that the transparency of gels varied with the amount of acid that was added. Figure 2.12 clearly shows this. All vials initially contained the same amounts of

resin solution but were catalysed with different amounts of acid. In Figure 2.12, the gel in the vial on the left contains three times as much acid as the one on the right (the pH of both gels was in the region of 4 when checked with pH paper).
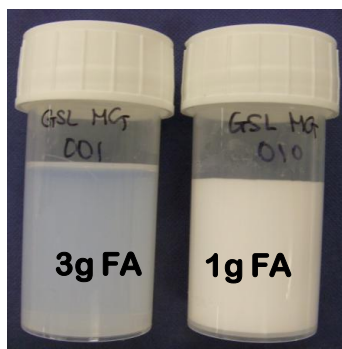
Figure 2.12: appearance of gels with different amounts of formic acid. The gel on the left has been catalysed with 3 g of formic acid whereas the one on the right has been catalysed with 1 g formic acid.

Objects can only scatter white light if the size of the particles or pores within materials is approximately of the same wavelength as visible light (400-700 nm) assuming that the refractive index of both gels is the same. Ruben *et al.*[75] mentioned for studies carried out on the synthesis of MF aerogels, that in order to form transparent gels the pH of the solution must be within a certain range. Although their work involved using hydrochloric acid to cross-link resins, it seems that it is still applicable when using formic acid. This group also showed that the opaque aerogels had horizontal tunnel-like cavities of 328±130 nm by 107±19 nm which were not present in the transparent aerogels, and these cavities must therefore be responsible for strongly scattering visible light. They also

proved that the surface area of the opaque material was 12% less than that of the transparent ones.

Figure 2.13: Appearance of final materials synthesised with different amounts of formic acid

The photo above (Figure 2.13) shows how the appearance of room temperature dried, pure MF materials synthesised with different amounts of formic acid and dried at room temperature. The final materials, like the gels, vary in opacity. Interestingly, the opaque material on the left, synthesised with 0.5 g formic acid, exhibits little shrinkage (higher retention of porosity) whereas the material at the furthermost right has undergone large shrinkage (low retention of porosity). This is further proof that transparent gels contain smaller pores, as the Young-Laplace equation states that the radius of pores affects the capillary pressure, *i.e.* the smaller they are, the higher the pressure within them thus leading to collapsing (note however the material on the far left is very brittle and exhibits poor mechanical strength).

3.1.2   Drying Methods

As smaller pores are the most susceptible to pore collapsing when dried at room temperature, it was thought that the use of the two different post-treatment methods with butanol and glutaraldehyde could aid in retaining pores. However, both post treatments had little effect in retaining pores in very transparent gels (gels containing high amounts of formic acid, see details in Table 2.2). Evidently, there was no significant pore retention enhancement in those made with small amounts of formic since these specimens already displayed low shrinkage even when dried at room temperature (a sign of rather large pores not affected by capillary pressures).

A very small range of MF gels did however display successful pore retention with the post- treatment methods. These samples, with a melamine-to-formaldehyde(M:F) ratio of 1:1.5, were acid catalysed with 1-2 g of formic acid. The photo below (Figure 2.14) shows one such example, where post-treatments with butanol and glutaraldehyde have significantly enhanced pore retention. The part of the gel dried at room temperature has undergone high shrinkage, only retaining 15% porosity. The other two parts post-treated prior to room temperature drying, however, have retained approximately 80% porosity (this is expected as the MF solid content was 25% by weight, 75% by weight is water).
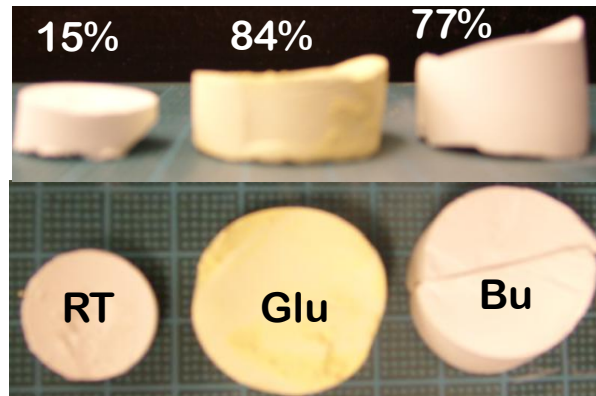
Figure 2.14: The effect of post treatment of gels: after gel synthesis, the sample was cut into 3 parts. The first was left to dry at room temperature (RT), the second was immersed in an aqueous glutaraldehyde solution at 80°C for 2 hours and then allowed to dry at room temperature. The final part was immersed in a butanol aqueous solution at 80°C for 2 hours prior to drying at room temperature.

The graph below (Figure 2.15) displays the final porosities of the different materials synthesised as a function of the molar MF/Formic acid ratio (MF/FA).
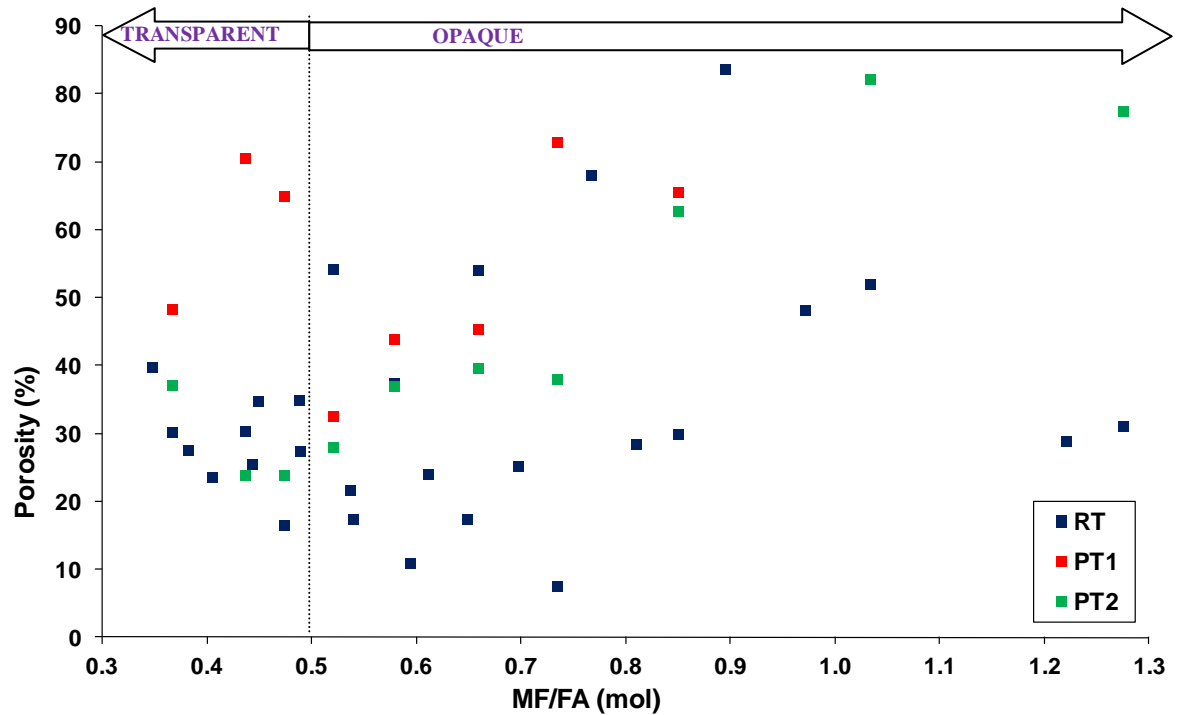
Figure 2.15: Graph showing Porosity *vs.* MF/FA ratio. The samples in blue were dried at room temperature, the samples in red were post treated with butanol prior to room temperature drying and the samples in green were post treated with glutaraldehyde prior to room temperature drying.

A general trend seems to be that the higher the MF/FA ratio, the higher the porosity volume. This seems to suggest that pore retention is enhanced when small amounts of formic acid are used to cross-link a resin solution. Plus, post-treated materials seem to generally show a larger pore volume than those dried at room temperature (although there is no clear differentiation between butanol or glutaraldehyde post-treatment) especially after an MF/FA ratio of 0.6. In fact there seems to be a transition occurring between MF/FA =0.6 to MF/FA =0.8 where most samples go from virtually non-porous to very porous. Also, in some cases, it is difficult to reproduce the same material twice

(*e.g.* the two blue points at MF/FA= 0.5 have a porosity difference of 10%). This may be due to the lack of control on the various equilibrium reactions occurring in the resin synthesis but also to slight variations in other parameters such as temperature, amount of catalyst and reaction times.

3.1.3 Introduction of different monomers

The final variable in this study was the incorporation of different melamine based monomers into MF networks. Three commercially available melamine derivatives acetoguanamine **23**, benzoguanamine **24** and caprinoguanamine **25** along with monomers 1 and 2 synthesised previously were incorporated into MF networks (monomer 3 was kept aside as the conversion of the ester moiety to the acidic function has not yet been carried out). The reaction scheme is shown below in Scheme 2.1.

Acetoguanamine	Benzoguanamine	Caprinoguanamine
23	**24**	**26**
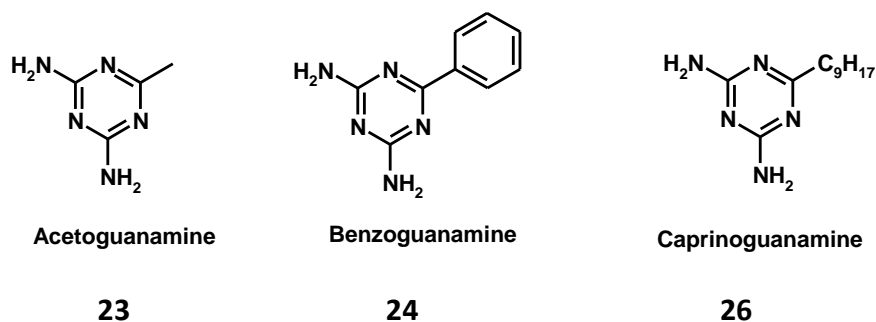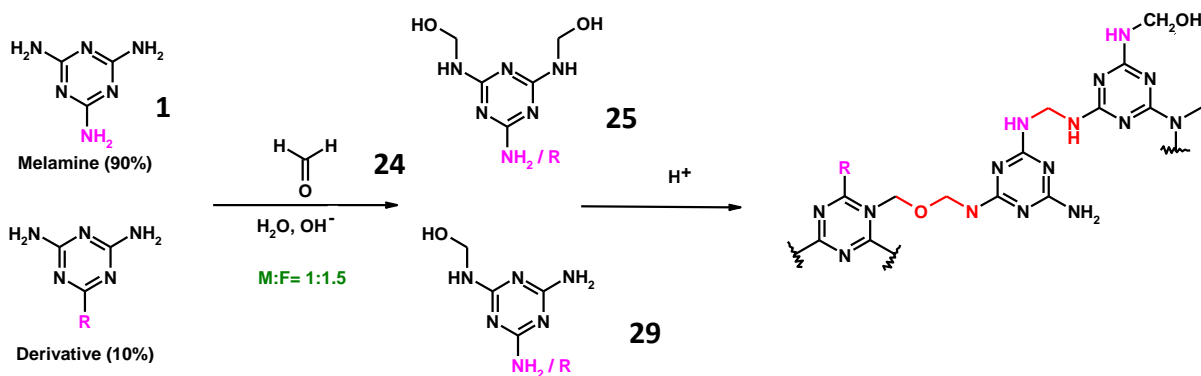
Scheme 2.1: Reaction scheme for the introduction of melamine derivatives into MF resins and subsequently the final cross-linked MF networks

The derivatives were added in 10% molar quantities with melamine during resin synthesis and then acid catalysed to yield materials in the same way that pure MF materials were produced. Acetoguanamine **26** and benzoguanamine **27** easily dissolved in water to produce clear solution with very little solid residue left over after filtration (benzoguanamine **27** gave a slight yellow colouration to the solution). The dissolution of caprinoguanamine **28** was a lot more difficult hence why the solid content of the resins was less than 25%. This may be due to the long alkyl chain group, a very hydrophobic group, on caprinoguanamine hindering its solubility.

The ratio of melamine and derivative to formaldehyde [(M+M'): F] is kept at 1:1.5. Theoretically this still produces mono and di-substituted precursors. The solid content (*i.e.* precursor concentration in aqueous solution) was approximately 20% depending on the solubility of monomers during resin synthesis. The following graphs present the calculated porosities for the monomer-containing MF materials. They are plotted against the [(M+M')F/FA] ratio , which is still referred to as MF/FA in the graphs below (Figure 2.15).
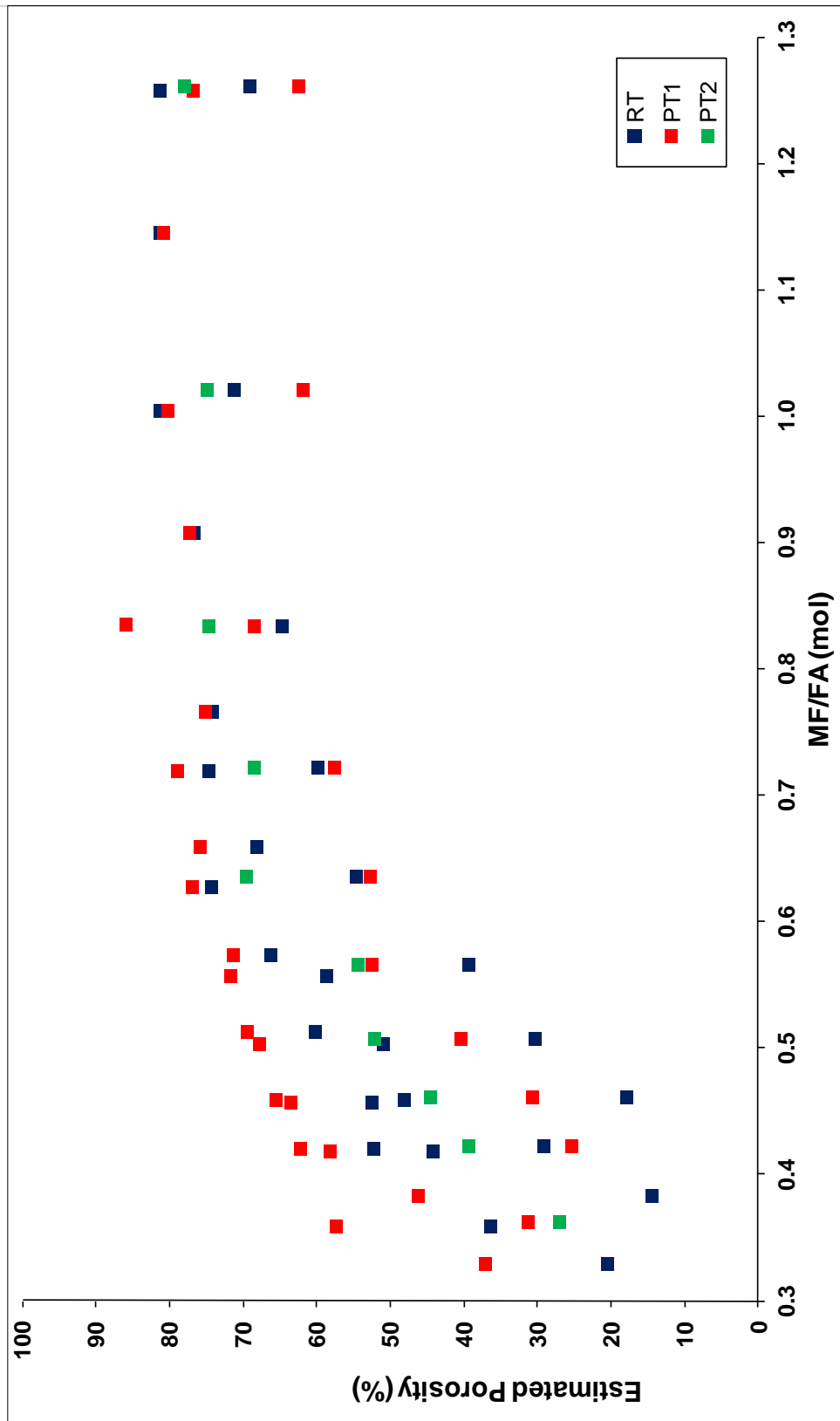
Figure 2.16: Graph showing Porosity *vs.* MF/FA ratio of materials containing benzoguanamine. The data points in blue are samples dried at room temperature, the samples in red are those post treated with butanol and the ones in green are post treated with glutaraldehyde.
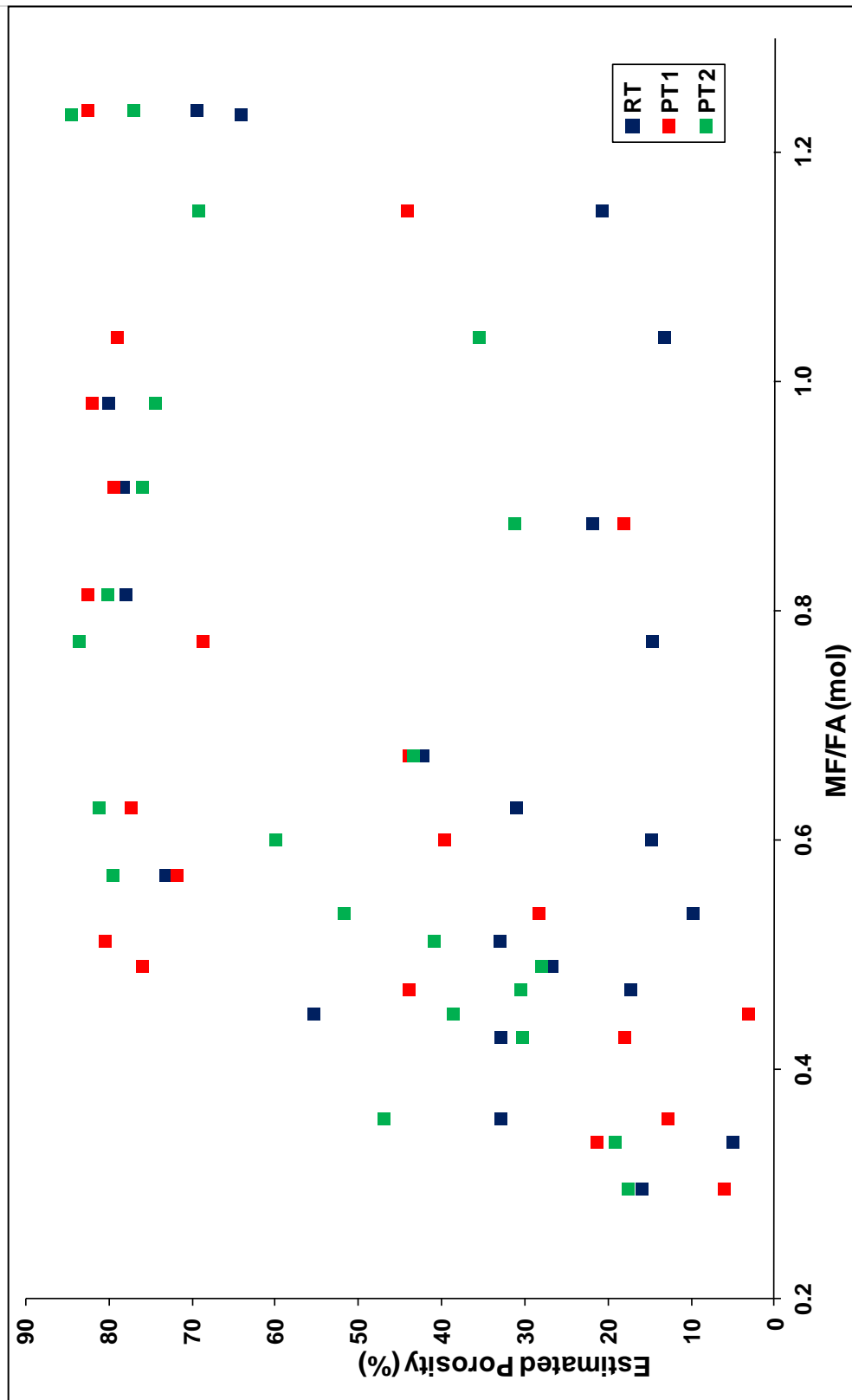
Figure 2.17: Graph showing Porosity *vs.* MF/FA ratio of materials containing acetoguanamine. The data points in blue are samples dried at room temperature, the samples in red are those post treated with butanol and the ones in green are post treated with glutaraldehyde.
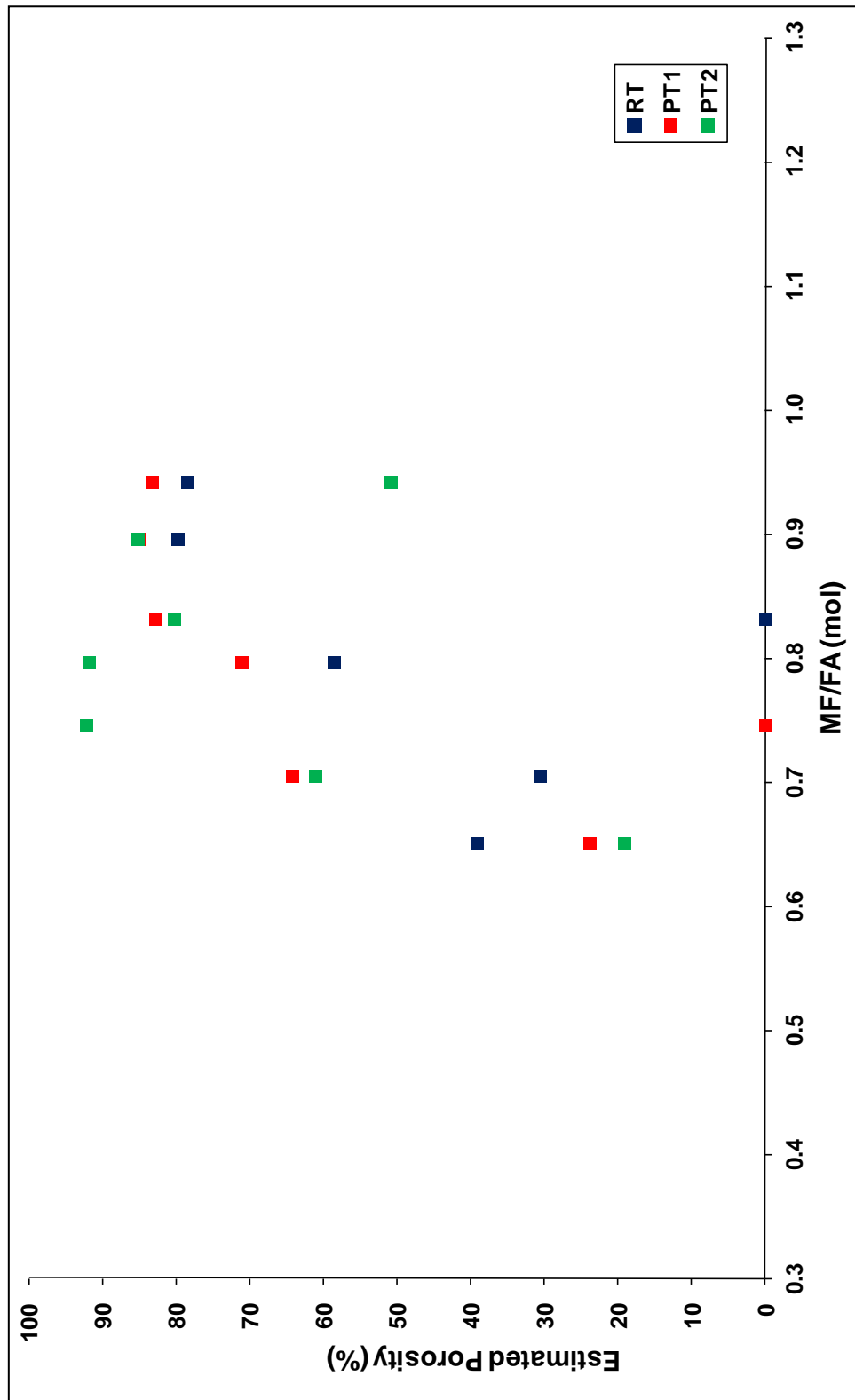
Figure 2.18: Graph showing Porosity *vs.* MF/FA ratio of materials containing caprinoguanamine. The data points in blue are samples dried at room temperature, the samples in red are those post treated with butanol and the ones in green are post treated with glutaraldehyde.

These graphs show a very similar trend to the one observed for pure MF materials (Figure 2.15). There is very clearly a link between the amount of formic acid and the retention of porosity: the greater the amount of acid added to cross-link precursors, the less porous the final material is. This re-emphasises that the amount of formic acid can somehow affect pores sizes within a gel (and eventually a material upon successful drying). Again, the region of transition between non-porous and very porous is at MF/FA=0.6 to 0.8. The mid-point of this region, MF/FA=0.7 indicates that the ratio of formaldehyde to formic acid (F:FA)is 2:1, meaning that approximately two moles of formic acid is required per mole of cross-linker to obtain materials with decent pore volumes (pore volumes above 60%). If the ratio MF/FA is higher than 0.7 (FA is lower than 0.5 mole per mole of formaldehyde) then, although, materials with high porosities are obtained, they are very opaque, brittle and dry very well at room temperature, a sign of rather large pores. If the ratio is lower than 0.7, transparent materials with very low pore volumes are formed. This then questions whether formic acid "catalyses" the reactivity of (supra)molecular units of melamine or if more generally it controls the overall pH of the reaction mixture?

From the knowledge gained about the region of interest (0.6<MF/FA<0.8) from the pure MF materials and those containing benzoguanamine and acetoguanamine, the caprinoguanamine containing resin mixture was catalysed with a narrower range of formic acid so that the MF/FA ratio was kept between 0.6 and 1.

In Figure 2.16, the graph of benzoguanamine containing materials has a very different profile to the other types of materials. Here the transition of non-porous to porous range has shifted to lower ratios (0.5 to 0.8) and for MF/FA ratios above 0.6, even

the room temperature dried samples display high porosities. Also there is no opaque-transparent transition in benzoguanamine containing materials. The substitution of amino groups for bulkier and more hydrophobic phenyl groups may therefore change the mechanism of phase separation and the resulting materials probably have large porous structures.

On the following page (Figure 2.19 and 2.20) similar graphs have been made for samples containing the synthesised monomers, monomer 1 and monomer 2.
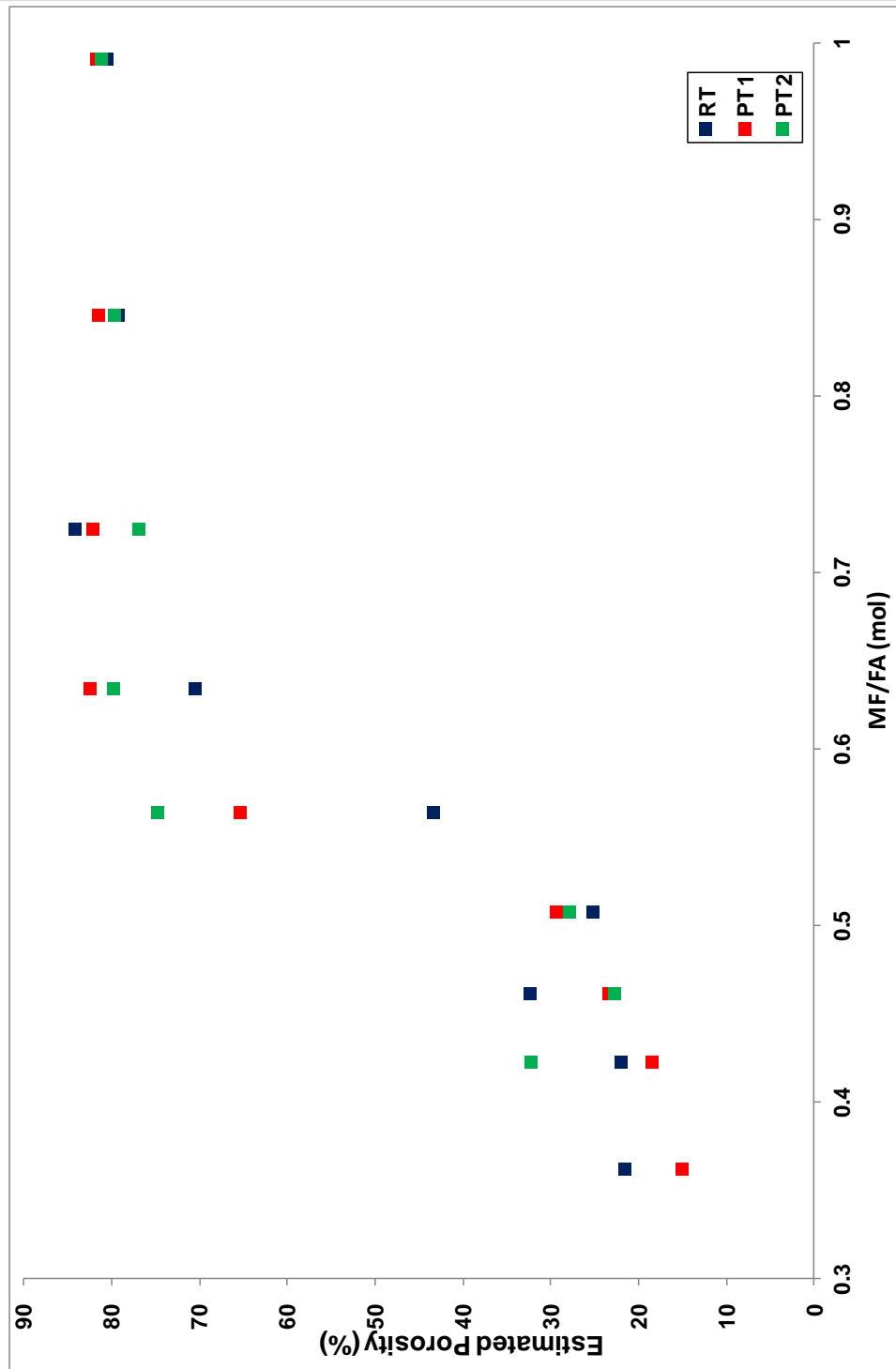
Figure 2.19: Graphs showing Porosity *vs.* MF/FA ratio of samples containing monomer 1. The samples in blue have been dried at room temperature, the samples in red have been post treated with butanol prior to room temperature drying and the samples in green have been post treated with glutaraldehyde prior to room temperature drying.
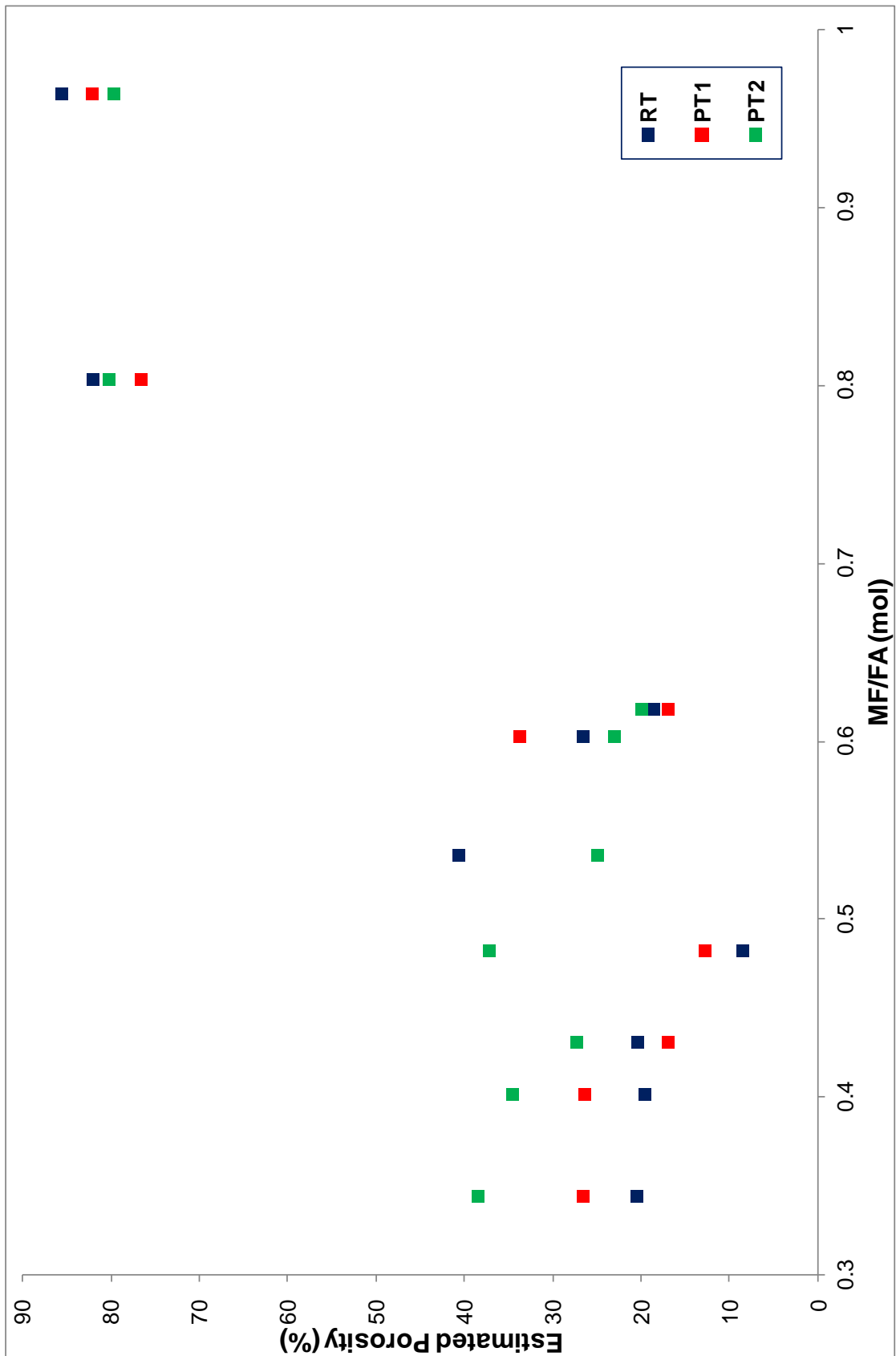
Figure 2.20: Graphs showing Porosity *vs.* MF/FA ratio of samples containing monomer 2. The samples in blue have been dried at room temperature, the samples in red have been

post treated with butanol prior to room temperature drying and the samples in green have been post treated with glutaraldehyde prior to room temperature drying.

The graphs in Figure 2.19 and 2.20 shows the same transition at 0.6<MF/FA<0.8 (although data points close to MF/FA = 0.7 are missing in the case of monomer 2 containing materials). The same shift towards lower MF/FA ratios for the non-porous/porous transition is observed in the case of monomer 1 (this may be due to the introduction of the phenyl moiety).

Incorporation of different functionalities in the MF network theoretically has the same effect as post treating (*i.e.* it increases pore retention due to the increase in hydrophobicity). In order to study this effect, the above graphs were separated into Porosity *vs.* MF/FA plots for the different drying methods. Firstly, Figure 2.21 represents the Porosity *vs.* MF/FA molar ratio of all the specimens dried at room temperature, with the different colours representing the different monomers.
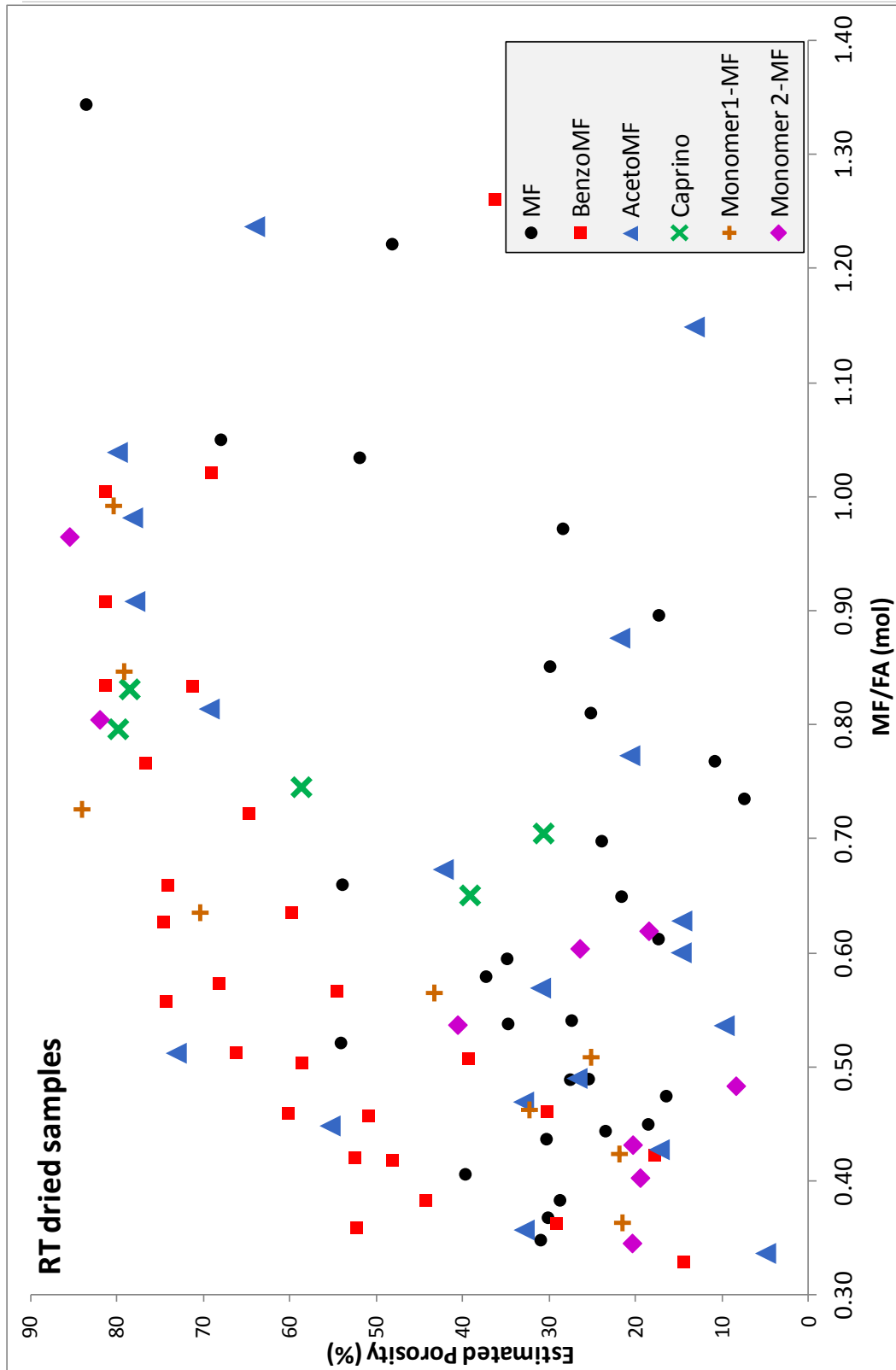
Figure 2.21: Graph showing the combined Porosity *vs*. MF/FA (mol) plots for all room temperature dried specimens. Different colours and shapes are used to differentiate the different monomers, as shown in the key.

The black dots represent pure MF samples. Most materials with additional derivatives tend to have higher prosities even after merely drying at room temperature. This suggests that the addition of hydrophobic groups into materials, in amounts as little as 10%, has an effect on the overall drying. It may be analogous to the way that the post treatment method changes the contact angle of the solvent in the pores of the materials. However, incorporation of different monomers during materials synthesis must have a greater effect on the material formation, *i.e.* phase separation during sol-gel synthesis (which can affect grain sizes of the network, Figure 2.38).

An attempt was made to incorporate larger amounts of benzoguanamine and acetoguanamine (20% molar quantities). The incorporation of 20% benzoguanamine was not very successful, leaving a large amount of solid residue on the filter paper. It is very likely due to the initial poor solubilisation of the precursors. The dissolution of 20% acetoguanamine, on the other hand, was successful. Figure 2.22 shows both graphs of 10% acetoguanamine and 20% acetooguanamine results for direct comparison.
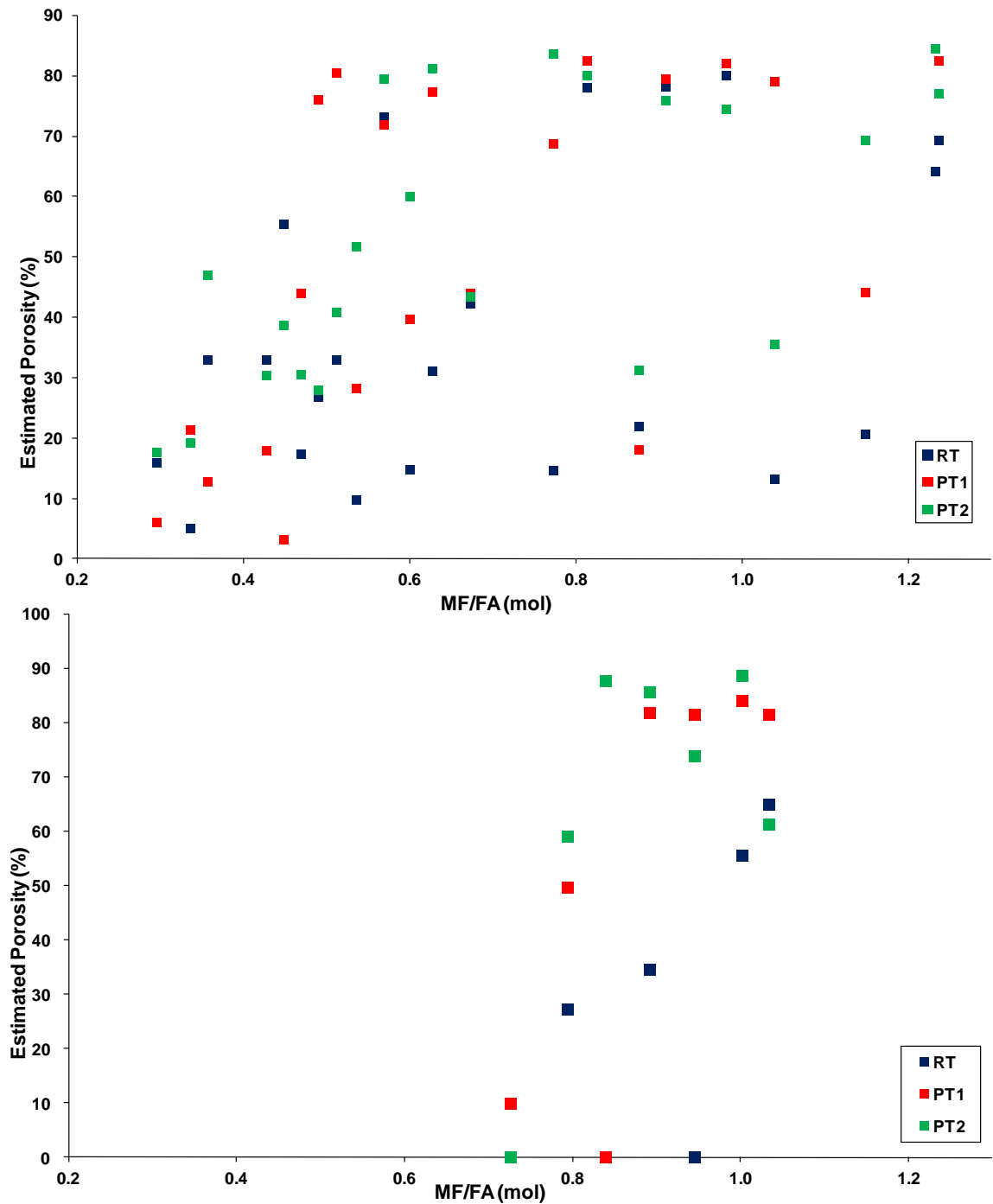
Figure 2.22: Graphs displaying the Porosity *vs*. MF/FA molar ratio for MF materials

containing 20% acetoguanamine (top) and 10% acetoguanamine (bottom).

The graphs interestingly show that the incorporation of acetoguanamine in higher concentrations seems to shift the 0.6-0.8 transition region to 0.8 -1. This may be due to less available cross-linking units (therefore less formic acid is required). Alternatively, it may be due to different mechanisms of phase separation modifying the final outcome.

Figure 2.23 and 2.24 show the plots of the different post treatment methods using butanol and glutaraldehyde respectively.
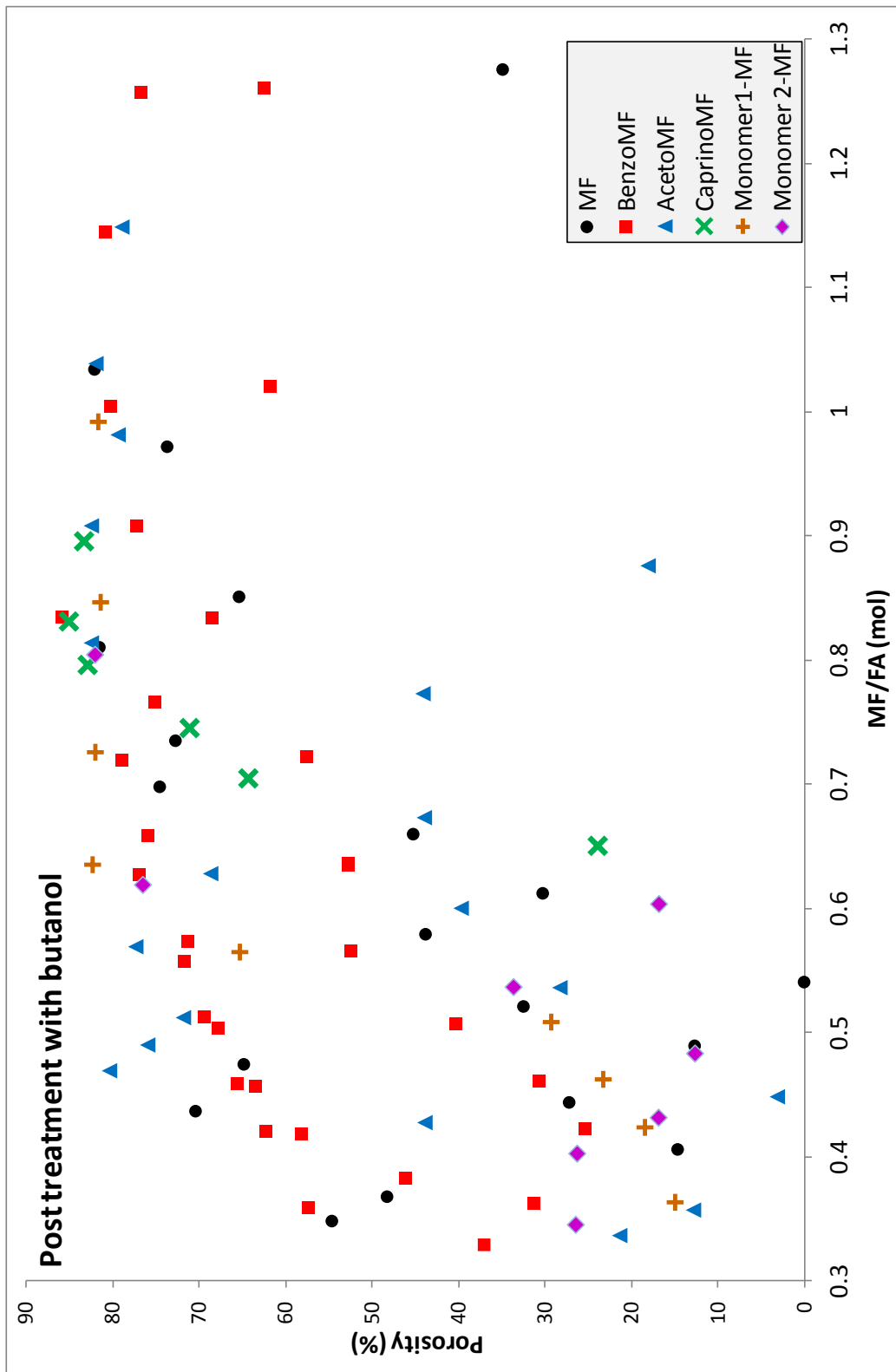
Figure 2.23: Graph showing the combined Porosity *vs*. MF/FA (mol) plots for all specimens post-treated with butanol. Different colours and shapes are used to differentiate the different monomers, as shown in the key.
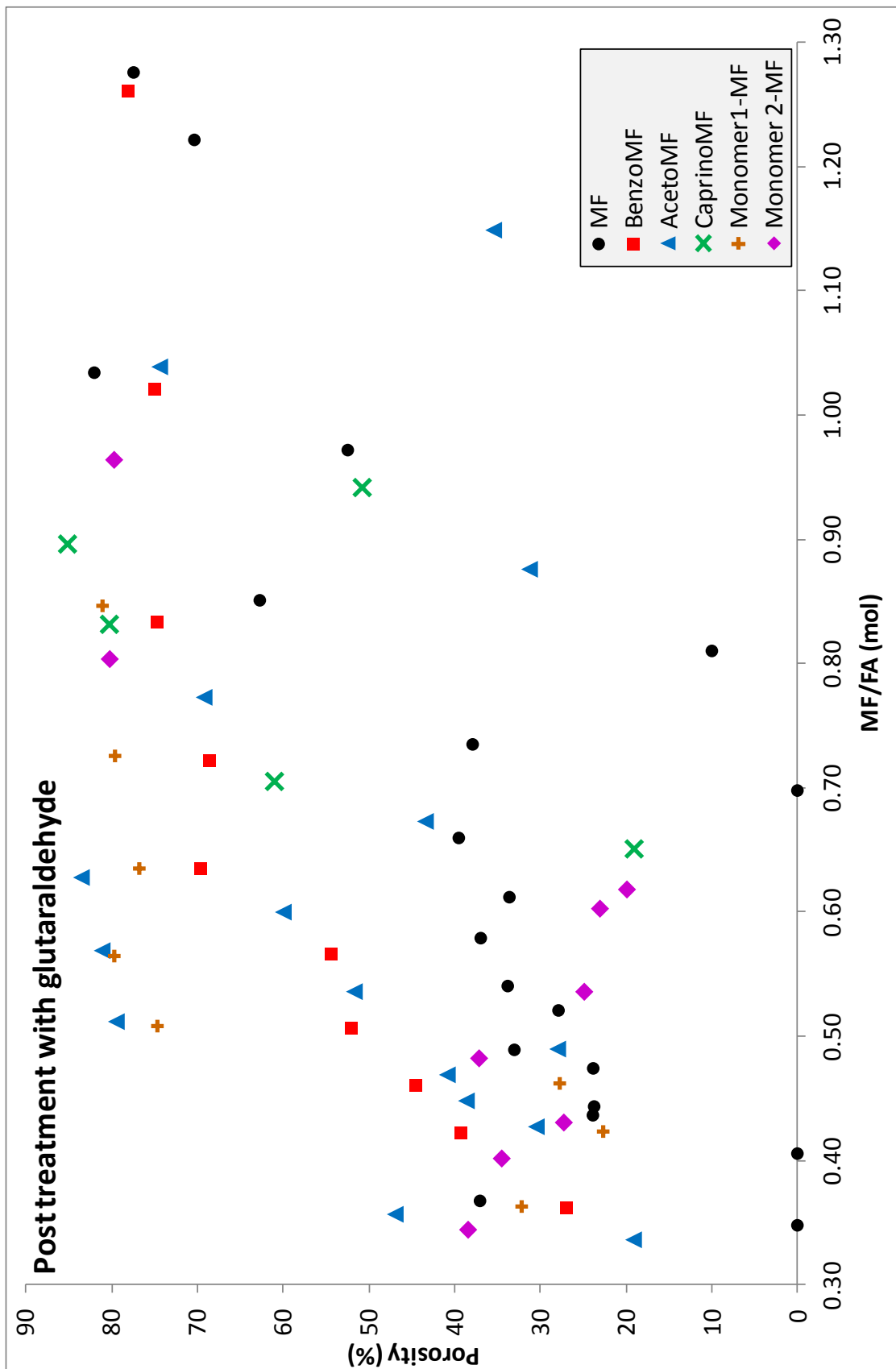
Figure 2.24: Graph showing the combined Porosity *vs*. MF/FA (mol) plots for all specimens post-treated with butanol. Different colours and shapes are used to differentiate the different monomers, as shown in the key.

Samples with low MF/FA ratios in Figure 2.23 have higher porosites compared to those dried at room temperature (Figure 2.21). It seems, however, that the glutaraldehyde post-treatment method (Figure 2.24) is not as sucessful as butanol, as most samples post treated with butanol seem to have higher porosities. Therefore questions which arise here are: (i) is the procedure used for post-treating with glutaraldehyde fully optimised? Or (ii) may be there are more hydroxyl sites in MF networks available for reactions with butanol, than primary amine groups for reaction with glutaraldehyde?

3.1.4   Post-treating samples with different aldehydes

In order to try to understand how the post-treatment with glutaraldehyde works (*i.e.* what sort of reactions occur), post-treatments of MF gels with glyoxal, in which aldol formation does not occur, and also with pentanal (the same number of carbons as glutaraldehyde but it is not a dialdehyde), for which the chemical structures are shown below (**30** and **31**), were carried out. This was done by immersing gels in 10% solution of aldehyde with water and raising the pH to 9 (pentanal was not very soluble in water alone, instead it was dissolved in a 25% acetone-water solution).
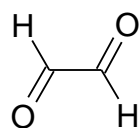
glyoxal
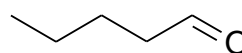
pentanal
(valeraldehyde)

30

31

The following image shows dried materials resulting from post-treatments with glyoxal and pentanal.

Figure 2.25: A set of samples (from the same gel) which were post treated with pentanal (val) and glyoxal (gly). The retention of porosity is visible by eye. (Porosity details available in the appendix section).

Most samples post treated with glyoxal had the same yellow colouration that samples post treated with glutaraldehyde displayed, this is indicative that imine formation has occurred[76,77] (Figure 2.26). As the pentanal post-treatment did not give this yellow coloration, it is thought that its reaction and incorporation into the MF matrix was not as successful. Perhaps, the reaction conditions for post-treating with all aldehydes including glutaraldeyde needs to be re-adapted. For instance, the reaction can be carried out in acidic conditions as most literature on organic reactions between amines and aldehydes favour acidic conditions[78].

Figure 2.26: Appearance of MF gels post treated with glyoxal. The samples on the left are non-porous and have a yellow coloration whereas those to the right are porous and do not have a strong yellow coloration.

3.1.5 Synthesis of materials with addition of amines directly in resin synthesis

It was thought that an alternative procedure to introduce functionality into MF materials could be that, rather than modifying the functionality on the monomers before resin synthesis, the direct attachment of the functional amine could occur during resin synthesis. For this 10% phenylethylamine (the amine used to synthesise monomer 1) with 90% melamine was reacted with the corresponding amount of formalin solution. Despite heating the mixture at 80°C for an hour, a clear solution was never obtained. A large amount of solid was left behind.

After filtration however, cross-linking the resin solution with formic acid was pursued as before (Figure 2.27). The materials were characterised by IR spectroscopy and the analysis revealed that there is no evidence to suggest that the functional amine had successfully been incorporated. Instead the spectra looked very similar to pure MF

materials, suggesting that the majority of the amine was lost in the solid residue. Photos of resulting materials after drying are given in Figure 2.27.
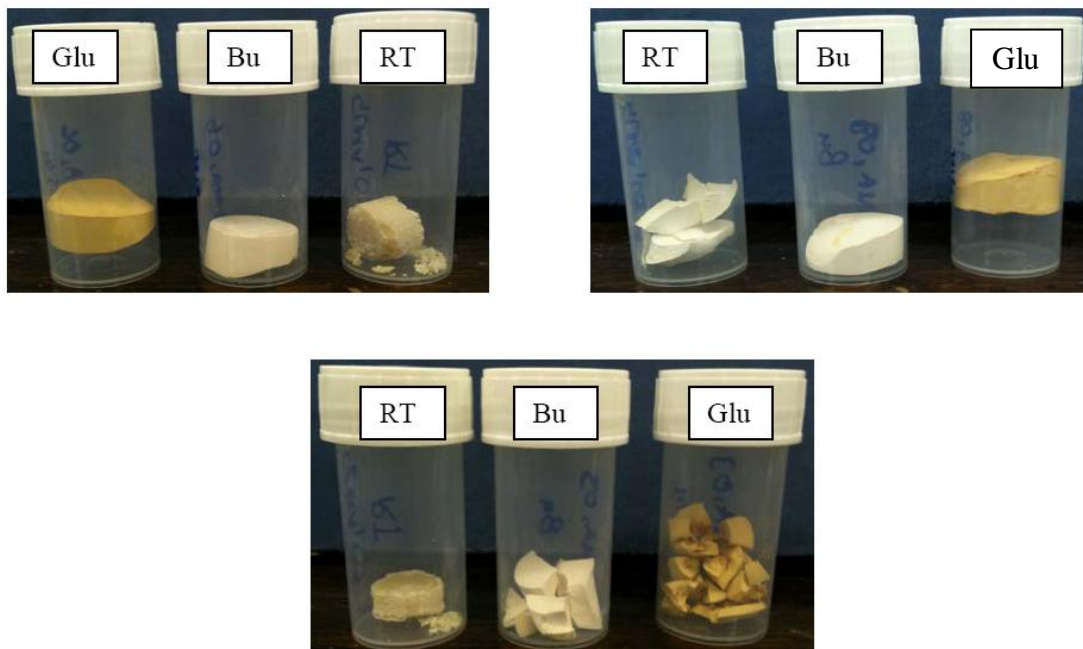
Figure2.27: A selection of samples synthesised via the direct introduction of functional amine. The set of samples differ in amounts of formic acid. The top left samples have MF/FA ratio of 0.34. The top right samples have MF/FA ratios of 0.39. The samples on the bottom have MF/FA ratios of 0.25.

Alternative ways to directly incorporate the amine into MF networks could be to find a post treatment method whereby functional amines are attached onto any of the available functional groups in the MF matrix.

Conclusions on the effect of the synthesis parameters on calculated porosity

Porosity has successfully been enhanced in MF materials. Firstly, this has been done by fine-tuning the formic acid content. Secondly, porosity has significantly been enhanced with post treatment methods. Thirdly, the incorporation of hydrophobic components also seems to have an effect of porosity.

3.2 Effect of the synthesis parameters on measured porosity

The materials described previously were expressed in terms of their overall porosity. Emphasis on pore sizes and pore size distributions still require quantification. For that purpose, nitrogen sorption and mercury porosimetry techniques were necessary and used next.

3.2.1 Nitrogen Sorption

A selection of samples was chosen for nitrogen sorption analysis by identifying post-treated materials displaying a significant change in porosity from their room temperature dried counter parts (using Table 2.2). Figure 2.28 shows a typical nitrogen adsorption and desorption isotherm for most materials studied.

Table 2.2: Information on the different materials synthesised alongside their estimated porosities. (Note: codes in the "M/F 1/1.5" column are codes that refer to sample numbers)

MF materials				Porosity (%)		
M/F 1/1.5	MF w/w%	MF/FA (mol)	F/FA (mol)	RT	PT (BuOH)	PT (Glu)
GSL011	24.03%	0.37	1.07	30	48	-
GSL012	24.03%	0.44	1.26	30	70	-
GSL013	24.03%	0.47	1.37	16	65	-
GSL014	24.03%	0.52	1.51	54	32	-
GSL015	24.03%	0.58	1.68	37	44	-
GSL016	24.03%	0.66	1.91	54	45	-
GSL017	24.03%	0.73	2.13	7	73	-
GSL018	24.03%	0.85	2.47	30	65	-
GSL019	24.03%	1.03	3.00	52	82	-
GSL020	24.03%	1.28	3.70	-	-	-
GSL021	22.68%	0.35	1.01	31	-	37
GSL022	22.68%	0.41	1.18	40	-	24
GSL023	22.68%	0.44	1.29	23	-	24
GSL024	22.68%	0.49	1.42	25	-	28
GSL025	22.68%	0.54	1.57	27	-	37
GSL026	22.68%	0.61	1.77	17	-	40
GSL027	22.68%	0.70	2.02	24	-	38
GSL028	22.68%	0.81	2.35	25	-	63
GSL029	22.68%	0.97	2.82	28	-	82
GSL030	22.68%	1.22	3.54	48	-	77
GLM040	25.00%	0.38	1.19	29	35	broken
GLM041	25.00%	0.45	1.39	19	55	24
GLM042	25.00%	0.49	1.52	28	15	33
GLM043	25.00%	0.54	1.67	35	27	34
GLM044	25.00%	0.59	1.84	35	13	34
GLM045	25.00%	0.65	2.01	22	broken	broken
GLM046	25.00%	0.77	2.38	11	30	10
GLM047	25.00%	0.90	2.78	17	75	52
GLM048	25.00%	1.05	3.26	68	82	70
GLM049	25.00%	1.34	4.17	84	74	broken

Benzo (10%)-MF				Porosity (%)		
M/F 1/1.5	MF w/w%	MF/FA (mol)	F/FA (mol)	RT	PT (BuOH)	PT (Glu)
GSLBZ011	23.80%	0.36	1.05	-	31	-
GSLBZ012	23.80%	0.42	1.23	29	25	-
GSLBZ013	23.80%	0.46	1.34	18	31	-
GSLBZ014	23.80%	0.51	1.47	30	40	-
GSLBZ015	23.80%	0.57	1.64	39	52	-
GSLBZ016	23.80%	0.64	1.84	55	53	-
GSLBZ017	23.80%	0.72	2.10	60	58	-
GSLBZ018	23.80%	0.83	2.42	65	68	-
GSLBZ019	23.80%	1.02	2.96	71	62	-
GSLBZ020	23.80%	1.26	3.66	69	62	-
GSLBZ021	23.60%	0.36	1.04	36	57	-
GSLBZ022	23.60%	0.42	1.22	52	62	-
GSLBZ023	23.60%	0.46	1.33	52	64	-
GSLBZ024	23.60%	0.50	1.46	51	68	-
GSLBZ025	23.60%	0.56	1.62	59	72	-
GSLBZ026	23.60%	0.63	1.82	74	77	-
GSLBZ027	23.60%	0.72	2.09	75	79	-
GSLBZ028	23.60%	0.83	2.42		86	-
GSLBZ029	23.60%	1.00	2.92	81	80	-
GSLBZ030	23.60%	1.26	3.65	81	77	-
GSLBZ031	21.60%	0.33	0.95	20	37	27
GSLBZ032	21.60%	0.38	1.11	14	46	39
GSLBZ033	21.60%	0.42	1.21	44	58	45
GSLBZ034	21.60%	0.46	1.33	48	66	52
GSLBZ035	21.60%	0.51	1.49	60	69	54
GSLBZ036	21.60%	0.57	1.66	66	71	70
GSLBZ037	21.60%	0.66	1.91	68	76	69
GSLBZ038	21.60%	0.77	2.22	74	75	75
GSLBZ039	21.60%	0.91	2.64	77	77	75
GSLBZ040	21.60%	1.14	3.32	81	81	78

Aceto (10%)-MF				Porosity (%)		
M/F 1/1.5	MF w/w%	MF/FA (mol)	F/FA (mol)	RT	PT (BuOH)	PT (Glu)
GSLMG001	25.00%	0.34	0.98	broken	Broken	broken
GSLMG002	25.00%	0.36	1.04	broken	21	broken
GSLMG003	25.00%	0.30	0.86	broken	13	19
GSLMG004	25.00%	0.45	1.30	5	6	47
GSLMG005	25.00%	0.49	1.42	33	3	18
GSLMG006	25.00%	0.54	1.56	16	Broken	39
GSLMG007	25.00%	0.60	1.74	55	Broken	28
GSLMG008	25.00%	0.67	1.95	27	Broken	52
GSLMG009	25.00%	0.88	2.54	10	76	60
GLMMG01	23.71%	0.43	1.24	15	28	43
GLMMG02	23.71%	0.47	1.36	42	40	broken
GLMMG03	23.71%	0.51	1.49	22	44	31
GLMMG04	23.71%	0.57	1.65	33	18	30
GLMMG05	23.71%	0.63	1.82	17	18	30
GLMMG06	23.71%	0.77	2.24	33	44	41
GLMMG1a- 09/01/09	23.71%	1.15	3.33	73	80	79
GLMMG1b-09/01	23.71%	1.04	3.02	31	72	81
GLMMG1c-09/01	23.71%	0.98	2.85	15	77	84
GLMMG1d-09/01	23.71%	0.91	2.64	21	69	69
GLMMG1e-09/01	23.71%	0.81	2.36	13	44	35
GLMMG07	23.71%	1.24	3.59	80	79	74
GMGMF1	22.93%	1.23	3.58	78	82	76
GMGMF2	22.93%	1.12	3.25	78	79	80
GMGMF3	22.93%	1.03	2.98	69	82	77
GMGMF4	22.93%	0.95	2.75	64	82	84
Aceto (20%)-MF						
M/F 1/1.5	MF w/w%	MF/FA (mol)	F/FA (mol)	RT	PT (BuOH)	PT (Glu)
GLMMG040	25.00%	0.73	2.25	broken	10	broken
GLMMG041	25.00%	0.79	2.46	27	50	59
GLMMG042	25.00%	0.84	2.60	broken	broken	88
GLMMG043	25.00%	0.89	2.76	34	82	86
GLMMG044	25.00%	0.95	2.93	broken	81	74
GLMMG045	25.00%	1.00	3.11	56	84	89
GLMMG046	25.00%	1.03	3.21	65	81	61

Caprino (10%)-MF				Porosity (%)		
M/F 1/1.5	MF w/w%	MF/FA (mol)	F/FA (mol)	RT	PT (BuOH)	PT (Glu)
M/F 1/1.5						
GLMCP01	18.70%	0.65	1.95	39	24	19
GLMCP02	18.70%	0.70	2.11	31	64	61
GLMCP03	18.70%	0.75	2.24	broken	broken	92
GLMCP04	18.70%	0.80	2.39	59	71	92
GLMCP05	18.70%	0.83	2.49	broken	83	80
GLMCP06	18.70%	0.90	2.69	80	85	85
GLMCP07	18.70%	0.94	2.82	79	83	51
Monomer 1 (20%) - MF	MF w/w%	MF/FA (mol)	F/FA (mol)	RT	PT (BuOH)	PT (Glu)
M/F 1/1.5						
GM1MF01	25%	0.36	1.11	22	15	broken
GM1MF02	25%	0.42	1.30	22	18	32
GM1MF03	25%	0.46	1.42	32	23	23
GM1MF04	25%	0.51	1.56	25	29	28
GM1MF05	25%	0.56	1.73	43	65	75
GM1MF06	25%	0.63	1.95	70	82	80
GM1MF07	25%	0.73	2.23	84	82	77
GM1MF08	25%	0.85	2.60	79	81	80
GM1MF09	25%	0.99	3.04	80	82	81
Monomer 2 (10%) - MF	MF w/w%	MF/FA (mol)	F/FA (mol)	RT	PT (BuOH)	PT (Glu)
M/F 1/1.5						
GM2MF011	23.75%	0.34	1.06	20	26	38
GM2MF012	23.75%	0.40	1.23	20	26	34
GM2MF013	23.75%	0.43	1.32	20	17	27
GM2MF014	23.75%	0.48	1.48	8	13	37
GM2MF015	23.75%	0.54	1.64	41	broken	25
GM2MF016	23.75%	0.60	1.85	26	34	23
GM2MF017	23.75%	0.62	1.90	19	17	20
GM2MF018	23.75%	0.80	2.47	82	77	80
GM2MF019	23.75%	0.96	2.96	86	82	80

Amine 1 (10%) +MF	MF w/w%	MF/FA (mol)	F/FA (mol)	Porosity (%)		
				RT	PT (BuOH)	PT (Glu)
M/F1:1.5						
GLMA101	12.50%		0.60	12	61	broken
GLMA102	12.50%	0.23	0.69	30	46	broken
GLMA103	12.50%	0.25	0.76	22	41	broken
GLMA104	12.50%	0.27	0.83	19	58	broken
GLMA105	12.50%	0.30	0.93	52	39	broken
GLMA106	12.50%	0.34	1.04	21	38	57
GLMA107	12.50%	0.39	1.19	16	45	11
GLMA108	12.50%	0.45	1.39	33	43	broken
GLMA109	12.50%	0.54	1.67	28	40	broken
GLMA110	12.50%	0.68	2.08	37	53	broken
MF materials						
M/F1:5	MF w/w%	MF/FA (mol)	F/FA (mol)	RT	PT (BuOH)	PT (Glu)
GLM001	24.4%	2.54	12.71	75	-	-
GLM002	24.4%	1.18	5.92	65	-	-
GLM003	24.4%	0.74	3.70	-	-	-
GLM004	24.4%	0.64	3.18	-	-	-
GLM005	24.4%	0.52	2.61	21	-	-
GLM006	24.4%	0.44	2.18	25	-	-
GLM007	24.4%	0.37	1.85	30	-	-
GLM008	24.4%	0.31	1.56	23	-	-
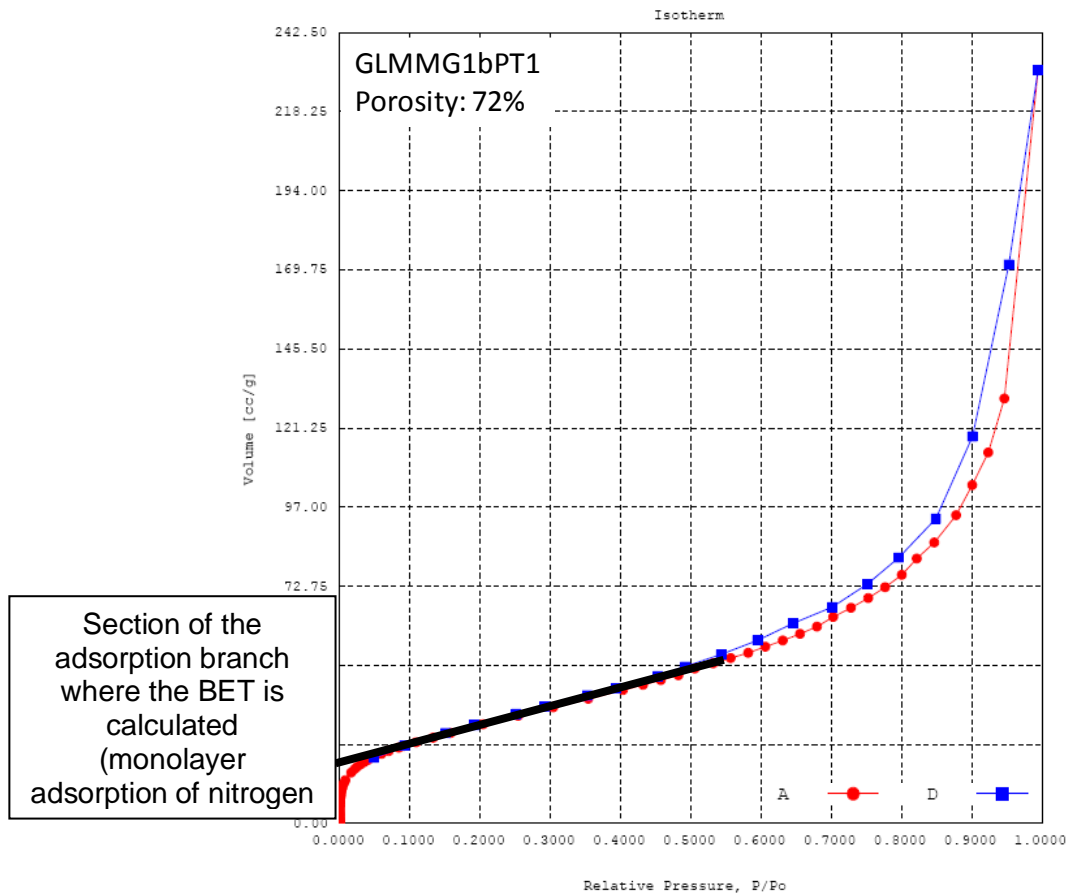
Figure 2.28: Typical adsorption/desorption isotherms of a MF material, here GLMMG1bPT1. The red curve represents the adsorption branch and the blue curve represents the desorption isotherm.

The isotherms obtained suggest that MF materials studied in this work are generally macroporous (no levelling off at p/p$_0$=1 suggesting that at higher pressures pores can still be filled). The findings of Gowerek *et al.*[65] and Baraka *et al.*[66], who classed their materials as mesoporous (type IV), carried out similar measurements on rather different MF systems though (porosity comes either from templating with colloidal silica of from grinding of bulk material). They concluded this because they observed levelling off of the

isotherm in the p/p$_0$=0.9 to 1 region suggesting that multilayer adsorption was occuring. However, the isotherms obtained in this work suggest we have large pores in the macroporous range instead with very little or no microporosity at all.

Also, according to Thomas *et al.*[79], isotherms (either adsorption or desorption) that are steep at intermediate relative pressures are characteristic of tubular shaped capillaries (not necessarily having circular cross sections) open at both ends. The advantage of the isotherms obtained in this work is the small gradient when p/p$_0$ is close to 0. This gives an accurate BET surface area.

Information obtained on the different samples studied is displayed graphically, in Figure 2.29. Triangles represent pure MF materials, circles represent acetoguanamine-MF materials, squares represent benzoguanamine-MF materials and diamonds represent caprinoguanamine-MF materials. Also included are the samples containing the synthetic monomers 1 (cross) and 2 (dash). Red is used for samples dried at room temperature, green for samples post treated with n-butanol and black represents samples post treated with glutaraldehyde.

The graph shows that in general there is a positive correlation between porosity and surface area. More specifically there does seem to be higher BET surface areas for samples that have been post treated. The majority of post treated samples (of 60% porosity and above) have surface areas above 80 m^2/g. Samples within the 60-65% porosity region exhibit high surface areas (~100 m^2/g) whereas those in the 70-90% porosity region fluctuate from BETs as low as 10 m^2/g to as high as 190 m^2/g. This suggests that materials with porosities of 70-90% can have large pores, giving high pore volume, but low surface area.

Also, materials with similar porosities, for example the pure MF sample post-treated with glutaraldehyde with 82% porosity has a surface area of 100 m^2/g and volume adsorbed was 164 cm$^{3/}$g (data not shown) whereas the acetoguanamine containing sample, post-treated with glutaraldehyde and of 81% porosity has a surface area of 80 m^2/g and the volume of nitrogen adsorbed is 275 cm$^{3/}$g (data not shown). Again this gives an indication that materials with high adsorbed volumes have large pores. It is very likely related to the quality of the phase separation[80] which can exhibit very different sorption behaviour.

Figure 2.30 displays BET values as a function of F/FA (formaldehyde/formic acid) ratios in order to ascertain whether there is a relationship that can be established between the amount of formic acid per cross-linker (formaldehyde) and the BET surface area *i.e.* if large amounts of formic acid increase the cross-linking density, resulting in smaller domains (grains and pores) leading to rather high surface areas for such materials. However, materials are formed across the F/FA range with low and large surface areas as if no correlation between amount of catalyst and BET can be established. The samples with extremely low BET surface areas were transparent materials and the plots in Figure 2.29 and 2.30 verify that these samples are completely non-porous.

Note: analysis of a pure MF sample (GSL017PT1) was carried out at a later stage, thus the point has not been added to Figure 2.29 and 2.30. This sample had the largest surface area (218m^2/g) out of all the samples studied.
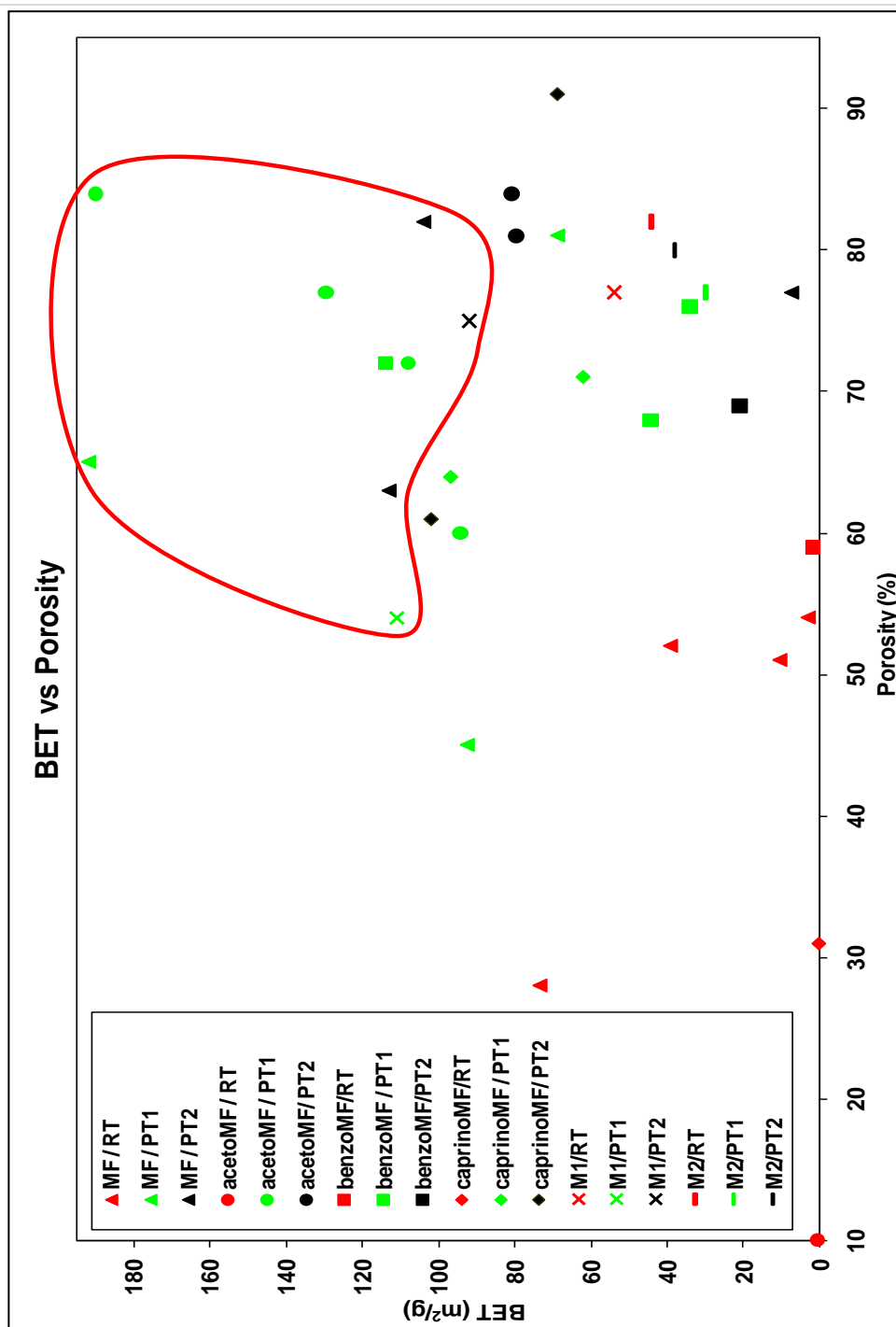
Figure 2.29: Porosity *vs*. BET of a selection of samples. Triangles represent pure MF materials, circles represent acetoguanamine-MF materials, squares represent benzoguanamine-MF materials and diamonds represent caprinoguanamine-MF materials. Also included are the samples containing the synthetic monomers 1 (cross) and 2 (dash). Colours are used to differentiate the drying methods. Red is used for samples dried at room temperature, green for samples post treated with butanol and black represents samples post treated with glutaraldehyde. The samples circled in red were also characterised by mercury intrusion measurements.
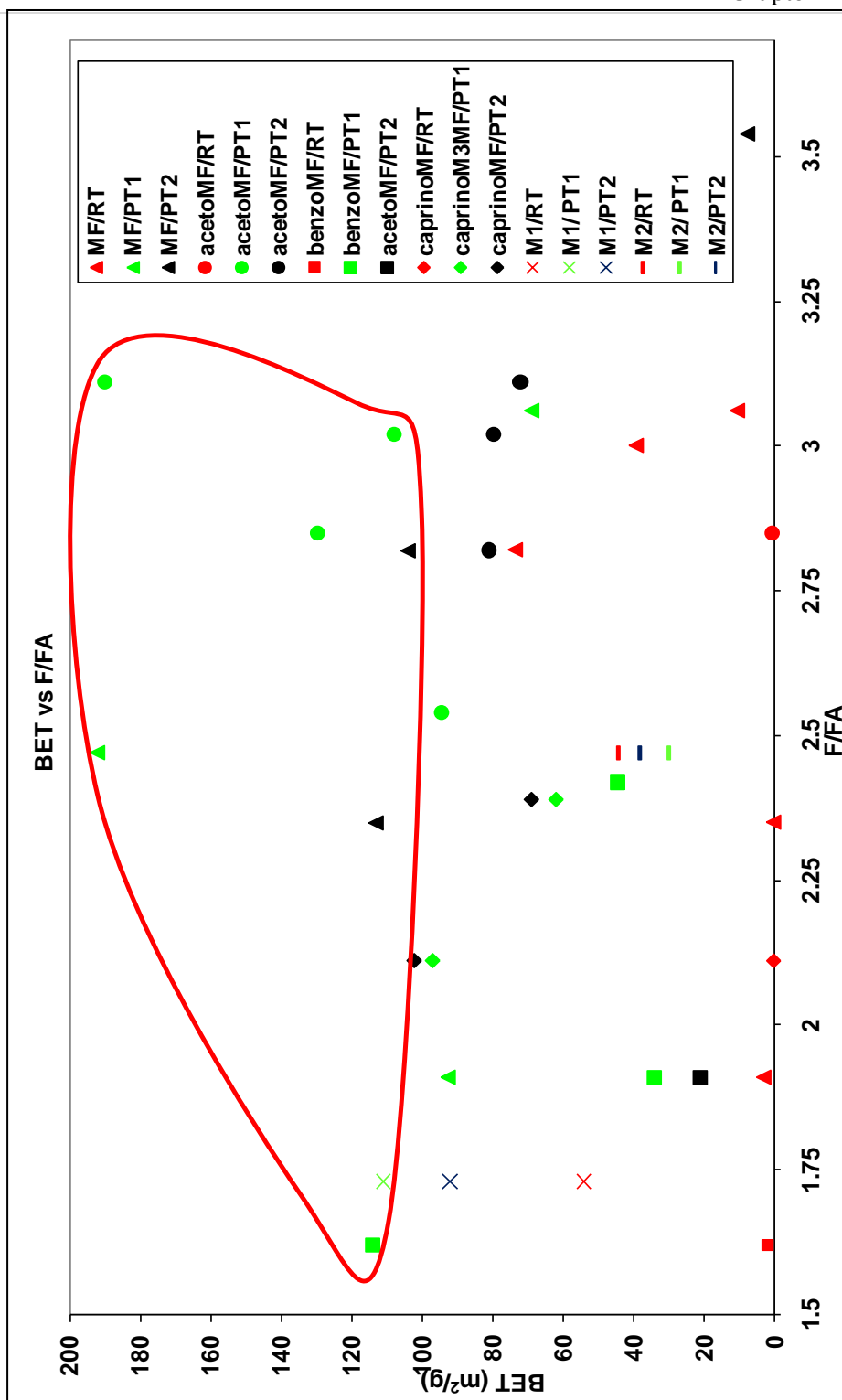
Figure 2.30: BET *vs* F/FA of a selection of samples. The triangles represent pure MF materials, the circles represent acetoguanamine-MF materials, the squares represent benzoguanamine-MF materials and the diamonds represent caprinoguanamine-MF materials. Also included are the samples containing the synthetic monomers 1 (cross) and 2 (dash). Colours are used to differentiate the drying methods. Red is used for samples dried at room temperature, green for samples post treated with butanol and blue represents samples post treated with glutaraldehyde. The samples circled in red were sent off for mercury intrusion measurements.

Although it was stated as a general observation, that nitrogen isotherms of MF materials studied in this work display similar characteristics, this is not completely true. Even though materials exhibit pores in the macroporous range, there are nuances as to whether the adsorption/desorption branches are similar or not. Figure 2.31 shows the isotherms of a pure MF material (GSL017PT) and materials containing the commercially available monomers (10% acetoguanamine-GLMMG1bPT1, 10% caprinoguanamine - GLMCP04PT1 and 20% acetoguanamine GLMMG045PT1). All samples have approximately the same porosities.
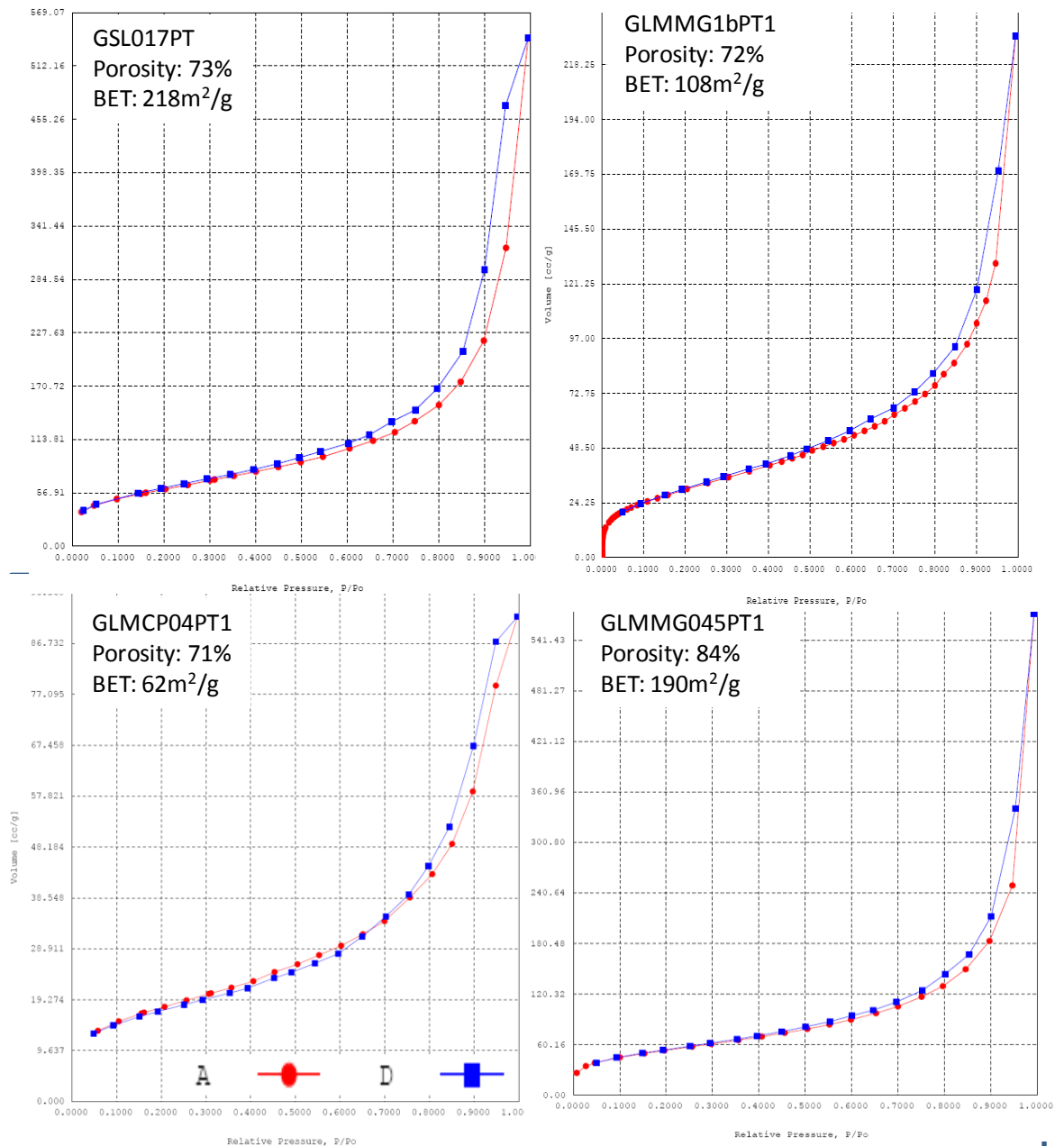
Figure 2.31: Typical isotherms of different MF materials with similar adsorption (red curve)/desorption (blue curve) isotherms. Top left: a pure MF sample. Top right: a MF sample containing 10% acetoguanamine. Bottom left: a MF sample containing 10% caprinoguanamine. Bottom right: a MF sample containing 20% acetoguanamine.

For each of the isotherms shown in Figure 2.31, the adsorption isotherm is very similar to the desorption branch (especially at low p/p_0). This indicates that the pores fill and empty in a similar way. This however is not the case for materials containing 10% benzoguanamine, 10% monomer 1 and 10% monomer 2, as shown in Figure 2.32.
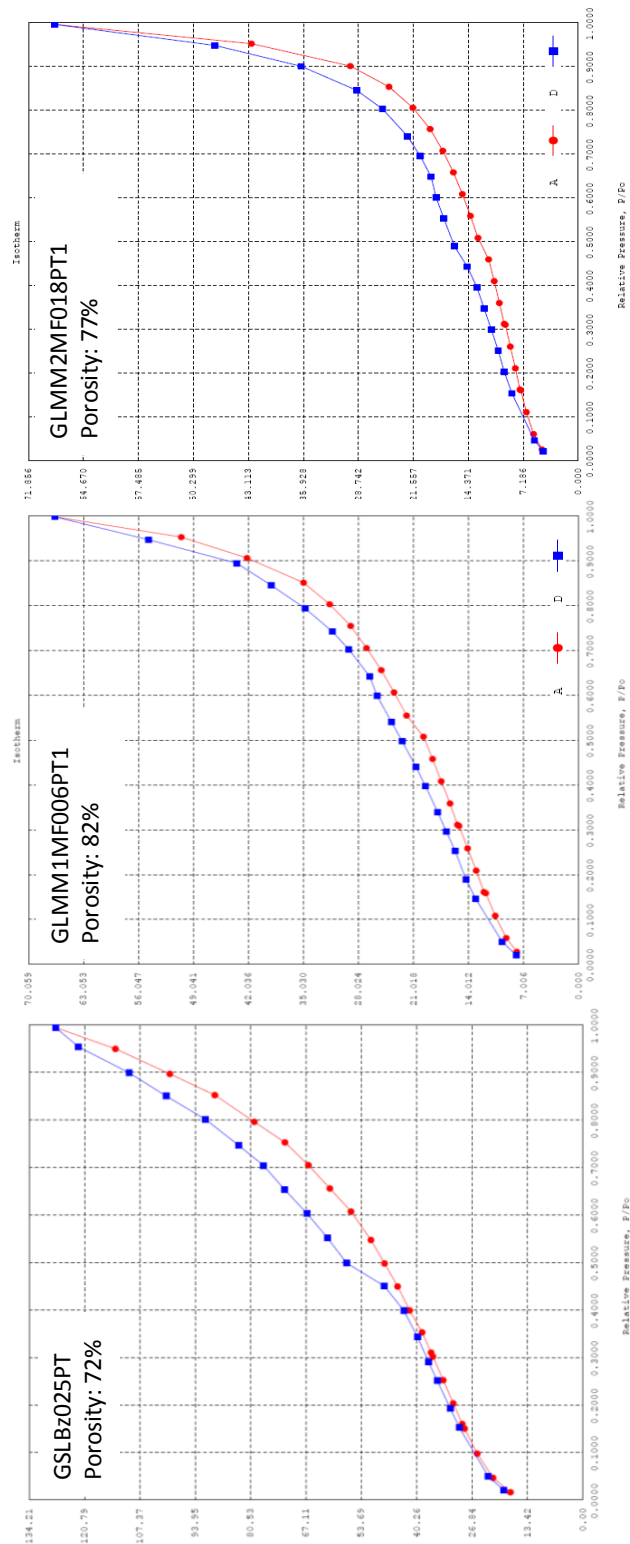
Figure 2.32: Typical isotherms of different MF materials containing hysteresis loops. Top:

a sample containing 10% benzoguanamine. Middle: a sample containing 10% monomer 1.

Bottom: a sample containing 10% monomer 2.

Here the adsorption and desorption isotherms produce a hysteresis loop. This indicates that the pores empty less easily than they fill, suggesting that pores are shaped like ink bottles. This may be due to the presence of more bulky substituents on these monomers directing pore sizes in the gel formation step[71].

Going back to Figure 2.29 and Figure 2.30, the samples circled in red were further analysed by mercury porosimetry.

3.2.2   Mercury Porosimetry

Mercury porosimetry is a well suited technique for the characterisation of macroporous networks as long as the material is strong enough (have high mechanical strength) to sustain the pressures applied to intrude mercury, a non-wetting liquid. Figure 2.33 shows the mercury intrusion trace of a particular sample.
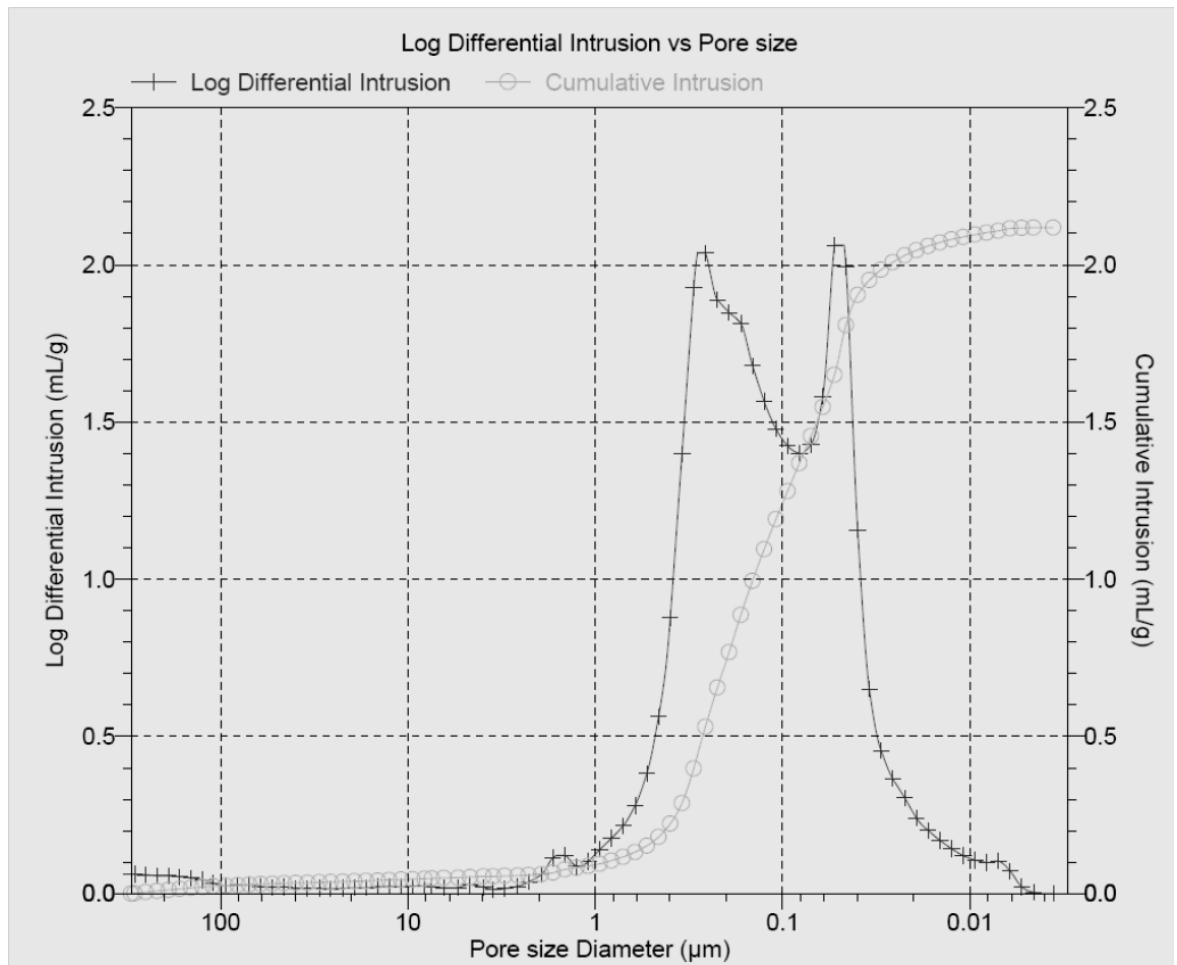
Figure 2.33: Mercury intrusion trace of GLMMG1bPT1. The trace shows that this

particular sample has a bimodal pore size distribution at 0.3µm and 0.05µm.

The cumulative intrusion trace shows the cumulative amount of mercury intruded for

each interval of pressure (already given here as pore size diameter, thanks to the

Washburn equation). Instead the differential intrusion, given as a log scale depicts the

amount of mercury intruded for each interval of pressure (pore size). The derivative plot

has the virtue of clearly identifying points of inflection, which in the case above shows

that the particular sample has a bimodal pore size distribution.

Mercury porosimetry is unavailable at Keele University, therefore samples were

analysed at BASF-SE. The different measurements carried out in-house (nitrogen sorption,

estimated porosity) are tabulated in Table 2.3 with the information obtained from

mercury intrusion.

Table 2.3: measurements using the different techniques described on a selection of samples.

Sample *	Estimated Porosity (%)	Calculated Mercury Porosimetry (%)	BET (m²/g)	Hg surface area (m²/g)	Hg Pore Sizes (µm)
GSL017PT1	73	75	218	107	0.8
GSL018PT1	65	75	192	109	0.5
GSL028PT2	63	61	113	114	0.05
GSL029PT2	82	71	50	44.5	0.2
GSLBZ025PT1	72	72	114	81	0.005 and 6
GLMMG1BPT1	77	78	108	114	0.15 and 0.05
GLMMG1CPT1	72	75	129	126	0.3 and 0.05
GSLMMG045(20%)	84	81	190	213	1
GM1MF05PT1	65	65	111	88	0.2
GM1MF05PT2	75	70	92	83	0.2
GM2MF018PT1	77	77	29	30	2

*the sample name refers to the names in Table 2.2.

Firstly, porosity estimations by geometric considerations are very similar to those

calculated using data from the mercury porosimetry measurements. The only

measurements that are different are for materials GSL018PT1 and GSL029PT2. However,

they still stand in the 10% error window for estimated porosities. Secondly the surface

area measurements obtained by mercury porosimetry and the BET calculations are also

very similar. This set of data consequently gives sufficient confidence that structural

characterisation of the MF networks prepared in this work are reliable (although, truly, as

pore sizes have only been tackled by mercury porosimetry, x-ray scattering measurements could also be useful).

3.3 Effect of synthesis parameters on the thermal behaviour

In the majority of the TGA/DSC traces, there are three main transitions corresponding to a steep vertical drop in the TGA trace and an endothermic peak in the DSC trace. Figure 2.34 shows the TGA and DSC profile of a pure M:F 1.5 sample post treated with butanol with a porosity of 54%. The different regions observed in the traces have been assigned to the following possible reactions occurring:

1- Loss of water around 100°C

2- Removal of formaldehyde and/or post treatment solvent and/ or strongly adsorbed water around 150-200°C

3- Thermal decomposition of the material around 300-400°C
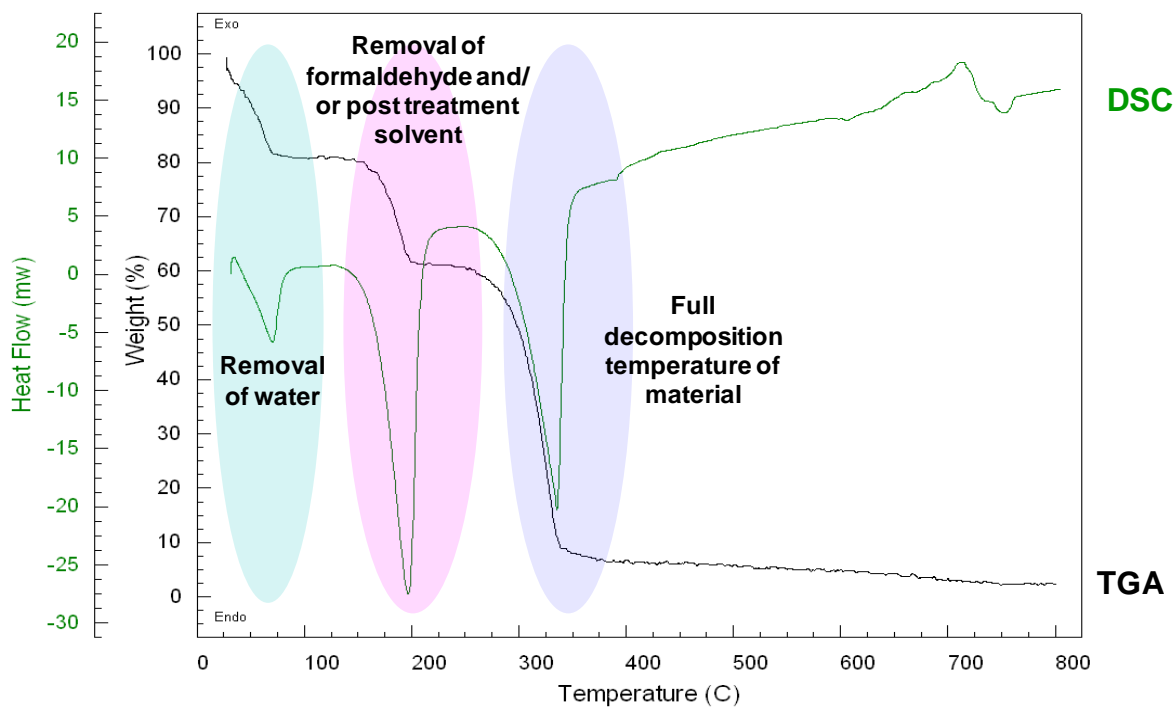
Figure 2.34: TGA/DSC trace of GSL014PT1, a 1:1.5 M:F sample post treated with butanol. The different transitions have been highlighted and labelled.

Most traces showed that the transition temperatures of decomposition are similar and that the addition of different monomers in 10% quantities does not have a significant impact the thermal stability of cross-linked MF materials.

In some cases, however, there seemed to be a slight increase in decomposition temperature with post treatments. This is shown in Figure 2.35, where the sample is post treated with glutaraldehyde. The DSC trace in this particular case suggests that thermal decomposition temperature is 450°C. (Note: the measurement was carried out all the way to 800°C, however).
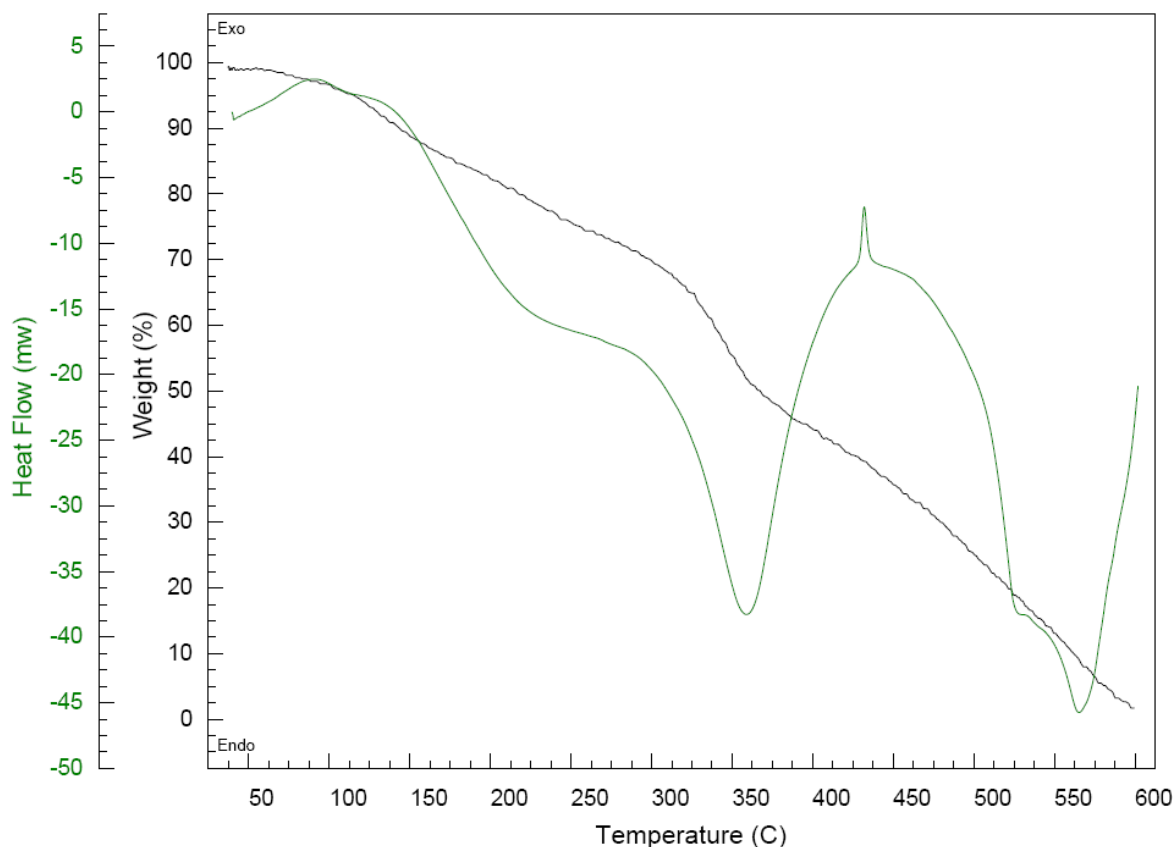
Figure 2.35: The TGA/DSC trace of GLMMG1cPTGlu, an acetoguanamine containing material post treated with glutaraldehyde. This particular sample has been post treated with glutaraldehyde and the traces suggest that the thermal decomposition has been increased compared to other systems usually displaying temperature within the 300-400°C.

Some traces show the merging of peaks due to loss of water and of formaldehyde, an example of which is displayed in Figure 2.36. This may be due to the heating ramp rate being set to 20°C a minute, which meant that the two steps were not distinct during the recording of the data.
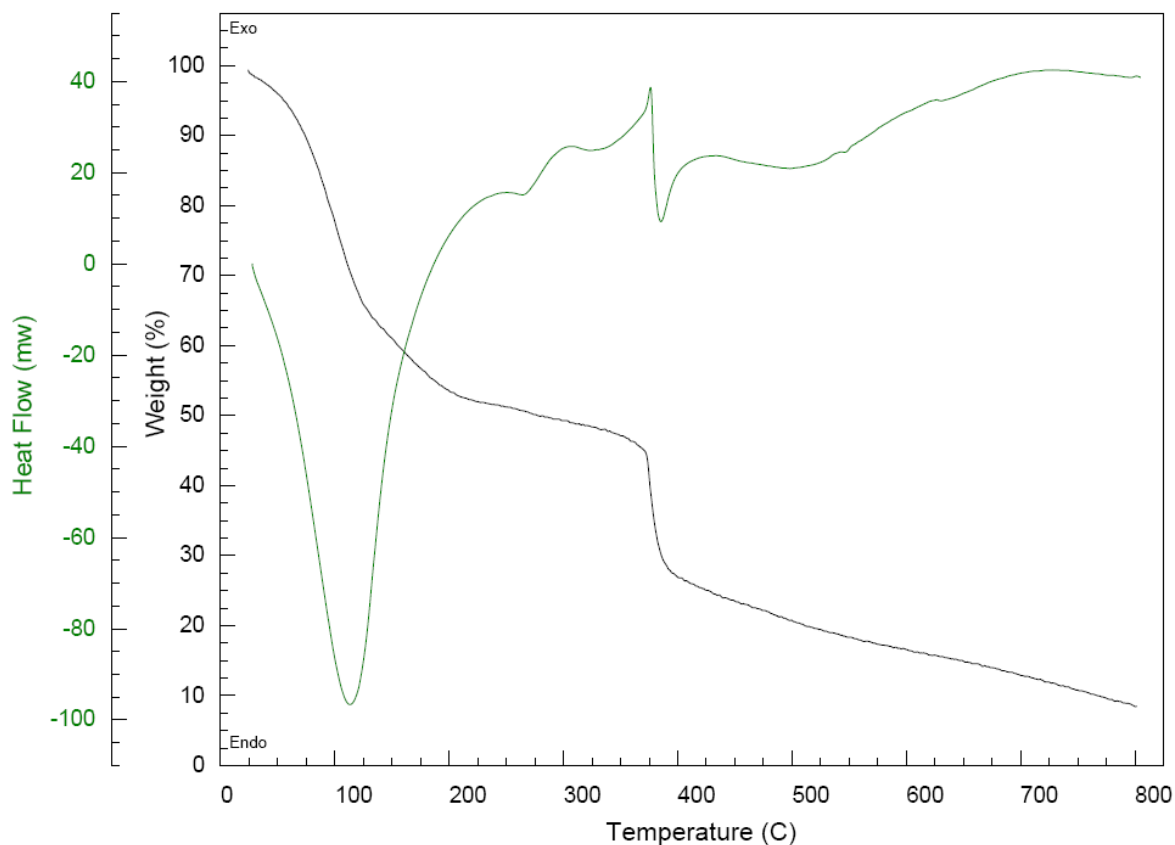
Figure 2.36: TGA/DSC trace of GLM05PT, a MF sample post-treated with butanol. In this trace the first two steps of formaldehyde release and water/post treatment solvent release have been merged and the loss occurs above 100°C.

To improve the TGA/DSC traces shown in Figures 2.35 and 2.36, the heat ramp rate could be lowered to 10°C/min. Also, In order to be more certain of what the dehydration/ decomposition temperatures correspond to, these experiments could be analysed using a TGA coupled to an FT-IR spectrometer, as used in the works of Hong *et al.* [72]and Hwang *et al.*[73]

Using TGA to quantify the amount of grafted butanol

Interestingly it was thought that the TGA trace could be used to determine how much butanol could have been grafted onto MF networks. The method is displayed below.
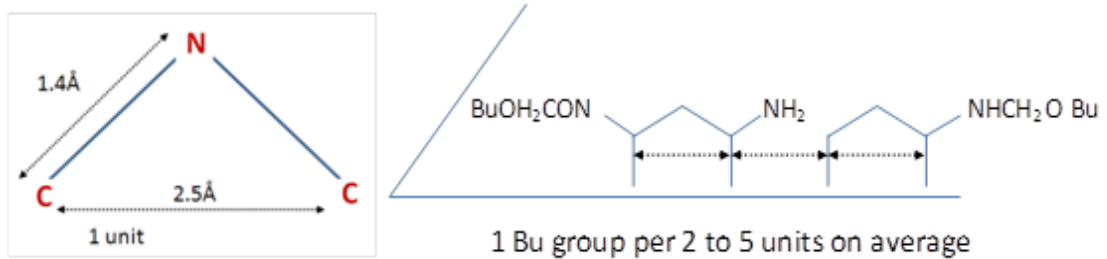
As an approximation, 1 Bu group in every 5Å to 12.5Å

In 1 g of a sample, on average the surface area is $100\ m^2$ ∴ $10m \times 10m$

$10m = 1 \times 10^{11}\text{Å}$

In 10^{11}Å there are $\dfrac{10^{11}}{12.5} = 8 \times 10^9$ Bu sites (min)   or $\dfrac{10^{11}}{5} = 2 \times 10^{10}$ Bu sites (max)

in $100\,m^2$ there are $(8 \times 10^9)^2 = 6.4 \times 10^{19}$ Bu sites (min)   or $(2 \times 10^{10})^2 = 4 \times 10^{20}$ Bu sites (max)

∴ 1.063×10^{-4} mol of Bu   ∴ 6.642×10^{-4} mol of Bu

∴ 7.88×10^{-3} g   ∴ 0.04923 g

∴ 1 g of sample contains 1 - 5% butanol

Figure 2.37: Approximate calculation strategy to quantify the grafting of butanol within the materials.

The calculation in Figure 2.37 assumes that all available hydroxyl sites react with butanol. Once the TGA traces of butanol post treated samples and their room temperature counterparts are obtained, the difference in weight loss calculated in the second decomposition temperature could then allow the interpretion of how much butanol has truly reacted on the available OH sites. However, as the weight loss is

between 1 and 5%, it is not obvious that the difference could easily be picked up on the TGA traces. However, this method could not be investigated further in the duration period of this project but may be worth looking into in future.

3.3 Effect of the synthesis parameters on phase separation

A sol is a dispersion of solid particles or polymers in a liquid. It is usually submicronic and acts as a nucleation site. A gel network results from the cross-linking of these polymeric clusters within the reaction solvent[24]. Phase separation, a competing process, occurs when a given polymer molecular weight of a polymer is reached and consists of it precipitating out from the solvent. Whether polymerisation is faster than phase separation (or even depolymerisation) will affect domain sizes and consequently pore sizes. Stability of polymeric aggregates will also influence the homogeneity of the final network[81.] Important factors that can hence influence this process are the nature of the precursors and the solvent, as well as the reaction conditions such as amount of acid catalyst and temperature of gelling.

When trends are identified between the porosity and the synthesis parameters, it is probably related to the thermodynamics and kinetics of phase separation. The amount of formic acid for instance affects gel transparency. Therefore both the degree of cross-linking and the size of the pore domain are parameters highly dependent on the phase separation process. Also, the incorporation of different monomers, notably benzoguanamine, seems to have an impact on the reaction mechanisms occurring during phase separation which carries over into the final material.

The higher porosities achieved with the incorporation of these monomers, even when dried at room temperature, could therefore be resulting from an earlier phase separation. As noticed previously, the incorporation of hydrophobic components, even in a 10% ratio, will decrease the overall polymer solubility, thus promoting early phase separation. Early phase separation can create MF networks with different morphologies, for instance thread like MF skeletons when strong acid catalysts are used[70] or more commonly, globular textures as shown in this work (SEM for benzoguanamine materials given in Figure 2.40). In both cases, though, large pore domains are formed. Pore/grain size is governed by interfacial energy and if solubility is decreased in the solvent, the surface area in contact with the solvent must be decreased. Table 3 shows the hydrophobic parameters associated with different organic substituents.

Table 2.4: Hydrophobic parameters of some common substituents.

| Substiuent	Hydrophobic parameter (π)[82]
Amino	-0.42
Hydrogen	0.00
Alanine	0.16 [83]
Methyl	0.58
Isopropyl	1.53
Phenyl	1.80
Butyl	2.13

The trend in this table helps to clarify why the dissolution of certain monomers is difficult during resin synthesis and may also give an insight into the mechanism of phase separation occurring at a microscopic level. However, viewing in-situ and dynamically the

process of phase separation (gelation) is virtually impossible to do. It is easier, but still challenging, to access the structure of the gel once it is formed[43, 84]. More commonly, the result of the phase separation process is investigated in the dried gel (the final material) using common structural techniques such as nitrogen sorption, mercury porosimetry and more routinely scanning electron microscopy (SEM).

In treated samples, the post-treatment is applied after gel synthesis; therefore it cannot affect phase separation. Instead it refrains pores from completely collapsing, so that pores accessed are a truer representation of the result of the phase separation process. (Note however the limitation in studying transparent gels containing high amounts of formic acid, where even post-treatment does not help pore retention).

Electron micrographs of all samples shown in Table 2 were carried out, to link pore sizes and grain size of the materials with BET surface area, mercury intrusion measurements and estimated porosity.

Firstly, it was noticed that successfully dried, pure MF materials had very fine textures with small grain sizes and open, homogenous networks, as shown in Figure 2.38.
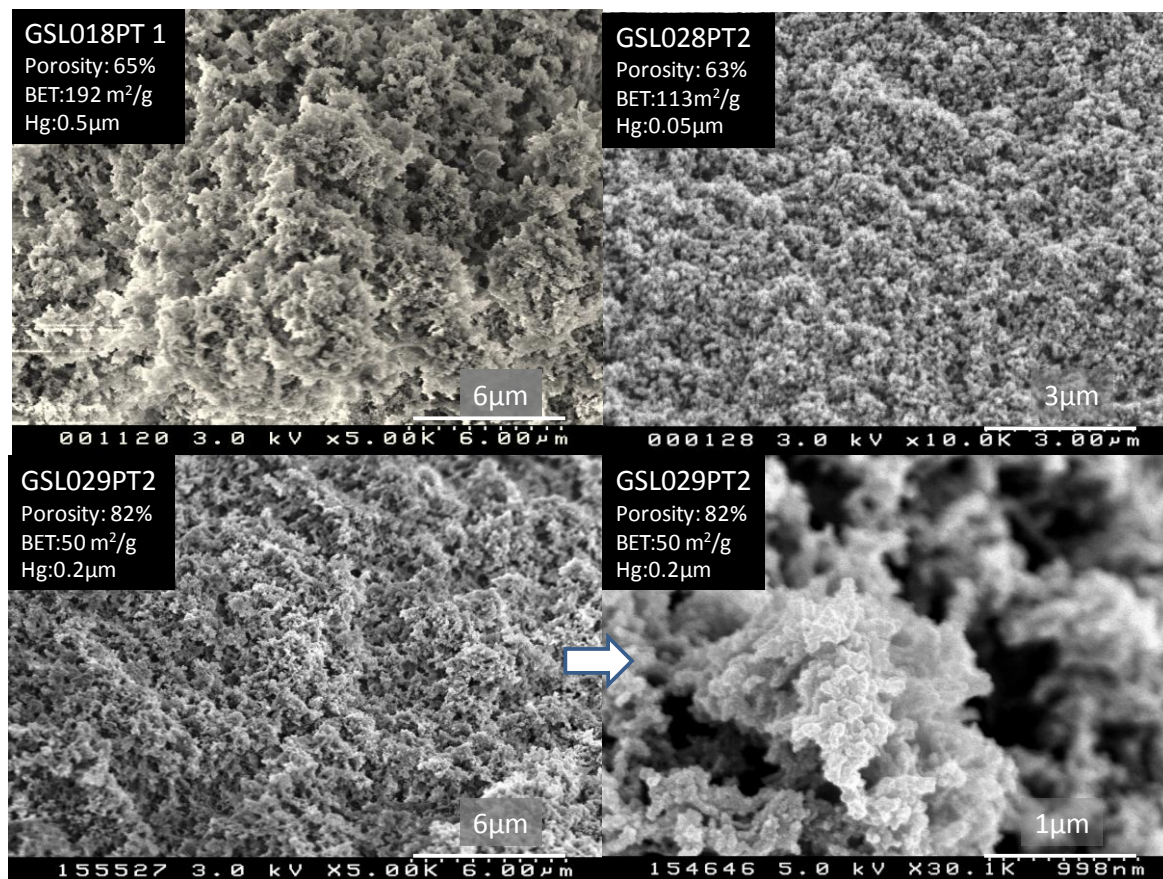
Figure 2.38: SEM micrographs of pure MF samples. GSL029PT2 (bottom left) has been magnified and shown on bottom right to display the grain size. These samples were all post-treated before drying and the micrographs show fine textures with homogenous, open networks (very small MF globules defining pores below 1μm).

Interestingly, materials formed with acetoguanamine had very similar textures to the pure MF samples, as shown in Figure 2.39. In fact the SEM micrographs suggest that GLMMG1cPT1, which has a similar porosity and slightly lower surface area than GSL018PT1, has a slightly more open structure. GLMMG045PT contains 20% acetoguanamine and the SEM micrographs show that a further change in hydrophobicity, by 20%, can still be successfully accommodated.
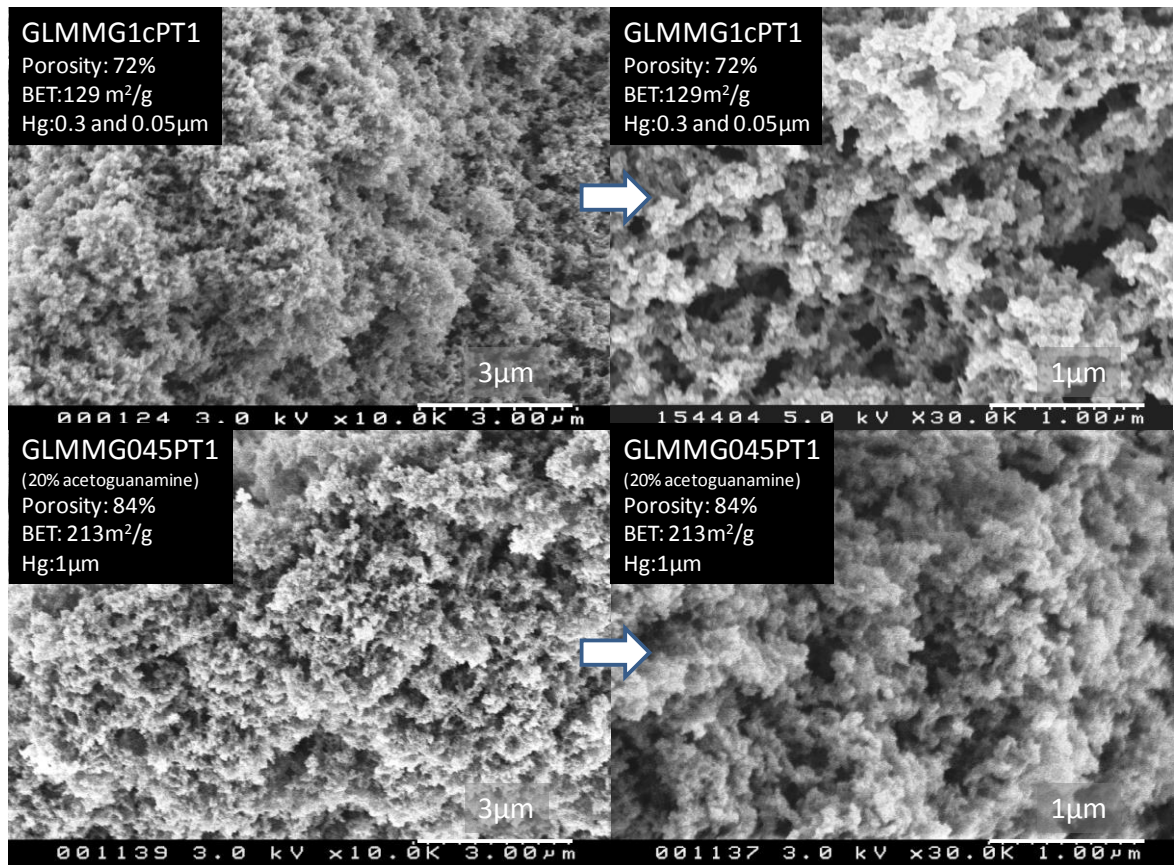
Figure 2.39: SEM micrographs of (top) GLMMG1cPT 1 a material containing 10% acetoguanamine and (bottom) GLMMG045PT, a material containing 20% acetoguanamine. The micrographs on the left are magnifications of the samples on the right. The networks are fine and open explaining why high surface areas are obtained with the incorporation of acetoguanamine into certain samples.

As suspected, the incorporation of benzoguanamine containing materials, however seems to lead to a different type of phase separation process. The structure is not as homogenous as previously encountered, the network is less fine and the MF globules are less defined (agglomerated into plaques or so). Pores seem much larger, even for a sample displaying a high surface area.
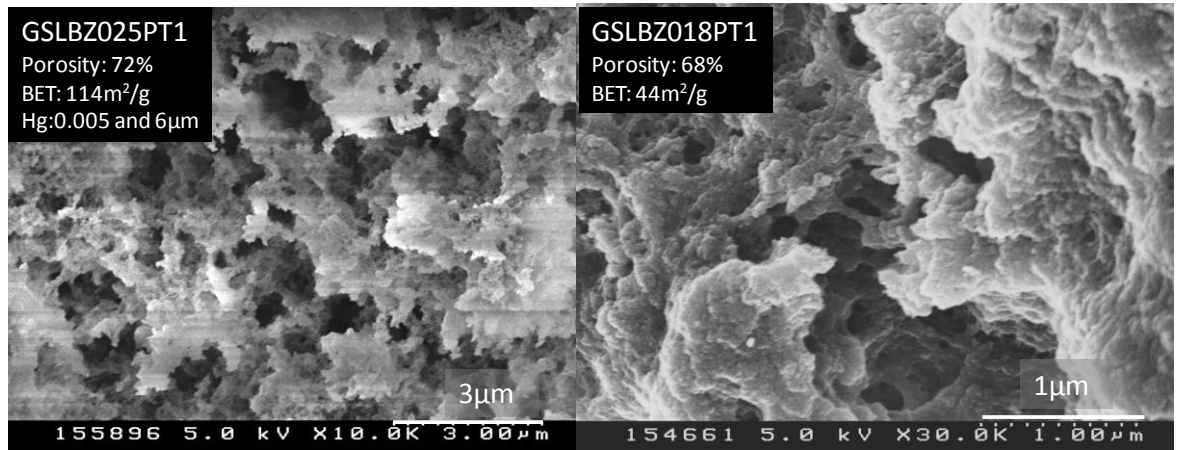
Figure 2.40: SEM micrographs of two samples containing 10% benzoguanamine with different BET surface areas. The images explain that samples have high calculated porosity value due to large voids within the material but the pore/grain sizes are not as fine as the samples seen previously. No mercury porosimetry data was carried out on GSLBZ018PT1.

Table 3 suggests that caprinoguanamine has a lower affinity for water than benzoguanamine. This was already seen by the amount of solid content remaining during resin synthesis, questioning if a substantial amount had actually dissolved. The SEM micrograph of one sample (GLMCP05RT) suggests that, even though it may not have fully dissolved, the amount that had has strongly changed the grain size of the network (Figure 2.41).
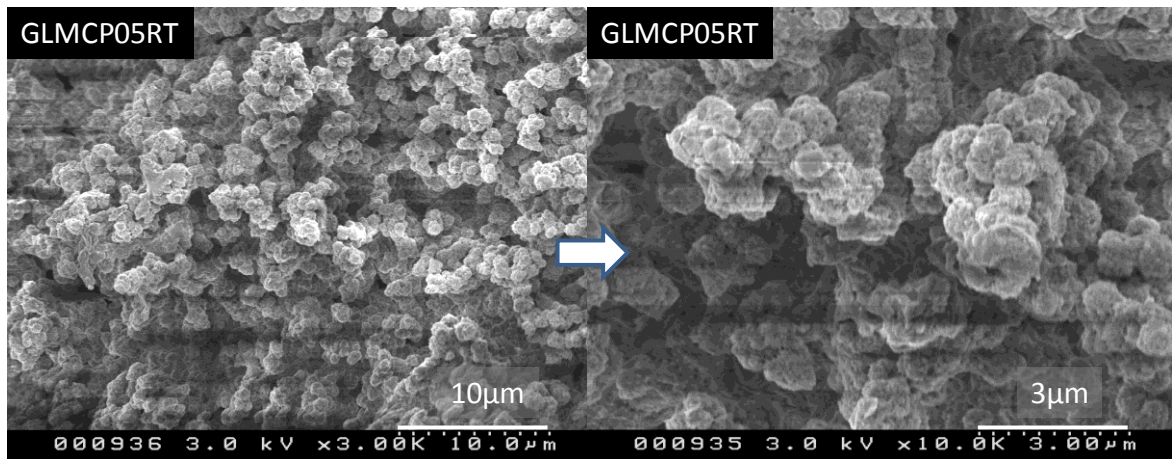
Figure 2.41: SEM micrographs of GLMCP05RT, a material containing 10%

caprinoguanamine. The presence of caprinoguanamine has affected the grain size of the

network thus suggesting that the pre polymer particles were larger clusters than those for

pure MF and acetoguanamine materials and even larger than that of benzoguanamine

materials (no estimated porosity or surface areas were measured due to sample cracking

during drying).

Finally, Figure 2.42 shows micrographs of materials containing the synthesised

monomers monomer 1 and 2. It was expected that the texture of the material containing

monomer 1 would be similar to that of the materials containing benzoguanamine. This,

however, does not seem to be the case. The material has quite a dense homogenous

surface, with smaller pores observed than those seen for GSLBZ025PT1. The texture is

alike that of MF or acetoguanamine containing MF materials (grains forming the network

delimiting pore domains).
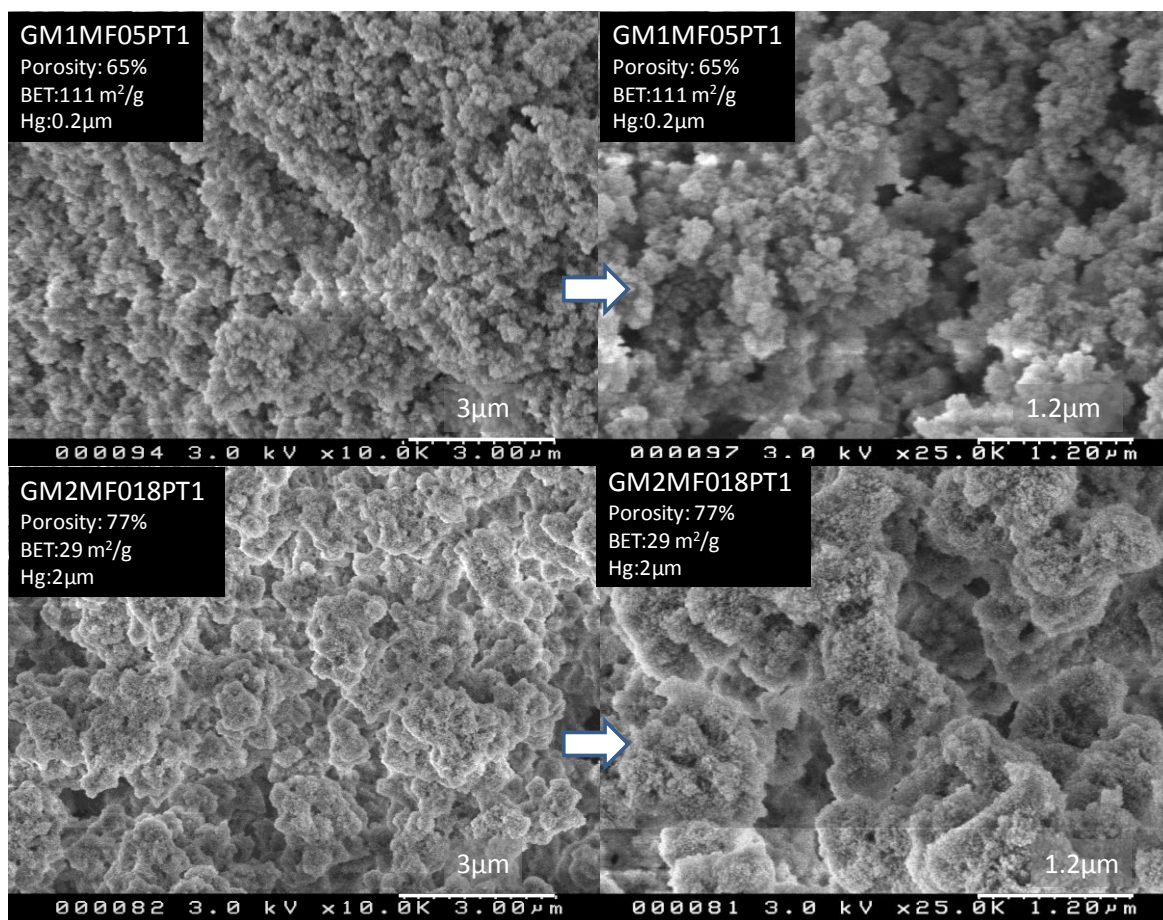
Figure 2.42: SEM micrographs of porous materials containing synthesised monomers, monomer 1 (top) and monomers 2 (bottom). The images on the right are higher magnifications of the micrographs on the right. The inclusion of monomer 1 in MF materials, give different surface textures to that observed for benzoguanamine. Materials containing monomer 2 have a dense heterogeneous structure.

The material containing monomer 2 also has a very different surface texture to the micrographs of the materials containing acetoguanamine. The phase separation seems coarser producing a dense heterogeneous network with rather large pore sizes (above 1μm), not too dissimilar to materials formed with caprinoguanamine.

4. Conclusions

From the results described and knowledge gained in this chapter, it is possible to say that the MF/FA window can be narrowed down in terms of porosity percentage. Samples go through a non-porous-porous transition from ratios of 0.6< MF/FA< 0.8. Below this region samples are completely non-porous, dense, transparent materials and post-treatment methods show no effect in enhancing pore retention. Above this ratio samples display maximum porosity as the samples are not fully cross-linked and pore sizes are too large to succumb capillary pressures to collapse pores within the structure. These findings are supported by nitrogen sorption data (high BET surface areas for post-treated samples visually showing evidence of enhancement in pore retention) and mercury porosimetry (small pore size distributions).

Also, with the work carried out with SEM shows that rather similar textures (essentially globular) are obtained with the use of formic acid, a weak catalyst, whatever the synthesis conditions used in this work compared to the SEMs carried out by other research groups using strong acids. SEM has also allowed to conclude that the quality of phase separation cannot be successfully predicted based on chemical structure of monomers, meaning the mechanism of phase separation is still eludes unclear. As Blank[63] mentioned, the counter anion from using the weak acid may play a significant role in this.

5. References

[1] Ishizaki, K., Komarneni, S., Nanko, M. (1998). *Porous materials: process technology and applications*, Kluwer Academic Publishers.

[2] Mueller, U., Schubert, M., Teich, F., Puetter, H., Schierle-Arndt, K., Pastre, J. (2006). "Metal-organic frameworks-prospective industrial applications." *J. Mater. Chem.* **16**(7): 626-636.

[3] Yu, J.-S., Kang, S,, Yoon, S. B., Chai, G., (2002). "Fabrication of Ordered Uniform Porous Carbon Networks and Their Application to a Catalyst Supporter." *J. Am. Chem. Soc*. **124**(32): 9382-9383.

[4] Sayers, C. M. (1981). "Ultrasonic velocity dispersion in porous materials." Journal of Physics D: Applied Physics **14**(3): 413.

[5] Yang, P. D., Rizvi, A. H., Messer, B., Chmelka, B. F., Whitesides, G. M., Stucky, G. D. (2001). "Patterning porous oxides within microchannel networks." *Adv. Mater.* **13**(6): 427-431.

[6] Ellerby, L. M., Clinton, R. N., Nishida, F., Yamanaka, S. A., Dunn, B., Valentine, J., S., Zink, J I. (1992). "Encapsulation of Proteins in Transparent Porous Silicate Glasses Prepared by the Sol-Gel Method." *Science* **255**(5048): 1113-1115.

[7] Whitesides, G. M., Ostuni, E., Takayama, S., Jiang, X., Ingber, D E. (2001). "Soft Lithography in Biology and Biochemistry." *Annual Review of Biomedical Engineering* **3**(1): 335.

[8] Avnir, D., Coradin, T., Lev, O., Livage, J. (2006). "Recent bio-applications of sol-gel materials. " *J. Mater. Chem.* **16**(11): 1013-1030.

[9] Davis, M. E. (2002). "Ordered porous materials for emerging applications." *Nature* **417**(6891): 813-821.

[10] Zaworotko, M. J. (2008). "Materials science: Designer pores made easy." *Nature* **451**(7177): 410-411.

[11] Sing, K. S. W.; Everett, D., Haul, R. A. W., Moscou, L., Pierotti, R. A., Rouquerol, J., Siemieniewska, T. (1985)." Reporting Physisorption Data for gas/ solid systems with Special Reference to the Determination of Surface Area and Porosity". *Pure Appl.Chem.* **1985**, *57*, 603.

[12] Yanagisawa, T., Shimizu, T., Kuroda, K., Kato, C. (1990). "The Preparation of Alkyltrimethylammonium-Kanemite Complexes and Their Conversion to Microporous Materials." *Bull. Chem. Soc. Jap.* **63**(4): 988-992.

[13] Kresge, C. T., Leonowicz, M. E., Roth, W. J., Vartuli, J. C., Beck, J. S. (1992). "Ordered Mesoporous Molecular-Sieves Synthesized by a Liquid-Crystal Template Mechanism." *Nature* **359**(6397): 710-712.

[14] Zhao, X. S., Su, F., Yan, Q., Guo, W., Bao, X. Y., Lv, L., Zhou, Z. (2006). "Templating methods for preparation of porous structures." *J. Mater. Chem.* **16**(7): 637-648.

[15] Hoa, M. L. K., Lu, M., Zhang, Y. (2006). "Preparation of porous materials with ordered hole structure." *Adv. Colloid Interface Sci.* **121**(1-3): 9-23.

[16] Studart, A. R., Gonzenbach, U. T., Tervoort, E. and Gauckler, L. J. (2006), Processing Routes to Macroporous Ceramics: A Review. *J. Am. Cer. Soc.,* 89: 1771–1789.

[17] Brian, F., Henry, R., Richard, T., Rodney, R., Robert, R. K. (2000). "Bilayer, nanoimprint lithography." *J. Vac. Sci. Technol. B*. **18**(4): 1866-1873.

[18] Hench, L. L. and West J. K. (1990). "The Sol-Gel Process." *Chem. Rev.* **90**(1): 33-72.

[19] Hüsing, N. and Schubert U. (1998). "Aerogels-Airy Materials: Chemistry, Structure, and Properties." *Angew. Chem. Inter. Ed.* **37**(1-2): 22-45.

[20] Hüsing, N. and Schubert U. (2000). *Aerogels*, Wiley-VCH Verlag GmbH & Co. KGaA.

[21] Pierre, A. C. and Pajonk , G. M., (2002). "Chemistry of Aerogels and Their Applications." *Chem. Rev*. **02**(11): 4243-4266.

[22] Egger, C. C. (2009). *Modern Trends in Macromolecular Chemistry*, Nova. Editor: Lee, J. N. (chapter 4, pages 81-88)

[23] Jeffrey Brinker C. and Scherer, G. W. (1990). *Sol-gel science: the physics and chemistry of sol-gel processing*, Academic Press.

[24] Gonzalez, R. D., Lopez, T., Gomez, R. (1997). "Sol-Gel preparation of supported metal catalysts." *Catalysis Today* **35**(3): 293-317.

[25] Schmidt, M. and Schwertfeger F. (1998). "Applications for silica aerogel products." *J. Non-Cryst. Sol.* **225**: 364-368.

[26] Kumar, A., Gaurav, Malik, A. K., Tewary, D. K., Singh, B. (2008). "A review on development of solid phase microextraction fibers by sol-gel methods and their applications." *Anal. Chim. Acta* **610**(1): 1-14.

[27] Avnir, D. (1995). "Organic Chemistry within Ceramic Matrixes: Doped Sol-Gel Materials." *Acc. Chem. Res.* **28**(8): 328-334.

[28] Schubert, U., Huesing, N., Lorenz, A. (1995). "Hybrid Inorganic-Organic Materials by Sol-Gel Processing of Organofunctional Metal Alkoxides." *Chem. Mater.* **7**(11): 2010-2027.

[29] Bandyopadhyay, A., Sarkar, M., Bhowmick, A. K. (2005). "Polymer–filler interactions in sol–gel derived polymer/silica hybrid nanocomposites." *J. Polym. Sci. B: Polym. Phys.* **43**(17): 2399-2412.

[30] MacCraith, B. D., McDonagh, C. M., O'Keeffe, G., McEvoy, A. K., Butler, T., Sheridan, F. R. (1995). "Sol-gel coatings for optical chemical sensors and biosensors." *Sensor Actuat. B. Chem.* **29**(1-3): 51-57.

[31] Brinker, C. J., Hurd, A. J., Schunk, P. R., Frye, G. C., Ashley, C. S. (1992). "Review of sol-gel thin film formation." *J. of Non-Cryst. Sol.* **147-148**: 424-436.

[32] Innocenzi, P., Kidchob, T., Yoko, T. (2005). "Hybrid organic-inorganic sol-gel materials based on epoxy-amine systems." *J. Sol-Gel Sci Tech.* **35**(3): 225-235.

[33] Lev, O., Wu, Z. , Bharathi, S., Glezer, V., Modestov, A., Gun, J., Rabinovich, L., Sampath, S. (1997). "Sol-Gel Materials in Electrochemistry." *Chem. Mater.* **9**(11): 2354-2375.

[34] Nakanishi, K., Minakuchi, H., Soga, N., Tanaka, N. (1998). "Structure Design of Double-Pore Silica and Its Application to HPLC." *J. Sol-Gel Sci Tech.* **13**(1): 163-169.

[35] Chen, Z., Uchiyama, K., Hobo, T. (2002). "Chemically modified chiral monolithic silica column prepared by a sol-gel process for enantiomeric separation by micro high-performance liquid chromatography." *J. Chromatogr. A* **942**(1-2): 83-91.

[36] Siouffi, A. M. (2003). "Silica gel-based monoliths prepared by the sol-gel method: facts and figures." *J. Chromatogr. A* **1000**(1-2): 801-818.

[37] Egger, C. C. internal communication

[38] Hans-Jürgen Butt, Karlheinz Graf, Michael Kappl (2003). *Physics and chemistry of interfaces,* Wiley VCH.

[39] Kirkbir, F., Murata, H., Meyers, D., Chaudhuri, S. R. (1998). "Drying of aerogels in different solvents between atmospheric and supercritical pressures." *J.Non-Cryst. Sol*. **225**(1): 14-18.

[40] Shi, F., Wang, L. J., Liu, J. X. (2006). "Synthesis and characterization of silica aerogels by a novel fast ambient pressure drying process." *Mater. Lett.* **60**(29-30): 3718-3722.

[41] Hwang, S. W., Kim, T. Y., Hyun, S. H. (2008). "Optimization of instantaneous solvent exchange/surface modification process for ambient synthesis of monolithic silica aerogels." *J. Colloid Interface Sci.* **322**(1): 224-230.

[42] Egger, C. C., Schadler, V., Hirschinger, J., Raya, J., Bechinger, B. (2007). "H-1-C-13 CPMAS and T-2 relaxation solid-state NMR measurements of melamine-based polycondensed chemical gels." *Macromol. Chem. Phys.* **208**(21): 2375-2375.

[43] Rigacci, A., Marechal, J. C., Repoux, M., Moreno, M., Achard, P. (2004). "Preparation of polyurethane-based aerogels and xerogels for thermal superinsulation." *J. Non-Cryst. Solids* **350**: 372-378.

[44] Pekala, R. W., Farmer, J. C., Alviso, C. T., Tran, T. D., Mayer, S. T., Miller, J. M., Dunn, B.. (1998). "Carbon aerogels for electrochemical applications." *J. Non-Cryst. Solids* **225**: 74-80.

[45] Pekala, R. W. and Schaefer, D. W. (1993). "Structure of organic aerogels. 1. Morphology and scaling." *Macromolecules* **26**(20): 5487-5493.

[46] Zhang, R., Li, W., Liang, X. Y., Wu, G. P., Lu, Y. G., Zhan, L., Lu, C. X., Ling, L. C. (2003). "Effect of hydrophilic groups in the polymer matrix on the porosity of organic and carbon aerogels produced from melamine, phenolic resole and formaldehyde." *Microporous Mesoporous Mater.* **62**(3): 17-27.

[47] Ruben, G. C., (1995). "High-resolution transmission electron microscopy of the nanostructure of melamine-formaldehyde aerogels." *J. Non-Cryst. Solids* **186**: 219-231.

[48] Blank, W. and Hensley, W. L. (1974). "Use of Amino Based Resins in Water Based Coatings." *J. Paint Technol.* **46**(593): 46-53.

[49] Jones, F. N., Chu, G. B. Samaraweera, U. (1994). "Recent studies of self-condensation and co-condensation of melamine-formaldehyde resins- cure at low-temperatures." *Prog. Org. Coat.* **24**(1-4): 189-208.

[50] Parfitt, G. D. (1986). "Curing of Melamine Resins." *Org. Coat. Sci. and Techn.* **8**: 125-138.

[51] Dieter Stoye, Werner Freitag, Günter Beuschel (1996). *Resins for coatings: chemistry, properties, and applications*, Hanser (pg 109-122).

[52] Rätzsch, M., Bucka, H., Ivanchev, S., Pavlyuchenko, V., Leitner, P., Primachenko, O. N. (2004). "The Reaction Mechanism of the Transetherification and Crosslinking of Melamine Resins." *Macromolecular Symposia* **217**(1): 431-443.

[53] Larkin., P. J. (1998). "Vibrational analysis of some important group frequencies of melamine derivatives containing methoxymethyl, and carbamate substituents: mechanical coupling of substituent vibrations with triazine ring modes." *Vib. Spectrosc.* **17**: 53-72.

[54] Scheepers, M. L., Gelan, J. M. Carleer, R. A., Adriaensens, P. J., Vanderzande, D. J. Kip, B. J., Brandts, P. M. (1993). "Investigation of Melamine-Formaldehyde Cure by Fourier-Transform Raman-Spectroscopy." *Vib. Spectrosc.* **6**(1): 55-69.

[55] Chang, T. T. (1994). "Characterization of (Methoxymethyl)melamine Resins by Liquid Chromatography/Mass Spectrometry." *Anal. Chem.* **66**(19): 3267-3273.

[56] Chang, T. T. "Novel approaches to characterization of melamine coating resins." *Prog. Org. Coat.* **29**(1-4): 45-53.

[57] Tomita, B. and H. Ono (1979). "melamine-formaldehyde resins – constitutional characterisation by fourier-transform C-13-NMR spectroscopy." *J. Polym. Sci., Part A: Polym. Chem.* **17**(10): 3205-3215.

[58] Ebdon, J. R., Hunt, B. J. Orourke, W. T. S., Parkin, J. (1988). "Characterization of Some Melamine Formaldehyde Condensates and Some Cured Resins by H-1, C-13 and N-15 Nmr-Spectroscopy." *Br. Polymer J.* **20**(4): 327-334.

[59] Hirt, R. C. and Schmitt R. G. (1958). "Ultraviolet absorption spectra ot derivatives of symmetric triazine--II: Oxo-triazines and their acyclic analogs." *Spectrochim. Acta.* **12**(2-3): 127-138.

[60] Dixon, J. K., Woodberry, N. T., Costa, G. W. (1947). "The Dissociation Constants of Melamine and Certain of its Compounds." *J.Am. Chem. Soc.* **69**(3): 599-603.

[61] Kim, S. and Kim H.-J. (2005). "Comparison of standard methods and gas chromatography method in determination of formaldehyde emission from MDF bonded with formaldehyde-based resins." *Bioresour. Technol.* **96**(13): 1457-1464.

[62] Blank, W. J. (1979). "Reaction-Mechanism of Melamine Resins." *J. Coat. Technol.* **51**(656): 61-70.

[63] Nelson G. L, Hoyle C. E, Storey R. F. (1988). "New approaches to overcoming kinetic limitations of the latent catalysts for the curing of the high solids coatings." *Proceedings of the fifteenth water-borne and higher solids coatings symposium:* 33-37.

[64] Berge, A. and Mejdell T. (2006). "Melamine formaldehyde compounds. The active species in acid catalyzed reactions." *Polymer* **47**(9): 3249-3256.

[65] Lide, D. R. (1993). *CRC handbook of chemistry and physics*, CRC Press, p 845

[66] Scheepers, M. L., Meier, R. J., Markwort, L., Gelan, J. M., Vanderzande, D. J., Kip, B. J. (1995). "Determination of free melamine content in melamine-formaldehyde resins by raman-spectroscopy." *Vib. Spectrosc*. **9**(2): 139-146.

[67] Goworek, J., Derylo-Marczewska, A., Stefaniak, W., Zgrajka, W., Kusak, R. (2003). "Absorption/adsorption properties of porous phenolic-formaldehyde and melamine-formaldehyde polymers." *Mater. Chem. Phys.* **77**(1): 276-280.

[68] Baraka, A., Hall, P. J., Heslop, M. J. (2007). "Preparation and characterization of melamine-formaldehyde-DTPA chelating resin and its use as an adsorbent for heavy metals removal from wastewater." *React. Funct. Polym.* **67**(7): 585-600.

[69] Egger, C. C., du Fresne, C., Schadler, V. (2008). "Characterization of highly porous polymeric materials with pore diameters larger than 100 mn by mercury porosimetry and X-ray scattering methods." *Langmuir* **24**(11): 5877-5887.

[70] Von Hohenesche, C. D., Schmidt, D. F. Schlader, V. (2008) "Nanoporous Melamine-Formaldehyde Gels by Microemulsion Templating" *Chem. Mat.* **20**(19): 6124-6129

[71] Hong, K. and Park S. (1999). "Melamine resin microcapsules containing fragrant oil: synthesis and characterization." *Macromol. Chem. Phys.* **58**(2): 128-131.

[72] Hwang, J.-S., Kim, J.-N., Wee, Y-J., Yun, J-S., Jang, H-G, Kim, S-H, Ryu, H-W (2006). "Preparation and characterization of melamine-formaldehyde resin microcapsules containing fragrant oil." *Biotechnol. Bioprocess. Eng.* **11**(4): 332-336.

[73] Devallencourt, C., Saiter, J. M., Capitaine, D.. (2000). "Reactions between melamine formaldehyde resin and cellulose: Influence of pH." *J. Appl. Polym. Sci.* **78**(11): 1884-1896.

[74] Costa L (1988). "Thermal Behaviour of Melamine." *J. Therm. Anal.* **34**: 423-429.

[75] Ruben G.C. (1995). "High-resolution transmission electron microscopy of the nanostructure of melamine-formaldehyde aerogels." *J. Non-Cryst. Solids.* **186**: 219-231.

[76] Ingleson, M. J., Perez Barrio, J. Guilbaud, J-B., Khimyak, Y. Z., Rosseinsky, M J. (2008). "Framework functionalisation triggers metal complex binding." *Chem. Commun.* (23): 2680-2682.

[77] Rajabi, F., Ghiassian, S., Saidi, M. R. (2010) "Efficient Co(ii) heterogeneously catalysed synthesis of [small alpha]-aminonitriles at room temperature via Strecker-type reactions." *Green Chem.* **12**(8): 1349-1352.

[78] Carey, F. A. and Sundberg R. J. (2007). p46 *Advanced organic chemistry: Reactions and synthesis*, Springer.

[79] Thomas, J. M. and Thomas, W. J. (1997). *Principles and practice of heterogeneous catalysis*, VCH.

[80] Egger, C., du Fresne, C., Schmidt, D., Yang, J., Schädler, V. (2008). "Design of highly porous melamine-based networks through a bicontinuous microemulsion templating strategy." *J. Sol-Gel Sci. Technol.* **48**(1): 86-94.

[81] Nakanishi, K. (1997). "Pore Structure Control of Silica Gels Based on Phase Separation." *J. Porous Mater.* **4**(2): 67-112.

[82] Corwin, H., Leo, A., Hoekman, D. H. (1995). *Exploring QSAR.: Fundamentals and applications in chemistry and biology*, American Chemical Society.

[83] Sotomatsu-Niwa, T. and Ogino A.,(1997). "Evaluation of the hydrophobic parameters of the amino acid side chains of peptides and their application in QSAR and conformational studies." *J. Mol. Struct.* **392**: 43-54.

CHAPTER 3: Characterising Chemical Functionality within MF Networks

Contents

1. Introduction

In this chapter the nature of chemical functions within the MF networks prepared in this work is investigated so as to allow the possible evaluation of polarity and reactivity of the networks and therefore their potential ability to recognise analytes.

The methods available to analyse chemical functions which may be present within cross-linked polymers are fewer in number than those available to analyse monomers, mainly due to the insolubility of such polymers in solvents. Therefore techniques such as solution-state NMR and liquid or gas chromatography coupled to mass spectrometers are more difficult or even impossible to apply to highly cross-linked polymers. However, there are other analytical techniques for chemical characterisation adapted to solids. In this chapter the infrared characterisation of the different materials described in chapter 2 are primarily discussed, as well as their Raman and solid-state NMR spectra.

1.1 Infrared spectroscopy of melamine

Melamine **1** (1,3,5-triazine-2,4,6-triamine) contains an aromatic ring with alternating carbon-nitrogen bonds (triazine) and side chain nitrogen atoms (amino groups). Therefore its main infrared properties are characterised by the interactions between π-electrons in the triazine ring and lone-pair electrons in the amino groups. According to the works of Ashrafi et al.[1], if melamine is assumed to be planar, it falls into the point group D_{3h}, the same as 1,3,5 triazine which possesses seven infrared vibrations[2].

D_{3h}	E	2C3	3C_2	σ_h	2S_3	3σ_v		
A_1'	1	1	1	1	1	1		x^2+y^2, z^2
A_2'	1	1	-1	1	1	-1	R_z	x^2-y^2, xy
E'	2	-1	0	2	-1	0	x,y	
A_1''	1	1	1	-1	-1	-1		
A_2''	1	1	-1	-1	-1	1	z	
E''	2	-1	0	-2	1	0	R_x, R_y	xz, yz

$2A_2'' + 5E'$
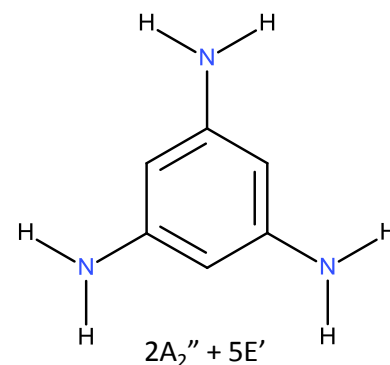
Figure 3.1: D_{3h} character table and ball and structure of melamine.[3]

Early IR studies by Padgett *et al.*[4] described triazine ring systems as having two main regions, one with strong bands at 1560-1450 cm^{-1} due to in-plane vibrations and one with weaker bands at 815 cm^{-1} due to out-of-plane vibrations. After analysing melamine and other mono-substituted melamine derivatives, the group noted that three regions occurred: one near 3000 cm^{-1}, another between 1660-1430 cm^{-1} and one just beyond 830 cm^{-1}.

The first region includes N-H stretching at 3500-3000 cm^{-1} and C-H stretching due to the C-H bond(s) present on substituted groups at 2900- 2800 cm^{-1}. The second region, as well as including the in-plane vibrations of the triazine ring also includes vibrations of the side chain amino groups usually with three or four large bands, the most intense being at 1550-1450 cm^{-1}.

According to the work done by Goubeau *et al.*[2] on the simple molecule 1,3,5-triazine, the bands at 1560 and 1410 cm^{-1} correspond to the ring stretching, therefore the weaker peaks at 1700-1600 cm^{-1} can be assigned solely to NH$_2$. In this region, C-H deformation vibrations should also occur and this will be discussed in more depth when analysing the

spectra of the commercially available melamine derivatives- acetoguanamine and caprinoguanamine. C-C aromatic ring vibrations are usually in this region too, and this will also be further discussed when looking into the spectrum of benzoguanamine, another commercially available melamine derivative.

Padgett *et al.*[4] also described the region after 850 cm^{-1} as "interesting" since it contains a sharp peak at around 810 cm^{-1}, which is present in melamine and all mono-substituted derivatives and is almost constant in position with slight variations depending on the electron donating/ accepting groups interacting with the triazine ring (according to Larkin *et al.*[5], it should always be in the region of 815± 7 cm^{-1} and is due to the triazine ring sextant out-of-plane bend).

In the formation of MF resins and crossed-linked materials, IR spectroscopy allows to see transformations primarily in the NH$_2$ region, as these functions disappear, plus a band due to OH stretching should appear near 3350 cm^{-1}. Other bands, due to the introduction of CH$_2$, should become visible as well as C-O stretching vibrations that should occur at 1040 cm^{-1}. The table below (Table 3.1) gathers the different vibrations in melamine discussed in this section.

Table 3.1: The different IR regions and assignments for melamine in 4000 cm^{-1} to 700 cm^{-1} region[1-5].

Vibration band region (cm^{-1})	Assignment in melamine
3000	-NH$_2$ stretching
1700-1600	-NH$_2$
1550-1450	Triazine ring stretching C-N side chain stretching
815	Out of plane triazine bend

1.2 Raman spectroscopy of melamine

Due to the various food incidents (pet food and baby food contamination) that occurred in the last decade, the uses of analytical techniques such as Raman spectroscopy were extended to solutions of melamine and cyanuric acid[6]. He *et al.*[7] were able to detect trace amounts of melamine using Raman spectroscopy coupled with gold nanosubstrates. The spectrum they obtained showed sharp peaks at 380, 582, 676 and 984 cm^{-1}. The most intense of these peaks appeared at 676 cm^{-1} and was assigned to in-plane deformations of the triazine ring, ring breathing mode 2 (carbon and nitrogen atoms of the triazine system move in phase in the direction towards and away from the centre of the ring).[8] The next most intense band at 984 cm^{-1} is due to ring breathing mode 1 (out of plane deformations of the triazine ring). Liu *et al.*[9] used Raman Spectroscopy to screen animal feed and foods and noticed that the vibration band at 670 cm^{-1} is very specific to free melamine.

As with infrared spectroscopy, there are reports in the literature on the Raman analysis of MF resins. Scheepers *et al.*[10,11] claimed that Raman Spectroscopy could be used to determine the presence of methylol groups (with low formaldehyde: melamine content at 999 and 1017 cm^{-1} and high formaldehyde: melamine at 950 and 1030 cm^{-1}), -NCH_2-N (1435 cm^{-1}) and N-CH_2-O (1450-1460 cm^{-1}). They also suggest that Raman analysis can complement NMR spectroscopy for quantitative analysis. They concluded that methylene bridges tend to occur for resins containing low formaldehyde: melamine ratios (1.7:1) whilst methylene ether bridges were favoured for high formaldehyde: melamine ratios (6:1).

Table 3.2 summarises the different infrared and Raman vibration band assignments given to melamine and melamine-formaldehyde resins. It includes the work of Meier *et al.*, who carried out in depth analysis on the vibrational spectroscopy of both by molecular modelling.[12]

Table 3.2: Vibration bands for melamine and MF resins in IR and Raman spectroscopy.[8-12]

Region (cm^{-1})	Assignment in Melamine	Assignment in Bridged methylolmelamine	Comments
675	in-plane ring deformation (R)	Decreases in intensity upon methylolation(R)	
811	Ring stretching motion (IR)	Persists on methylolation (IR)	Disappears in Raman
984	Ring breathing mode (R)	Constant upon methylolation	
999-1350	1028 cm^{-1} (IR and R) triazine ring and NH motion	999/1015-1020 cm^{-1} (IR and R) methylol groups and triazine motion. Intensity depends on change of symmetry	Does not change upon ether bridge formation.
1390-1470	1443 cm^{-1} (IR and R) Ring breathing mode	1390 cm^{-1} (CH$_2$ vibrations) and 1360 (ring breathing) (IR and R)	1435 cm^{-1} due to -NCH$_2$N- 1450-1460 cm^{-1} due to -NCH$_2$O-
1550	NH bend and CN stretching (IR and R)	Decreasing intensity (R) upon methylolation (due to decrease in symmetry)	Does not change upon ether bridge formation
1650	Strong in IR but weak (R). Due to NH$_2$ deformations	Decreasing intensity with decreasing symmetry in Raman.	
2800-3500	3120 cm^{-1} broad band (R) due to interacting NH$_2$ groups 3420-3470 cm^{-1} sharp peaks due to free NH$_2$ groups	3050-3380 cm^{-1} secondary amines (R) 2800-3100 cm^{-1} CH or CH$_2$ vibrations	

R= Raman bands   IR=IR bands

Meier *et al*. works interestingly show that a particular band of interest is the one at 675 cm^{-1}; for which the Raman intensity dramatically drops upon methylolation. The group also concludes that the 910 cm^{-1} vibration band is due to CH$_2$ and not C-O-C, as mentioned by Scheepers *et al*.[10]

1.3 Solid-state NMR of MF species

Solid-state NMR has previously been carried out on MF resins (^{13}C and ^{15}N) [13,14] and MF materials in the gel state (^{1}H-^{13}C -CP MAS)[15]. MF resins or gels produce distinct ^{15}N and distinct ^{13}C signals (165-170ppm for the triazine ring region, at 40-60ppm for aminal- N-C-N bonds and at 70-80ppm for ether N-C-O bridges in ^{13}C NMR specta). Furthermore, the work carried out by Egger *et al.*[14] showed that the functional type and functional density of resulting MF gels can be adjusted by varying the amount melamine: formaldehyde ratio, the solid concentration in the resin mixture prior to gel formation and the catalyst amount (formic acid). They proved that methylene bridges rather than methylene ether bridges form for low formaldehyde content (melamine: formaldehyde of 1:1.5), a similar conclusion to that drawn by Scheepers *et al.*[10], using Raman Spectroscopy.

The table below (Table 3.3) summarise the important regions that exist in the solid-state NMR spectra of MF resins and networks.

Table 3.3: Different ^{13}C and ^{15}N NMR signals for cross-linked MF (resins or gels). [12-14]

^{13}C NMR (TMS reference)		Chemical Shift (ppm)
Triazine carbon	**Ar**-NH$_2$	167-170
	Ar-NH-(CH$_2$OR)	165-170
	Ar-N-(CH2OR)$_2$ or C=N[11]	150-160
Ether bridge:	N-**CH**$_2$-O	70-80
Free alcohol:	N-**CH**$_2$-OH	65-70
Methylene bridge:	N-**CH**$_2$-N	40-60
^{15}N NMR (Nitromethane reference)		
Amine		-280
Triazine		-200 to -211

2. Experimental Methods

2.1 IR analysis

The instrumentation used for the analysis of the samples in this work was a Thermo Nicolet 380 FTIR with Smart Omnic-sample and a germanium crystal ATR attachment. A germanium crystal is useful in the range of 5000-550 cm^{-1} and has a refractive index of 4.0 (refractive index of diamond is 2.4). The parameters used were 800 scans (unless stated otherwise) and a resolution of 4 (1.928 cm^{-1} spacing). The samples analysed were ground into a fine powder before use. In the spectra, the region between 2700 cm^{-1} and 1900 cm^{-1} has been omitted for clarity as there are no peaks of interest in this area. Please note also that spectra have been shifted on the y-axis and the intensity of peaks has at times been modified for clarity.

2.2 Raman analysis

The instrumentation used for this work was the Avalon RamanMicro Instrument R3 coupled to an Olympus BX410 microscope. The laser power was of 100 mW. The number of scans was 100, the scan time was 0.1 s, and the data collection range was 2000 - 200 cm^{-1}. The samples were analysed directly as bulk solids mounted upon a glass support.

2.3 CP-MAS NMR

The samples were analysed at the EPSRC solid-state NMR facility (Department of Chemistry, Durham University) using a Varian VNMRS spectrometer with a 9.4 T magnet (operating at 100.56 MHz for ^{13}C and 40.53 MHz for ^{15}N). The specimens were ground

down to a powder (500mg) for analysis. The chemical shift references are trimethylsilane for ^{13}C NMR and nitromethane for ^{15}N NMR.

3. Results and Discussion

3.1 General variations in IR vibration bands of melamine, MF resins and cross-linked MF materials

Figure 3.2 shows the IR spectra obtained for melamine (red), MF resin 20% in water (green) and cross-linked dry MF material (blue).

The main vibration bands for melamine using the ATR-IR method has given a very compatible spectrum to those carried out by both Wang *et al.* [16] (carried out in the gas phase in a solid argon-matrix at 10K) and Costa *et al.*[17] (using the KBr disc technique). There are three main areas of importance in the spectrum of melamine shown in Figure 3.2. Firstly, the two very sharp peaks at 3470 cm^{-1} and 3420 cm^{-1} are typical of primary amine N-H bonds (associated to N-H asymmetric stretching). They disappear as resin and material formation takes place i.e. the primary amine becomes a secondary and/or tertiary amine. Secondly, most of the vibrations in melamine or melamine derivatives occur in the region between 1700 cm^{-1} and 1400 cm^{-1}, responsible for vibrations due to the triazine ring and side chain amino groups. Finally, the very well defined, sharp peak at 811 cm^{-1} identifies triazine bending vibrations.

As the reaction of formaldehyde onto melamine proceeds, new bonds (C-H, **N-C**H$_2$- and C-O) are formed. According to IR tables[18], C-H aliphatic stretching occurs at 2950-2850 cm^{-1}, C-O stretching at 1300-1000 cm^{-1} and **N-C**H$_2$ stretch vibrations at 1190-1170 cm^{-1}. In Figure 3.2, the spectrum of a MF resin (green) shows new vibration

bands in the OH areas. Major transformations that occur as melamine reacts with formaldehyde is (1) disappearance of the amine doublet at 3470 and 3420 cm^{-1}, (2) appearance of aliphatic stretching at 3000-2900 cm^{-1} region and (3) presence of a new peak in the 1700-1400 cm^{-1} region. This new peak at 1350 cm^{-1} is of medium intensity and must be due to either C-O or N-C (side chain) type bonds that are not present in melamine.
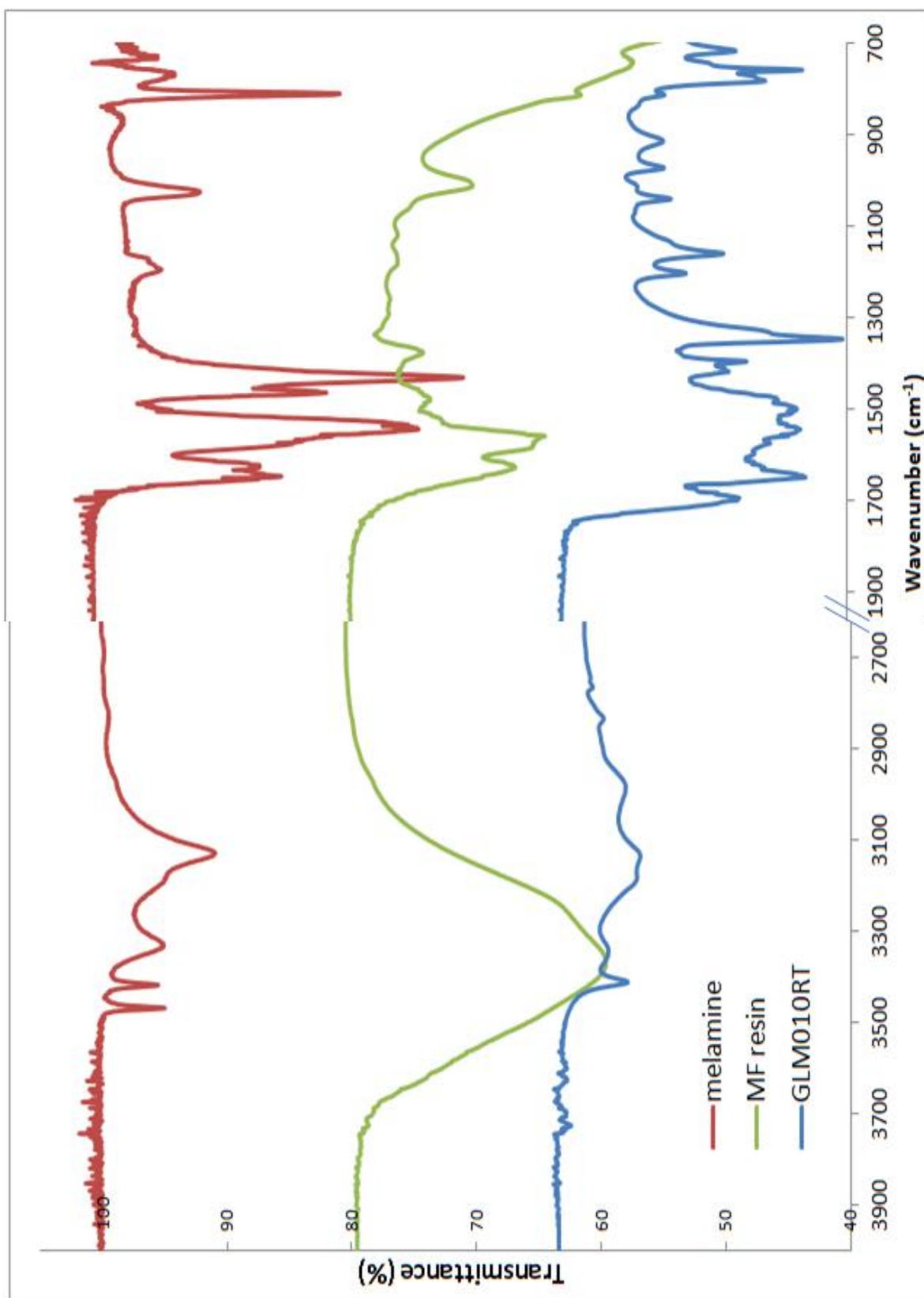
Figure 3.2: IR spectrum of melamine (red), a melamine formaldehyde resin (green) and a cross-linked melamine formaldehyde material (blue).

The spectrum of a cross-linked material (blue spectrum in Figure 3.2) shows that the major transformations from resin to material are (1) better defined amine stretching peak at 3400 cm^{-1} and peaks thereafter (H-bonding is high in the resin due to the state of the specimen, in aqueous solution), (2) appearance of a new vibration at 1700 cm^{-1} which could correspond NH_2 scissor or OH bending but also to C=N imine type stretching (3) a much more intense peak at 1350 cm^{-1} (4) many weak peaks appearing from 1200 to 900 cm^{-1}.

What can be noted for all material samples is that the peak at 1350 cm^{-1} is always present weakly (resins) or strongly (cross-linked materials), and therefore seems characteristic of cross-linking and will be further discussed throughout the chapter. Also, an interesting remark is that the peak at 811 cm^{-1} in melamine, is still present in both resin and materials, although it seems weaker in the latter. Interestingly, a stronger peak just below at 780 cm^{-1} has appeared perhaps due to isomeric forms of the triazines in the MF network.

To date, very few accounts of IR analysis on cross-linked MF networks have been reported. Salaun et al. [19] synthesised MF microcapsules and determined their structure by FT-IR. Another group, Dante et al.[20], synthesised cross-linked resins at very high temperature and pressure from mixtures of both MF and phenolic-formaldehyde resins, which were also analysed by FT-IR.

Tables 3.4, 3.5 and 3.6 given below attempt to gather experimental data both from this work and key works found in the literature on assignments of infra-red vibration bands of triazine or melamine, melamine-formaldehyde resin solutions (only low degree of cross-linking without acid catalysis) and solid MF networks resulting from acid catalysis (high degree of cross-linking). They aim at emphasising the changes expected with forming a resin or a well defined solid MF matrix based on the literature and the work described here.

Table 3.4: IR assignments for melamine from Sigma Aldrich, 99% purity, used in this work compared to other references[15, 16] and related to IR tables[17]

Wang et al.[15] (cm^{-1})	Costa et al.[16] (cm^{-1})	This work (cm^{-1})	Assigned Vibration from IR tables[17]
3571	3470 / 3420	3468/3418	NH asymmetric stretching
3453	3335/3125	3331/3129	NH symmetric stretching
1598	1653	1649	NH$_2$ Scissor
1556	1580/1555	1546	Triazine ring stretching
1440	1470/1440	1466	Ring and side chain CN stretching
1000	1030	1197	C-N stretch, NH$_2$ swing, tertiary C
925		1025	C-N stretch, NH$_2$ swing, tertiary C
824	815	811	Out of plane triazine ring formation
752			Out of plane triazine ring formation

Table 3.5: IR assignments for the MF resin solution used in this work compared to other references[12, 20,21]and related to IR tables.[17]

Ebdon et al.[12]	Kim et al.[20]	Birinci et al.[21]	This work	Assigned Vibration from IR tables [17]
3395	3375	3385	3374	N-H stretching, O-H stretching
	1600	1635	1625	NH_2 scissor, O-H bending
	1550	1592	1560	Triazine ring stretching
	1470/1430	1491	1480	C-N, CH_2, N-H bend or N=C-N bend
1334		1358	1375	CH_2, C-N due to cross-linking
1149	1175	1143	1175	C-N, C-O due to cross-linking
993/881	1010	971	1011	C-O-C stretching
811	810	812		Out of plane triazine ring deformations
780				Out of plane triazine ring bending

Table 3.6: IR assignments for cross-linked MF matrices produced (GSL013RT where M:F=1:1.5 and GLM001RT where M:F=1:5) in this work compared to other references[18,19] and related to IR tables.[17]

Salaun et al.[18]	Dante et al.[19]	GSL013RT	GLM001RT	Assigned Vibration from IR tables [17]
3360	3371/3209	3412/3343/3135	3342	N-H stretching, O-H stretching
1651		1697/1651		NH_2 scissor, O-H bending
1557	1549	1546	1546	Triazine ring stretching
1482	1490/1450			C-N, CH_2, N-H bend or N=C-N bend
1306	1350	1420/1398/1348	1360	CH_2, C-N due to cross-linking
1199	1241	1204/1162	1199	C-N, C-O due to cross-linking
1021	1095	1042/974/915	998	C-O-C stretching
814	806	813		Out of plane triazine ring deformations
		783/760/717	791	Out of plane triazine ring bending

3.2 Comparison of the commercially available monomers to melamine

Figure 3.3: shows stacked spectra for the different commercially available monomers that were used in synthesising novel MF materials: benzoguanamine **24** (red), acetoguanamine **23** (green) and caprinoguanamine **25** (purple) with the IR spectrum of melamine **1** (blue).

At a first glance, the three specific regions observed by Padgett *et al.* [4] are still valid for these triazine structures: 3500-3000 cm^{-1} corresponding to amine stretching, the side-chain amino deformation and triazine ring stretching region at 1700-1300 cm^{-1} and finally one just beyond 830 cm^{-1} for triazine ring bending.

However upon closer analysis there are many subtle differences. For example, a peak at 1270 cm^{-1} can be observed for acetoguanamine, benzoguanamine and caprinoguanamine (weak), but is absent in the melamine spectrum. This peak may therefore be due to C-H deformation vibrations, as these are the only bonds present in all three commercially available derivatives which are not present in melamine. However C-H deformation vibrations occur at 1700-1350 cm^{-1} in most alkanes and 900-720 cm^{-1} for most monosubstituted benzenes (=C-H).

The spectrum of caprinoguanamine shows extra sharp vibration bands below 3000 cm^{-1} compared to the melamine spectrum and these should be due to the presence of C-H aliphatic bonds (C-H stretching). Acetoguanamine has vibration bands in this region but they are weaker and cannot be seen clearly in the spectrum shown in Figure 3.3. Aromatic C-H bond stretching vibrations, on the other hand, occur in the 3150-3000 cm^{-1} region (as seen in the benzene spectrum) which is difficult to distinguish in the benzoguanamine spectrum in Figure 3.3 from the N-H stretching bands. The NH

asymmetric stretching bands in acetoguanamine are better defined (2 clear bands) at 3300 cm^{-1} compared to melamine.

From the region of 1700-1300 cm^{-1}, three peaks (at 1590 cm^{-1}, 1490 cm^{-1} and 1390 cm^{-1}) are present in the benzoguanamine spectrum and absent in the melamine spectrum. The peaks at 1590 cm^{-1} and 1490 cm^{-1} are characteristic of aromatic C=C peaks (the peak at 1490 cm^{-1} can also be observed in the spectrum of benzene in Figure 3.3). It is still unclear to what vibration band the peak at 1390 cm^{-1} can be assigned. Interestingly these peaks are also present in the Raman spectrum of benzoguanamine (red) in Figure 3.4.

It can also be noticed that benzoguanamine has two sharp peaks at 825 cm^{-1} and 775 cm^{-1} whereas melamine (and the other monomers) has one peak in this region (811 cm^{-1}) which has been assigned to the out-of-plane triazine ring bending. The peak at 775 cm^{-1} may therefore be due to the benzene ring, and according to IR spectroscopic tables, it corresponds to mono-substituted out-of-plane benzene ring vibrations. This could also be due to iso-melamine conjugating with benzene.

The region from 1700 cm^{-1} to 1400 cm^{-1} shows a strong peak present in the acetoguanamine spectrum at 1655 cm^{-1}, which may be specific to alkyl groups as this vibration band is present in exactly the same region for caprinoguanamine but absent in the benzoguanamine spectrum. However, it seems very high in frequency for C-H deformation vibrations. Other possibilities include an additional N-H deformation vibration band.

The Raman spectra of commercially available monomers in Figure 3.4 suggest that peaks present between 1390-1000 cm^{-1} are probably due to C-H deformation vibrations. More specifically peaks at 1160-1190 cm^{-1} are due to aromatic C-H deformations whereas the peaks at 1270-1300 cm^{-1} are due to aliphatic C-H deformations.

Figure 3.3 and Figure 3.4 suggest that both IR and Raman vibration techniques are more suitable for determining benzoguanamine and caprinoguanamine. The substitution of an -NH$_2$ group with a –CH$_3$ group does not significantly manifest itself in vibrational spectroscopy.
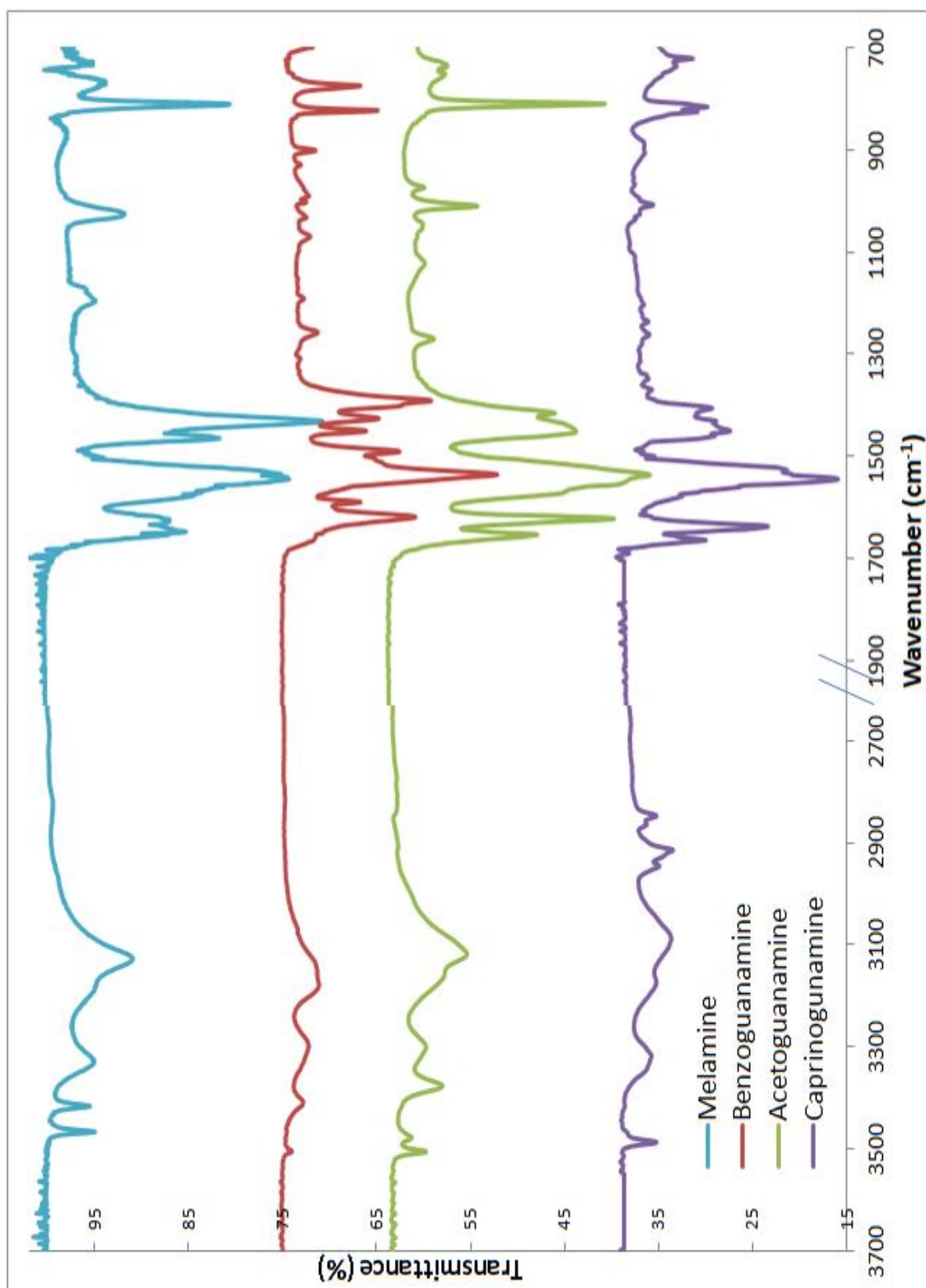
Figure 3.3: IR spectra of melamine (blue), benzoguanamine (red), acetoguanamine

(green), and caprinoguanamine (purple).
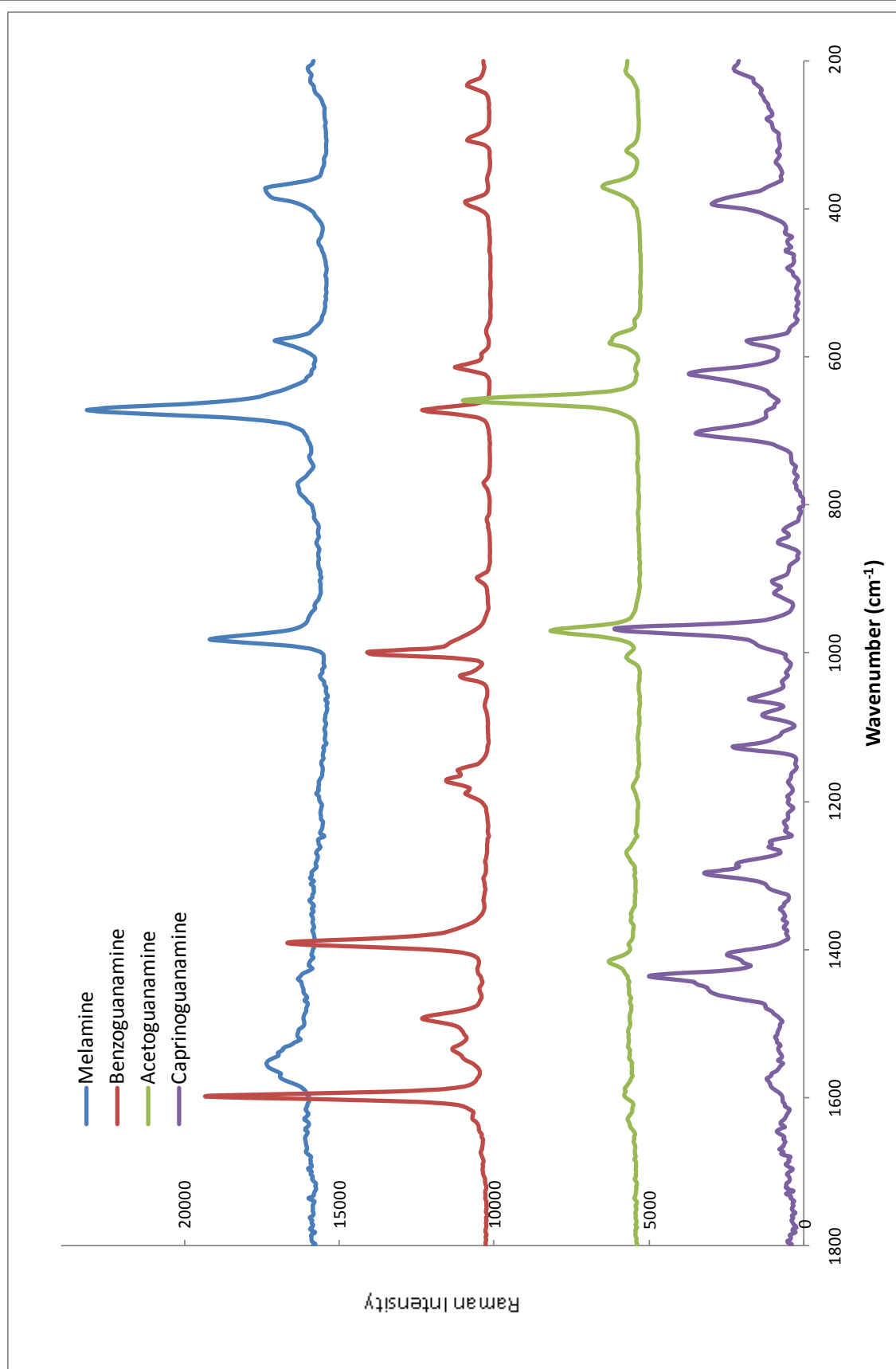
Figure 3.4: Stacked Raman spectra of melamine (blue), benzoguanamine (red), acetoguanamine (green) and caprinoguanamine (purple).

3.3 Comparison of both synthesised and commercial monomers with melamine

Figure 3.5 shows the stacked spectra of benzene (for easier comparison with phenyl moiety of benzoguanamine), benzoguanamine, melamine and monomer 1, **13**. The three regions typical of amino triazines (3000 cm^{-1}, 1660-1430 cm^{-1} and 830 cm^{-1}) still apply to the spectrum of monomer 1. Some weak broad bands at 2900 cm^{-1} occur, which can be seen if comparing this region to melamine. This is due to the presence of C-H alkyl groups.

Figure 3.6 shows the stacked spectra of acetoguanamine, melamine and monomer 2, **14**. A more pronounced peak at 2975 cm^{-1} can be seen for monomer 2, which is due to the presence of more alkyl groups in monomer 2 than in monomer 1. In the region of 1700-1300 cm^{-1} four sharp peaks can be seen which are not as well defined in the spectrum of acetoguanamine, corresponding to various triazine stretching. In the region of 1200-700 cm^{-1}, many weak, sharp peaks, notably the one at 811 cm^{-1} can be observed.

Figure 3.7 shows the stacked spectra of caprinoguanamine, melamine and monomer 3 ester **15**. The ester intermediate shows a peak at 1700-1730 cm^{-1} This vibration band is absent from all other spectra, as shown in Figure 3.7 thus it must be due to C=O. Additional peaks that appear strongly in the spectrum of the monomer 3 ester are at 1300 cm^{-1}, which could be due to C-O-C ester asymmetric stretching, 1065 cm^{-1} which is due to C-O-C ester symmetric stretching and two sharp peaks at 995 and 915 cm^{-1} which cannot be assigned but according to the tables produced by George Socrates *et al.*[17], butyrates have various peaks from 1095 to 580 cm^{-1}. Monomer 3 ester contains a long chain alkyl group attached to an ester moiety just like a butyrate and hence the bands may be related.
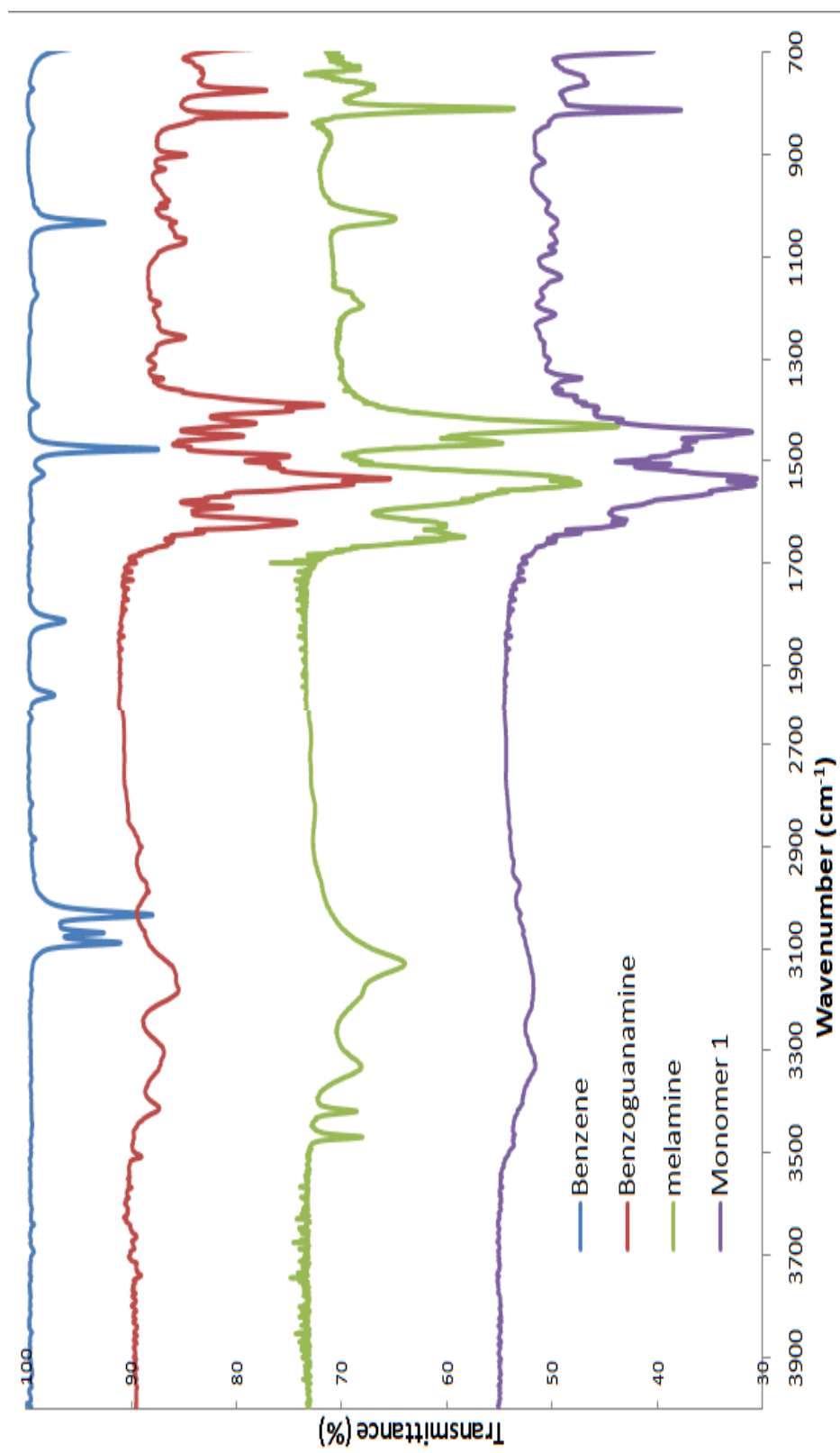
Figure 3.5: IR spectra of benzene (blue), benzoguanamine (red), melamine (green) and monomer 1 (purple).
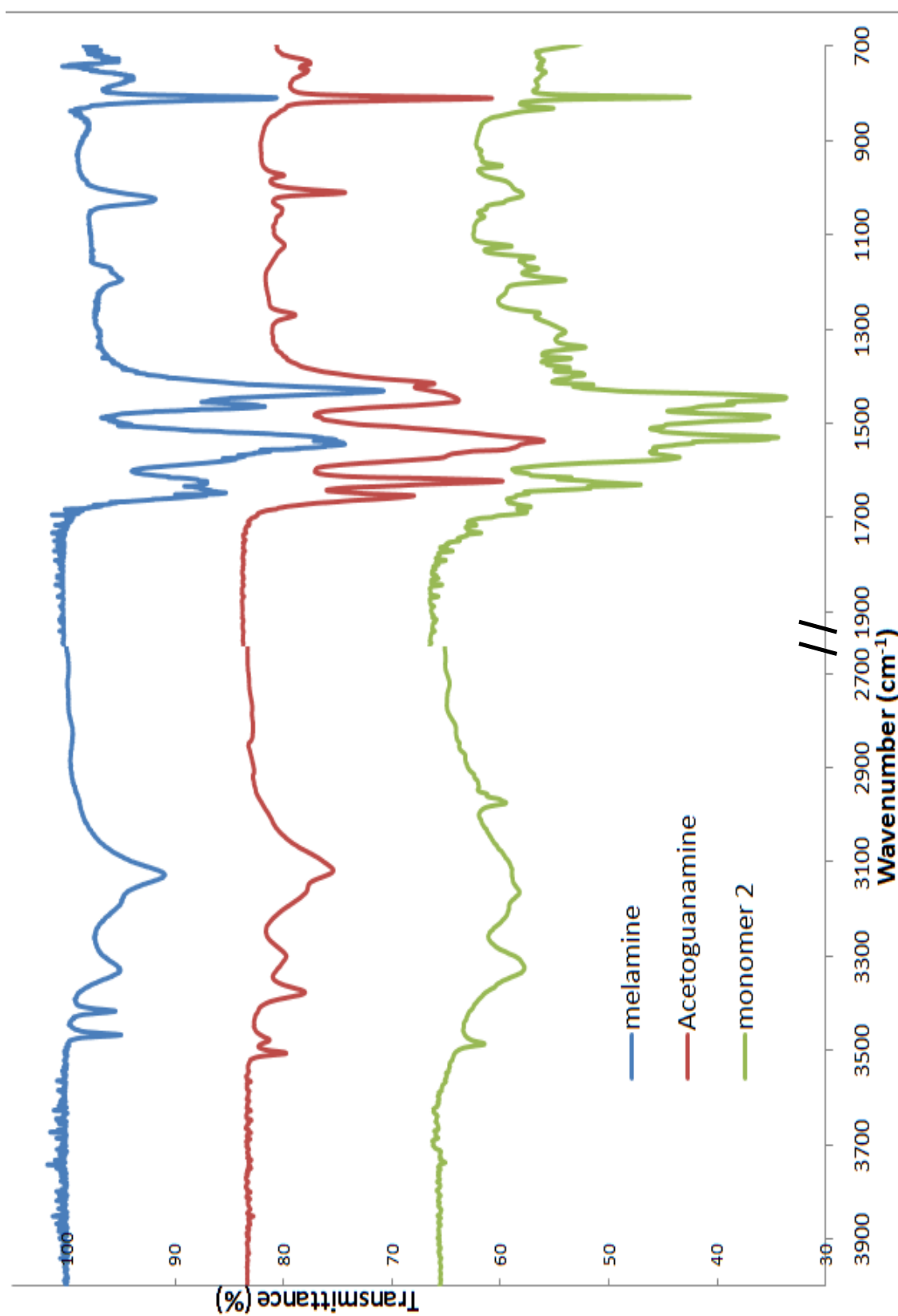
Figure 36: IR spectra of melamine (blue), acetoguanamine (red) and monomer 2 (green).
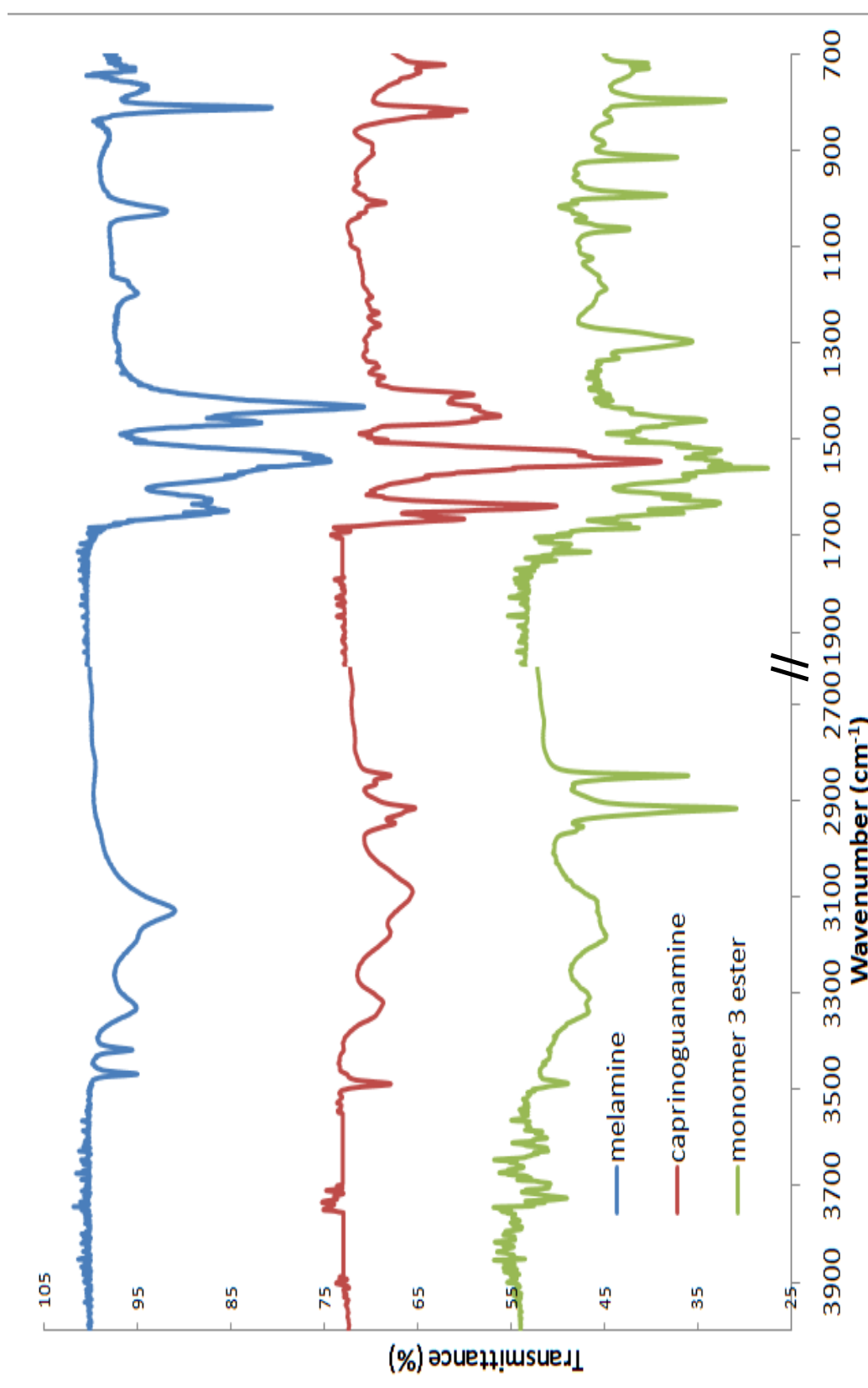
Figure 3.7: IR spectra of melamine (blue), caprinoguanamine (red) and monomer 3 ester (green).

3.4   From monomers to room temperature dried materials

3.4.1   Melamine-formaldehyde materials

As mentioned earlier in this chapter, all MF cross-linked networks, irrespective of synthesis and drying conditions, exhibit an intense characteristic IR peak in the 1300 cm^{-1} region, as displayed in Figure 3.8. Plus, as already briefly noted earlier, the primary amine vibrations at 3470 and 3420 cm^{-1} becomes a singlet (secondary amine) upon addition of formaldehyde onto melamine. GSL013RT may exceptionally contain more free NH$_2$ (not as fully cross-linked) than the other samples (for tertiary amines there are no peaks in this region).

The CH region at 2900 cm^{-1} becomes more apparent in GSL015RT, GSL013RT, GLM010RT and GSL016RT with cross-linking occurring via methylol groups, as does the N-CH$_2$ stretching at about 1150 cm^{-1}. The triazine bending vibration at 811 cm^{-1} remains upon cross-linking although it is less intense and stronger peaks just below 800 cm^{-1} appear, as briefly mentioned previously.
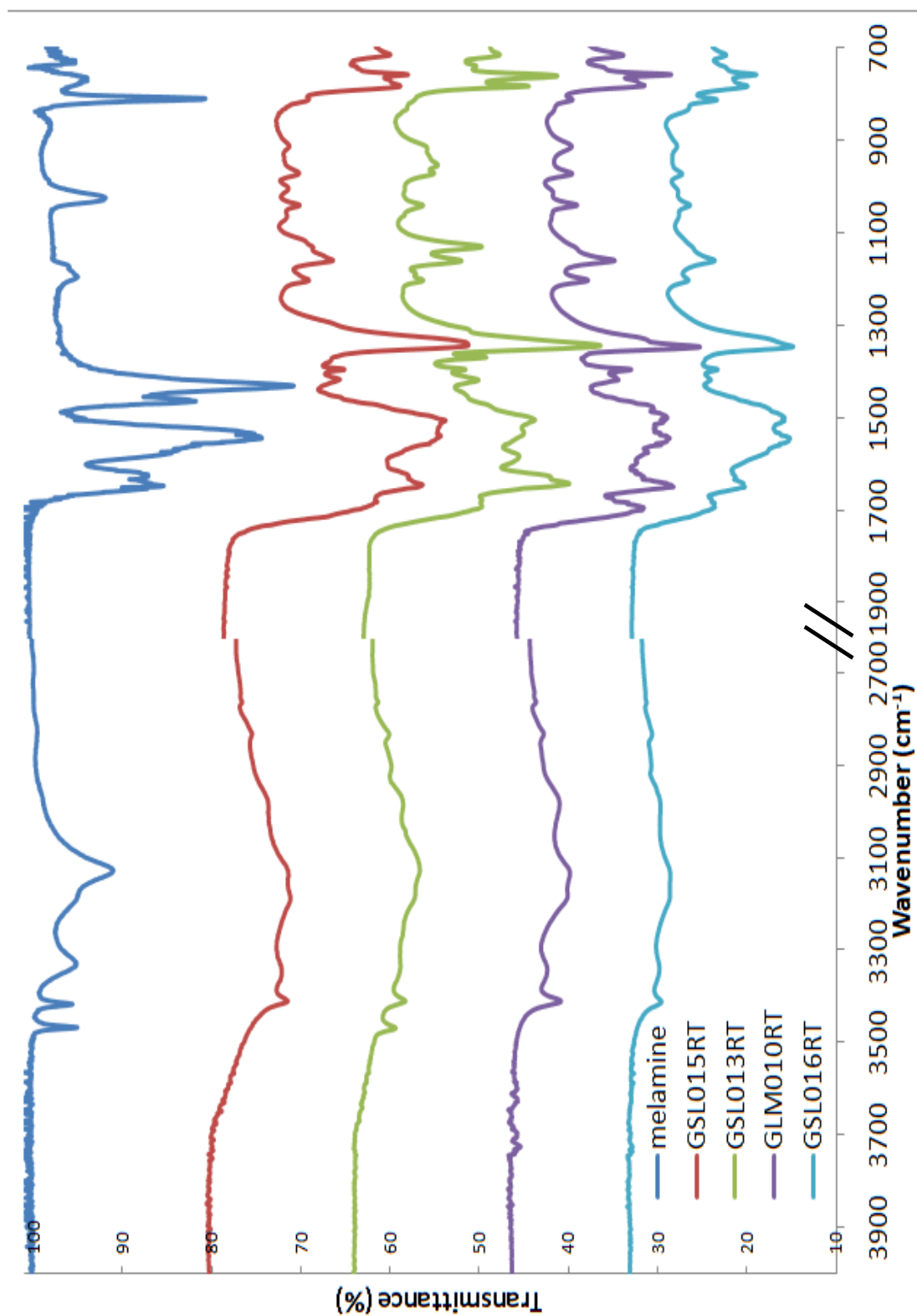
Figure 3.8: IR spectra of various cross-linked MF networks emphasising the presence of a strong vibration band at 1350 cm^{-1} compared to the spectrum of melamine.

In order to look in detail at the 1350 cm^{-1} band which appears to be specific to cross-linked materials, it is necessary to picture what the possible cross-linking units formed are. Figure 3.9 gives the possible branching occurring in MF networks along with their IR signatures.

Functional Group	Frequency (cm^{-1})	Comments
Ether	1310-1020 930-900 1140	symmetric asymmetric
Methylol	1260-1140	usually broad
Methylene	1360-1250 1280-1180	usually sharp

Figure 3.9: Possible cross-linking units present in MF materials along with corresponding IR data.

a) Investigating the Nature of the Cross-linking of MF resins by IR

According to IR tables, for C-O-C vibrations there would be two vibrations in the 1310-900 cm^{-1} region if the ether is asymmetric or just one at 1140 cm^{-1} if the ether is symmetric. However, if the peak is classed as broad then it would be due to –OH vibrations and a sharp peak would mean it is due C-N vibrations. It could also be that the peak occurs due to a combination of all three possibilities, i.e. the vibrations of all three possible cross-linking units overlap. In order to understand if one of the cross-linking mechanisms is predominant in this region, further analysis is required.

It is known that removal of formaldehyde from MF materials can occur through curing (heating)[21]. During this process, ether bridges are transformed into methylene bridges (-N-CH$_2$-N-) with the release of formaldehyde, and the result of this transformation could

potentially be observed by infrared spectroscopy. In order to investigate this possibility, a

finely ground sample (GSL024RT) was heated at either 60°C, 120°C or 200°C for 2 hours

and the resulting IR spectra, were recorded and are displayed in Figure 3.10.
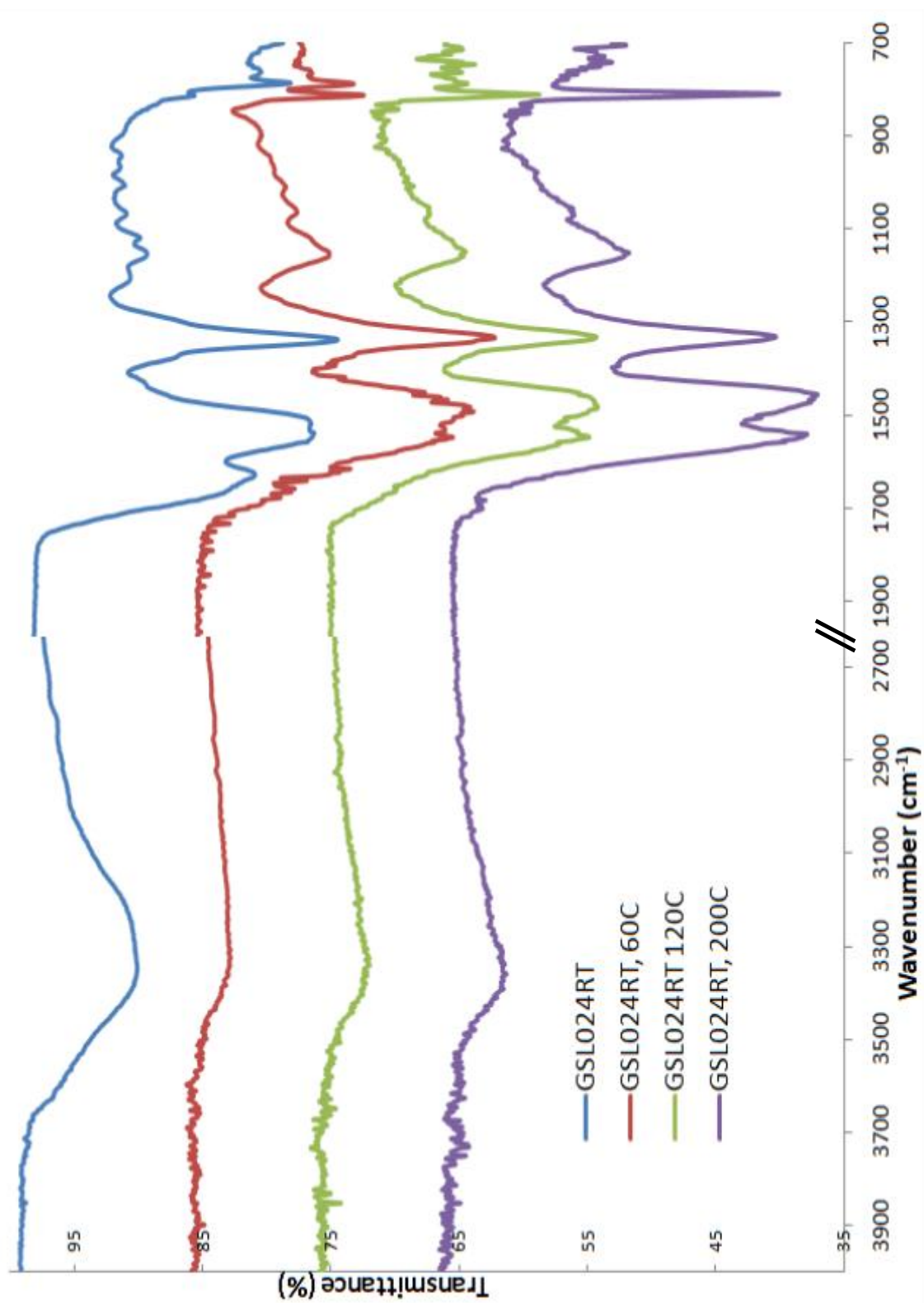
Figure 3.10: A semi-transparent MF sample heated at different temperatures in order to

see if the peak at 1350 cm^{-1} changes intensity or broadness.

GSL024RT is a semi-transparent material, thus the cross linking density is probably quite high and there should be a significant decrease in intensity if the peak at 1300 cm^{-1} was due to C-O-C bonds. The sample was first heated to 60°C to remove some of the water adsorbed in the pores in order to see if the 2990-2930 cm^{-1} region could be better defined (see work carried out by TGA/DSC analysis in chapter 2). However, the region does not appear to be much different. The same specimen was then heated to 120°C where most of the water adsorbed would be removed and some removal of formaldehyde would occur. It was finally heated to 200°C where full curing would occur.

It can be noticed that the intensity of the peak at 1300 cm^{-1} relative to the ones present at 1600-1450 cm^{-1} has decreased in the 200°C spectrum. This could therefore mean that this peak is partly due to ether vibrations; however as the peak does not disappear completely, it would suggest that vibrations due to C-O-C are not the only ones occurring in this region. (Note that the strength of the peak at 811 cm^{-1} increases with heating. This may be due to the triazine ring vibrating more strongly when the sample is less hydrated).

An additional analysis was pursued. GLM006RT is a sample synthesised using 1:5 M:F ratio (thus a high level of formaldehyde substitution at amino positions on melamine). It also has a low MF:FA ratio (thus a large amount of formic acid to enhance cross-linking). For comparison, the spectrum of GLM001RT, a specimen with M:F=1:5 but with a higher MF:FA ratio, was also recorded, and the two spectra are displayed in Figure 3.11.
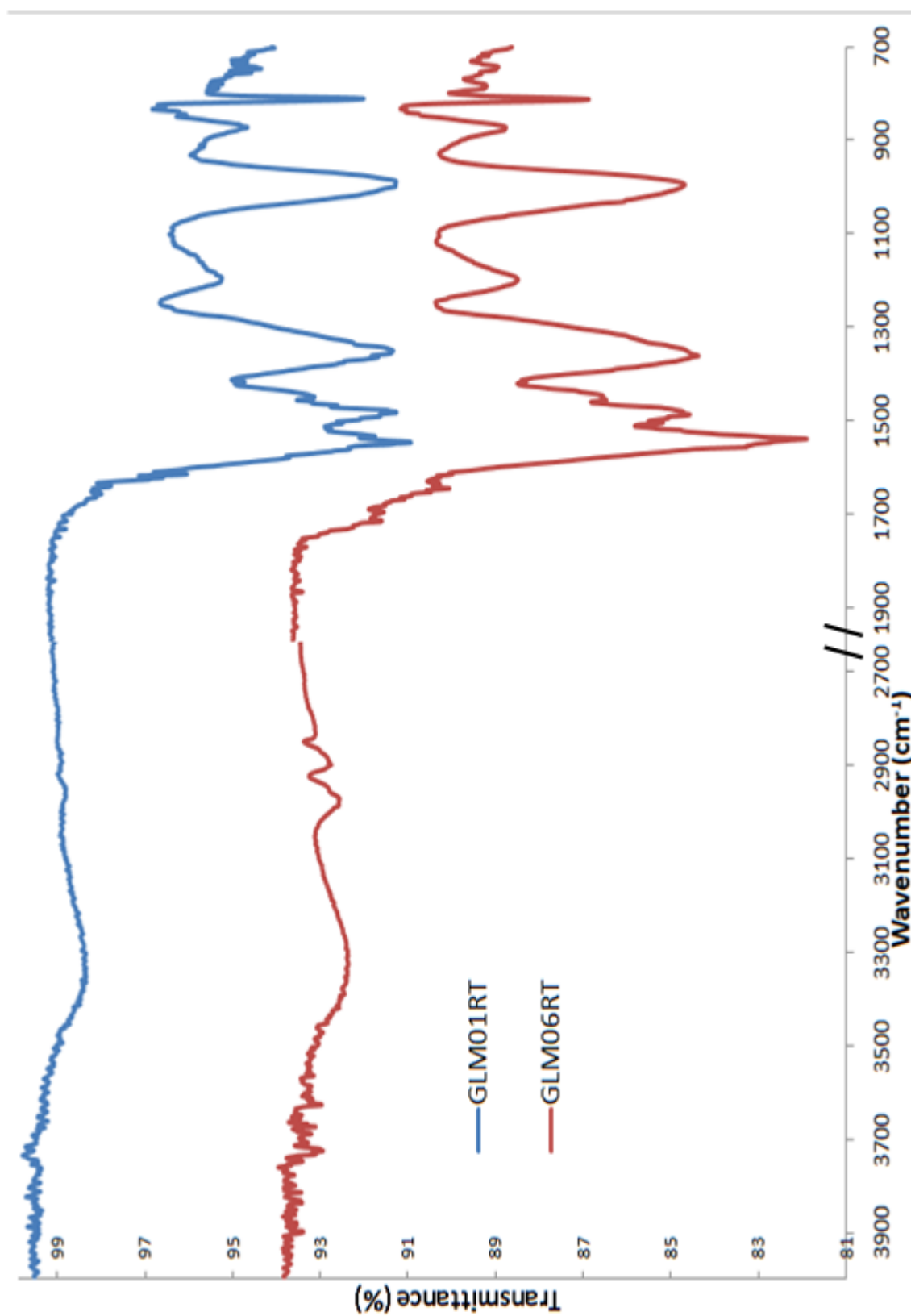
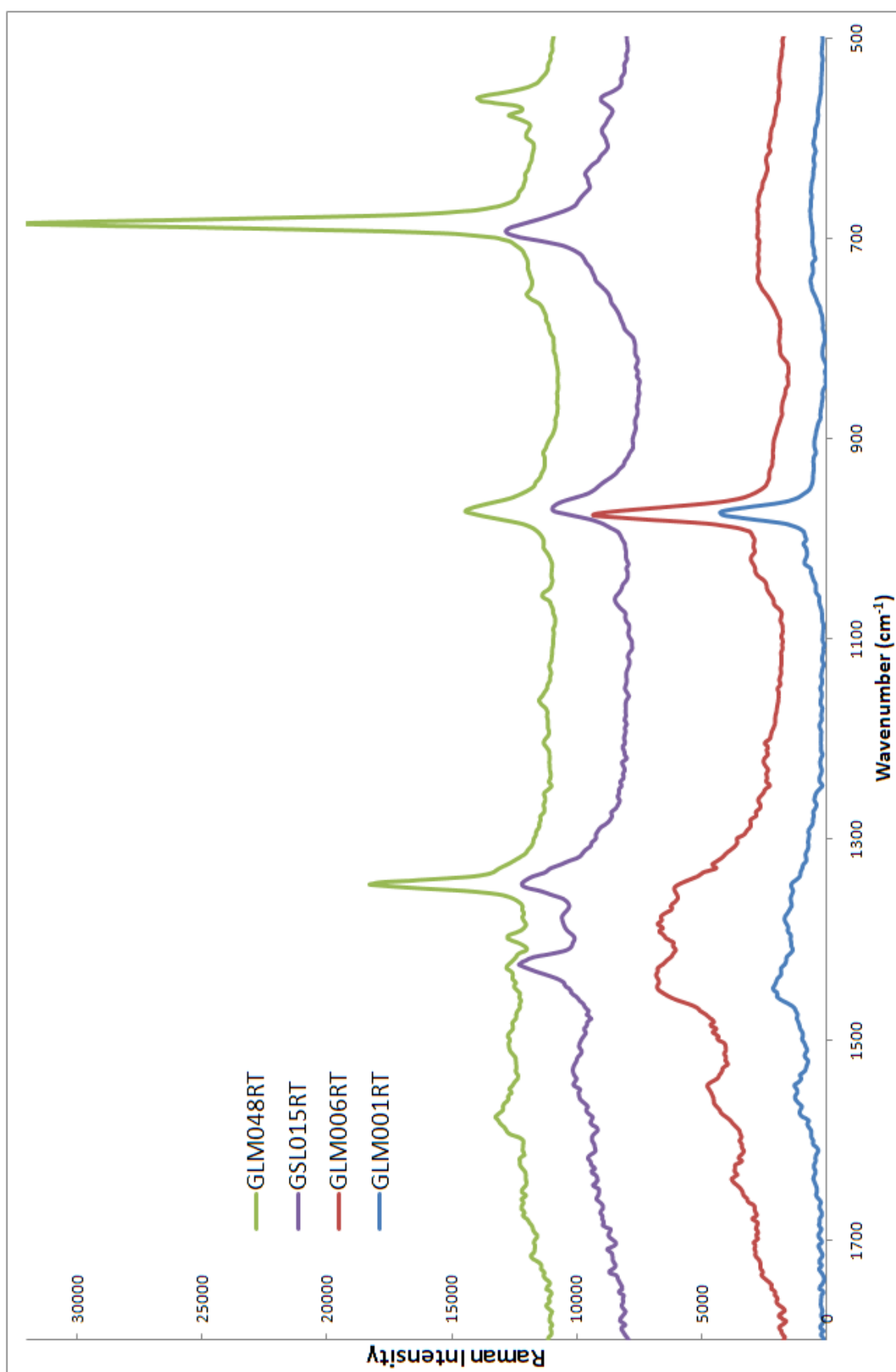**Figure 3.11:** IR spectra of GLM001RT and GLM006RT, both made from resins of M:F=1:5.

The samples are however catalysed with different amounts of formic acid (low for

GLM010RT and high for GLM06RT).

The broadness of the peak at 1350 cm^{-1} does not seem to change significantly with MF:FA ratio. In theory, the amount of acid added to a system is expected, to a certain extent, to increase the amount of cross-linking, and inversely to decrease the number of non cross-linked units (more CH_2OH groups are likely to be more present in GLM001RT with low FA content than GLM006RT with a high FA content). In Figure 3.11, since there is no variation in broadness for this band with the amount of catalyst added, it seems to suggest that this vibration is not due to CH_2-OH group and eliminates the possibility of this vibration being responsible for the peak observed. It can therefore be concluded that this peak may be partially due to -C-O-C vibrations, but is mostly due to C-N methylene vibrations after cross-linking. The peak broadness may be due to the fact that there are three different types of C-N bonds that form. (Note: yet again, the peak at 811 cm^{-1} is quite intense in this set of spectra).

b) Investigating the Nature of the Cross-linking of MF resins by Raman Spectroscopy

The curing of MF resins by physical means is discussed in a paper by Scheepers *et al*[10]. They managed to elucidate that the peaks occurring in Raman spectra at 1010-1070 cm^{-1} are due to methylol groups (CH_2OH). They also used ^{13}C NMR in conjunction with Raman spectroscopy to state that N-C-O bonds give vibration bands at 1450-1460 cm^{-1} whereas N-C-N bands occur at 1435 cm^{-1}. They concluded that methylene ether bridges tend to occur for resins containing high formaldehyde content whilst methylene bridges were favoured for low formaldehyde content per melamine (this was later confirmed on cross-linked MF gels by Egger *et al.*[14])

In order to differentiate between the different types of bridging, two samples containing low formaldehyde (GSL015RT and GLM048RT) and the two samples already mentioned with high formaldehyde content (GLM001RT and GLM006RT) were analysed by Raman spectroscopy (Figure 3.12).

Figure 3.12: Raman spectra of GLM01RT and GLM06RT (samples with a high degree of methylolation) and samples GSL015 and GLM048RT (samples with low degree of methylolation).

What seems to have occurred is that as mentioned in the introduction, the degree of methylolation has affected the intensity of the peak at 675 cm^{-1}. In Figure 3.12 above, for the high M:F (1:5)samples, this peak has disappeared and for the M:F 1:1.5, the amount of formic acid seems to have a large effect on the intensity of this peak compared to the peak at 975 cm^{-1}.

Also in the above spectra, GLM048RT and GSL015RT have peaks at 1425 cm^{-1} suggesting that the main type of bridging that is occurring could be –N-C-N- but the region between 1420-1470 cm^{-1} is too broadened and weak to unambiguously distinguish what type of bridging is occurring in materials, perhaps suggesting that it is not solely –N-C-N-.

c) *Investigating the Degree of the Cross-linking in MF materials*

The vibrations that are assigned specifically to the triazine ring, especially in triazine monomers, are the ones that appear at 811 cm^{-1}. The peak responsible for cross-linking in MF materials is the one at 1350 cm^{-1}. Therefore by obtaining the ratio between the areas of these two peaks, the degree of cross-linking could be estimated and the samples may then be cross- compared and potentially be related back to the synthetic steps (amount of acid catalyst, appearance of materials etc).

Many samples were screened and an interesting observation came about. The peak at 811 cm^{-1} is not always present. Stronger bands tend to appear at lower wavenumbers.[17] There is the possibility that if the vibration band appears at 795-750 cm^{-1} then it is due to the iso form in which one double bond is external to the ring by conjugation. If, however, the vibration band(s) occur in the 860-775 cm^{-1} region, it is due to "normal" (as opposed

to iso) out-of-plane bending vibrations, which can be more numerous than one. Adding the integrations of these peaks is also not a feasible option as the degeneracy of the mode of vibration is uncertain and the same vibration may be accounted for twice. The only vibration that is well defined, theoretically, is the one at 811 cm^{-1}.

Out of the library of collected IR spectra, only four samples showed intense 811 cm^{-1} vibration bands (compared to the intensity of peaks below 811 cm^{-1}) two of which were samples with a high formaldehyde content and two with a lower formaldehyde content (see Figure 3.13)
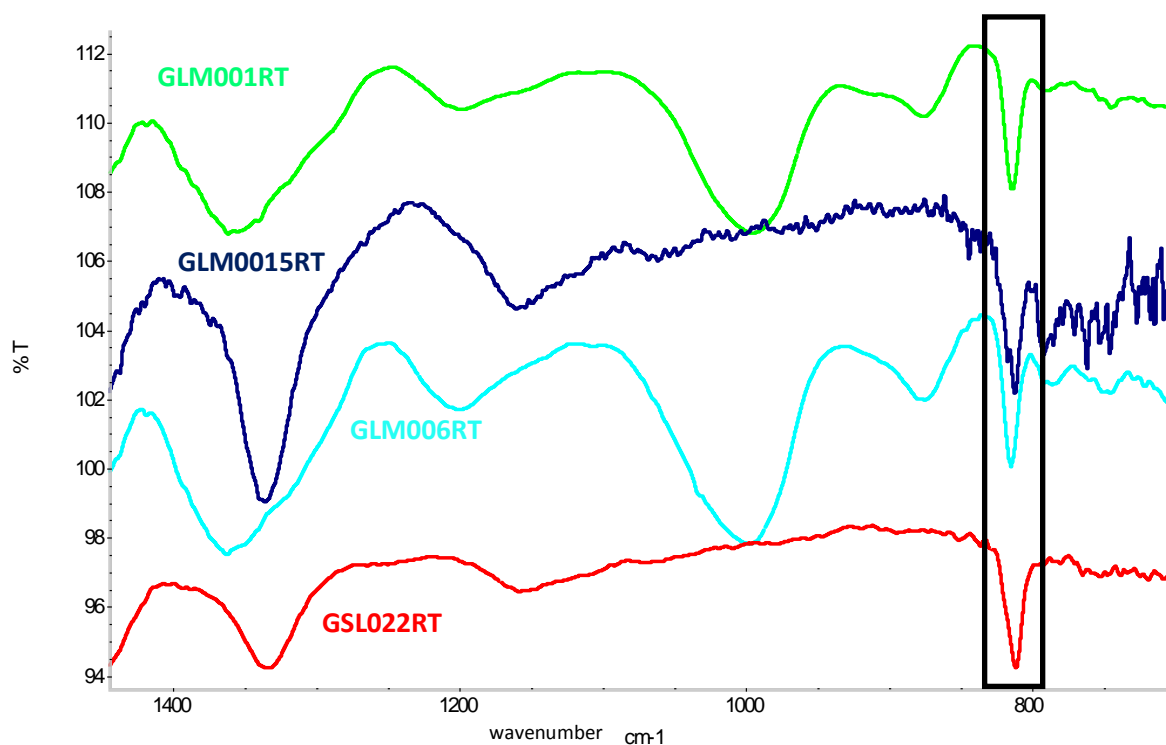
Figure 3.13: Spectra of four MF cross-linked samples that display quite intense peaks at 811 cm^{-1}.

The details of peak integration after converting spectra into the reflectance mode are given in Table 3.7. The ratio of the bands was calculated using the equation below:

$$\frac{I_{1350}}{I_{811}} = \frac{cross - linking}{triazine} \equiv \text{normalisation (amount of } cross - linking \text{ per triazine unit)}$$

This would allow more accurate cross-comparisons between specimens as the actual measurements were carried out non-quantitatively. The table below (Table 3.7) summarises the ratios obtained for the four samples.

Table 3.7: Samples for which the IR spectra showed peaks at 811 cm^{-1}. The integrated area of these peaks is shown alongside the integrated ratio of the peak at 1350 cm^{-1}. A ratio of the two areas is also calculated and displayed.

	Sample	Integration of peak at 811 cm^{-1} (I_{811})	Integration of peak at 1350 cm^{-1} (I_{1350})	Ratio (I_{1350}/I_{811})
Low	GLM001RT (M:F= 1:5)	0.088	1.15	1.31
FA	GLM015RT (M:F=1:1.5)	0.160	2.33	14.56
High	GLM006RT (M:F= 1:5)	0.157	3.15	20.06
FA	GSL022RT (M:F=1:1.5)	0.079	0.30	3.80

Table 3.7 shows that it is extremely risky to be conclusive as no correlation is seen between the MF/FA ratios or formaldehyde content on such a small selection of samples. It is still uncertain if an increase in MF/FA ratio leads to an increase in the cross-linking density or whether an increase in formaldehyde content leads to an increase in cross-linking density.

The 811 cm^{-1} peak was looked into more closely in order to understand what influences its presence. The samples were firstly dried under vacuum to see if this had an effect on the peak intensity. After analysis and ratio calculations, this procedure showed that there was very little difference between the room temperature dried sample and the vacuum dried one.

Instead a material (GSL024RT) was dried in an oven at different temperatures. The intensity of the 811 cm^{-1} peak seemed to increase as the temperature was increased (as shown in Figure 3.14). In Table 3.8, the ratio of the I_{1350}/I_{811} for each temperature decreases with temperature, the 811 cm^{-1} definitely becomes more intense.
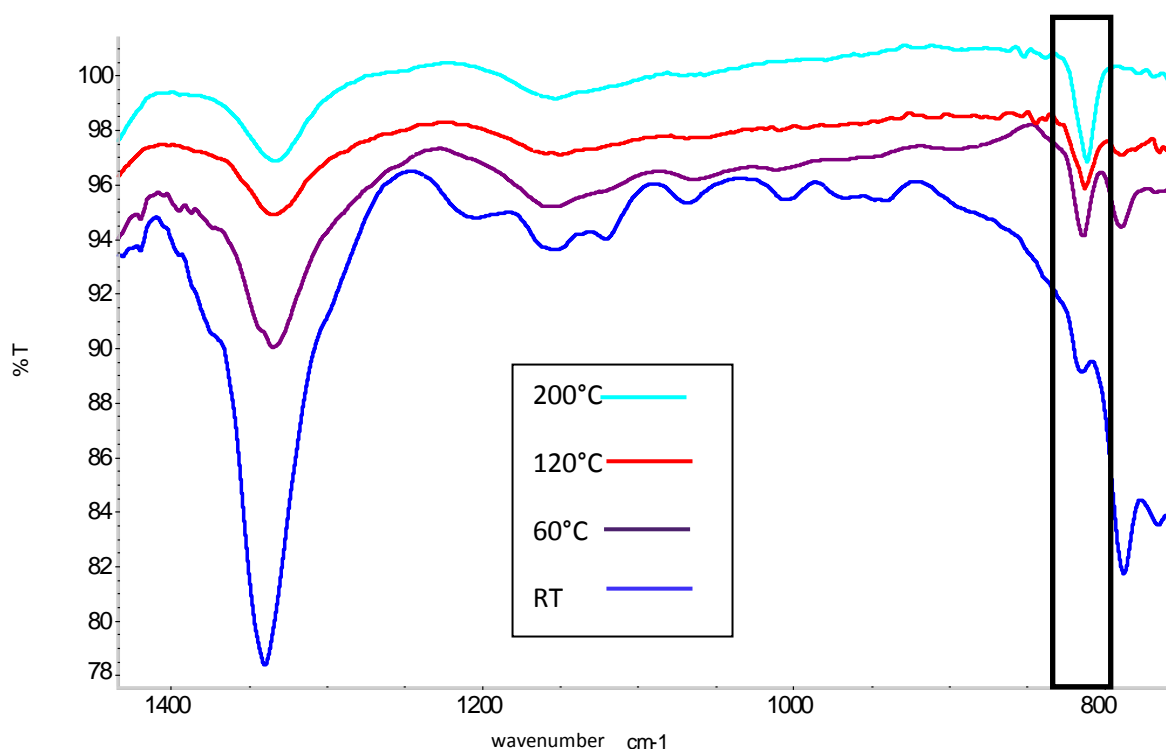
Figure 3.14: GSL024RT heated to different temperatures. The spectra are shown for the 1400-700 cm^{-1} region where there is an increase in intensity of the vibration band at 811 cm^{-1}.

Note that grinding the samples to very fine powders for analysis did not change the intensity of the 811 cm^{-1} peak either.

Table 3.8: The 811 cm^{-1} and 1350 cm^{-1} integrated intensities and calculated ratios between the two peak intensities.

Temperature of GSL024RT (°C)	Integration of peak at 811 cm^{-1} (I_{811})	Integration of peak at 1350 cm^{-1} (I_{1350})	Ratio (I_{1350}/I_{811})
RT	0.05	4.858	97.16
60	0.11	1.599	14.54
120	0.09	0.74	8.22
200	0.17	0.78	4.59

Another route towards estimating cross-linking density is by MAS NMR on final materials. According to Egger at *al.*[14] ^{13}C CP-MAS can show differences in gels with different synthesis parameters, such as how MF/FA and the M:F ratio can affect the presence and/or intensities of different signals in the ^{13}C spectra (of MF in an aqueous gel state).

The selected samples analysed by MAS NMR in this work are outlined in Table 3.9.

Table 3.9: Samples that were analysed by MAS NMR alongside composition details.

Sample	M:F (mol)	MF/FA (mol)	Porosity (%)
GLMCP05RT	1:1.5	0.83	Sample broken but in between 60 and 80%
GLM048RT	1:1.5	1.05	68%
GLMMG1aRT	1:1.5	1.15	73%
GSLBz019RT		1.02	71%
GLM013RT	1:1.5	0.47	16%
GLM06RT	1:5	0.44	25%

The spectra of these samples are shown in Figure 3.15 and 3.16.

Cross-linking can be identified in two different regions in ^{13}C MAS NMR shown. Firstly, there are signals in the 40-80ppm region which, as Table 3.3 outlines, is where the Ar-N-CH$_2$ bonds (methylene bridges) manifest themselves. Secondly, the region between 150-180 ppm is where the carbons of the triazine ring resonate. Within this region, it is possible to identify three sub-regions for carbons connected to primary (167-170 ppm), secondary (165-170 ppm) and tertiary amine groups (150-160 ppm).

For most of the samples (the first four in Table 3.9), ^{13}C MAS NMR exhibit similar signatures, even when MF/FA is different but with M: F still kept at a ratio of 1:1.5 (as seen with the ^{13}C NMR spectrum of GLM013RT in Figure 3.16). Therefore, in conclusion, the influence of formic acid is not easily observed. However when M: F increases from 1:1.5 to 1:5, an obvious change is noticed. New peaks appeared at 60-80 ppm, which in

Table 3.3 are assigned to -NCH$_2$O- bridges (either methylene ether or methylol, no distinction can be made between the two).
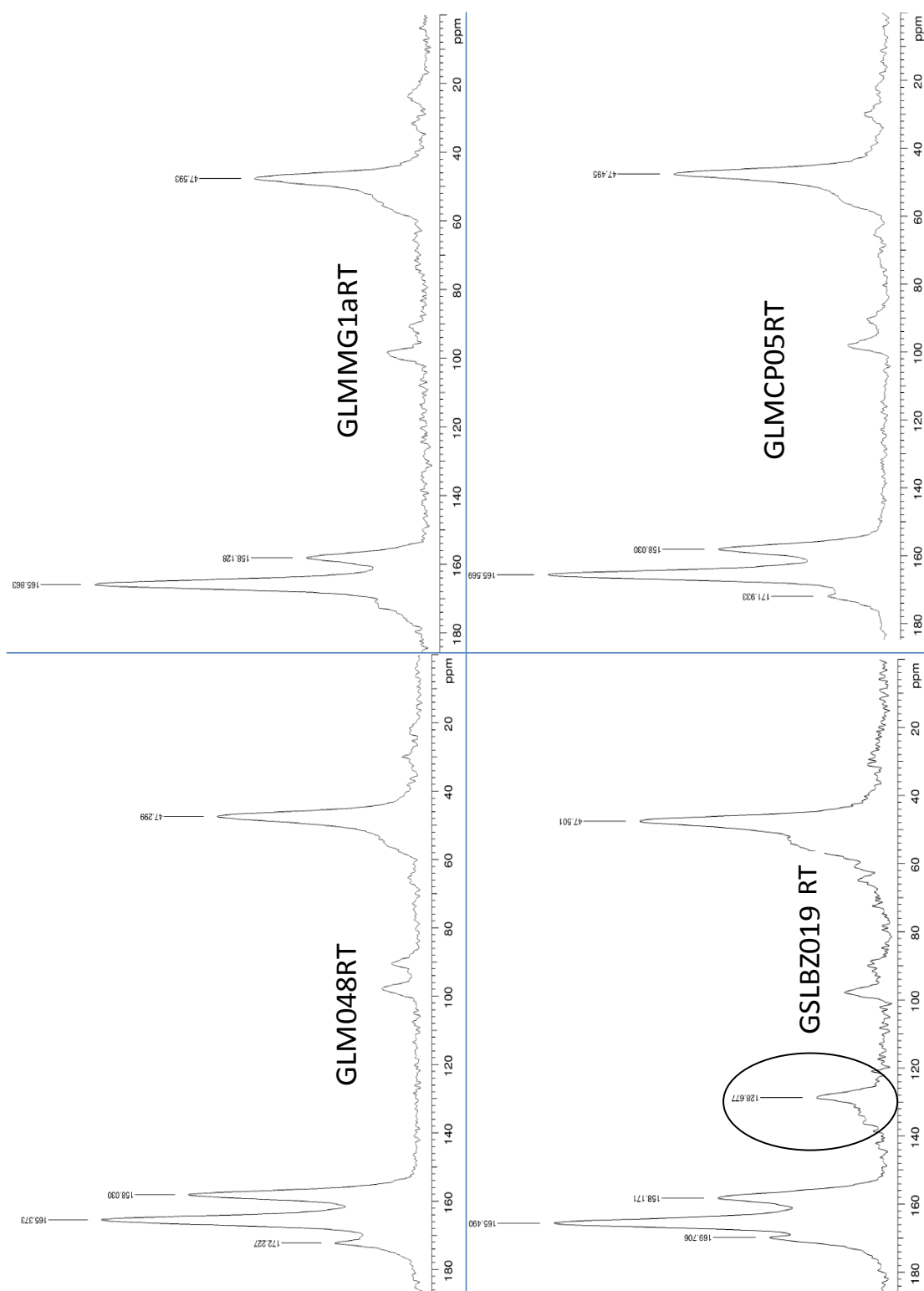
Figure 3.15: ^{13}C MAS NMR of four samples containing different monomers. All of these

samples have a M:F ratio of 1:1.5 and they all seem to display similar spectra. The circle

on the GSLBZ019RT spectrum is where peaks due to carbons on the benzene ring

resonate.
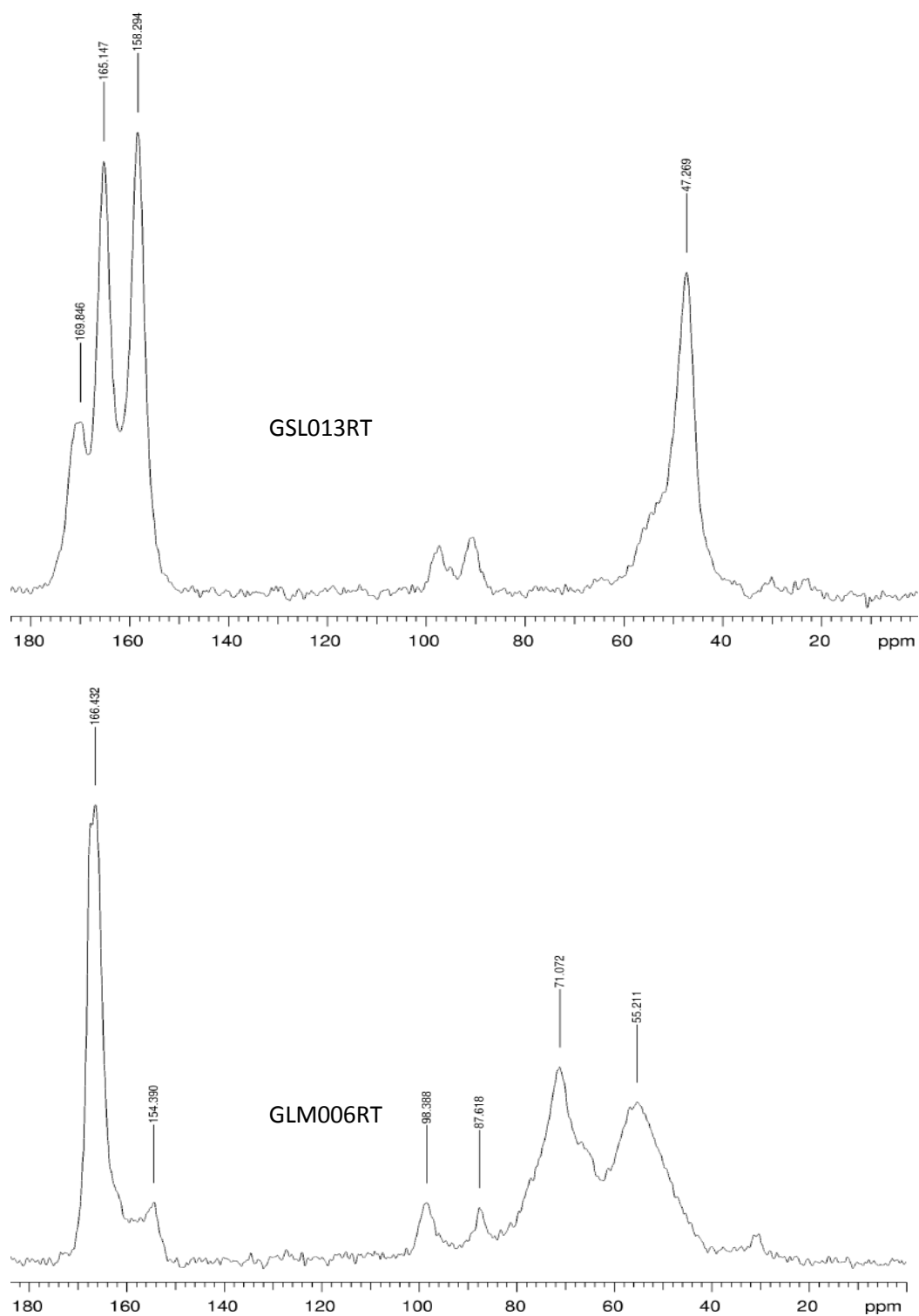
Figure 3.16: ^{13}C MAS NMR of two samples each consisting of similar MF/FA ratios but different M:F ratios. The MF/FA ratio of both samples are lower than the MF/FA ratios of samples shown in Figure 3.15.

Note: the spectrum of GLM006RT is very similar to the spectrum of the MF gel MFG2a (with M:F ratio of 1:3) produced by Egger *et al.*[17] Like the spectra displayed here in Figure 3.16, they showed that a peak at 60-80ppm appears in the samples with high M:F ratio and concluded that it was due to N-CH$_2$-O (of methylol or methylene ether units in the network).

Figure 3.16 shows that there are clear differences between spectra of GSL013RT and GLM006RT. The amount (or even the presence) of primary amines is modified considerably with M: F ratios. Also, the fact that different bridges have formed is a clear indication of the different cross-linking that has occurred within the material. ^{15}N CP-MAS NMR, with and without interrupted decoupling, was also carried out to use in conjunction with the ^{13}C MAS NMR data. These spectra, however, did not lead to conclusive data at this stage.

The IR spectra of GLM013RT and GLM06RT are shown below. An interesting remark is that GLM013 RT does not have a strong band at 811 cm^{-1} whereas GLM06RT does have an intense band at 811 cm^{-1}.
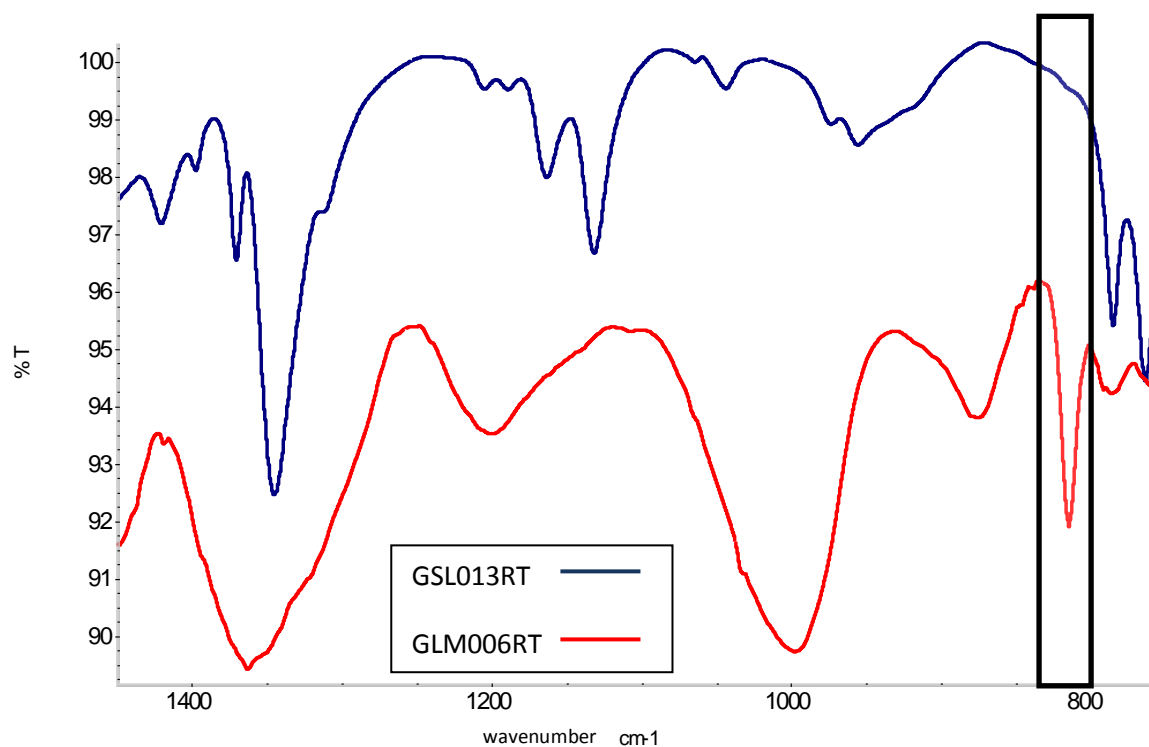
Figure 3.17: Expansion of IR spectra in the 1400-700 cm^{-1} region of GSL013RT and GLM006RT. The samples have different M:F ratios and GLM006 which has a high formaldehyde content has a stronger 811 cm^{-1} peak.

More work is required in understanding the factors influencing out-of-plane bending vibrations with IR spectroscopy. As for the NMR work, quantification of cross-linking would require peak deconvolution on ^{13}C CP MAS NMR and more experiments carried out by ^{15}N CP MAS NMR to start drawing conclusions.

3.4.2 MF materials containing commercial monomers

Table 3.10 below shows which vibrations should occur due to the introduction of benzene groups into the MF network.

Table 3.10: Expected changes to MF materials with the introduction of benzoguanamine.

Type of vibration	Frequency (cm^{-1})
=C-H	3105-3000 (stretching)
	900-720 (out-of-plane-deformation)
Aromatic C=C	1625-1430 (stretching)
	630-510 (ring deformation)

In Figure 3.18, IR spectra of benzoguanamine, a pure MF material and a material containing benzoguanamine are displayed.

MF materials tend to show very broad peaks in the region between 3500-2700 cm^{-1} of Figure 3.18 and they are even less defined and very weak in the spectrum of the benzoguanamine-MF materials. The region at 1800-1600 cm^{-1} seems quite distinct for benzoguanamine materials. The very intense and distinct vibration band in both benzoguanamine and pure MF materials at 1650 cm^{-1} has broadened and is no longer distinctive. The benzoguanamine materials show peaks at 1300 cm^{-1} and 1150 cm^{-1} that was also seen in all MF materials previously. And finally the region between 1200-900cm^{-1} is not very well defined and merged into two broad bands. The peak at 800 cm^{-1} which is characteristic of triazines is still observed, and another close by at 800-780 cm^{-1} which may be due to either benzene ring vibrations or iso-melamine conjugated with benzene.

Raman spectroscopy can potentially help to characterise vibrations from aromatic ring as this moiety is rather polarisable. Figure 3.19 shows a set of stacked Raman spectra for benzoguanamine, GSL015RT (a MF material) and GSLBZ019RT (a material containing benzoguanamine). There are vibrations in the benzoguanamine-MF sample specific to the benzene ring at 1000 cm^{-1}, 1025 cm^{-1} and 1600 cm^{-1}.
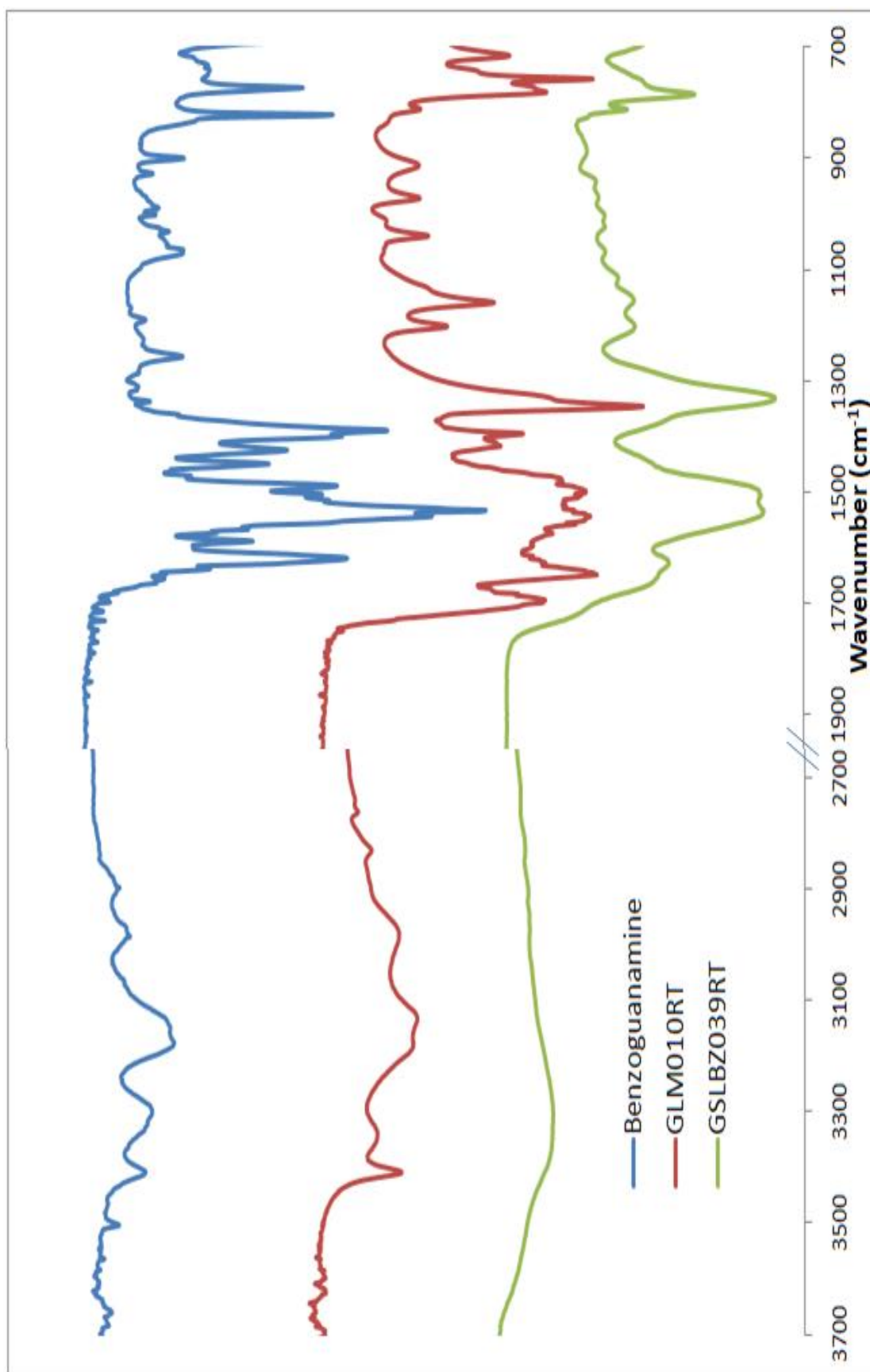
Figure 3.18: IR spectra of benzoguanamine (blue), a room temperature dried material

(red) and a benzoguanamine (10%)-MF sample dried at room temperature (green).
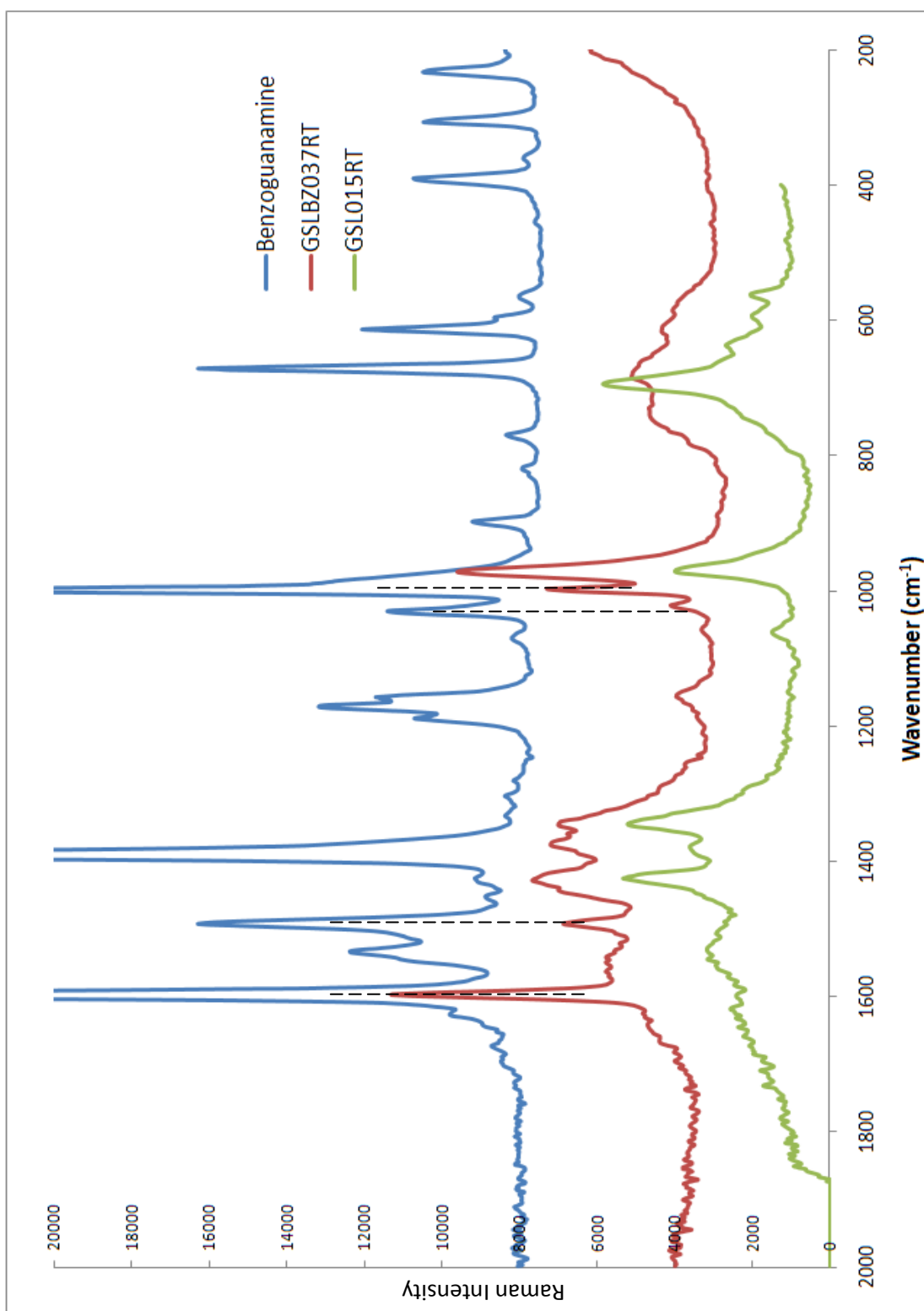
Figure 3.19: Raman spectra of benzoguanamine (blue), a benzoguanamine containing

material dried at room temperature (red) and a MF sample dried at room temperature

(green).

In Figure 3.20 the spectra of acetoguanamine, a MF material and an acetoguanamine-MF material are stacked.

As seen for the benzoguanamine containing materials, the region between 3500-2700 cm^{-1} is less defined and very weak in the spectrum (green) of the acetoguanamine material. The peaks present in the region 1800-1600 cm^{-1} in MF materials have also decreased in intensity as they did for benzoguanamine materials. The peaks present at 1300 cm^{-1} and 1150 cm^{-1} that were discussed previously seem very distinctive to all MF materials. The region between 1200-800 cm^{-1} shows very broad, undefined peaks. Again there is a series of sharper peaks around 800 cm^{-1}.
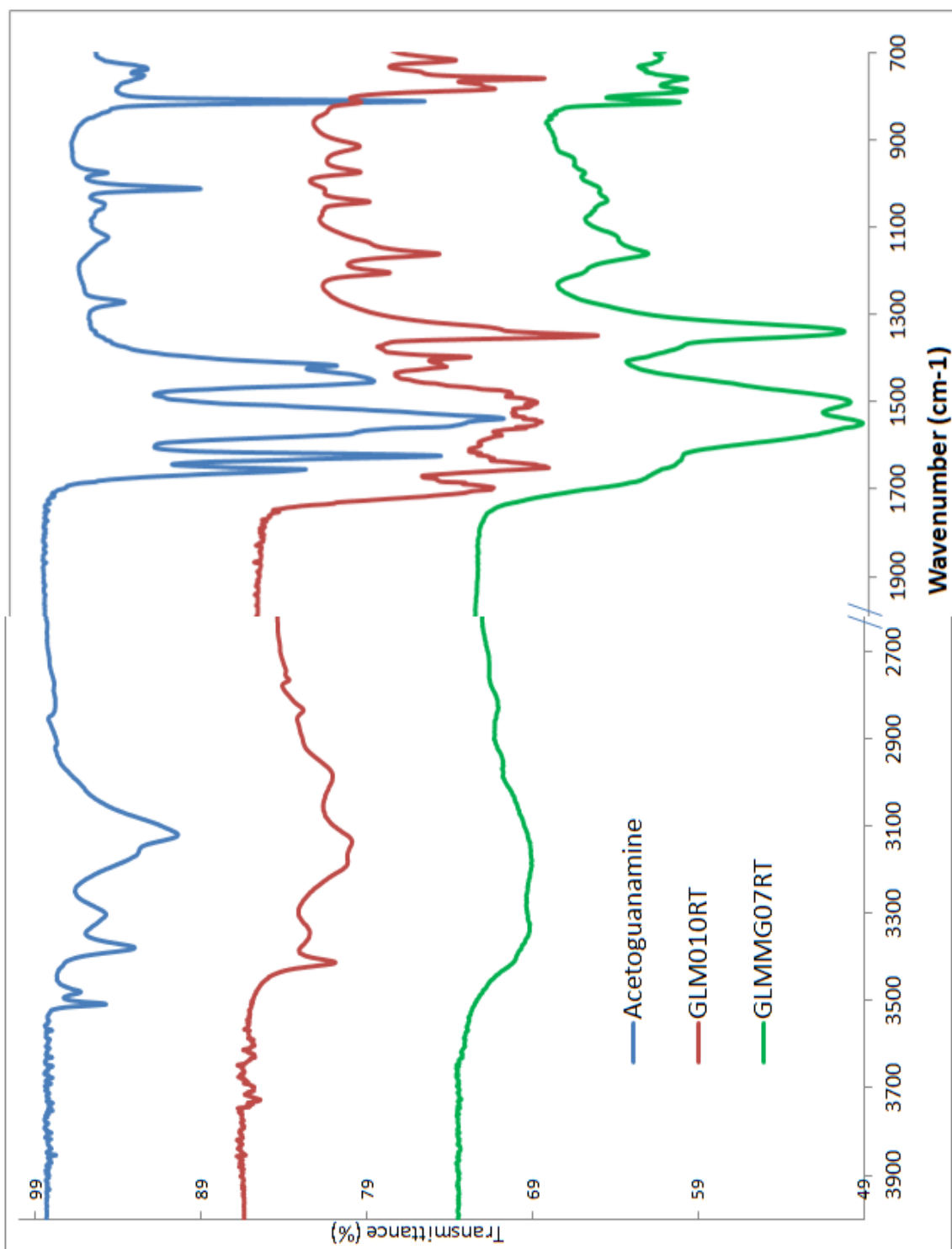
Figure 3.20: Stacked spectra of acetoguanamine (blue), a room temperature dried MF material (GLM010RT, red) and a room temperature dried acetoguanamine (10%)-MF material (green).

Figure 3.21 shows stacked spectra of caprinoguanamine, a MF material and a caprinoguanamine-MF material.

The material containing caprinoguanamine looks very similar to the spectra of materials containing acetoguanamine, discussed previously. The regions where changes occur are (i) 3500-2800 cm^{-1}, where broadening has occurred, (ii) 1800-1600 cm^{-1}, where the sharp peaks in pure MF materials have dramatically decreased in intensity to give broad shoulders to the main peak at 1600 cm^{-1} and (iii) 1200-800 cm^{-1}, weaker and sharper peaks in MF materials coalesce into two very broad, weak bands. There is also the very intense peak at 1300 cm^{-1} and the weaker one at 1150 cm^{-1}.

It is therefore possible to distinguish materials containing other monomers from pure MF materials solely using IR spectroscopy. The sharper stronger peaks at 1700 cm^{-1} and 1650 cm^{-1} present in the pure MF materials decrease and broaden significantly in the monomer containing materials. It is, however, difficult to be able to distinguish precisely which monomer is incorporated into materials. Raman Spectroscopy has proved to be a vital complementary tool in analysing benzoguanamine containing materials, due essentially to the fact that benzoguanamine itself has a very distinctive Raman signature.
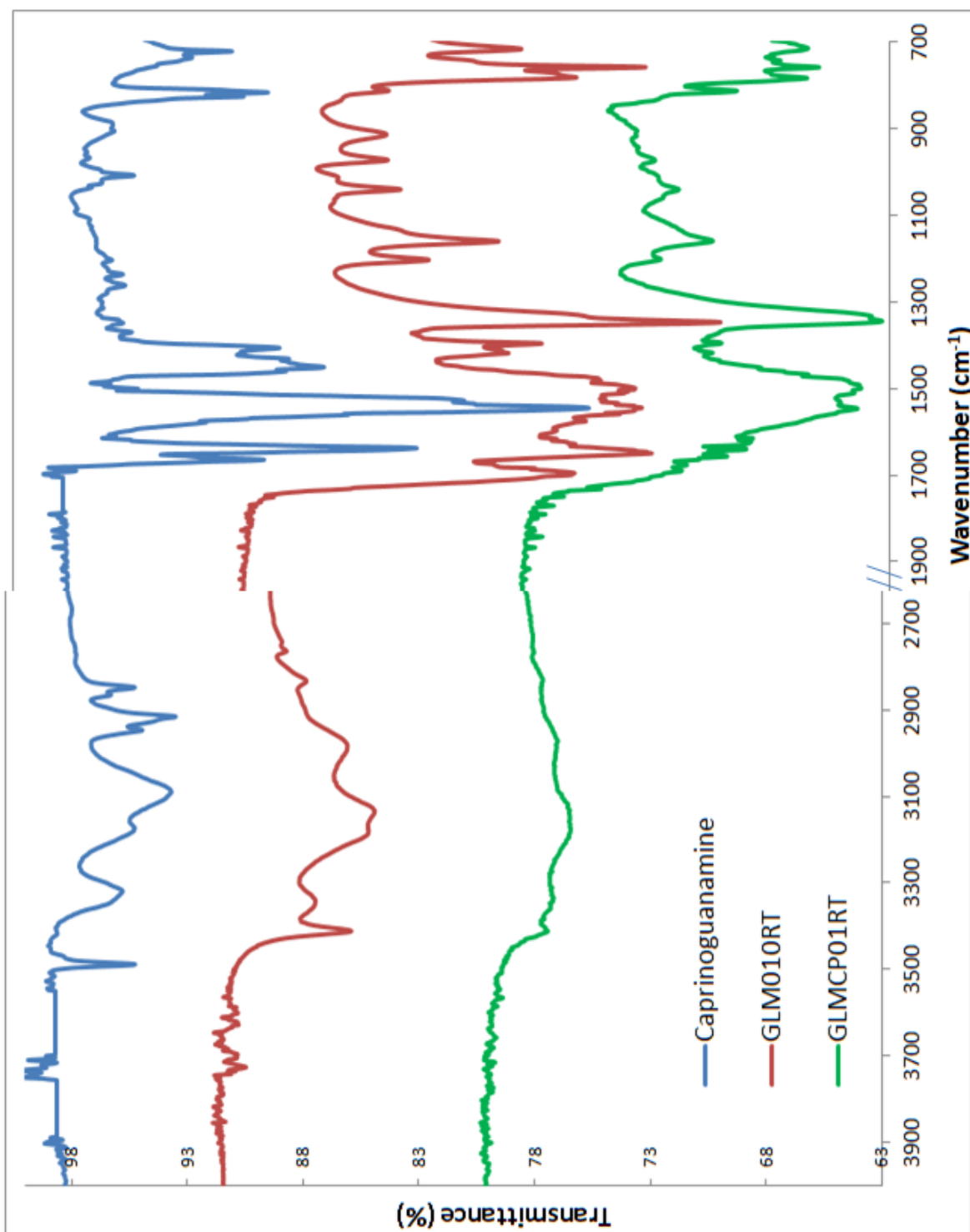
Figure 3.21: Stacked spectra of caprinoguanamine (blue), a room temperature dried MF material (red) and a room temperature dried caprinoguanamine(10%)-MF material (green).

3.4.3 MF materials containing monomers synthesised in-house

In this section, the IR spectra of materials containing monomers 1 and 2 are discussed. It is important to note that these monomers are not as pure as commercial monomers. Therefore the IR spectra were expected to be noisier. Primarily, the spectrum of materials containing monomer 1 should resemble the spectra of benzoguanamine containing materials. The expected change would be additional vibrations below 3000 cm^{-1} for the additional alkyl group and perhaps additional NH (**-CH(CH₃)**Ph) vibrations.

Figure 3.22 shows the IR of a monomer 1 containing material alongside monomer 1, a benzoguanamine containing material and a MF material. The peaks in 1700-1650 cm^{-1} region are slightly sharper for the blue spectrum than the benzoguanamine-MF one. Also as with all previous spectra of materials, the peaks at 1350 cm^{-1} and 1150 cm^{-1} are still present. There are also two peaks in the 800 cm^{-1} region.
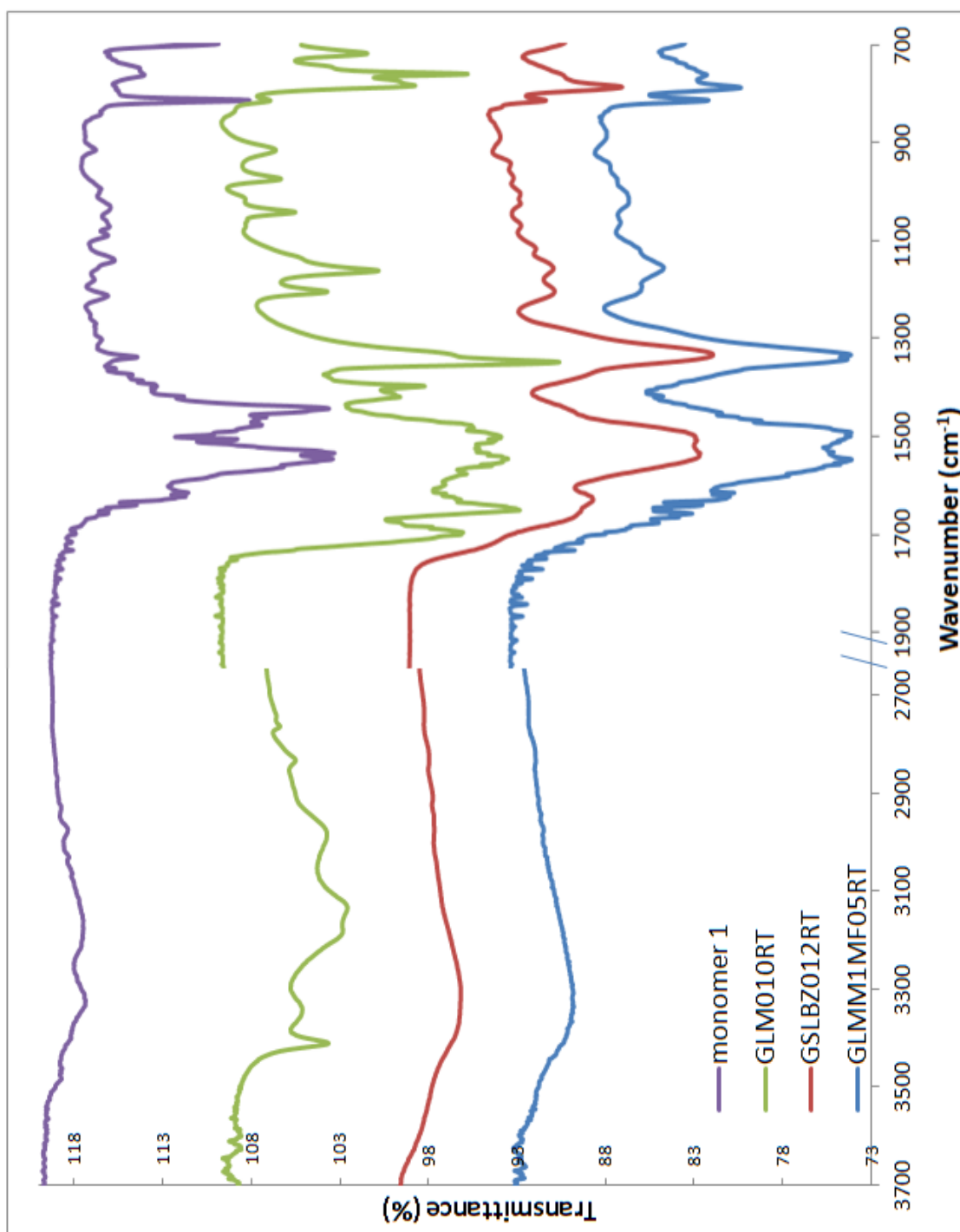
Figure 3.22: monomer 1(purple), a MF material (green) , a material containing

benzoguanamine (red) and a material containing monomer 1 (blue).

Figure 3.23 shows the IR of a monomer 2 containing material alongside monomer 2, an acetoguanamine containing material and a MF material. The spectrum of monomer 2-containing material is very similar to that of acetoguanamine materials. There is also the peaks characteristic of materials at 1350 cm^{-1} and 1150 cm^{-1}, with two peaks in the 800 cm^{-1} window.

As mentioned in chapter 2 on the synthesis of MF materials, materials containing monomer 3 were not synthesised thus the comparison of materials incorporating monomer 3 and caprinoguanamine containing materials has not been carried out.

It seems that, at this stage of the work, IR spectroscopy has not proved sufficient to easily differentiate between materials containing 10% of a melamine derivative.
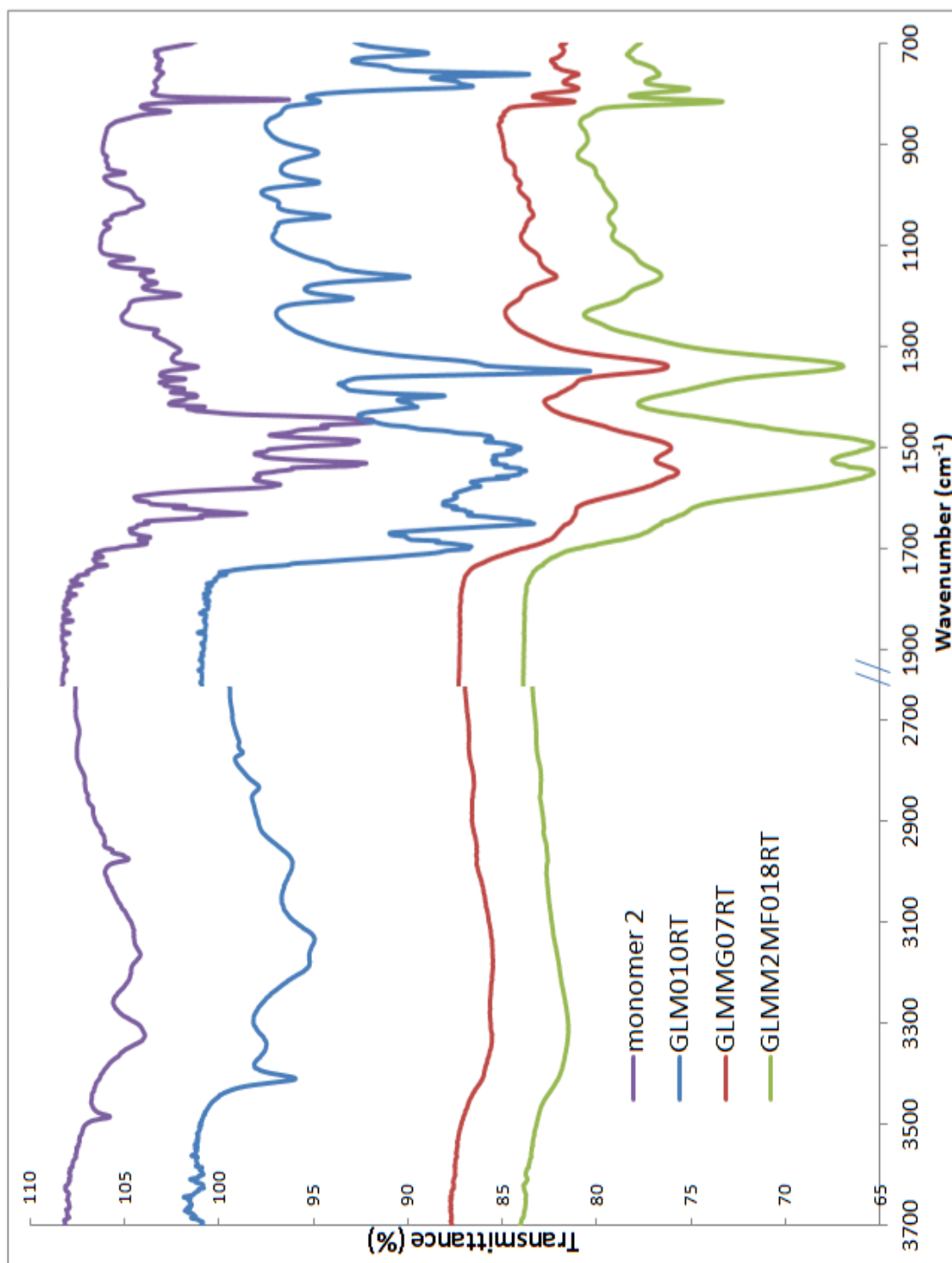
Figure 2.23: monomer 2 (purple), a MF material (green), a material containing acetoguanamine (red) and a material containing monomer 2 (blue).

3.5 The effect of post-treatment

3.5.1   Post- treatment with n-butanol
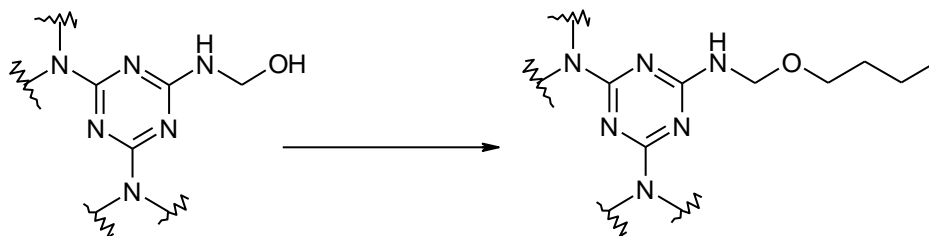
Figure 2.24: structural changes that may occur during butanol post-treatment

Figure 2.24 above shows what type of reaction is occurring upon post-treatment with butanol. The regions where the new vibrations occur when a MF gel is post-treated with n-butanol are given in Table 3.11.

Table 3.11: Expected functional groups present in n-butanol post-treated materials**.**

Expected functional groups	Wavenumber (cm^{-1})
-C-H (stretching)	2950-2800
-C-O (stretching)	1250-1100
-C-C	Not easily distinguishable

Figure 25 shows stacked spectra of butanol post-treated MF materials containing the different commercial monomers alongside the spectrum of a post-treated MF material.

At a first glance, it can be noted that many regions in the spectra of butanol post-treated samples are broader than the corresponding room temperature dried materials.

Notably, for the butanol post-treated MF material, sharp peaks can no longer be observed in the region of 3500-3000 cm^{-1}. It is difficult to notice any change for the materials containing the commercially available monomers as the peak in this region is already broad in the room temperature dried samples (3.18, 3.20 and 3.21). Both GLMMG07PT1 (an acetoguanamine containing material) and GLMCP05PT1 (a caprinoguanamine containing material) have alkyl stretching occurring at 2988 cm^{-1} and 2900 cm^{-1} in their spectrum. These peaks are cannot due to the presence of alkyl groups already present in the respective monomers since they are absent from the spectra of their room temperature dried counterpart (see Figure 3.26). Interestingly Larkin *et al.*[5], who carried out IR studies on alkylated MF resins, remarked that individual CH bonds of CH_2 or CH_3 are not identical when these groups are adjacent to an oxygen or nitrogen atom. If the substitution was O-CH_3, then the out-of-phase stretching occurs at 2988-2980 cm^{-1} and the in-phase stretching varies from 2965 to 2821 cm^{-1}. These two peaks could therefore be assigned to the two different CH_2-O stretching. However, when these butanol post-treated samples were dried under vacuum, these two peaks disappeared, suggesting that they were due to excess, non-grafted butanol on the MF matrix.

Like the observations made with the addition of different monomers to MF networks, in the region of 1800 to 1600 cm^{-1}, sharp peaks can no longer be observed in Figure 3.25. Instead a broad weak peak that produces a shoulder at 1700 cm^{-1} can be observed. That had already been remarked for materials containing a melamine derivative and dried at RT. This region therefore seems very specific to substitutions on side chain C-N groups. Any modifications to this group, whether it is a different functional group or a post-treatment, do manifest their presence.

More significant changes occur in the fingerprint region from 1250 to 850 cm^{-1}. In the post- treated materials, vibration in this region are no longer sharp compared to their room temperature dried counterparts, they have broadened considerably. Plus the vibration at 1065 cm^{-1} can increase significantly in the spectra of the post-treated materials. According to Larkin *et al.*[5], that could be due to C-O-C out-of-plane stretching. Peaks at ~1350 cm^{-1} and ~1150 cm^{-1} are still present in all these samples (which seem to be the vibration bands responsible for cross-linking are thus not affected by butanol post-treatment).
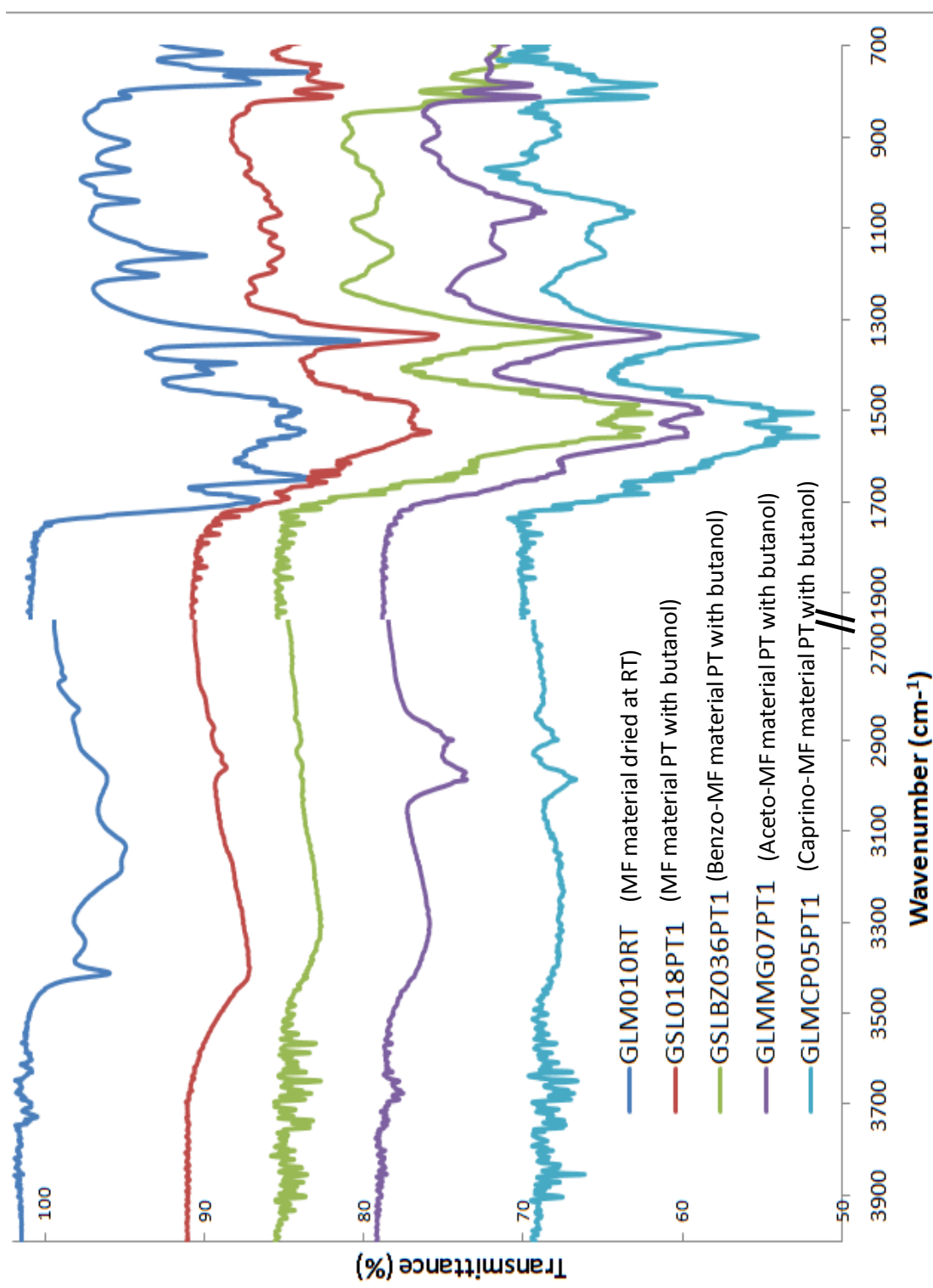
Figure 3.25: IR spectra of different cross-linked MF networks containing commercial monomers post-treated with n-butanol compared to the spectrum of a MF material dried at room temperature (dark blue). Note that the set of peaks at 2988 cm^{-1} and 2900 cm^{-1} disappear when the samples are dried under vacuum.
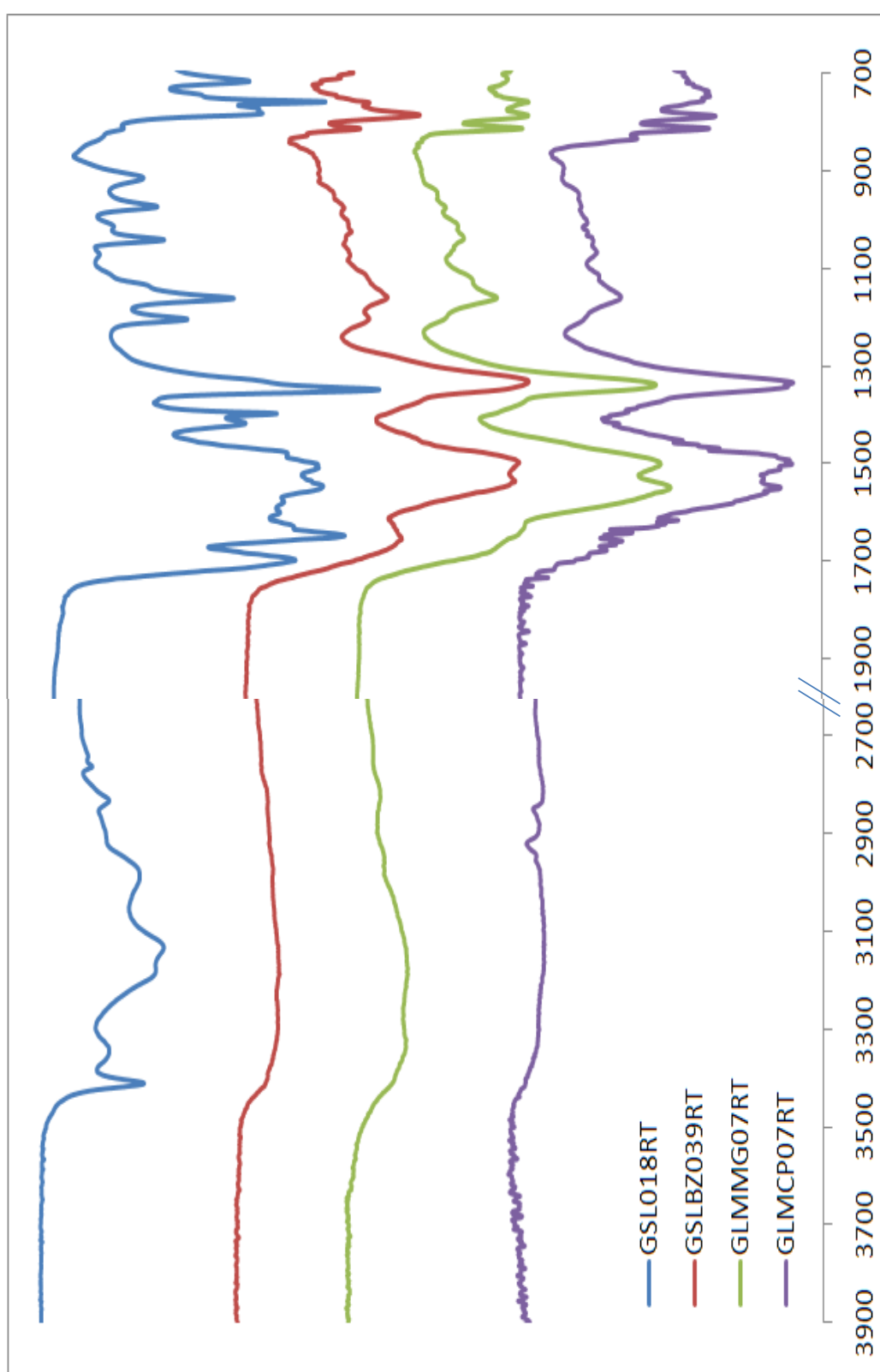
Figure 3.26: IR spectra of materials dried at room temperature for comparison with

Figure 3.25. The blue spectrum is of a pure MF sample, the red spectrum is for a

benzoguanamine containing material, the green spectrum is of an acetoguanamine

containing material and the purple spectrum is of a caprinoguanamine material.

3.5.2   Post-treatment with glutaraldehyde
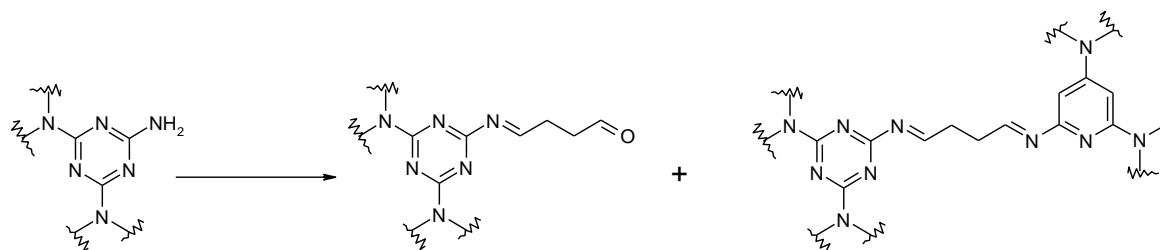
Figure 3.27: structural changes that may occur during n-butanol post-treatment.

Figure 3.27 above shows what types of reactions are occurring upon post-treatment with glutaraldehyde. The regions where changes should occur when a MF gel is post-treated with glutaraldehyde are given in Table 3.12.

Table 3.12: Expected functional groups present in glutaraldehyde post-treated materials.

Expected functional groups	Wavenumber (cm^{-1})
-C-H stretching	2950-2800
-C=N (stretching)	1700-1615
-C=O (stretching)	1700
-CH$_2$ (scissoring)	1470

As observed with the post-treatment with n-butanol, the sharp peaks in the MF room temperature dried samples at 3000 cm^{-1} have broadened, indicating that NH$_2$ stretching is not as distinctive. As Table 3.12 shows, the addition of alkyl groups to the materials should manifest as vibration bands in the 2900 cm^{-1}. In the spectra of Figure 3.28 there is a peak at 2930 cm^{-1} and for acetoguanamine and caprinoguanamine containing materials there is a smaller peak just after at 2870 cm^{-1}. These maybe explained by the observations

made by Larkin *et al.*[5] but as the heteroatom adjacent is nitrogen, there are slight variations in the position of the vibration bands. (Note: the samples were also dried under reduced pressure, as those post-treated with butanol, but even after 24 hours the peaks did not disappear, suggesting the material required heating under vacuum to be sure of the glutaraldehyde attachment to MF matrix).

At 1700 cm^{-1}, none of the glutaraldehyde post-treated samples have sharp, distinctive peaks as the room temperature dried MF material has. However, compared to the butanol post-treated samples, the 1700 and 1650cm^{-1} peaks may be more distinctive (although incredibly weak). They may be due to C=N imine type bonds, which commonly occur when aldehydes react with primary amines. C=O carbonyl stretching also occurs at 1700 cm^{-1}, it is therefore difficult to assign to what vibrations these peaks may be due.

What can also be noticed is that most MF materials have large broad bands in the 1600-1400cm^{-1}region. They manifest peaks at ~1550 and ~1500 cm^{-1}. In the spectra of glutaraldehyde samples, the region is still very broad but an additional peak is present at 1470-1460 cm^{-1}. This is the region in which CH$_2$ scissoring occurs.

The region from 1230 to 845 cm^{-1} region has changed from room temperature dried samples. This area seems very sensitive to peak broadening with addition of derivatives and/or post-treatments to the MF matrix as mentioned for butanol, but here a more resolved peak at 970 cm^{-1} is observed (not as well defined in the room temperature samples or the butanol post-treated samples) which surprisingly corresponds to C-O-C stretching. As with the butanol post-treatment, the peaks due to cross linking at 1350 and 1150 cm^{-1} are still intact.
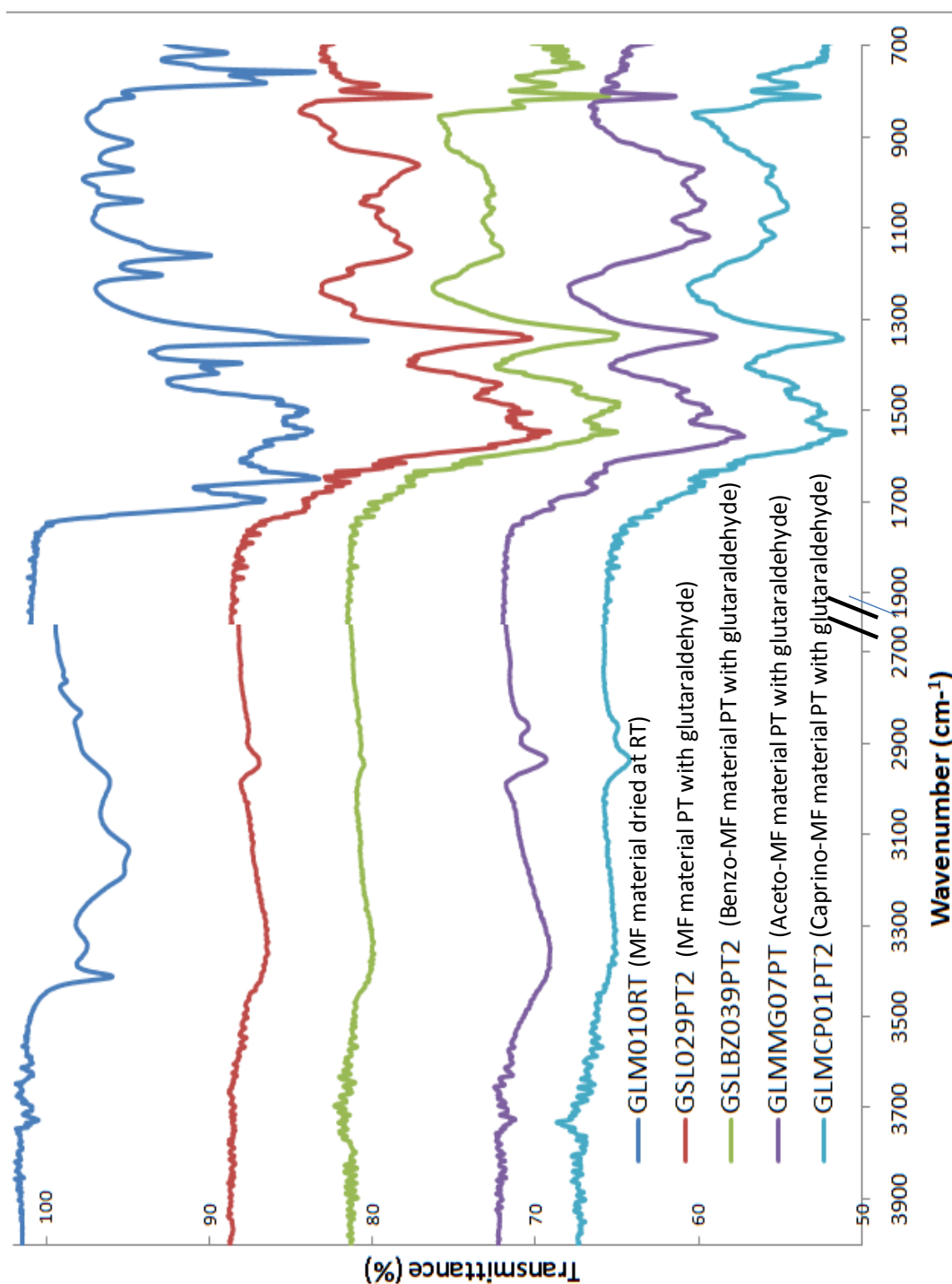
Figure 3.28: IR spectra of different cross-linked MF networks containing commercial monomers post-treated with glutaraldehyde n-butanol compared to the spectrum of a MF material dried at room temperature (dark blue).

### 3.5.2   Post-treatments of monomer 1 and 2 containing materials

Figure 3.29 and 3.30 show stacked spectra of monomer 1-MF materials dried at room temperature and post-treated with butanol and glutaraldehyde. The analyses previously carried out seem to remain applicable to these sets of spectra.

Firstly, as previously noticed the alkyl vibration bands at 2980 cm^{-1} and 2890 cm^{-1} become more intense for both post-treated samples. This is displayed in the post-treated monomer1-MF materials and monomer 2-MF materials.

In the 1700 cm^{-1} region a distinctive peak appears at 1670 cm^{-1} in both the glutaraldehyde post-treated materials. There seems to be a peak in both the butanol post-treated samples too at 1650 cm^{-1}, but it is also present in the room temperature samples, suggesting it originates from the monomers. The broad region around 1700-1400 cm^{-1} usually shows peaks at 1550 and 1500 cm^{-1} but as mentioned previously, the post-treatment with glutaraldehyde also shows a peak at 1450 cm^{-1}. This is also the case in both GM1MF05PT2 and GM2MF018PT2.

Both peaks (1350 and 1150 cm^{-1}) are still intact in the spectra of the materials. However in the region of 1200 to 900 cm^{-1}, both materials incorporated with synthesised monomers and post-treated with glutaraldehyde, show one large, broad band peaking at 1070 cm^{-1}. It was previously mentioned that one of the characteristic features of carrying out a post-treatment with butanol was that the weak peak at 1070 cm^{-1}. Although that still holds true for the monomer 2 containing materials, it has not occurred in the spectrum of GM1MF05PT1.
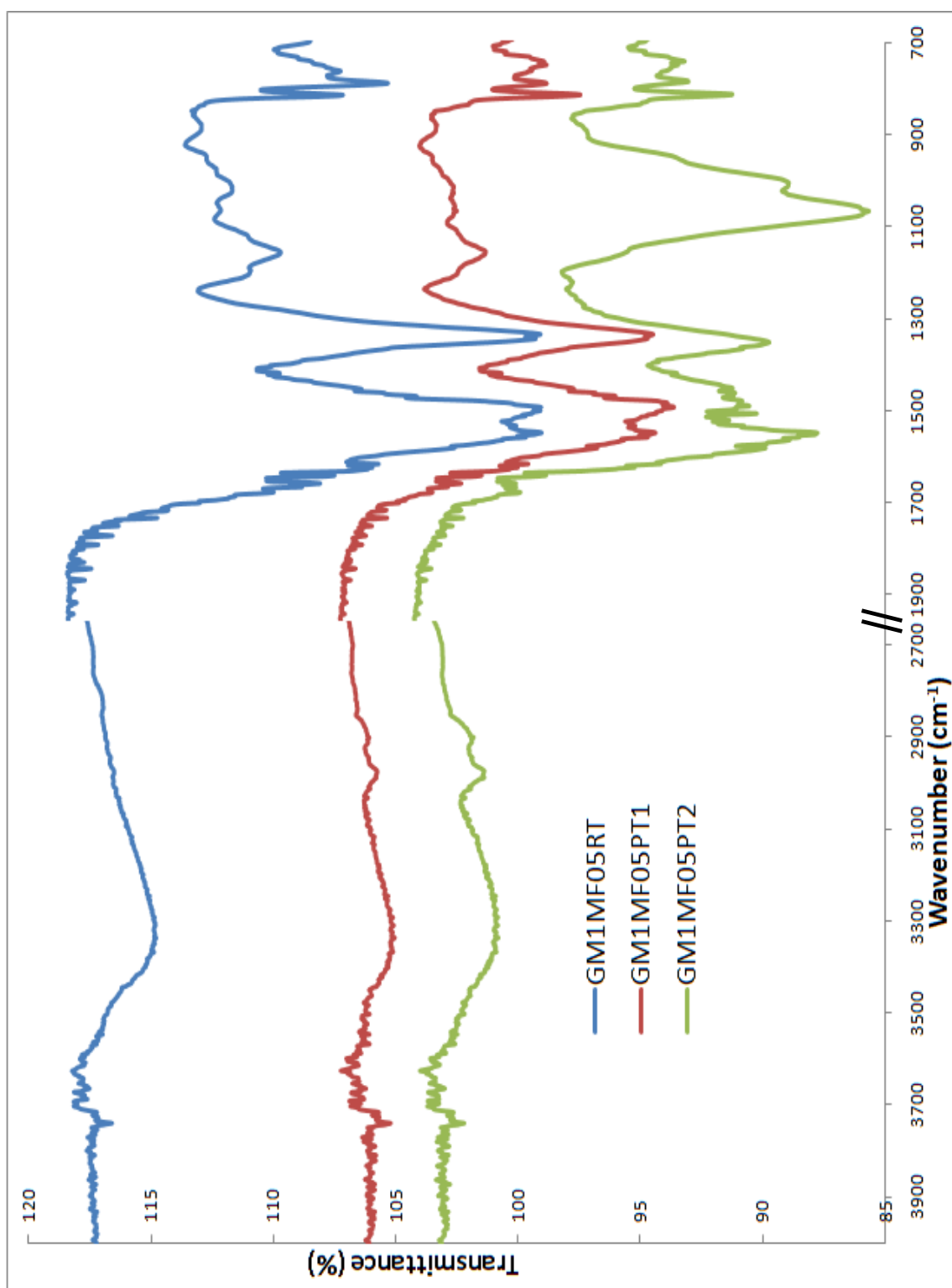
Figure 3.29: Stacked spectra of a material containing monomer 1 dried dusing different methods: i) at room temperature (blue), ii) post- treated with n-butanol (red) and iii) post-treated with glutaraldehyde (green).
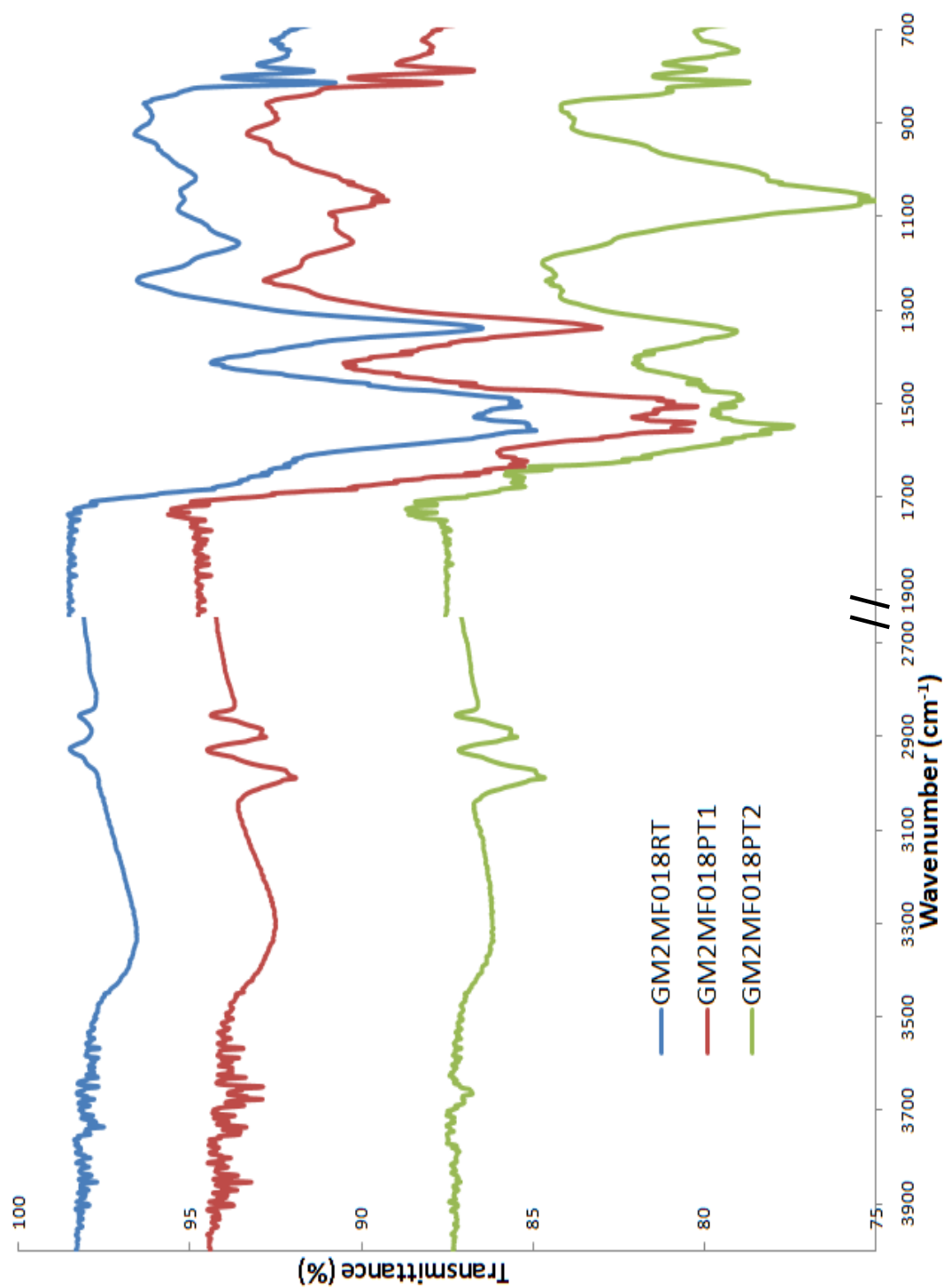
Figure 3.30: Stacked spectra of a material containing monomer 2 dried dusing different methods: i) at room temperature (blue), ii) post-treated with n-butanol (red) and iii) post-treated with glutaraldehyde (green).

3.5.4   Post-treatments with other aldehydes

Figure 3.31 and 32 show spectra of samples post-treated with glyoxal and pentaldehyde (valeraldehyde) respectively. They also show spectra of a glutaraldehyde post-treated MF sample and a room temperature dried MF material for comparison.

As described in chapter 2 on the material synthesis, these post-treatments were carried out to better understand the chemical reactions occurring during the glutaraldehyde post-treatment.

i)   Post-treatment with glyoxal

In the region of 3700 to 3000 cm^{-1}, the peaks present in room temperature dried MF sample have broadened, similarly to what had occurred during the post-treatment with glutaraldehyde. In the case of glyoxal however the peaks seem to be much broader and more intense.

Glyoxal does not add alkyl groups to the MF matrix, it is therefore normal not to observe any alkyl vibrations as seen for the post-treatment with glutaraldehyde.

A peak appears at 1670 cm^{-1}, which can sometimes be seen for glutaraldehyde but here it is better defined. This could again be due to either C=O stretching or C=N stretching.

In the region where there are large broad vibration bands at 1700 to 1400 cm^{-1}, for glutaraldehyde there was an additional peak that appeared at 1450 cm^{-1}. In the spectra of both the glyoxal post-treated samples, this additional peak is present too.

As with all post-treatment methods seen, glyoxal has not modified the peak at 1350 cm^{-1} and a small shoulder on the broad vibration band at 1200 cm^{-1} is observed. This broad band covers the 1200-900 cm^{-1} region and has a maximum at 1065 cm^{-1}. This region looks very similar to what was seen for the monomer 1 and monomer 2 containing samples and further post-treated with glutaraldehyde. Overall the spectra seem to show that glyoxal has reacted with the MF matrix.

ii)   *Post-treatment with pentaldehyde (valeraldeyhde)*

The region from 3700-3000 cm^{-1} has slightly broadened with pentaldehyde. However, the sharp singlet due to N-H stretching can still be seen, which completely disappeared for sample post-treated with glutaraldehyde and glyoxal. Contrary to glyoxal, addition of pentaldehyde to a MF matrix should manifest in vibration bands appearing at 2900 cm^{-1}, which is not the case. Both these observations seem to suggest that pentaldehyde had not reacted with MF.

In the region at 1700 cm^{-1}, however, a slight change can be observed. There is a shoulder on the broad region of 1700-1400 cm^{-1}, where there were sharp peaks in the room temperature dried MF samples. The region of 1200 to 900 cm^{-1} has also been broadened. These changes are consistent with the observations made with all post-treated samples and or addition of derivatives to MF. It is therefore difficult to unambiguously conclude if pentaldehyde has reacted with the material or if its presence as a coating has affected these regions. The samples therefore need to be dried beforehand.
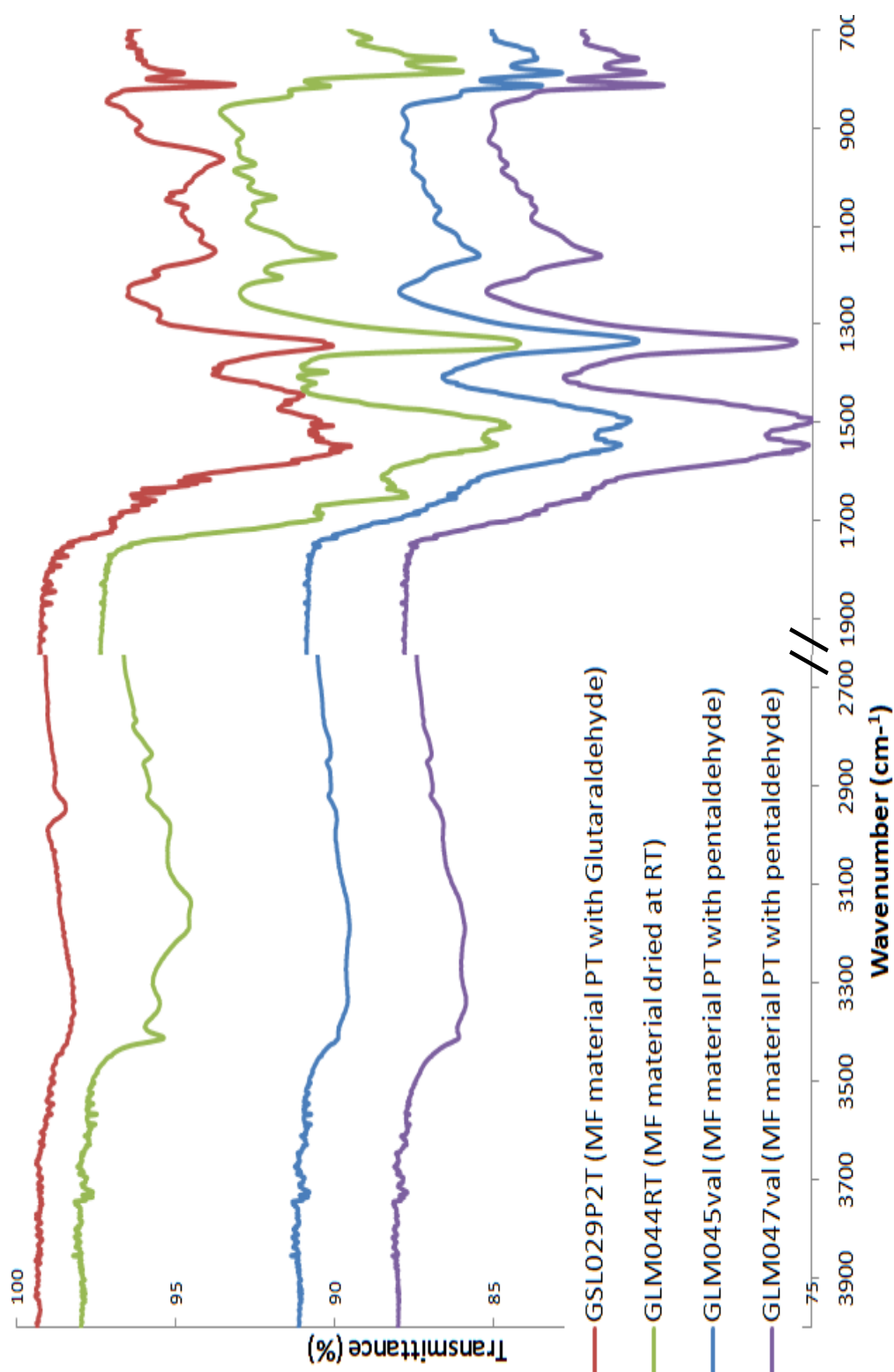
Figure 3.31: Stacked spectra of a MF materials post-treated with glutaraldehyde (red), a MF material dried at room temperature (green) and two MF materials post-treated with pentaldehyde (blue and purple).
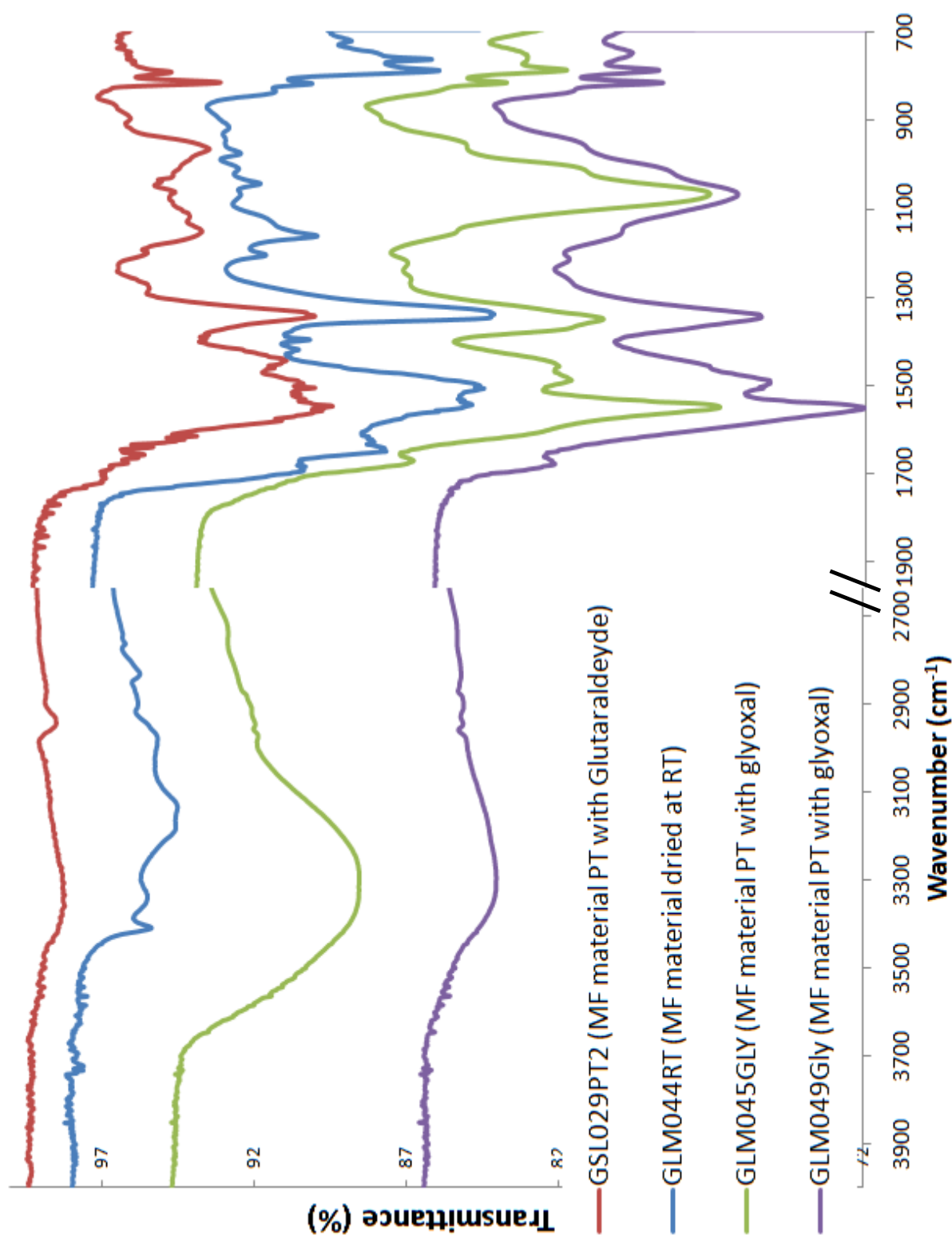
Figure 3.32: Stacked spectra of a MF materials post-treated with glutaraldehyde (red), a MF material dried at room temperature (blue) and two MF materials post-treated with glyoxal (green and purple).

4. Conclusions

In this work, both IR spectroscopy and Raman spectroscopy and have successfully been employed to produce well defined spectra for melamine as a single molecule. To date, highly cross-linked melamine-formaldehyde networks by acid catalysis had not been previously investigated and this work shows that two distinctive peaks feature at 1350 cm^{-1} and 1150 cm^{-1}, which are vibrations due to the bridging of resin precursors (-C-N units or C-O-C).

Incorporation of melamine derivatives, however, is not easily distinguishable at 10% ratio by IR or Raman spectroscopy, but produces slightly different spectra to that of pure MF materials. Nevertheless, distinguishing between monomers is yet to be achieved.

On the other hand, post-treatment methods with butanol or glutaraldehyde can be noticed on spectra. In both cases, there is an increase in intensity for the $1070cm^{-1}$ band; and for the glutaraldehyde post-treatment, a peak appears at 1460 cm^{-1}.

Determining the degree of cross-linking was attempted but the data obtained at this stage is not yet conclusive. Further work is required by solid-state NMR, especially ^{15}N CP-MAS NMR, to elucidate the nature of bridging occurring between precursors and also to relate the findings back to synthesis conditions (concentration of M:F and MF:FA).

5. References

[1] Ashrafi, A. R. (2005). "Full Non-Rigid Group Theory and Symmetry of Melamine." *J Iran. Chem. Soc.* **2**(2): 135-139.

[2] Goubeau, J., Jahn, E. L., Kreutzberger, A., .Grundmann, C. (1954). "Triazines. X. The Infrared and Raman Spectra of 1,3,5-Triazine." *J. Phys. Chem.* **58**: 1078-1080.

[3] Atkins P., *Physical Chemistry*, Oxford, 8th Edition, 2006

[4] Padgett, W. M., Hamner, W. F. (1957). "The Infrared Spectra of Some Derivatives of 1,3,5-Triazine." *J. Am. Chem. Soc.* **80**(4): 803-808

[5] Larkin, P. J., Makowski, M. P., Colthup, N. B., Flood, L. A. (1998). "Vibrational analysis of some important group frequencies of melamine derivatives containing methoxymethyl, and carbamate substituents: mechanical coupling of substituent vibrations with triazine ring modes." *Vib. Spectrosc* **17**: 53-72.

[6] Sun, F., Ma, W. Xu, L., Zhu, Y., Liu, L., Peng, C., Wang, L., Kuang, H. Xu, C.(2010) "Analytical methods and recent developments in the detection of melamine." *Trends Anal Chem* **29**(11): 1239-1249.

[7] He, L., Liu, Y., Lin, M., Awika, J., Ledoux, D., Li, H., Mustapha, A. (2008). "A new approach to measure melamine, cyanuric acid, and melamine cyanurate using surface

enhanced Raman spectroscopy coupled with gold nanosubstrates." *Sens. Instrum. Food Qual. Saf.* **2**(1): 66-71.

[8] Larkin, P. J., Makowski, M. P., Colthup, N. B. (1999). "The form of the normal modes of s-triazine: infrared and Raman spectral analysis and ab initio force field calculations." *Spectrochim. Acta.* **55**: 1011-1020.

[9] Liu, Y. L., Chao, K. L., Kim, M. S., Tuschel, D., Olkhovyk, O., Priore, R. J. (2009). "Potential of Raman Spectroscopy and Imaging Methods for Rapid and Routine Screening of the Presence of Melamine in Animal Feed and Foods." *Appl. Spectrosc.* **63**(4): 477-480.

[10] Scheepers, M. L., Gelan, J. M., Carleer, R. A., Adriaensens, P. J., Vanderzande, D. J., Kip, B. J., Brandts, P. M. (1993). "Investigation of Melamine-Formaldehyde Cure by Fourier-Transform Raman-Spectroscopy." *Vib. Spectrosc.* **6**(1): 55-69.

[11] Scheepers, M. L., Meier, R. J. Markwort, L., Gelan, J. M., Vanderzande, D. J., Kip, B. J.. (1995). "Determination of Free Melamine Content in Melamine-Formaldehyde Resins by Raman-Spectroscopic." *Vib. Spectrosc.* **9**(2): 139-146.

[12]Meier, R. J., Tiller, A., Vanhommerig, S. A. M. (1995). "Molecular Modeling of Melamine-Formaldehyde Resins .2. Vibrational-Spectra of Methylolmelamines and Bridged Methylolmelamines." *J. Phys. Chem.* **99**(15): 5457-5464.

[13] Ebdon, J. R., Hunt, B. J., Orourke, W. T. S., Parkin, J. (1988). "Characterization of Some Melamine Formaldehyde Condensates and Some Cured Resins by ^{1}H-, ^{13}C- and ^{15}N- NMR-Spectroscopy." *Br. Polym. J.* **20**(4): 327-334.

[14] Baraka, A., Hall, P. J, Heslop, M. J. (2007). "Preparation and characterization of melamine-formaldehyde-DTPA chelating resin and its use as an adsorbent for heavy metals removal from wastewater." *React. Funct. Polym.* **67**(7): 585-600.

[15] Egger, C. C., Schadler, V., Hirschinger, J., Raya, J., Bechinger, B. (2007). "H-1-C-13 CPMAS and T-2 relaxation solid-state NMR measurements of melamine-based polycondensed chemical gels (vol 208, pg 2204, 2007)." *Macromol. Chem. Phys.* **208**(21): 2375-2375.

[16] Wang, Y.-L., Wu, C. J., Chen, Y. T., Lin, C. E., Jiang, J. C. (1997). "IR spectroscopy and theoretical vibrational calculation of the melamine molecule." *Faraday* **93**(19): 3445-3451.

[17] Costa, L. and Camino G. (1988). "Thermal behaviour of melamine." *J. Therm. Anal. Calorim.* **34**(2): 423-429.

[18] Socrates, G. (2001). *Infrared and Raman Characteristic Group Frequencies: Tables and Charts*, Wiley.

[19] Salaun, F., Vroman, I. (2008). "Influence of core materials on thermal properties of melamine-formaldehyde microcapsules." *Eur. Polym. J.* **44**: 849-860

[20] Dante, R. C., Gil, J. M., Pallavidino, L., Geobaldo, F.. "Synthesis under Pressure of Potential Precursors of CNx Materials Based on Melamine and Phenolic Resins." *J. Macromol. Sci., Phys.B* **49**(2): 371-382.

[21] Blank, W. J. (1979). "Reaction-Mechanism of Melamine Resins." *J. Coat. Technol.* **51**(656): 61-70.

CHAPTER 4: Evaluating Molecular Recognition Properties within Novel MF Materials

Contents

1. Introduction

As mentioned in chapter 1, molecular recognition is the ability for particular functional groups of a molecule to bind to other functional groups in another molecule or another part of a molecule through weak and reversible interactions such as hydrogen bonding, electrostatic interactions and π- π stacking. This association is based on complementary donor-acceptor sites between the receptor and donor, as seen with cyanuric acid and melamine. In order to suppress any interference, the solvents used to bring these molecules together in solution are typically aprotic organic solvents such as chloroform, particularly in the case of hydrogen bonding, where protic solvents would compete with the association of molecules[1].

However, molecular recognition defines many binding processes in biological entities (receptor-ligand association, enzyme-substrate binding, antibody-antigen complexes, etc.), which occur in aqueous environments. Therefore artificial receptors able to perform recognition in water are of great interest. This challenging concept has been documented previously[2,3] and the conclusion reached was that molecular recognition in aqueous media was successful due to cooperative effects of π stacking or electrostatic interactions.

In fact, in biological systems, extreme selectivity is fully achieved not only by the functional groups acting in a cooperative manner, but also because the cavity has a shape to match that of the substrate. In 1972, Wulff *et al.* [4,5] introduced these types of cavities into organic polymers in order to form synthetic materials capable of mimicking molecular binding of biological systems. These materials are called molecularly imprinted

polymers (MIPs) and they provide a promising area of development in chromatography, catalysis research, biosensor technology and the production of artificial antibodies[6,7].
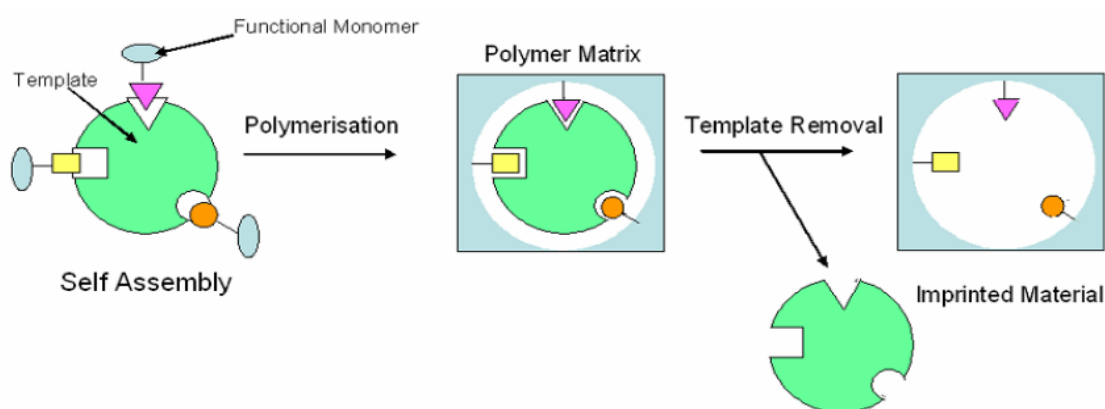
1.2   Molecular imprinting

Molecular imprinting was recognised in 1931 when Polyakov reported on the unusual adsorption of solvent (benzene, toluene, xylene) in silica polymeric gels which had been pre-exposed to them during gel synthesis.[8] Slightly after this date Linus Pauling also proposed his antibody formation theory[9]. He stated that biological specificity resulted from complementary association due to molecular structures of the interacting entities[10]. From the early 80's onwards, however, interest in this field has soared considerably due primarily to the possibilities that the introduction of molecular recognition properties in bulk macromolecular structures would offer[11].

Molecular imprinting has been defined in a review by Alexander, Andersson, Ansell *et al.* as: 'The construction of ligand selective recognition sites in synthetic polymers where a template (atom, ion, molecule, complex or a molecular, ionic or macromolecular assembly, including micro-organisms) is employed in order to facilitate recognition site formation during covalent assembly of the bulk phase by polymerisation or poly-condensation process, with subsequent removal of some or all the template being necessary for recognition to occur in the spaces vacated by the templating species.'[8]

The concept is schematically illustrated in Figure 4.1 where, in the first step, functional monomers that bear specific functional groups interact with a template molecule through weak interactions. These functional monomers are then polymerised into a solid matrix with a cross-linker and the template is removed. This leaves behind a

vacant space within a material that can then rebind to a template-like molecule when re-exposed to it.

Figure 4.1: A schematic representation of the molecular imprinting technique adapted from [11]. In the first instance polymerisable molecules interact with different functional groups on a template via weak interactions. In the second step they are held in place by polymerisation around them. The template is then removed and a vacant site is left behind for recognition.

The very first types of precursors used for the polymeric (backbone) matrix were silicates[10,12], where it was found that the silica pore structure was influenced by benzene, toluene or xylene which were used as porogens.[13] Over the few decades that followed, however, more and more work on organic molecularly imprinted polymers was reported, typically using vinyl-containing precursors[11]. This is mainly due to the wider range of functionality available with such precursors as well as the ease and rapidity of cross-linking by radical polymerisation.

As with supramolecular recognition, molecular imprinting within vinyl polymers was limited to uses in apolar solvents. In 1995, however, Mosbach *et al.*[14] reported that MIPs, initially produced in non-polar solvents, could still be applied to recognition in water, (conditions which are more relevant to biological systems) just as well as they did in solvents such as toluene. Again this was most probably due to cooperative weak forces acting together. Mosbach *et al.*[10,15,16] then reported soon after that imprinting can actually occur in water by incorporating functional groups adapted for hydrophobic interactions and ionic bonding.

The library of commercially available silica precursors bearing functional groups has recently been extended; hence the sol-gel chemistry of silicates has resurged. In fact, a wide variety of organic silicates now contain functional groups such as amino, phenyl and alkyl, plus the milder conditions used in sol-gel processing with silicates (aqueous media, mild temperature and pH) are more compatible with molecules similar to biological systems. As discussed in chapter 2, the sol-gel process offers versatility in precursors (organic-inorganic hybrids), final shape of material (film, bulk or powder) and the incorporation of additional entities such as dyes and of course template molecules. In fact, the encapsulation of enzymes[17], proteins[18], bacteria and viruses (E-coli[19], tobacco mosaic virus[20]) within sol gel materials, without modifying the physical and chemical properties of the polymer matrix, has been successfully reported and reviewed[21,22].

Other advantages of sol-gel materials include high thermal stability meaning that removal of template molecules through liquid-liquid extractions (which is often incomplete and some template molecules remain within the material) can be avoided and that instead the template molecules can fully be destroyed by combustion. Also, the

introduction of porosity by solvent removal and its relative control (size and density) within the materials mean materials can have a greater reactive surface area as well as good diffusion of analytes through the material, which is not easily achievable with vinyl polymers[8].

Some researchers have gone as far as inducing chirality in sol-gel (silicate-based) MIPs[23]. They describe this concept by taking three approaches (i) using silanes bearing a chiral group and covalently grafting them on the surface of pores within given materials; (ii) using chiral silanes as monomers or co-monomers in sol-gel polycondensations; and finally (iii) physical entrapping of chiral molecules via sol-gel processing and subsequent removal of the molecule to leave behind chirally imprinted cavities. These materials can have application in sensing, catalysis, chromatography[24], and optics. In fact, there is a lot of scope in enhancing chirality in most MIPs, notably those based on vinyl monomers, as current MIPs have displayed high binding site heterogeneity (binding mainly occurs at the surface of materials) and there is generally a low density of high-affinity binding sites (the number/type of binding sites needs to be enhanced)[25].

Most of the previous reports on sol-gel MIPS has been restricted to silica, titanium, zirconium and aluminium oxide based precursors[8]. It is, however, possible to extend sol-gel processing to organic precursors (as previously discussed in chapter 2) such as urea-formaldehyde, resorcinol-formaldehyde and melamine-formaldehyde but interestingly these have not yet been widely reported to date as having uses in synthesising MIPs.

The triumph of molecular imprinting is also impeded by the size of the template. It is often more difficult to imprint bio-molecules such as enzymes and proteins. Notably sol-gel systems have shown certain adaptabilities to these fragile structures [17-22], but in most

polymer systems it is often very difficult to fully control the homogeneity of cross-linking. The final material might be very highly cross-linked and it is too dense for analytes to access active sites within it or, on the contrary, too loose (very porous sol-gel systems) for good analyte retention. Some heterogeneously cross-linked materials may even demonstrate both of these problems.

However, control, to a certain extent, of porosity (final pore size and volume but also distribution) within melamine-formaldehyde systems has been reported[26,27,28]. Plus, the MF systems synthesised in these works are completely compatible with the aqueous phase (solvent used for the synthesis). Also, chiral recognition with melamine has already been achieved[29]. The potential, therefore, of such resins in preparing MIPs is enormous and the interest they generate has started to show slowly in the literature.[40,41,42]

1.3   Role of melamine and triazines in molecular imprinting

Many herbicides, notably atrazine, simazine and propazine, belong to the chemical group of triazines. They have played a role in molecular imprinting as template molecules to produce sensors[30] or solid phase extraction sorbents[31] for environmental pollution monitoring. In both cases the functional monomer, which has to initially form complexes with the template molecule, is methacrylic acid (MAA). The polymer matrix which binds MAA into place is cross-linked with ethylene glycol dimethacrylate (EGDMA), as shown in Figure 4.2.
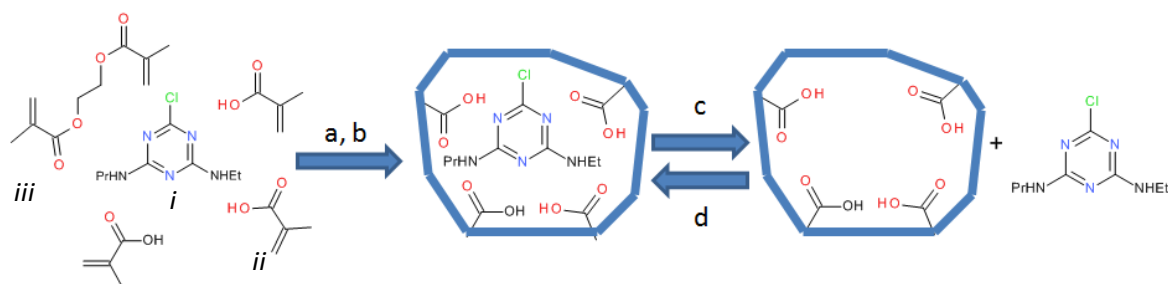
Figure 4.2: Reaction scheme of molecular imprinting of a triazine herbicide, atrazine, used by Matsui *et al.*[31] In the first instance, the template molecule *i* and a functional monomer methacrylic acid *ii* are mixed to form complexes (a). The atrazine– methacrylic acid complexes are cross-linked with ethylene glycol dimethacrylate *iii* (b). *i* is extracted from the cross-linked polymer network (shown with bold lines) using dichloromethane (c). The resultant cavities, complementary to *i*, work as selective binding sites (d).

However, Matsui *et al.*[32] reported that a flaw to using atrazine directly as the template was that incomplete removal of it during MIP synthesis led to it seeping out when the polymer was used for atrazine capture, falsifying the results. Using a different template molecule to the one that is to be locked into the cavities was therefore a better method. The group used trialkylmelamines instead as dummy molecules. Also, in 2002, Turiel *et al.*[33] produced MIPs using propazine as a template and found that their materials were able to bind with many other triazine based compounds equally as well as binding to propazine.

The synthesis of all of the above MIPs was carried out in *organic* solvents such as DMF and chloroform due to the organic nature of the precursors. The MIPs were however used to remove triazine herbicides from *aqueous* solutions after grinding the formed polymers

and packing into columns or cartridges. This echoed work reported by Mosbach *et al.*[13, 14] before this date whereby aprotic organic solvents (chloroform, tetrachloromethane) were used because protic solvents compete for hydrogen bonds with the target molecule.

He *et al.* [34] and Curcio *et al.*[35] reported on the specific extraction of melamine in water. He *et al.* used cyromazine as the template molecule (to prevent seepage, as described above) and the synthesis of the polymer was carried out in water compatible solvents (mixture of methanol/water). They concluded that their method eliminated the use of costly organic and toxic solvents. Curcio *et al.* reported that their MIP system was only possible in partial aqueous medium.

Due to the recent incidents in 2007-2008 of melamine contaminants found in pet food and milk formula, many research groups have reported on the use of molecularly imprinted polymers for detecting melamine in milk and dairy products (Liang 2009[36], Yang 2009[37], Wang 2011[38]). The polymerisation to form the MIPs is carried out in both organic solvents (THF, benzene) and aqueous conditions. They all use MAA and EGDMA, which undergo radical polymerisation with AIBN. Combining their analysis with other techniques such as HPLC and flow analysis, they concluded that they were able to accurately detect the levels of melamine added to spiked milk samples.

To date, very little work has been reported on sol-gel MIP materials featuring melamine, however. Going back to the work briefly mentioned by Arrachart *et al.*[39] in chapter 1, upon which the synthesis of monomers was based, the group incorporated cyanuric acid functionality into hybrid silica materials using a sol-gel process and used melamine as a template molecule. They used nitrogen sorption, FTIR and solid state NMR to provide evidence that their materials could retain melamine. They, however, suggested

that the harsh treatments of template removal (in strong acids) created structural modifications to the MIP and that the complete re-introduction of melamine was not obtained.

In 1996, Asanuma *et al.*[1,40] used poly(vinyldiaminotriazine), a triazine-containing polymer, as a back-bone material to bind to heterocyclic bases in water (uracil and thymine were better candidates than the other three bases found commonly in nucleotides). In 1998[41] the group reported the use of the same type of polymers to bind to nucleotides. They found that the binding constant between thymidine and the polymer was extremely large. They claimed that this was due to the additional interactions between the phosphate moiety and the diaminotriazine residues, as depicted in Figure 4.3.
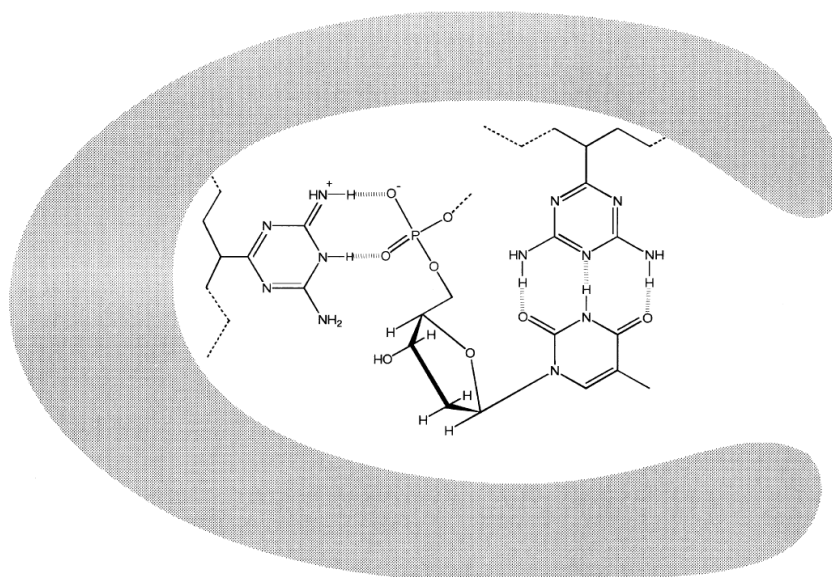
Figure 4.3: Asanuma *et al.*[39] found that thymidine bound better to poly(vinyldiaminotriazine) than thymine due to the added phosphate moiety strengthening weak interactions between the polymer and the target molecule.

In 1997, Iuliano *et al.*[42] reported on using a triazine-based (2-chloro-4(S)-1-(1-naphthylyl)ethylamino-6-L-Val-L-Val-L-valine isopropyl ester 1,3,5-triazine) stationary phase in high- performance liquid chromatography (HPLC). The triazine derivative contained two chiral centres and was linked to a silica stationary phase. The group reported successful separation of N-3,5-dinitrobenzoyl amino acid alkylesters and 2,2′-disubstituted-1,1′-binaphthyl compounds.

Interestingly one research group, Prasad *et al.* reported many accounts of the use of melamine to produce actual melamine based MIPs. They used melamine with chloranil to form prepolymeric chains that were then mixed with the template in DMF and refluxed at high temperatures. The template was then removed by liquid extraction and the resulting MIP was placed onto a mercury drop surface. The templates they used for recognition

purposes were barbituric acid[43], creatinine[44,45], uric acid[46,47] , dopamine[48] and ascorbic acid[49,50]. They managed to successfully detect trace levels of the given analytes in biological samples (water and blood serum).

Guo *et al.*[51] used a co-polymer featuring melamine (a melamine-urea-formaldehyde resin) to form MIPs capable of trapping ligustrazine out of the extracts of a Chinese herb. SEM micrographs showed that the imprinted resins produced were porous and the authors claimed they achieved high absorbability compared to the non-imprinted counterparts despite not displaying solid proof of this. Imprinted sites were claimed to be important for molecular retention, possibly due to the shape of cavities constituting a very important feature for molecular binding.

Grunule *et al.*[52] reported on how the incorporation of salicylic acid into MF resins enabled the high selectivity of metal ions such as Fe^{3+}, Cu^{2+} and Ni^{2+}. Baraka *et al.* [53, 54] reported on the attachment of chelating groups (DTPA, NTA, EDTA) onto MF materials for the removal of copper (Cu^{2+}) and cobalt (Co^{2+}) from waste waters. Aydin *et al.*[55] and Yirikoglu *et al.*[56] reported on the incorporation of thiourea with MF to form resins capable of selectively uptaking gold (Au^{3+}) and silver (Ag^{+}) from solutions containing other ions (Cu^{2+} and Zn^{2+}). Yang *et al.*[57] reported the use of melamine-based porous networks to remove aqueous mercury ions. Although the cited references above are not examples of molecular imprinting, it shows that molecular imprinting with melamine-based materials has scope for use in bio-molecular recognition featuring metals (vitamin B12 for example).

From the work cited above and other reports on molecular imprinting, there seems to be a real potential in adapting melamine based sol-gel systems (and MF networks

containing other functional groups) to carry out recognition in water. Indeed, there is no clear evidence of well-defined, successfully imprinted MF networks, for which the pore structure is designed, functionality is controlled and the whole recognition process is carried out in aqueous media. Therefore, it implies that functional porous MF networks designed in this work can potentially absorb all molecules that have shown a particular affinity to melamine in supramolecular and recognition chemistry. It would be interesting, for instance, to evaluate the ability to carry out enatiomeric separation of chiral amino acids by incorporating the melamine derivatives produced by Lui *et al.*[28] in MF networks. Numerous accounts of the incorporation of chirality into materials has been reported [58,59,60,61,62,] suggesting that this is a very intense area of research.

2. Preparation for carrying out recognition

In this work, molecular imprinting was not targeted straight away. The intention of incorporating melamine derivatives onto the pore walls of MF networks was (i) to locally increase hydrophobicity in order to potentially strengthen weak interactions with neighbouring groups and (ii) to introduce chirality so that diverse analytes were better retained. In other words, molecules could potentially be attracted into local pore pockets within the material by various weak forces: electrostatic effects, π-π stacking and the hydrophobic effect as well as cooperatively exploiting the effect of hydrogen bonding sites of neighbouring amino or hydroxyl groups. So as a preliminary step, molecular retention in MF materials was evaluated. Firstly the different preparative steps that were carried out to do this are described below.

2.1   Preliminary idea: passive diffusion vs. active adsorption

A very preliminary study involved evaluating the uptake into a piece of bulk MF material by using a coloured dye. The extent of retention would hence be visual within the material. Also, cutting cross-sections of the material would allow checking whether the dye has diffused through the material or not. Therefore a piece of MF material (with 25% porosity and without any additional derivative or post-treatment) was immersed into a pink solution of Fuschin Acid (10^{-7} M). Interestingly, after 24 hours the material had adsorbed all of the dye from the solution; the solution was colourless and the material had adopted the pink colour from the solution (as seen in Figure 4.4).
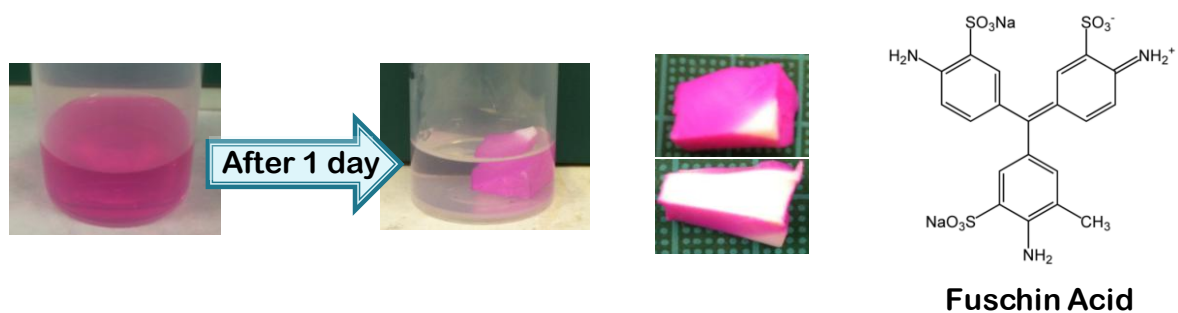
Fuschin Acid

Figure 4.4: Adsorption of Fuschin Acid with a MF material after a day. A cross-section from cutting across the material showed that the dye was adsorbed at the surface of the material and did not diffuse through the material.

Figure 4.4 is a photograph of the material cross-section after 24 hours. It shows how the dye has been adsorbed onto the exposed surface but has not managed to diffuse through the material.

This simple test shows that either the binding capacity limit of the material has been reached or that the use of bulk materials (even if porous) may not be optimal for the adsorption of given molecules. Instead another option considered was grinding the material (with adequate porosity) to powder forms as they would exhibit larger surface areas and could also be packed into a column to make use of the chromatographic effect and also to allow for easy detection of the analyte as simply depicted in Figure 4.5.

Chapter 4: Molecular Recognition in MF
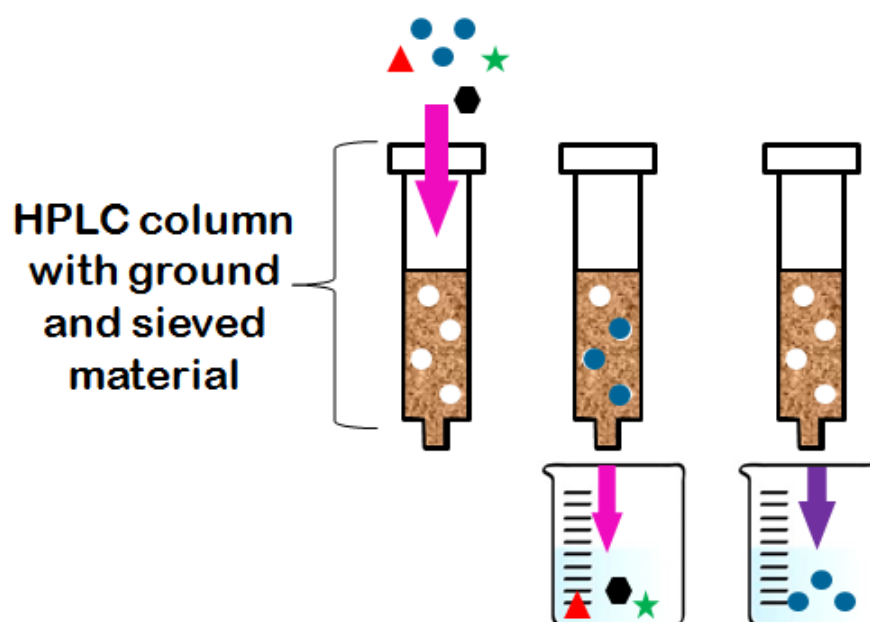
Figure 4.5: Evaluating molecular recognition by packing materials into HPLC columns and detecting the retention. Firstly molecules that are do not contain chemical functionality that shows strong interactions with the pores of the material and eluted quickly. Subsequently due to a change of conditions (polarity, pH, temperature of solvent conditions), the strongly retained molecules can be eluted.

2.2   Packing materials into HPLC columns

The packing of MF materials/powder into chromatographic columns was carried out by Dr Richard Ansell at Leeds University. Five sets of samples were selected based on their porosities but also more practically whether the materials were available in sufficient quantities. In fact, materials with similar synthesis condition and similar porosities had to be paired for the packing of one column (see details in Table 4.1).

Table 4.1: Materials used to pack five HPLC columns alongside their porosity. For each column, two finely ground samples had to be used.

Column	Material 1- Porosity	Material 2-Porosity
1	GSLBZ017RT-60%	GSLBZ018RT-65%
2	GSL014RT1-54%	GSL016RT-54%
3	GSL018PT1-65%	GSL019PT1-82%
4	GSLBZ019RT-71%	GSLBZ020RT-69%
5	GSLBZ021PT1-57%	GSLBZ025PT1-72%

A powder was produced by grinding dry bulk MF material with a pestle and mortar and then by placing the resulting powder into acetone to produce a slurry. The slurry was then poured through a 38μm sieve and the aliquot was collected. The acetone was evaporated and a fine powder was left behind. Note: The group that packed the HPLC columns (150 x 4.6 mm columns from Hichrom) suggested that the particle sizes of the material were not uniform and were larger than 38 μm, which may have been due to the unfortunate use of a damaged sieve. This meant that the packing was not homogenous throughout the column, which would lead to issues concerning consistency.

To verify that porosity was not destroyed by the grinding and sieving process described above, three samples previously analysed as bulk by mercury intrusion measurements and nitrogen sorption underwent the same grinding and sieving process. They were then reanalysed as powders using the same techniques. Table 2 shows the BET and pore size distribution results obtained before and after powder formation. Mercury porosimetry measurements revealed that the pore size distribution remained intact (see Appendix 4). The nitrogen sorption showed that the surface area of the material had not changed significantly upon grinding of the sample, which was initially expected.

Table 4.2: BET surface area and pore size distributions (by mercury measurements) of three samples as bulk materials and as fine powders.

Sample	BET surface area (m^2/g)		Mercury pore size distribution (μm)	
	Bulk material	*Powder*	*Bulk material*	*Powder*
GSL028PT2	113	96	0.02-0.1	0.02-0.1
GLMMG1bPT1	110	108	0.04-0.4	0.06-0.4
GLMM105PT1	70	80	0.04-0.2	0.04-0.2

As the results of the mercury intrusion measurements showed that porosity was not lost, the columns were used with confidence for retention work. When packing a HPLC column, one has to bear in mind that the density of packing might affect the back pressure generated upon trying to run a solvent through the column. In this particular case however, MF columns behaved extremely well under low flow rates (0.1 mL/min) as well as higher flow rates (1 mL/min) with back pressure varying only from 60 to 430 psi respectively.

The method used was as outlined in Table 4.3 with "curve 1" corresponding to a step change and curve 6 referring to a gradient change. The mobile phase (methanol/water) was chosen following [65-66] (1 mL/min flow rate is the flow rate generally used with standard C18 reverse phase silica column).

Table 4.3: The HPLC method used to carry out chromatographic runs on the prepared columns

Time	% methanol	% water	Curve
0-25 mins	5	95	1
25-35 mins	5	95	6
35-50 mins	5	95	1

2.3   Choosing the appropriate analyte

Analytes had to be judiciously chosen so that a positive interaction with the MF material was expected. Important factors to consider for this were polarity of both the column and the analyte, size of the analyte and also the nature of the functional groups present on the material and the analyte molecule.

It was anticipated that the analyte had to be polar in order for retention to occur on a polar column. The size of the analyte was also restricted to being small at this stage so as to optimise the interaction between the analyte and the different MF matrices. Typically cyanuric acid **2** is a very good candidate[63, 64, 65] but also phenol **26** which has a benzene ring, that is potentially able to form π-π interactions with the triazine ring or incorporated benzoguanamine moieties. Also amino acids could be a viable option[29]. In this work, alanine **27**, phenylalanine **28** and tryptophan **29** were investigated.
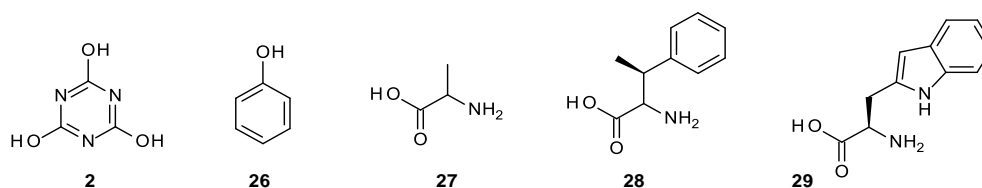
2.4 Towards quantitative analysis: calibration curves

In order to quantitatively study any uptake of the various analytes attempted with the different MF matrices, accurate calibration curves had to be plotted. When analytes of a known concentration were eluted onto the packed columns, final solutions were collected and from this analyte concentrations were able to be accurately determined by relating back to the appropriate calibration curve. The plotting of calibration curves in this work was carried out by using two independent methods, HPLC and ^{13}C NMR spectroscopy.

Cyanuric acid (pK$_a$ =6.5[66]) is not a strong chromophore and cannot easily be detected by UV spectroscopy (UV-visible spectrometer and UV detector in the HPLC instrument) but it has been known to display high UV absorbance maxima at a elevated pH[66,67,68,69]. This is due to its tautomerism into the enol form in alkaline conditions.[70] Cantu *et al.* [66] described, however, that cyanuric acid under acidic conditions (at pH<6.5 thus when primarily in its keto form) gives an absorbance maximum in the 196 nm region. Solutions of different concentrations, kept at the original pH, were analysed directly by the HPLC UV detector (injection of solutions with no column) and also with a UV-visible spectrometer (note: only spectra of solutions with high concentrations -10^{-2} M- presented a clear maximum at 198nm). The calibration trace of the absorbance values taken at

λ=198 nm for the various concentrations prepared here (10^{-2} to 10^{-4} M) is given in Figure 4.6.

Calibration at 198nm using 1mm cuvette

$y = 218.14x + 0.0926$
$R^2 = 0.9986$
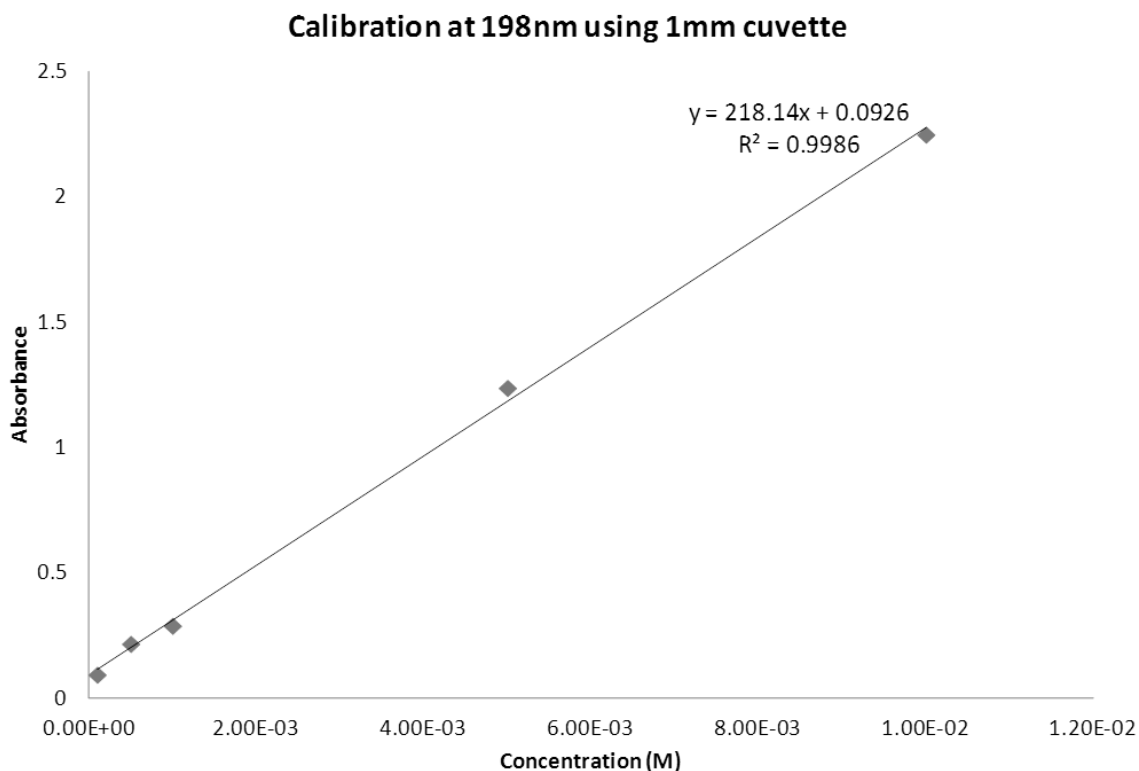
Figure 4.6: Calibration plot produced from taking UV absorbance measurements at λ = 198 nm for 5 solutions of different concentration.

The calibration curve based on UV seems reliable (high R^2 value) and as a precaution a blind experiment was conducted whereby a solution of known concentration (8×10^{-3} M) was tested and confirmed to be 8×10^{-3} M.

^{13}C NMR was used to help building up a second calibration curve, independently to the one created from UV data. However, after running spectra even for long scan times (more than 3 days), no strong ^{13}C signal was observed for the lowest concentration. This

is due to the natural abundance of ^{13}C being so low (1.07%). Consequently, ^{13}C enriched cyanuric acid was purchased for easy analysis by ^{13}C NMR. A batch solution of 10^{-2} M ^{13}C-enriched cyanuric acid was prepared and through appropriate dilutions, four solutions of different concentrations resulted: 5 x 10^{-3}, 10^{-3}, 5 x 10^{-4} and 10^{-4} M. A typical ^{13}C NMR spectrum of cyanuric acid shows a single peak at 152 ppm. Figure 4.7 shows the peak area *vs.* concentration calibration curve. Note the solution of 10^{-4} M was too low to be detected, thus only four points are presented. Also the data point in red was used as a verification method to see if it is reliable for determining unknown concentrations.
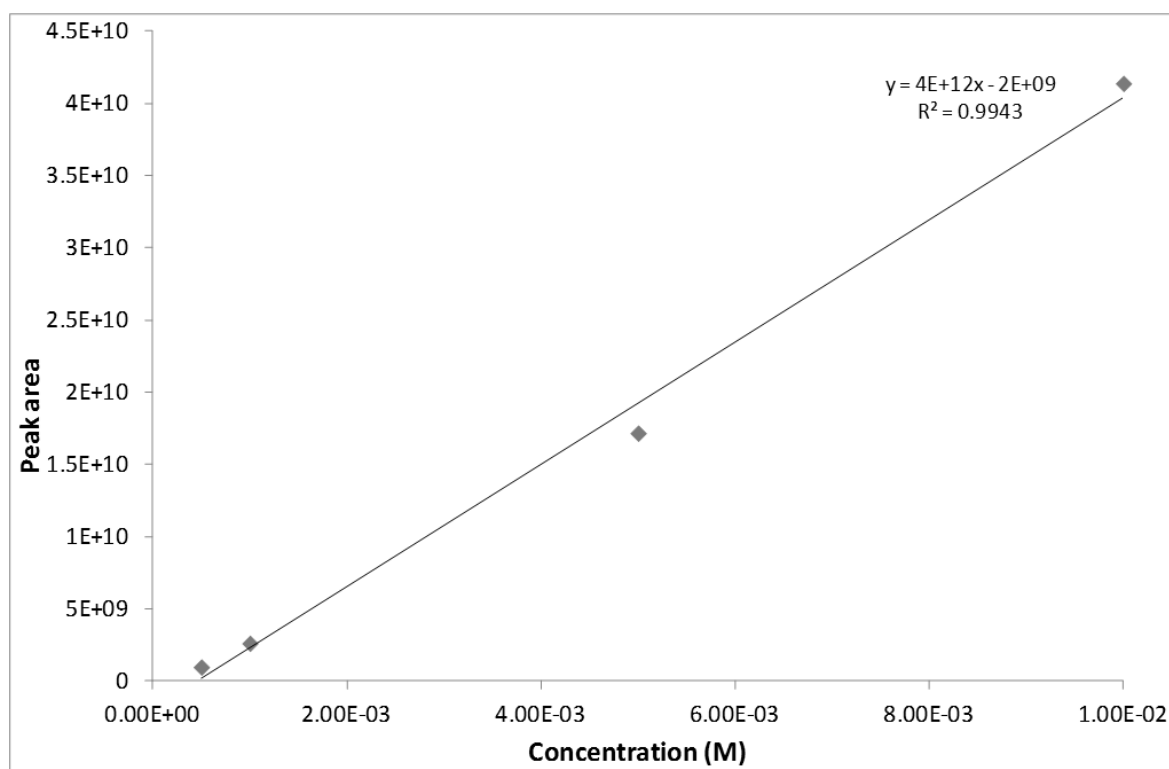
Figure 4.7: Calibration plot produced from conducting ^{13}C NMR analysis on solutions of ^{13}C-enriched cyanuric acid and plotting integrated peak values against the concentration.

The data points determine that the calibration curve is accurate. Also to consolidate this, The UV traces of the ^{13}C enriched cyanuric acid solutions prepared for NMR analysis were re-analysed by UV spectrometry. The previous calibration plot in Figure 4.6 confirmed that the concentrations were reliable.

3.   Results and Discussion

Analytes were injected in both the MF packed column and a commercial C18 reversed phase column (a column packed with octadecyl carbon chain bonded silica particles). Ideally a commercial normal phase column should have been used as a reference but it was not available at Keele University and was not purchased.

Injecting on an apolar column however shows how fast or slow a given analyte is eluted and whether it can be detected easily using the HPLC set-up. Initially column 1 and the C18 column were used for all analytes.

Both cyanuric acid and phenol were eluted within 2 and 10 minutes, respectively, on the C18 column. However, on column 1 only phenol seems to be partially eluted between 36 -50 minutes, whereas cyanuric acid is fully retained. Despite longer runs (50 minutes) and changes to conditions such as the pH, flow rate and polarity of mobile phases, cyanuric acid was not eluted out of column 1 (see composition in previous table, Table 4.1), as shown in Figure 4.8.
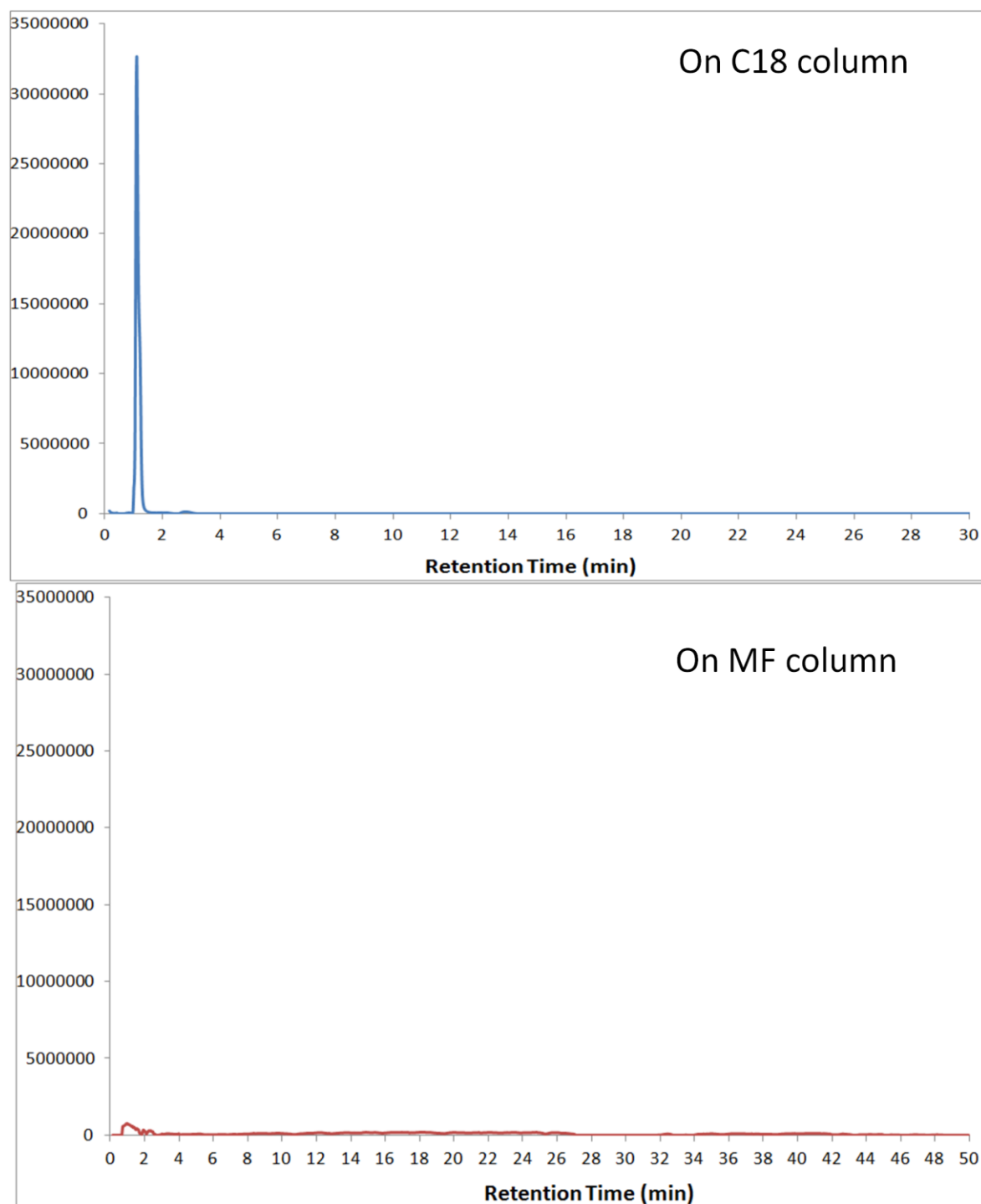
Figure 4.8: Chromatograms of cyanuric acid on a reverse phase C18 column (blue) and
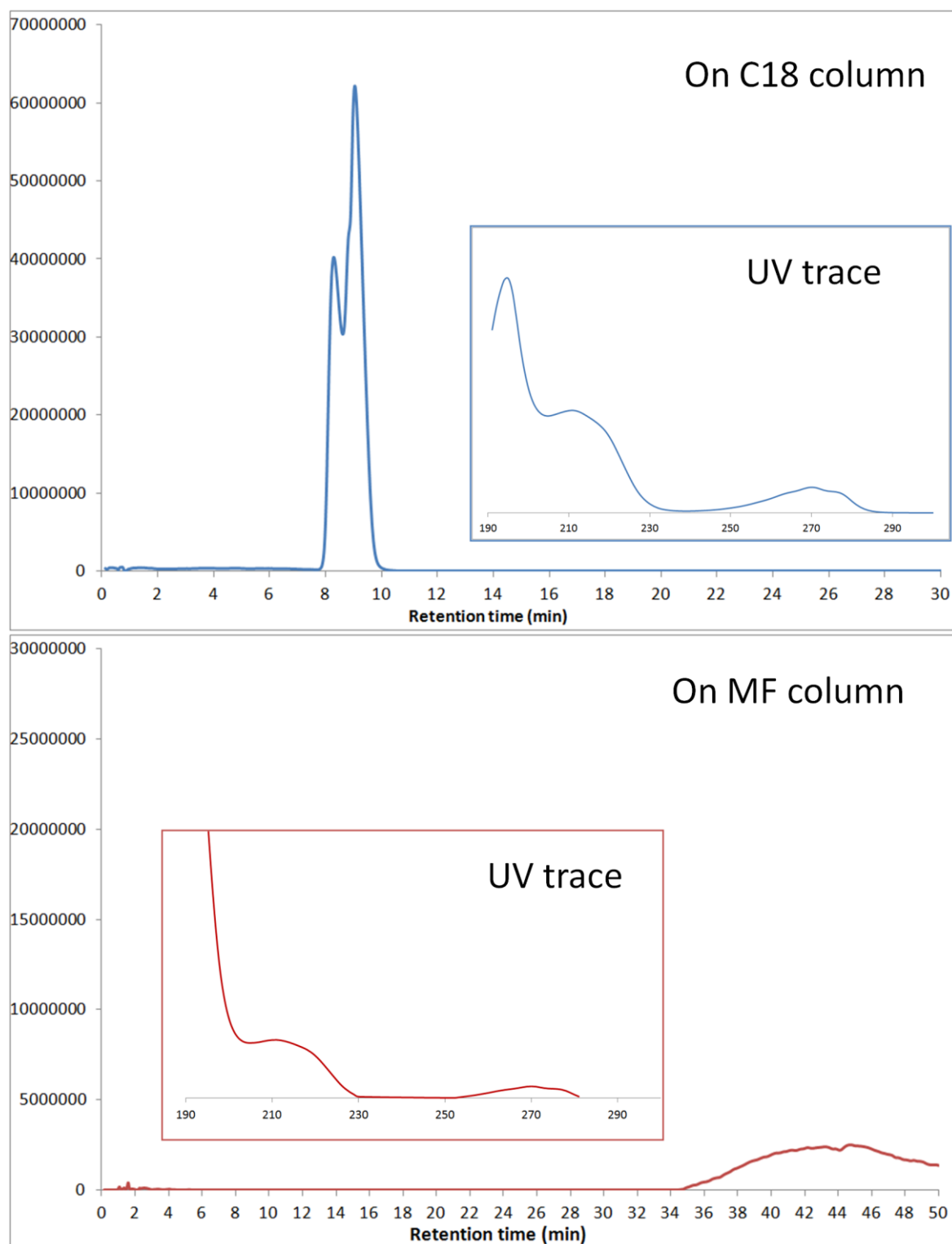
column 1 (red).

Figure 4.9: Chromatograms of phenol on a reverse phase C18 column (blue) and column 1 (red).

Solutions of 10^{-2} M of the three amino acids were prepared. The pH was not altered and was approximately 7. The three amino acid solutions (alanine, phenylalanine, tryptophan) were also injected in both the reverse phase column and column 1. Apart from alanine, which is not a very good chromophore, the amino acids used here have characteristic UV traces. As previously shown and as expected, all three amino acids were eluted rapidly on the C18 column. However, more surprisingly, all were also eluted on the more polar column 1, Figure 4.10, 4.11, 4.12.
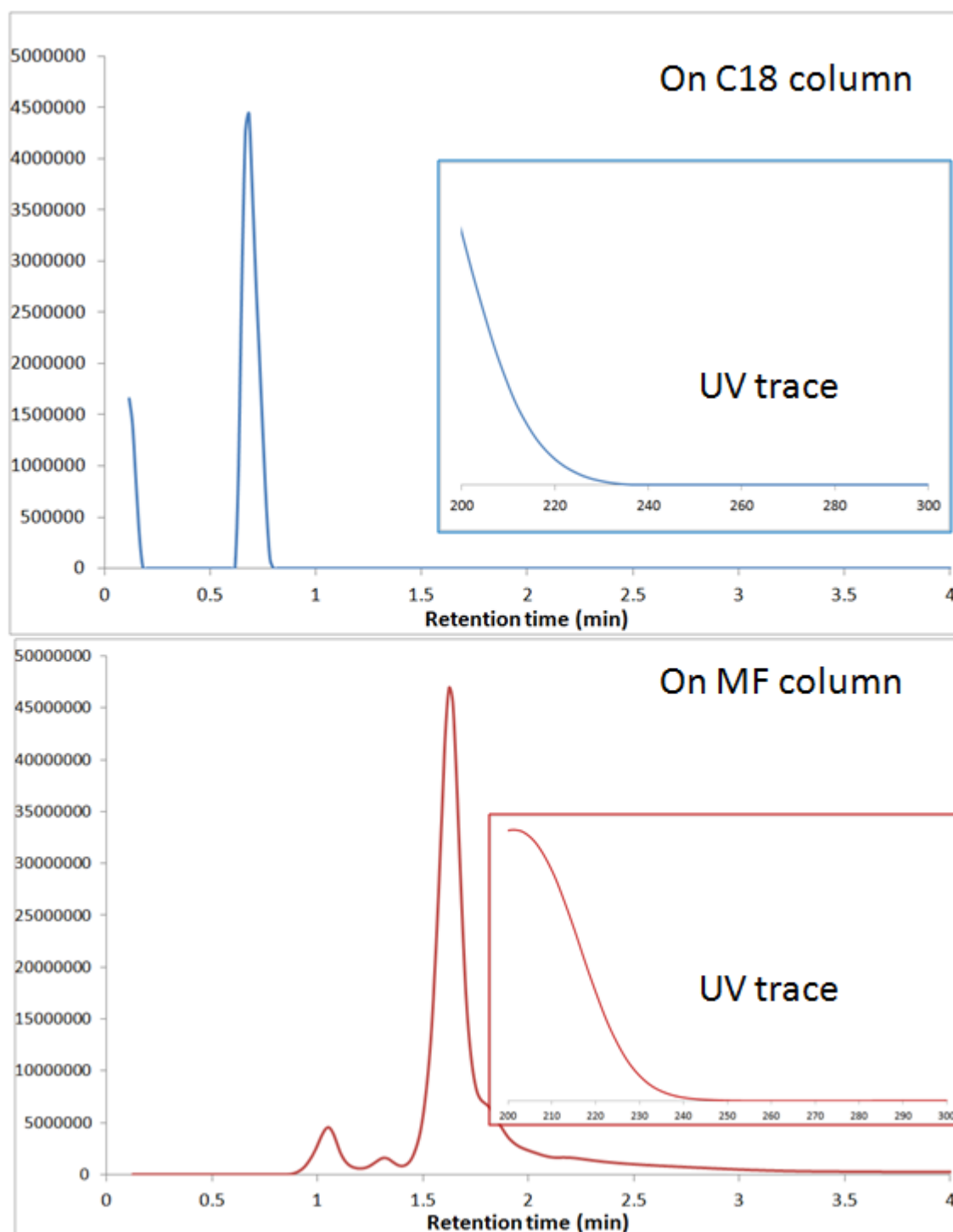
Figure 4.10: Chromatograms of alanine on a reverse phase C18 column (blue trace) and

column 1 (red trace) with their corresponding UV traces. Note that the UV trace taken for

the C18 chromatogram does not correspond to the UV trace taken on the column 1.
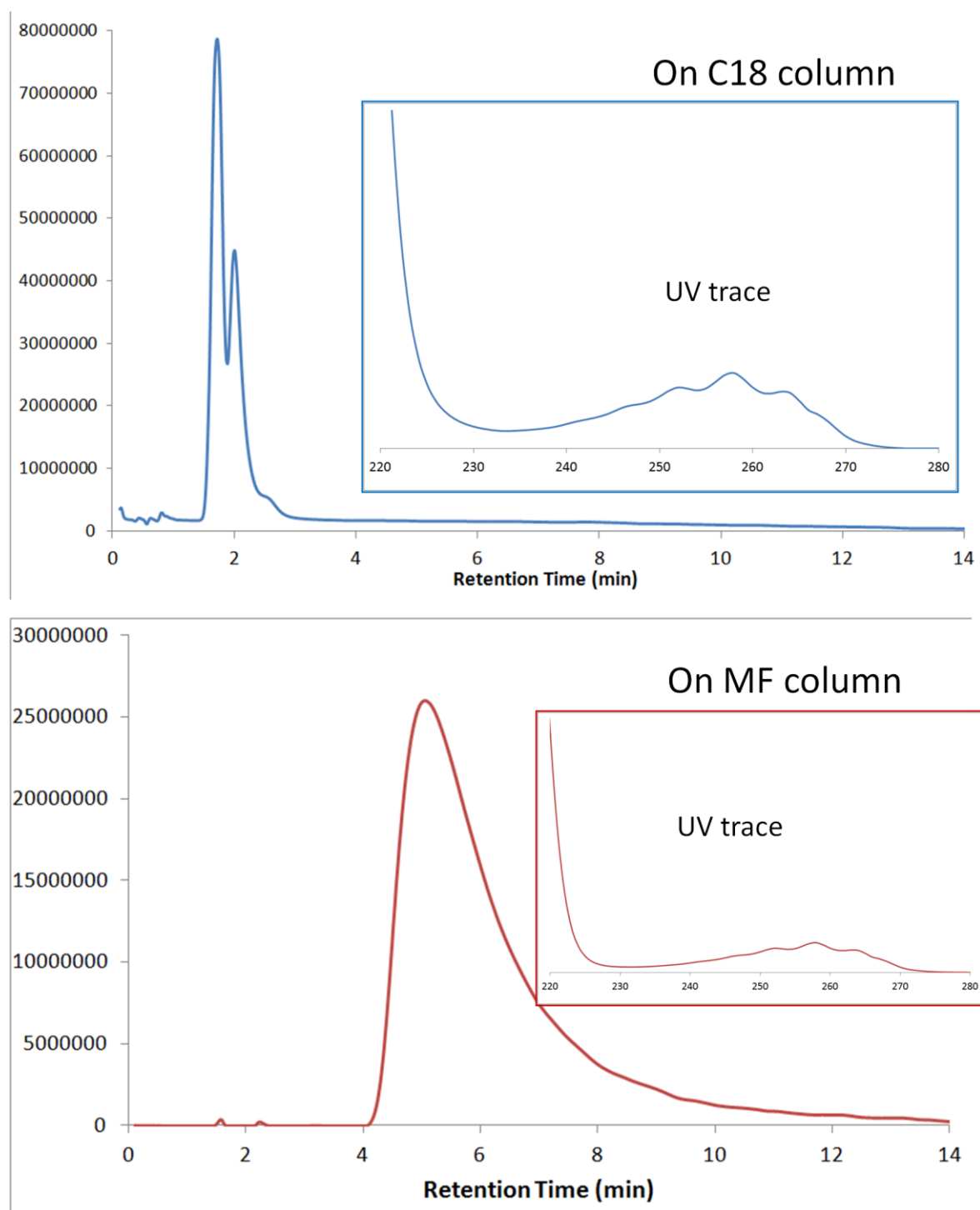
Figure 4.11: Chromatograms of phenylalanine on a reverse phase C18 column (blue trace) and column 1 (red trace) with their corresponding UV traces. The elution times varies from 2 to 5 minutes.
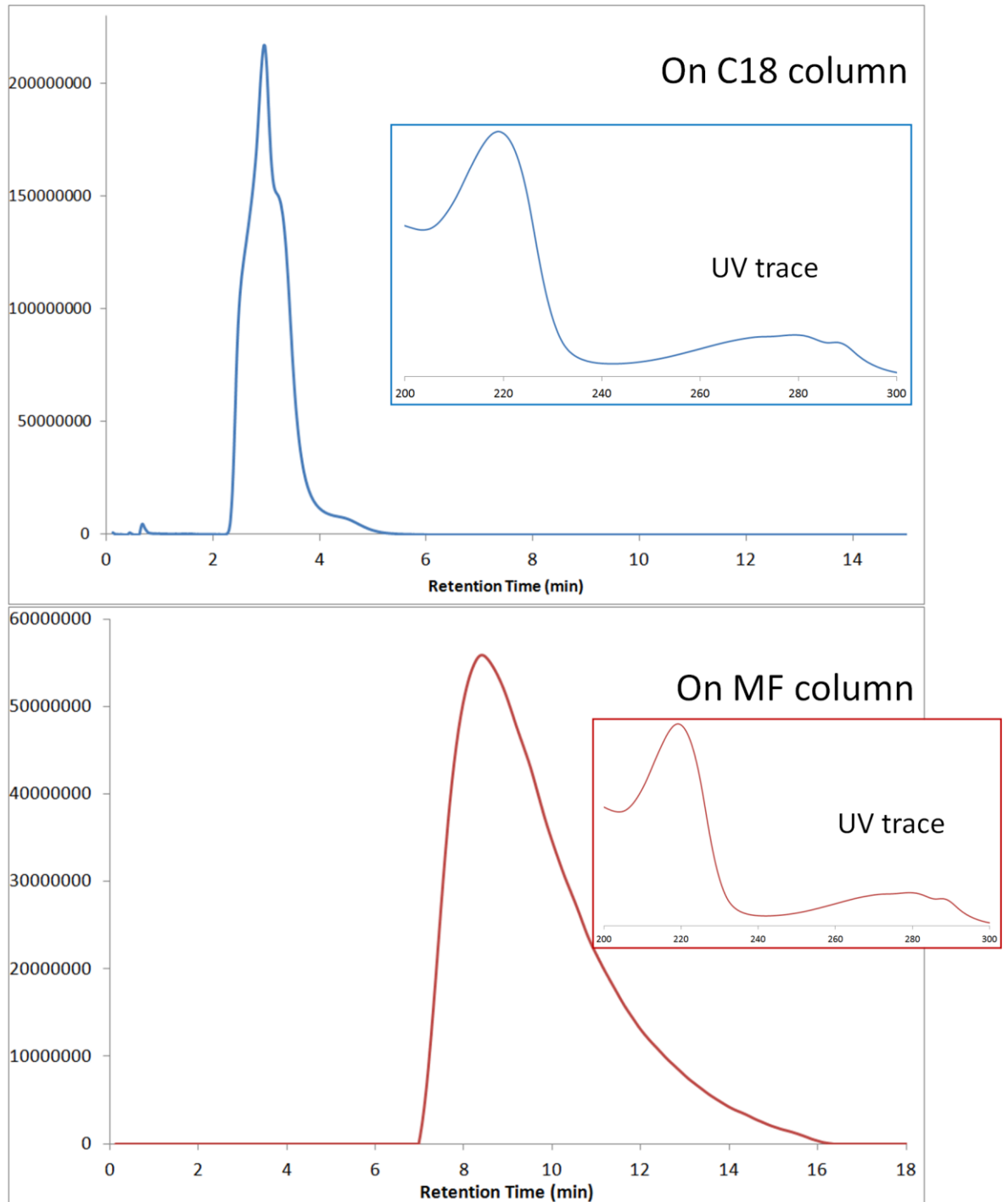
Figure 4.12: Chromatograms of tryptophan on a reverse phase C18 column (blue trace) and column 1 (red trace) with their corresponding UV traces. The elution time for tryptophan varies from 3 to 9 minutes.

As alanine is not a UV active compound it is difficult to detect. The UV traces of the two chromatograms (one on the C18 column, the other on column 1) do not display the same UV absorbance maximum. It is difficult to say if the peak is due to alanine with certainty. Phenylalanine and tryptophan, however, show a slightly higher retention time on column 1. The retention time of phenylalanine has increased by 3 minutes and tryptophan, which has an extra hydrogen donor site, has a retention time of 9 minutes on column 1 whereas it had a retention time of 3 minutes on the C18 column. Plus, the UV traces confirm very well that the peaks on the chromatogram are due to phenylalanine and tryptophan respectively.

As the latter two amino acids showed positive results, they were later injected onto the remaining 4 columns (columns 2, 3, 4 and 5, as shown in Table 1). Figures 4.13 and 4.14 show the stacked chromatograms obtained. The UV traces confirm that the peaks are due to their respective analytes. (Note: there was a heavy leakage when column 3 was connected to the HPLC system. This column required repacking and therefore had to be discarded for the time being).
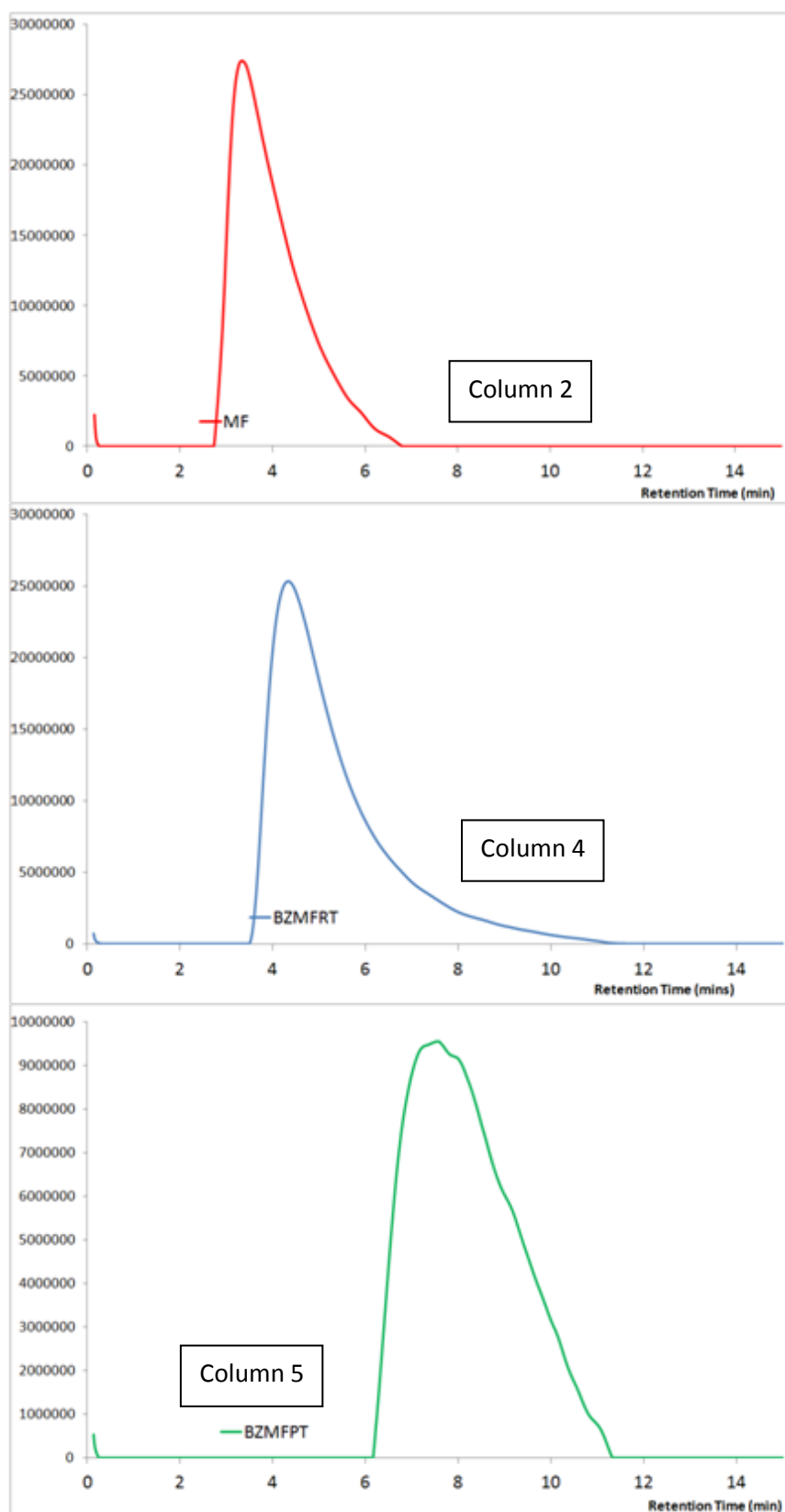
Figure 4.9: Elution of phenylalanine on different MF columns: chromatograms are shown

for column 2(red), column 4 (blue), column 5 (green)
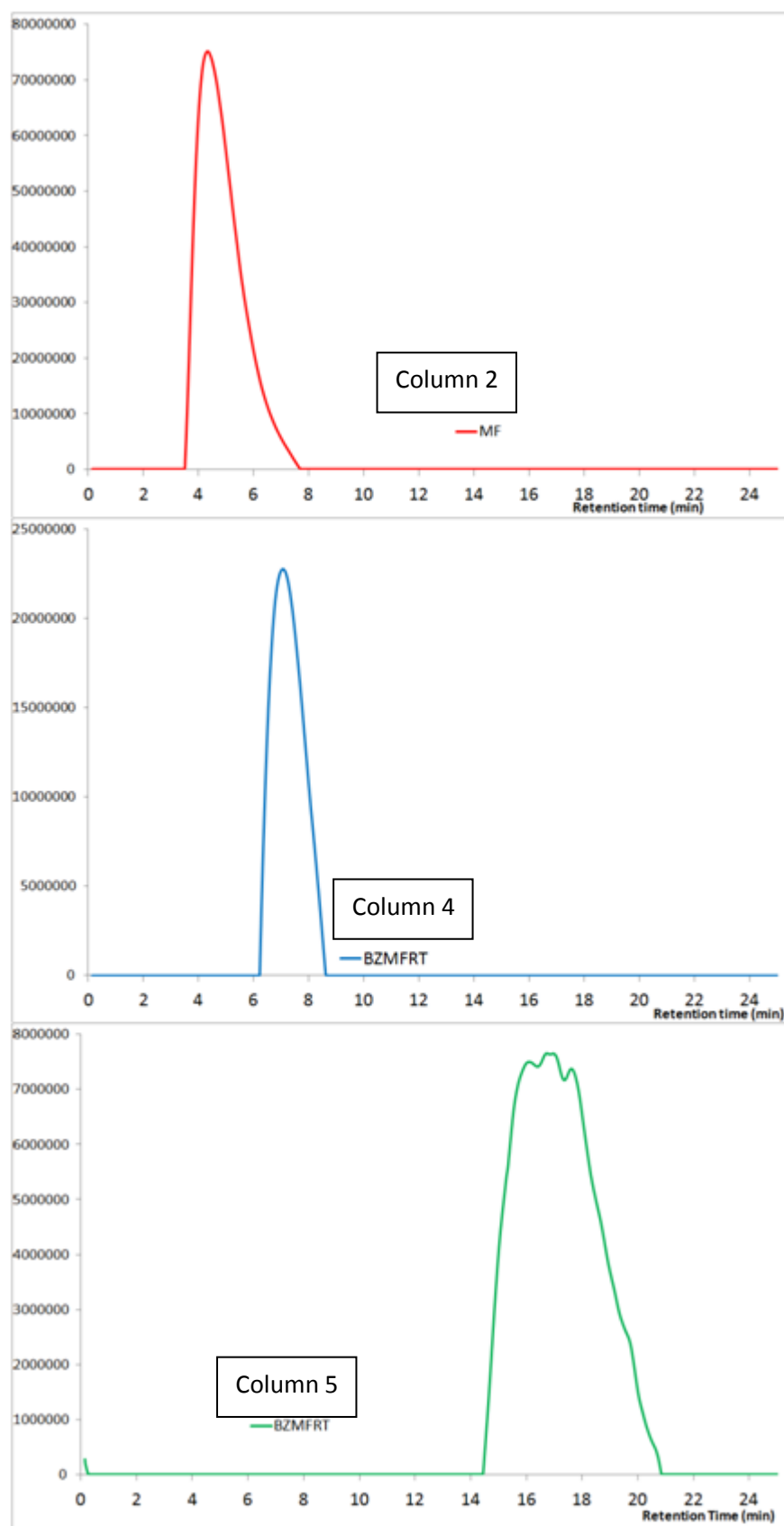
Figure 4.14: Elution of tryptophan on different MF columns. chromatograms are shown

for column 2(red), column 4 (blue), column 5 (green)

Figure 4.13 shows that there is a slight increase in retention from 4 minutes to 5 minutes when the column used is packed with a MF material that contains 10% benzoguanamine. However, the retention time of phenylalanine increases significantly (by 4 minutes) when the material has been post-treated. These observations seem to suggest that lowering the polarity of the MF matrix does in fact enhance retention of phenylalanine.

The chromatograms shown in Figure 4.14 display similar results. From column 2 to column 4 a slight increase in retention time is observed due to a small difference of polarity of the MF matrix within the column (incorporation of benzoguanamine). A much more significant increase in retention time (from 5 minutes to 17 minutes) is observed with the post-treated MF matrix, maybe because the polarity has decreased further.

The general difference observed between phenylalanine and tryptophan may be due to the additional heterocyclic system on tryptophan enhancing its retention properties. The above runs were repeated once each time and similar retention times (±1 minute) were observed.

4. Conclusions

This work has shown that the packing of MF materials into columns is very compatible with a HPLC system. There was very little back pressure, even at high flow rates.

The calibration curves were not as straight forward to carry out as originally thought (detector saturation and limits, poor chromophoric properties of certain analytes, low natural abundance of ^{13}C for NMR analysis, *etc.*) and were only carried for cyanuric acid. A chromatographic system coupled to a mass spectrometer could help to overcome problem of a lack of chromophores and further calibration plots need to be produced for the amino acids.

The choice of analytes in this work has proven to be crucial. Some are too compatible at forming complementary bonds with melamine and hence are strongly retained, typically what was seen here with cyanuric acid. However, the studies carried out on the uptake of phenylalanine and tryptophan have shown that other amino acids such as histidine, proline and tyrosine can also be further investigated. The calibration curves of each analyte needs plotting to check that the measurements are quantitative. Once the process has been optimised and is proven to be successful, then can molecular imprinting be carried out.

5. Experimental Details

All chemicals were bought from major suppliers and used as received with no further purification. Cyanuric acid (99% purity), (+/-)-phenylalanine (99% purity) and L-tryptophan (Sigma grade) were purchased from Sigma-Aldrich. Phenol (99%) was purchased from Merck. ^{13}C enriched cyanuric acid (purity) was purchased from Toronto Research Chemicals. D,L-Alanine (99% purity) was purchased from Acros. HPLC grade methanol was purchased from Fischer.

In order to pack HPLC columns with chosen materials a powder was produced by grinding dry bulk MF material with a pestle and mortar and placing the resulting powder into acetone to produce a slurry. The slurry was then poured through a 38μm sieve and the aliquot was collected. The actone was removed and a fine powder was left behind. Empty columns (150x4.6mm) were purchased from Hichrom.

Nitrogen sorption measurements were carried out using the same instrumentation described in chapter 2: a Quantachrome Autosorb 1. The adsorbate used was nitrogen, the vacuum pressure was 10^4-10^5 Torr, the equilibrium time was 1 minute and the tolerance was 3. The powder samples were placed in sample cells of 6 or 9mm diameter with a glass rod. Prior to analysis, the samples were out-gassed at 50°C for 12 hours. The porosity analysis comprised adsorption and desorption of nitrogen at 77K into the sample pores and the working range was p/p_0=0 to 1. The software used to view the isotherms produced was Autosorb version 1.50.

Mercury Intrusion was carried out at BASF-SE. Approximately 200 mg of the powder samples were necessary for each measurement. The instrumentation used was Autopore

IV Micromeritics, and the software was Micrometics Version V1.09. The range of pore sizes checked was from 0.0037 μm to 200 μm.

The UV measurements were carried out on a UV-visible spectrometer Varian Cary 50 Bio. The range was set from 190 nm to 300 nm. The corresponding software used was Scan program Varian Win UV. Samples were prepared by dissolving cyanuric acid (purchased from Aldrich 99% purity) in deionised water. The samples were then transferred to 1 mm quartz cuvettes.

The ^{13}C NMR spectra were recorded on a Bruker spectrometer, 75 MHz, at room temperature in [D_6] DMSO. The number of scans taken per sample were 8192.

The HPLC equipment used was a Waters Alliance 2690 separation mode. The UV detector attached was a Waters 996 Photodiode Array detector. The corresponding software used was Mass Lynx V3.5 Global with inlet editor V3.5.

- HPLC method on C18 column

Time (mins)	% methanol	% water	Flow	Curve*
0-25	5	95	1	1
25-30	0	100	1	6
30-35	5	95	1	6

- HPLC method on MF columns

Time (mins)	% methanol	% water	Curve*
0-25	5	95	1
25-35	5	95	6
35-50	5	95	1

*6 is the curve that corresponds to a gradient (gradual linear) change whereas

curve 1 is for a step change.

6. References

[1] Asanuma, H., Ban, T., Gotoh, S., Hishiya, T., Komiyama, M. (1998). "Hydrogen Bonding in Water by Poly(vinyldiaminotriazine) for the Molecular Recognition of Nucleic Acid Bases and Their Derivatives." *Macromolecules* **31**(2): 371-377.

[2] Fan, E., Van Arman, S. A., Kirkaid, S., Hamilton A. D. (1993). "Molecular recognition: hydrogen-bonding receptors that function in highly competitive solvents." *J. Am. Chem. Soc.* **115**(1): 369-370.

[3] Kato, Y., Conn, M. M., Rebek, J. (1995). "Hydrogen bonding in water using synthetic receptors." *Proc. Natl. Acad. Sci. U.S.A.* **92**(4): 1208-1212.

[4] Wulff, G. and Sarhan A. (1972). "Use of Polymers with Enzyme-Analogous Structures for Resolution of Racemates." *Angew. Chem. Int. Ed.* **11**(4): 341.

[5] Wulff, G., Sarhan, A., Zabrocki, K. (1973). "Enzyme Analogue Built Polymers and Their Use for the Resolution of Racemates." *Tetrahedron Lett.* **44**: 4329-4332.

[6] Wulff, G. (1995). "Molecular Imprinting in Cross-Linked Materials with the Aid of Molecular Templates— A Way towards Artificial Antibodies." *Angew. Chem. Int. Ed. English* **34**(17): 1812-1832.

[7] Janiak, D. and Kofinas P. (2007). "Molecular imprinting of peptides and proteins in aqueous media." *Anal. Bioanal. Chem.* **389**(2): 399-404.

[8] Alexander, C., Andersson, H. S. Andersson, L. I., Ansell, R. J., Kirsch, N., Nicholls, I. A., O'Mahony, J., Whitcombe, M. J. (2006). "Molecular imprinting science and technology: a survey of the literature for the years up to and including 2003." *J. Mol. Recognit.* **19**(2): 106-180.

[9] Remcho, V. T. and Tan, Z. J. (1999). " MIPs as Chromatographic Stationary Phases for Molecular Recognition." *Anal. Chem.* **71**(7): 248A-255A.

[10] Pauling, L. (1959) Molecular Structure in Relation to Biology and Medicine. *Ciba Foundation Symposium - Significant Trends in Medical Research*, John Wiley & Sons, Ltd.**:**. 3-17.

[11] Cormack, P. A. G. and Mosbach, K. (1999). "Molecular imprinting: recent developments and the road ahead." *React. Funct. Polym.* **41**(1-3): 115-124.

[12] Díaz-García, M. E. and Laínño, R. B. (2005). "Molecular Imprinting in Sol-Gel Materials: Recent Developments and Applications." *Microchim. Acta.* **149**(1): 19-36.

[13] Polyakov, M.V. (1931)." Adsorption properties and structure of silica gel." *Zhur. Fiz. Khim.* 2: 799-805.

[14] Andersson, L. I., Müller, R. Vlatakis, G., Mosbach, K. (1995). "Mimics of the binding sites of opioid receptors obtained by molecular imprinting of enkephalin and morphine." *Proc. Natl. Acad. Sci. U.S.A* **92**(11): 4788-4792.

[15] Haupt, K., Dzgoev, A., Mosbach, K. (1998). "Assay System for the Herbicide 2,4-Dichlorophenoxyacetic Acid Using a Molecularly Imprinted Polymer as an Artificial Recognition Element." *Anal. Chem.* **70**(3): 628-631.

[16] Mosbach, K. and K. Haupt (1998). "Some new developments and challenges in non-covalent molecular imprinting technology." *J. Mol. Recognit.* **11**(1-6): 62-68.

[17] Braun, S. (2007). "Biochemically active sol-gel glasses: The trapping of enzymes." *Mater. Lett.* **61**: 2848-2846.

[18] Ellerby, L. M., Clinton, R. N. Nishida, F., Yamanaka, S. A., Dunn, B., Valentine, J. S., Zink, J. I. (1992). "Encapsulation of Proteins in Transparent Porous Silicate Glasses Prepared by the Sol-Gel Method." *Science* **255**(5048): 1113-1115.

[19] Fennouh, S., Guyon, S. Livage, J., Roux, C. (2000). "Sol-Gel Entrapment of Escherichia coli." *J. Sol-Gel Sci. Technol.* **19**(1): 647-649.

[20] Royston, E., Lee, S.-Y., Culver, J N., Harris, M. T. (2006). "Characterization of silica-coated tobacco mosaic virus." *J. Colloid Interface Sci.* **298**(2): 706-712.

[21] Livage, J. (2001). "Encapsulation of biomolecules in silica gels." *J. Phys. Condens. Matter* **13**: R673–R691.

[22] Gupta, R. (2007). "Entrapment of biomolecules in sol–gel matrix for applications in biosensors: Problems and future prospects." *Biosens. Bioelectron.* **22**: 2387-2399.

[23] Marx, S. and Avnir D. (2007). "The Induction of Chirality in Sol-Gel Materials." *Acc. Chem. Res.* **40**(9): 768-776.

[24] Ansell, R. J. (2005). "Molecularly imprinted polymers for the enantioseparation of chiral drugs." *Adv. Drug Delivery Rev.* **57**(12): 1809-1835.

[25] Maier, N. and Lindner, W. (2007). "Chiral recognition applications of molecularly imprinted polymers: a critical review." *Anal. Bioanal.Chem.* **389**(2): 377-397.

[26] Egger, C., du Fresne, C., Raman, V. I., Schadler, V., Frechen, T., Roth, S. V., Muller-Buschbaum, P. (2008). "Design of highly porous melamine-based networks through a bicontinuous microemulsion templating strategy." *J. Sol-Gel Sci. Technol.* **48**(1): 86-94.

[27] Egger, C. C., du Fresne, C., Hirschinger, J.,Raya, J.,Bechinger, B. (2008). "Characterization of highly porous polymeric materials with pore diameters larger than

100 mn by mercury porosimetry and X-ray scattering methods." *Langmuir* **24**(11): 5877-5887.

[28] du Fresne von Hohenesche, C., Schmidt, D. F., Schadler, V. (2008). "Nanoporous Melamine-Formaldehyde Gels by Microemulsion Templating." *Chem. Mater.* **20**: 6124-6129.

[29] Liu, Q., Zhang, S. Wu, B., Guo, J., Xie, J., Gu, M., Zhao, Y., Yun, L., Liu, K. (2005). "Chiral Melamine Derivatives: Design, Synthesis, and Application to Mass Spectrometry-Based Chiral Analysis." *Anal. Chem.* **77**(16): 5302-5310.

[30] Piletsky, S., Piletskaya, E. V., Elgersma, A. V., Yano, K., Karube, I., Parhometz, Yu P. El'skaya, A. V. (1995). "Atrazine sensing by molecularly imprinted membranes." *Biosens. Bioelectron.* **10**: 959-964.

[31] Matsui, J., Okada, M., Tsuruoka, M., Takeuchi, T. (1997). "Solid-phase Extraction of a Triazine Herbicide Using a Molecularly Imprinted Synthetic Receptor." *Anal. Commun.***34**: 85-87.

[32] Matsui, J., Fujiwara, K. Takeuchi, T. (2000). "Atrazine-selective polymers prepared by molecular imprinting of trialkylmelamines as dummy template species of atrazine." *Anal. Chem.* **72**(8): 1810-1813.

[33] Turiel, E., Martin-Esteban, A. Martin-Esteban, A.,Fernandez, P.,Perez-Conde, C.,Camara, C. (2001). "Molecular recognition in a propazine-imprinted polymer and its application to the determination of triazines in environmental samples." *Anal. Chem.* **73**(21): 5133-5141.

[34] He, L. M., Su, Y. J. Zheng, Y. Q., Huang, X. H., Wu, L., Liu, Y. H., Zeng, Z. L., Chen, Z. L. (2009). "Solid-phase extraction of melamine from aqueous samples using water-compatible molecularly imprinted polymers." *J. Sep. Sci.* **32**(19): 3310-3318.

[35] Curcio, M., Puoci, F., Cirillo, G., Iemma, F., Spizzirri, U. G., Picci, N..(2010) "Selective Determination of Melamine in Aqueous Medium by Molecularly Imprinted Solid Phase Extraction." *J. Agric. Food Chem.* **58**(22): 11883-11887.

[36] Liang, R. N., Zhang, R. M. Qin, W.. (2009). "Potentiometric sensor based on molecularly imprinted polymer for determination of melamine in milk." *Sens. Actuators, B.* **141**(2): 544-550.

[37] Yang, H.-H., Zhou, W.-H. Guo, X-C., Chen, F-R., Zhao, H-Q., Lin, L-M., Wang, X-R. (2009). "Molecularly imprinted polymer as SPE sorbent for selective extraction of melamine in dairy products." *Talanta* **80**(2): 821-825.

[38] Wang, B., Wang, Y. Yang, H., Wang, J., Deng, A. "Preparation and characterization of molecularly imprinted microspheres for selective extraction of trace melamine from milk samples." *Microchim. Acta* **174**(1): 191-199.

[39] Arrachart, G., Carcel, C. Trens, P., Moreau, J. J. E, Man, M. W. C. (2009). "Silylated Melamine and Cyanuric Acid as Precursors for Imprinted and Hybrid Silica Materials with Molecular Recognition Properties." *Chem. Eur. J.* **15**(25): 6279-6288.

[40] Asanuma, H., Gotoh, S., Ban, T., Komiyama, M. (1997). "Molecular Recognition of Nucleic Acid Bases in Water by Hydrogen Bonding of Poly(vinyldiaminotriazine)." *J. Inclusion Phenom.Macrocyclic Chem.* **27**(3): 259-264.

[41] Asanuma, H., Ban, T. S. Komiyama, M et al. (1998). "Precise recognition of nucleotides and their derivatives through hydrogen bonding in water by poly(vinyldiaminotriazine)." *Supramol. Sci.* **5**(3-4): 405-410.

[42] Iuliano, A., Pieroni, E., Salvadori, P. (1997). "New 1,3,5-triazine based chiral stationary phase for the high performance liquid chromatographic separation of enantiomers." *J. Chromatogr. A* **786**: 355-360.

[43] Prasad, B. B. and Lakshmi D. (2005). "Barbituric acid sensor based on molecularly imprinted polymer-modified hanging mercury drop electrode." *Electroanalysis* **17**(14): 1260-1268.

[44] Lakshmi, D., Sharma, P. S., Prasad, B. B. (2007). "Imprinted polymer-modified hanging mercury drop electrode for differential pulse cathodic stripping voltammetric analysis of creatine." *Biosens. Bioelectron.* **22**(12): 3302-3308.

[45] Lakshmi, D., Prasad, B. B., Sharma, P. S. (2006). "Creatinine sensor based on a molecularly imprinted polymer-modified hanging mercury drop electrode." *Talanta* **70**(2): 272-280.

[46] Prasad, B. B., Sharma, P. S., Lakshmi, D. (2007). "Molecularly imprinted polymer-based solid-phase extraction combined with molecularly imprinted polymer-based sensor for detection of uric acid." *J. Chromatogr. A* **1173**(1-2): 18-26.

[47] Lakshmi, D., Sharma, P. S., Prasad, B. B. (2006). "Development of uric acid sensor based on molecularly imprinted polymer-modified hanging mercury drop electrode." *Electroanalysis* **18**(9): 918-927.

[48] Prasad, B. B., Srivastava, S., Tiwari, K., Sharma, P. S. (2009). "Trace-level sensing of dopamine in real samples using molecularly imprinted polymer-sensor." *Biochem. Eng. J.* **44**(2-3): 232-239.

[49] Prasad, B. B., Srivastava, S. Tiwari, K., Sharma, P. S. (2009). "Ascorbic acid sensor based on molecularly imprinted polymer-modified hanging mercury drop electrode." *Mater. Sci. Eng., C -Biomimetic and Supramolecular Systems.* **29**(4): 1082-1087.

[50] Prasad, B. B., Tiwari, K., Lakshmi, D. (2008). "Molecularly imprinted polymer-based solid-phase microextraction fibre coupled with molecularly imprinted polymer-based sensor for ultratrace analysis of ascorbic acid." *J. Chromatogr. A.* **1198**: 59-66.

[51] Guo, Z. F., Guo, T. T., Guo, M. F. (2008). "Preparation of molecularly imprinted adsorptive resin for trapping of ligustrazine from the traditional Chinese herb Ligusticum chuanxiong Hort." *Anal. Chim. Acta* **612**(2): 136-143.

[52] Gurnule, W. B., Juneja, H. D., Paliwal, L. J. (2002). "Ion-exchange properties of a salicylic acid-melamine-formaldehyde terpolymer resin." *React. Funct. Polym.* **50**(2): 95-100.

[53] Baraka A and Hall, P. J. (2007). "Melamine–formaldehyde–NTA chelating gel resin: Synthesis, characterization and application for copper(II) ion removal from synthetic wastewater." *J. Hazard. Mater.* **140**: 86-94.

[54] Baraka, A., Hall, P. J., Heslop, M. J. (2007). "Preparation and characterization of melamine-formaldehyde-DTPA chelating resin and its use as an adsorbent for heavy metals removal from wastewater." *React. Funct. Polym.* **67**(7): 585-600.

[55] Aydin, A., Imamoglu, M., Gulfen, M. (2008). "Separation and recovery of gold(III) from base metal ions using melamine-formaldehyde-thiourea chelating resin." *J. Appl. Polym. Sci*. **107**: 1201-1206.

[56] Yirikoglu, H. and Gulfen, M. (2008). "Separation and recovery of Silver(I) ions from base metal ions by melamine-formaldehyde-thiourea (MFT) chelating resin." *J. Sep. Sci.* **43**(2): 376-388.

[57] Yang, G. W., Han, H. Y. Du, C. Y., Luo, Z. H., Wang, Y. J. (2010). "Facile synthesis of melamine-based porous polymer networks and their application for removal of aqueous mercury ions." *Polymer* **51**(26): 6193-6202.

[58] Shunai, C., Zheng, L. Ohsuna, T. Sakamoto, K. Terasaki, O. Tatsumi, T.. (2004). "Synthesis and characterization of chiral mesoporous silica." *Nature* **429**(6989): 281-284.

[59] Yoshikawa, M., Shimada, A. , Izumi, J. (2001). "Novel polymeric membranes having chiral recognition sites converted from tripeptide derivatives." *Analyst* **126**(6): 775-780.

[60] Marx, S. and Avnir, D. (2007). "The Induction of Chirality in Sol-Gel Materials." *Acc. Chem. Res.* **40**(9): 768-776.

[61] Kuschel, A., Sievers, H., Polarz, S. (2008). "Amino Acid Silica Hybrid Materials with Mesoporous Structure and Enantiopure Surfaces." *Angew. Chem.* **120**(49): 9655-9659.

[62] Qiu, H., Inoue, Y., Che, S. (2009). "Supramolecular Chiral Transcription and Recognition by Mesoporous Silica Prepared by Chiral Imprinting of a Helical Micelle." *Angew. Chem. Int. Ed.* **48**(17): 3069-3072.

[63] Mathias, J. P., Simanek, E. E. Zerkowski, J. A., Seto, C.T., Whitesides, G. M. (1994). "Structural Preferences of Hydrogen-Bonded Networks in Organic Solution - the Cyclic CA3.M3 "Rosette". *J. Am. Chem. Soc.* **116**(10): 4316-4325.

[64] Zerkowski, J. A., MacDonald, J. C., Seto, C. T., Wierda, D. A., Whitesides, G. M. (1994). "Design of Organic Structures in the Solid State: Molecular Tapes Based on the Network of Hydrogen Bonds Present in the Cyanuric Acid. Melamine Complex." *J. Am. Chem. Soc.* **116**(6): 2382-2391.

[65] Mathias, J. P., Simanek, E. E., Whitesides, G. M. (1994). "Self-Assembly through Hydrogen Bonding: Peripheral Crowding - A New Strategy for the Preparation of Stable Supramolecular Aggregates Based on Parallel, Connected CA3.cntdot.M3 Rosettes." *J. Am. Chem. Soc.* **116**(10): 4326-4340.

[66] Sancier, K. M., Brady, A. P., Lee, W. W. (1964). "Absorption spectra of solutions of cyanuric acid and its chlorinated derivatives." *Spectrochim. Acta* **20**(3): 397-403.

[67] Cantú, R., Evans, O., (2000). "An HPLC Method with UV Detection, pH Control, and Reductive Ascorbic Acid for Cyanuric Acid Analysis in Water." *Anal. Chem.* **72**(23): 5820-5828.

[68] Cantú, R., O. Evans, Magnuson, M., Kawahara, F. K., Shoemaker, J. A., Dufour, A. P. (2001). "Rapid analysis of cyanuric acid in swimming pool waters by high performance liquid chromatography using porous graphitic carbon." *Chromatographia* **53**(7): 454-456.

[69] Yu, C., Zhu, L., Xiao, J., Tang, H., Guo, G., Zeng, Q., Wang, X. (2009). "Ultrasonic extraction and determination of cyanuric acid in pet food." *Food Control* **20**(3): 205-208.

[70] Klotz, I. M. and Askounis T. (1947). "Absorption Spectra and Tautomerism of Cyanuric Acid, Melamine and Some Related Compounds." *J. Am. Chem. Soc.* **69**(4): 801-803.

CHAPTER 5:
Conclusions and Future Work

From the work described in this thesis, preliminary data has been provided to suggest that MF materials have potential applications in the field of molecular recognition. These materials are unique as, to date, no work has been reported on designing melamine- formaldehyde based cross-linked networks via sol-gel synthesis for use in molecular recognition. Even though many reports have been made on the use of sol-gel MIPs and, in parallel, much research has been carried out in producing melamine derivatives which show binding through weak interactions, the two have not been cohesively tied together.

The initial steps of this very broad project involved designing and synthesising melamine derivatives from 2-chloro,-4, 6-diamine-1,3,5-triazine plus a functional amine. We have shown that derivatives can be tailored and tuned, using a simple route, to provide a plethora of derivatives containing diverse functionality such as high aromaticity and chiral groups. Although the starting material (2-chloro-4,6-diamine-1,3,5-triazine) in this method is costly in large quantities, we discuss alternative synthesis routes that can be used, depending on the amounts required.

In this work, we successfully show the incorporation of commercial melamine derivatives and two synthesised derivatives into MF networks via the sol-gel process to produce porous materials. The various measurements and data have shown that porous

materials (≤1 µm) with surface areas of around 100 m^2/g were produced. Plus, the materials, like MF resins displayed high thermal stability (~400°C).

We learnt that the incorporation of the derivatives can strongly affect the final properties of materials such as the pore and grain sizes of the network. Various post-treatment methods can be applied successfully to enhance pore retention (and consequently increase the surface area) due to extended reactions with the diverse functional groups present in the MF matrix.

Various spectroscopic techniques (infrared, Raman and solid-state NMR) can be applied to bulk MF materials for characterisation of the different functional groups. Surprisingly, analyses of cross-linked MF materials by infrared spectroscopy have not been reported in depth to date and trends were observed with the modification of the M: F ratio and the application or not of post-treatment to samples (to enhance porosity). It was difficult, however, to differentiate materials containing different derivatives solely using IR spectroscopy. Materials containing phenyl groups could be differentiated with solid-state NMR and Raman spectroscopy but further in-depth work is required here, especially in evaluating the cross-linking.

Additionally, when the presence of the different functional groups within the MF matrix is coupled with properties such as good surface area and porosity, the potential for producing materials for recognition is significantly enhanced. Ultimately, an increased amount of binding activity can occur due to the high reactive surface areas available and good analyte diffusion can occur through the materials with high porosity.

Evaluating molecular recognition was the ultimate final challenge in this work. Analytes were eluted on MF materials packed into HPLC columns and the retention time was compared to retention on a non-polar reverse phase C18 silica column. Here, we saw complete retention of cyanuric acid, the enhanced retention of phenol and the retention and elution of amino acids phenylalanine and tryptophan. The latter two analytes showed however that their retention could be enhanced if the MF matrix was more apolar (included an incorporated derivative or was post-treated).

Due to time constraints, however, the work carried out in this area was limited and time permitted, the analysis would have been extended to various columns packed with different materials (matrices containing acetoguanamine, caprinoguanamine, monomers 1 and 2 and/or different post-treatments) to see how the retention times of the amino acids change. Also, more importantly, however, the column packing conditions require optimising. Materials need to be ground down to the correct size, with thorough particle characterisation (surface area and pore size distribution) to maximise their potential.

Further work that could also be carried out subsequently, in the recognition area, include fine tuning the material and judiciously incorporating specific functional groups for chosen analytes. The synthesis procedure to design melamine derivatives is now clear as well as how to achieve high porosities in MF materials. Therefore, materials containing mixtures of functional groups and mixture of post-treatments may ameliorate retention, porosity and surface area.

Also, other work that needed to be completed in this project is the full cleavage of the ester moiety on monomer 3. This would have provided an acid functionality onto a triazine core and such molecules have not, to our knowledge, been reported before.

Further work that can be carried out to enhance functionality in MF matrices include incorporating various other derivatives such as esters, amides, metal chelating ligand (for ionic bonding), thio-ligands (for metal binding etc.). As MF chemistry is very versatile, the cross-linker does not have to be restricted to formaldehyde. In fact, one group reported on using soy flour based cross-linkers that were a much more environmentally viable option[1], and also thio-based cross-linkers (for the retention of mercury) has also been reported[2].

Another way to modify porosity (towards enhancing it) could be to change the weak acid used for gelation. Blank reported on the importance of the counter ion produced with the MF precursors. Di-acids would certainly be an interesting alternative. Alternatively, functionality can also be enhanced with the post-treatment method and the diverse functionalities present in MF offer the possibility of different reactions to try out such as attaching carboxylic acid derivatives to amine groups to form amides.

Finally, once all the above possibilities have been explored and confidence has been gained in the analysis of recognition of small molecules, molecular imprinting of bio-molecules in MF materials would be the final hurdle, especially if this was to be adapted for chiral recognition. One can design the MF derivatives for a specific template molecule, and the imprinting technique is easily adaptable in aqueous media in which most biological systems are found. The template has the possibility of being removed, either by several washes, or as MF materials display high thermal stability, thermal treatment may be investigated. Very recently Sigma-Aldrich commercialised MIP solid phase extractors (SupelMIP[TM]-SPE). Fourteen different types are available, one of which is adapted to triazine analytes. Although the composition of the material was not revealed, it seems as

though the material is formed from vinyl-based precursors (from IR spectral analysis performed on the MIP). It would be of interest to compare the performance of the materials produced from melamine-based materials with these solid-phase extractors.

References

[1]   Amaral-Labat, G. A., A. Pizzi, et al. (2008). "Environment-friendly soy flour-based resins without formaldehyde." *J. Appl. Polym. Sci.* **108**(1): 624-632.

[2] Yang, G. W., H. Y. Han, et al. (2010). "Facile synthesis of melamine-based porous polymer networks and their application for removal of aqueous mercury ions." *Polymer* **51**(26): 6193-6202.

Appendix

Contents

Appendix 1: Additional analytical data for monomer synthesis

Structures and molar masses of mono and di-substituted monomers

Monomer 1 is actually a mixture of desired and undesired compounds:

Molecular Weight =230.27
Exact Mass =230
Molecular Formula =C11H14N6

Molecular Weight =334.43
Exact Mass =334
Molecular Formula =C19H22N6
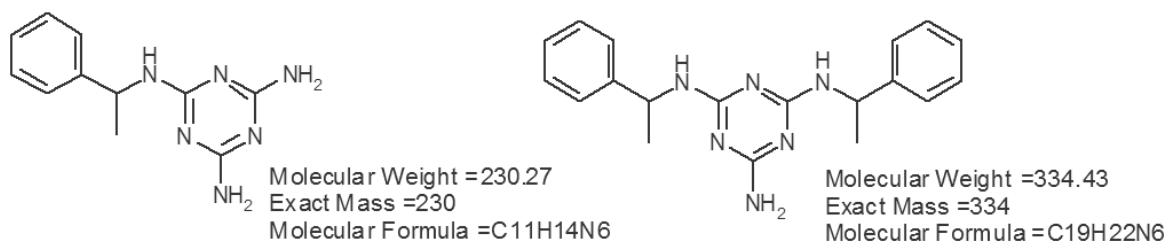
Monomer 2 is actually a mixture of desired and undesired compounds:

Molecular Weight =168.20
Exact Mass =168
Molecular Formula =C6H12N6

Molecular Weight =210.28
Exact Mass =210
Molecular Formula =C9H18N6
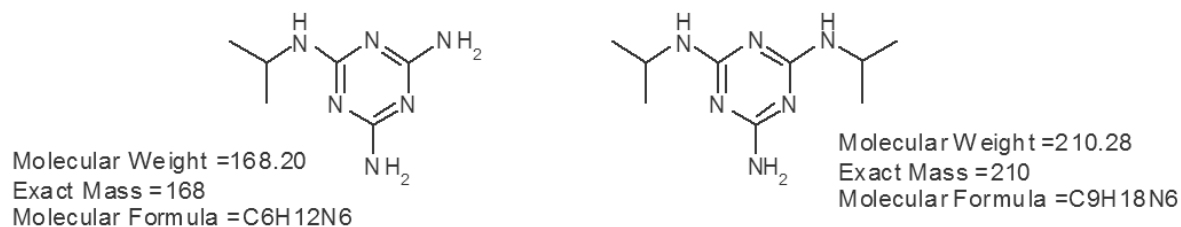
Monomer 3 is actually a mixture of desired and undesired compounds:

Molecular Weight =422.62
Exact Mass =422
Molecular Formula =C22H42N6O2

Molecular Weight =719.12
Exact Mass =718
Molecular Formula =C41H78N6O4
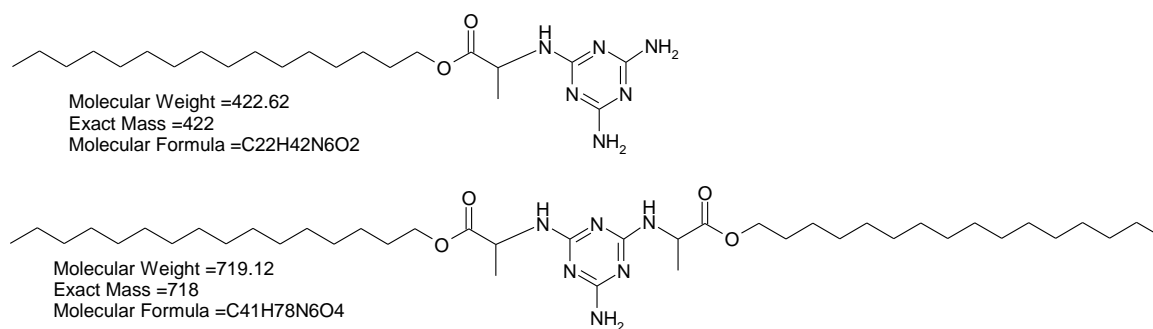
LC-MS data carried out at Keele University

Crude mixture from Monomer 1 synthesis (from cyanuric chloride)
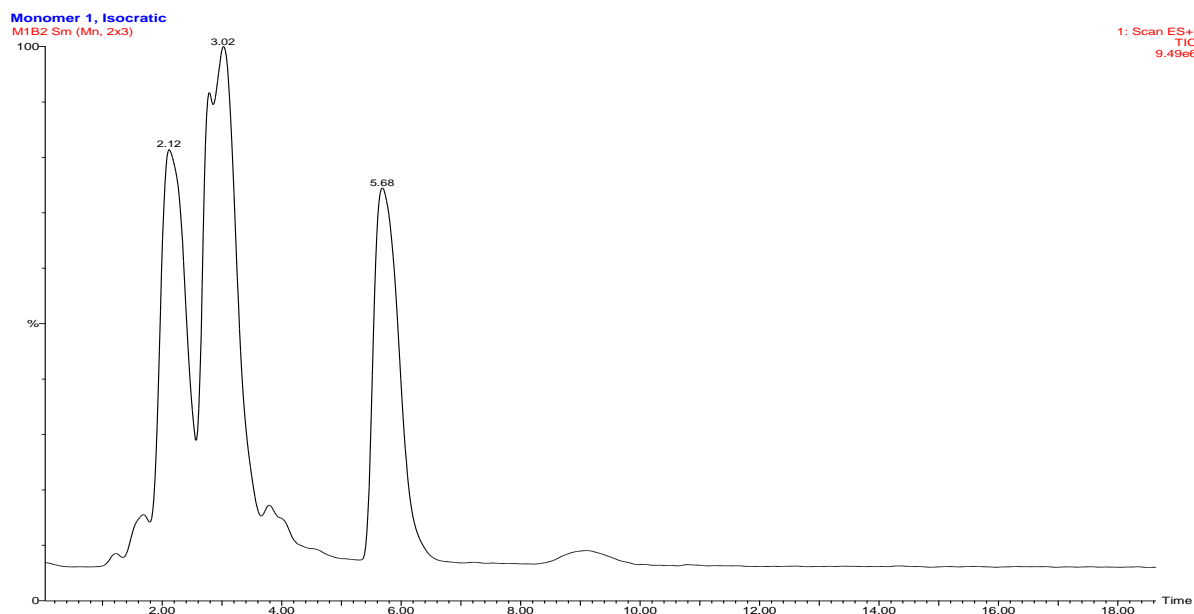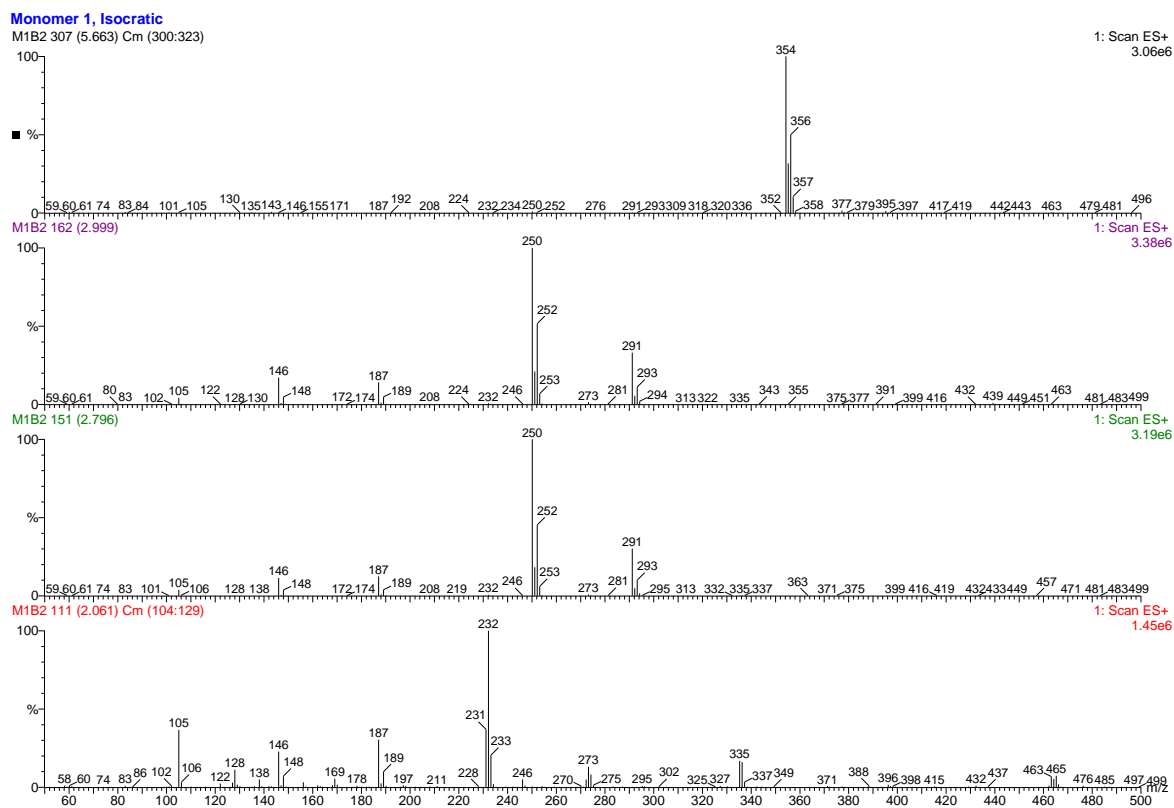
Crude mixture from Monomer 2 synthesis (from cyanuric chloride)

Monomer 2, isocratic
M2B 125 (2.317) Cm (119:127)   1: Scan ES+
                                                                                2.10e6
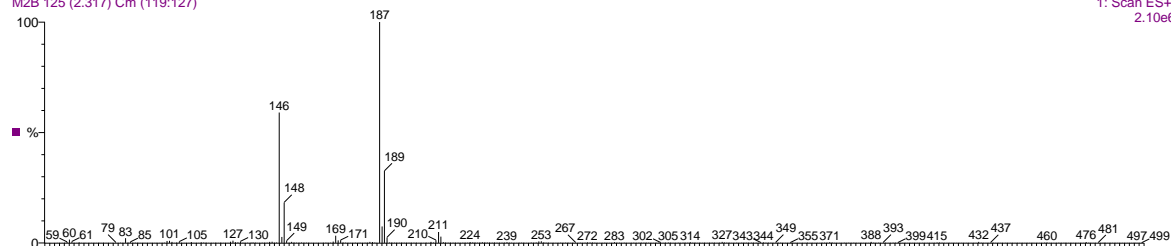
Monomer 2, isocratic
M2B 137 (2.537) Cm (133:143)   1: Scan ES+
                                                                                2.82e6
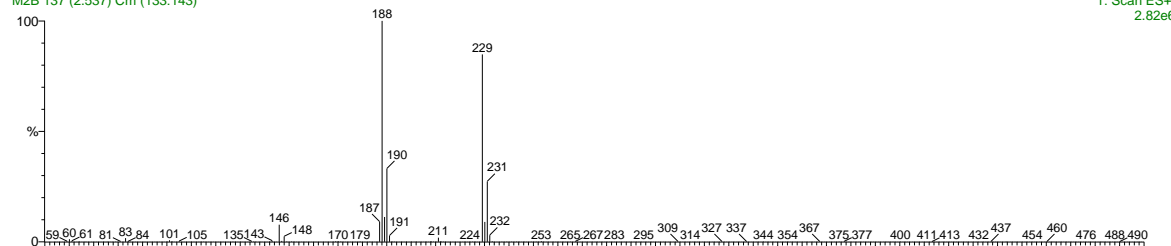
M2B 207 (3.820) Cm (202:210)   1: Scan ES+
                                                                                3.16e6
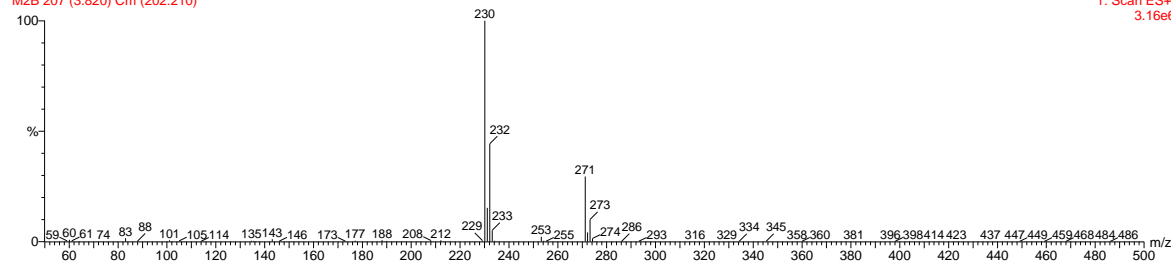
Monomer 2, isocratic
M2B   1: Scan ES+
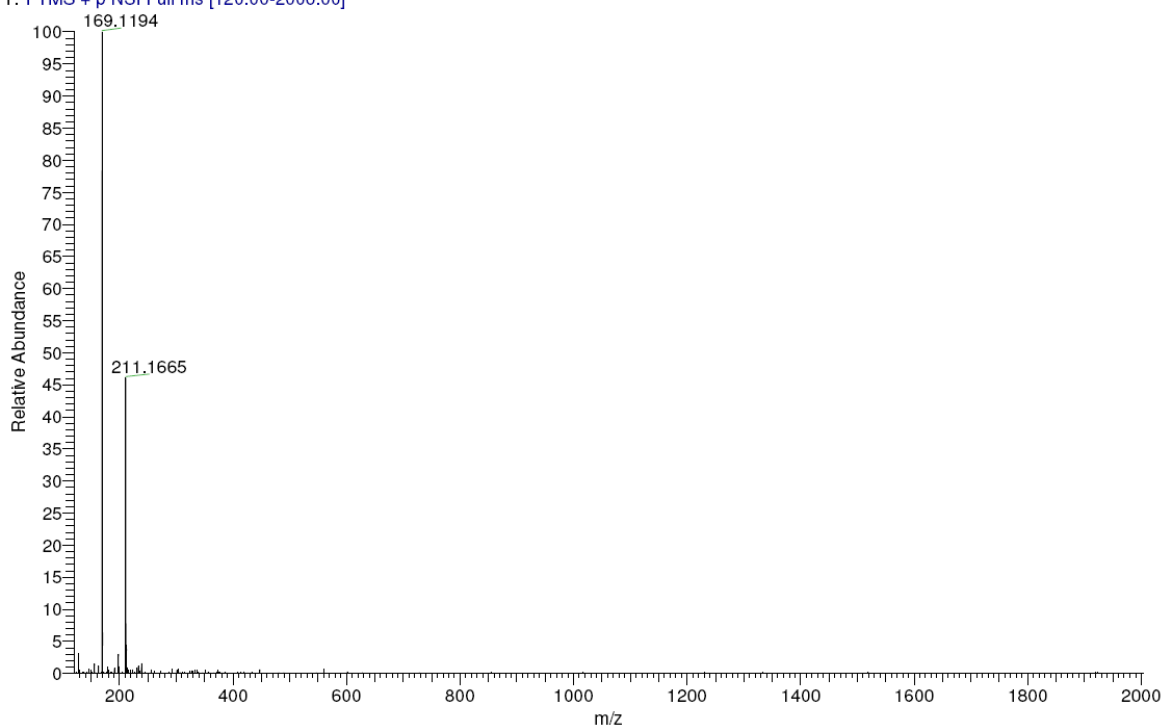   TIC
                                                                                9.56e6
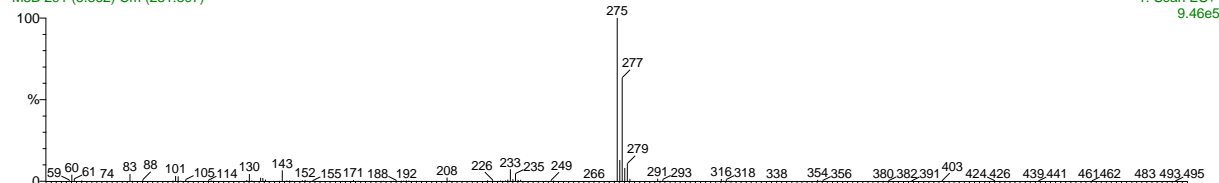
Crude mixture from Monomer 3 synthesis (from cyanuric chloride)
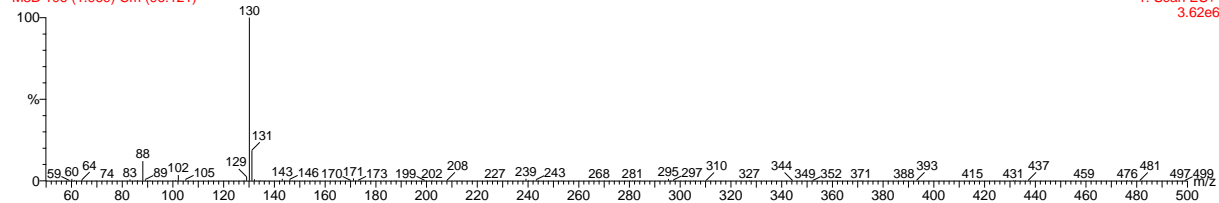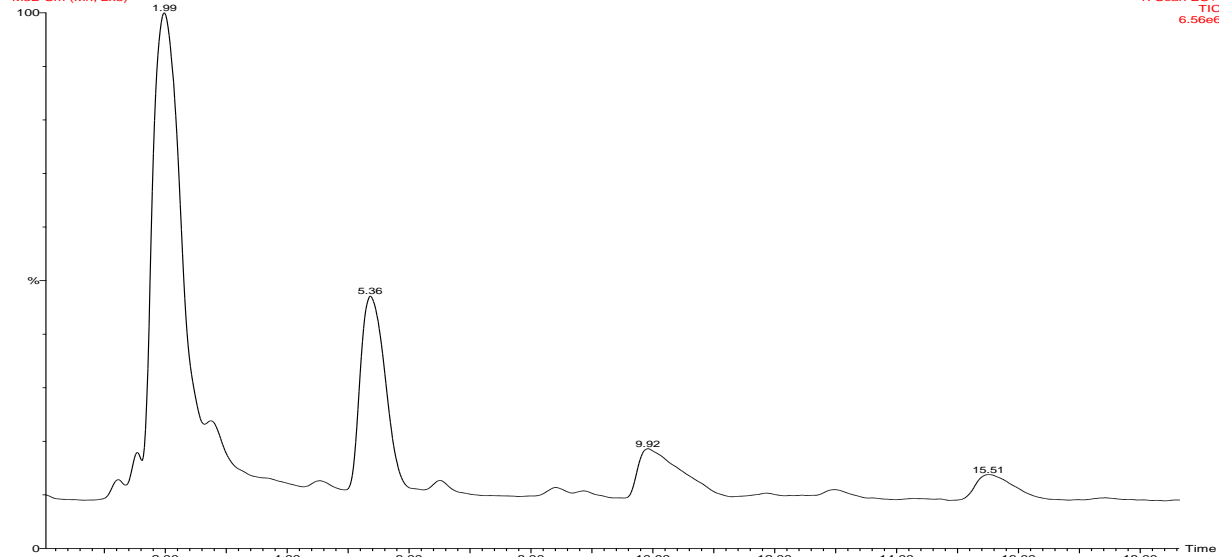
Various mass spectrometry analyses from EPSRC Swansea facilities

Crude mixture from Monomer 1 synthesis (from 2-chloro-4,6-diamino-1,3,5-triazine)

monomer 1 MW=230?
(DCM)/MeOH + NH4OAc
SM: 7G

EPSRC National Centre Swansea
LTQ Orbitrap XL

Dr Chrystelle Egger
01/06/2010 13:03:01

NL:
2.04E4

$C_{11} H_{14} N_6 H$:
$C_{11} H_{15} N_6$
p (gss, s /p:40) Chrg 1
R: 100000 Res .Pwr . @FWHM

Theoretical Isotope Model: [M + H]+

NL:
1.33E7

KEEEGG003-OM-HNESP#2-7
RT: 0.18-0.59 AV: 6 T: FTMS
+ p NSI Full ms
[120.00-2000.00]

Observed Data

Isotope:	Min. .. Max.		
14 N	0....16		
16 O	0....10		
12 C	0....60		
1 H	0....80		
23 Na	0....0		
Tolerance Window:	+- 5.00 ppm		
Db/Ring Equiv:	-3.. 100	N-Rule:	Do not use
Fits:	100	Charge:	1

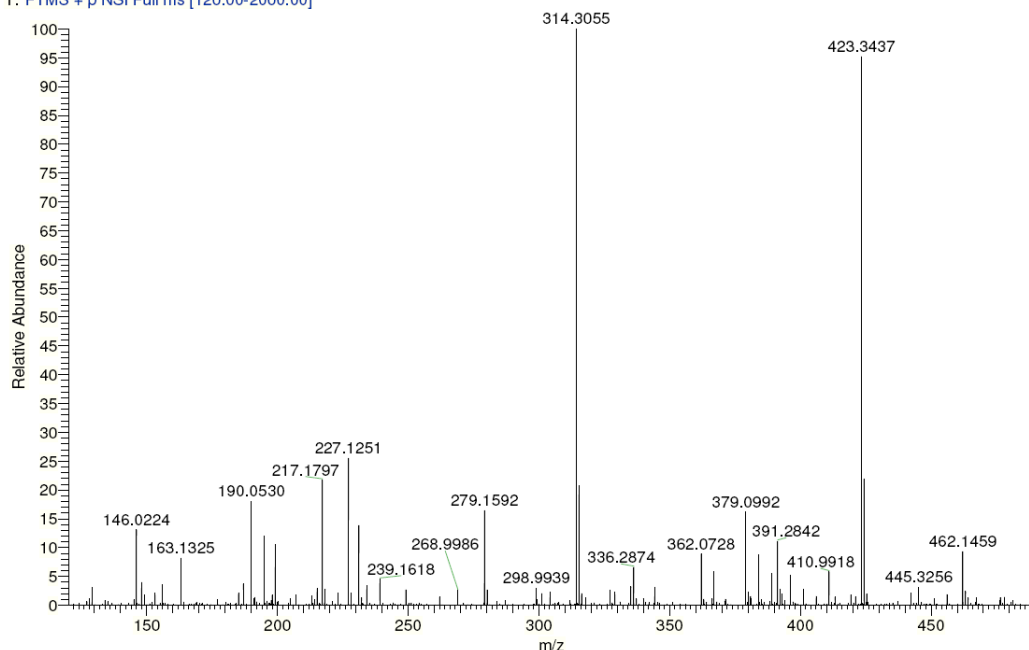| Mass	Theoretical Mass	Delta [ppm]	RDB	Composition
231.1353	231.1353	0.1	7.5	$C_{11} H_{15} N_6$

Crude mixture from Monomer 2 synthesis (from 2-chloro-4,6-diamino-1,3,5-triazine)

KEEEGG004-OE-HNESP #10-13 RT: 0.93-1.18 AV: 4 SM: 7G NL: 2.24E7
T: FTMS + p NSI Full ms [120.00-2000.00]
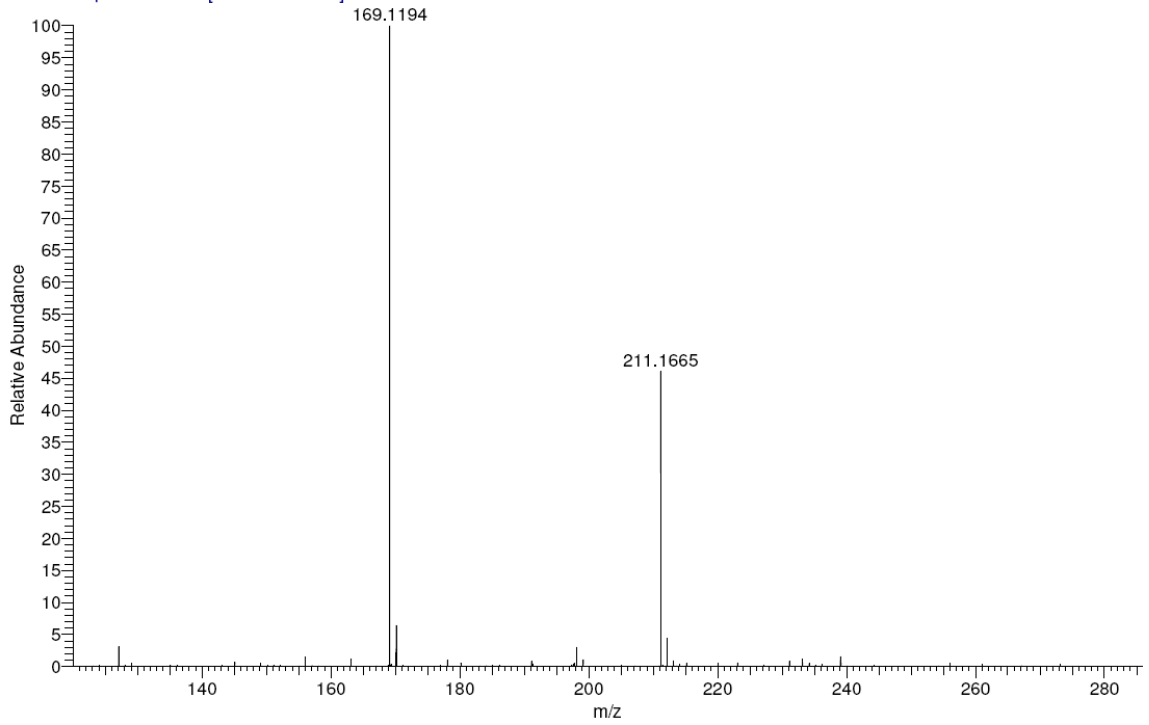
Isotope:	Min. .. Max.		
14 N	0....10		
16 O	0....20		
12 C	0....60		
1 H	0....80		
23 Na	0....0		
Tolerance Window:	+- 5.00 ppm		
Db/Ring Equiv:	-3.. 100	N-Rule:	Do not use
Fits:	100	Charge:	1

Mass	Theoretical Mass	Delta [ppm]	RDB	Composition
169.1194	169.1196	-1.3	3.5	$C_6 H_{13} N_6$

Crude mixture from Monomer 3 synthesis (from 2-chloro-4,6-diamino-1,3,5-triazine)

monomer 3 MW=422?
(DCM)/MeOH + NH4OAc
KEEEGG002-OM-HNESP #1-7 ̄ RT: 0.18-0.58 ̄ AV: 6 ̄ SM: 7G ̄ NL: 2.27E6
T: FTMS + p NSI Full ms [120.00-2000.00]
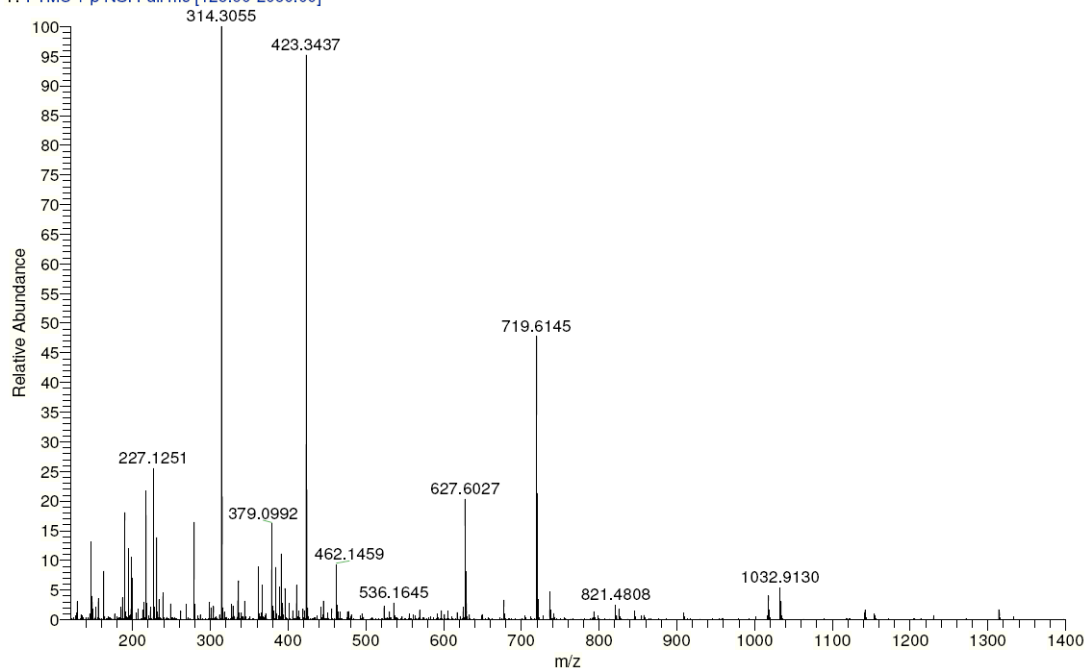
EPSRC National Centre Swansea
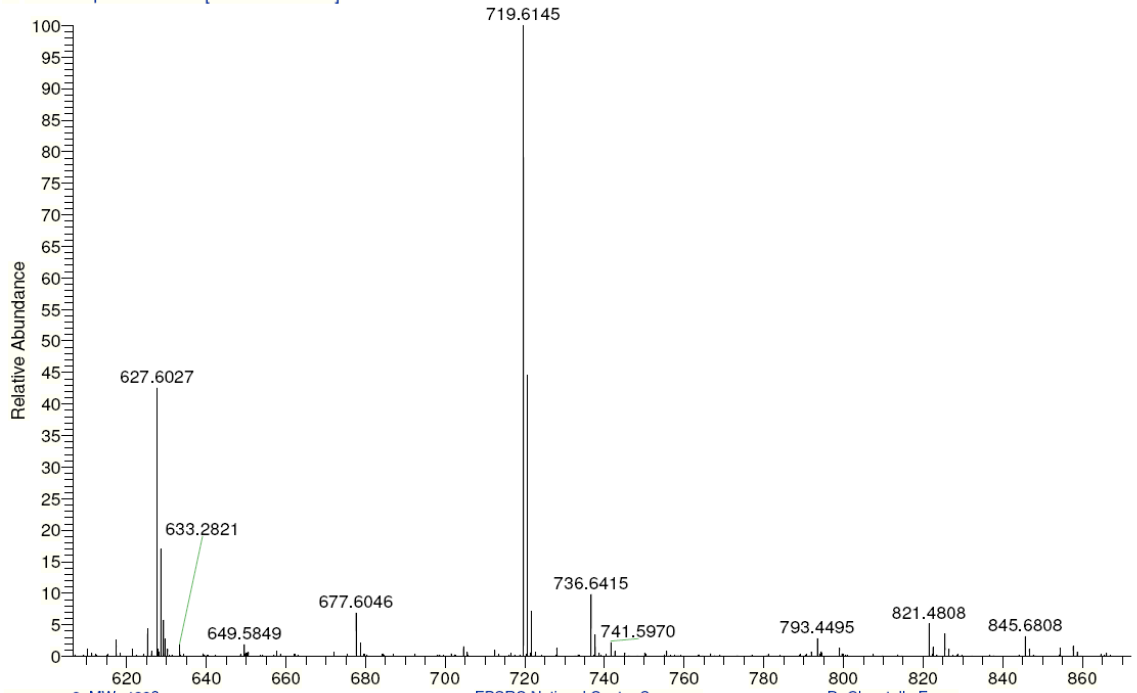LTQ Orbitrap XL

Dr Chrystelle Egger
01/06/2010 12:59:53

monomer 3 MW=422?
(DCM)/MeOH + NH4OAc
KEEEGG002-OM-HNESP #1-7 ̄ RT: 0.18-0.58 ̄ AV: 6 ̄ SM: 7G ̄ NL: 2.54E5
T: FTMS + p NSI Full ms [120.00-2000.00]

EPSRC National Centre Swansea
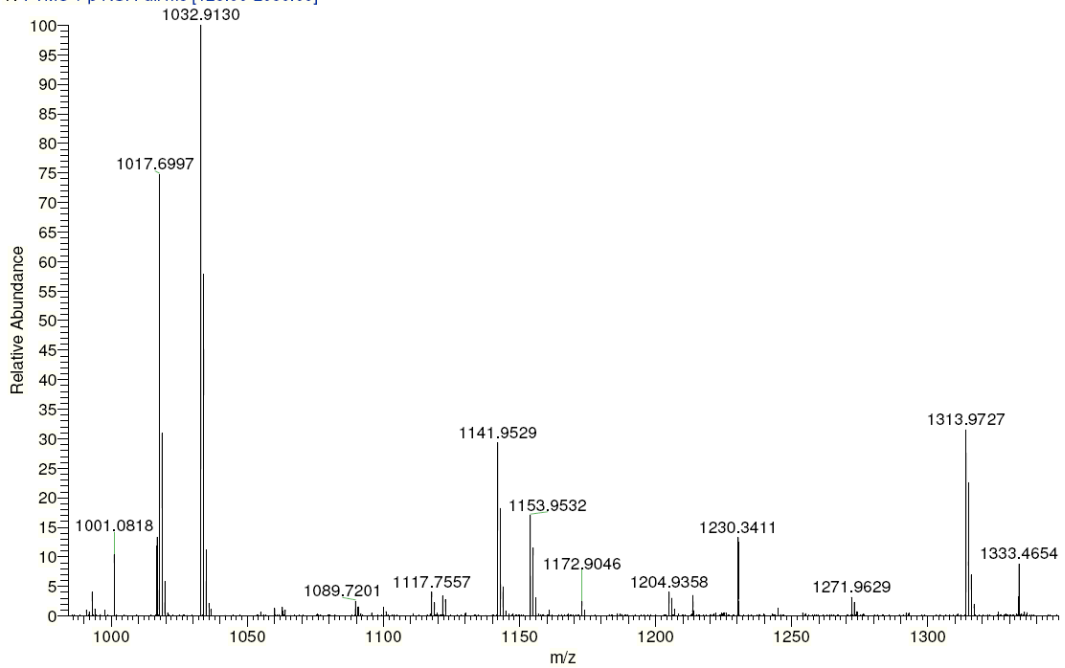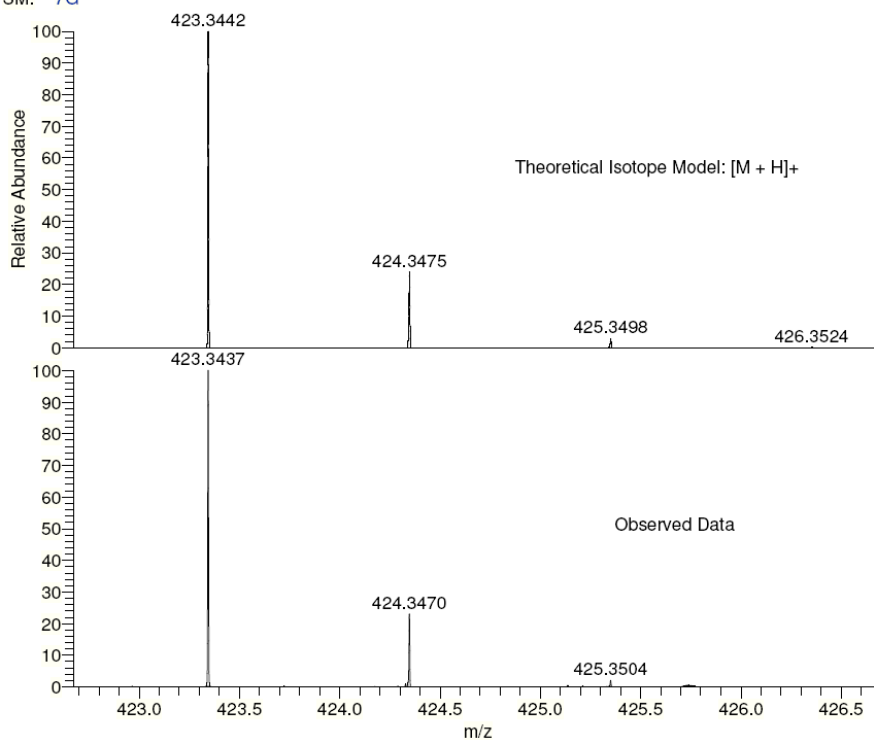LTQ Orbitrap XL

Dr Chrystelle Egger
01/06/2010 12:59:53

monomer 3 MW=422?
(DCM)/MeOH + NH4OAc
SM: 7G

EPSRC National Centre Swansea
LTQ Orbitrap XL

Dr Chrystelle Egger
01/06/2010 12:59:53

NL:
1.79E4

$C_{22} H_{42} N_6 O_2$ H:
$C_{22} H_{43} N_6 O_2$
p (gss, s /p:40) Chrg 1
R: 100000 Res .Pwr . @FWHM

Theoretical Isotope Model: [M + H]+

NL:
4.51E6

KEEEGG002-OM-HNESP#1-7
RT: 0.18-0.58 AV: 6 T: FTMS
+ p NSI Full ms
[120.00-2000.00]

Observed Data

Isotope:	Min. .. Max.	
14 N	0....16	
16 O	0....12	
12 C	0....60	
1 H	0....80	
23 Na	0....0	
Tolerance Window:	+- 5.00 ppm	
Db/Ring Equiv:	-3.. 100	N-Rule: Do not use
Fits:	100	Charge: 1

| Mass	Theoretical Mass	Delta [ppm]	RDB	Composition
423.3437	423.3442	-1.2	4.5	$C_{22} H_{43} O_2 N_6$
	423.3429	2.0	-0.5	$C_{21} H_{47} O_6 N_2$
	423.3429	2.0	5.0	$C_{20} H_{41} O_1 N_9$
	423.3455	-4.4	4.0	$C_{24} H_{45} O_3 N_3$

Appendix 2: Analytical techniques

Techniques for structural characterisation

I   Nitrogen Sorption

The efficiency of a porous solid to uptake a large volume of condensable gas depends on the porous volume and the amount of surface area exposed. Therefore, by studying the adsorption of gases or vapours within such materials, information on surface area can be obtained. One of the most common adsorbates used for this purpose is nitrogen, in a process commonly known as nitrogen sorption. In this technique a monolayer of nitrogen molecules is adsorbed at 77K onto the surface of a material which is then quantified and converted into a measure of the surface coverage. This is called the BET method, as it was formulised by Brunauer, Emmett and Teller in 1938[i]. The concept is an extension of the Langmuir theory (a theory for monolayer molecular adsorption) applicable to multilayer adsorption with the following hypotheses:

(a) gas molecules physically adsorb infinitely on a solid in layers;

(b) there is no interaction between each adsorption layer;

(c) the Langmuir theory can be applied to each layer.
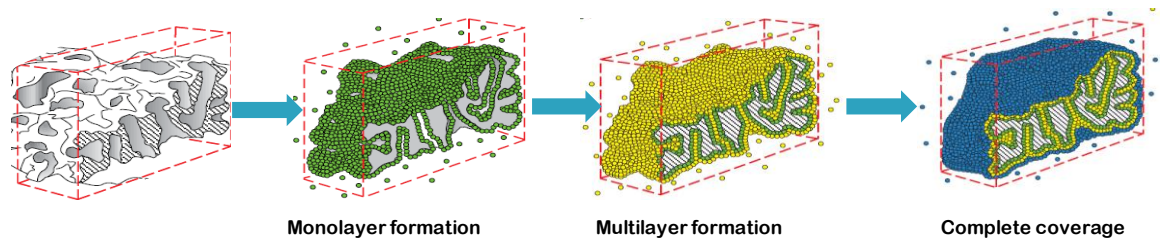
Figure 1: Principle of nitrogen sorption adapted from Quantachrome brochure[ii].

Adsorption is usually described through isotherms, i.e. the amount of adsorbate on the adsorbent (V_{ads}) as a function of its pressure at a constant temperature (p/p_0, where p is equilibrium pressure and p_0 is the saturation pressure of nitrogen at 77K). Brunauer *et al.* divided physical adsorption isotherms into five classes.

Type I isotherms correspond to true microporous adsorbents for which the size of pores within them is not much greater than the diameter of the sorbate molecule, hence why saturation limit is reached very rapidly corresponding to complete filling of the micropores. If intermolecular interactions are large and multi-layers start to form, then isotherms of type V are observed. An isotherm of type IV suggests the formation of two layers either on a plane surface or the wall of a pore that is much higher in diameter than the sorbate. Isotherms of type II and III are observed generally in adsorbents in which there is a wide range of pore sizes. In such systems there is a continuous progression of adsorption from monolayer to multilayer formation and then to capillary condensation. Type VI isotherms are of step-wise multilayer adsorption on a uniform non-porous surface.
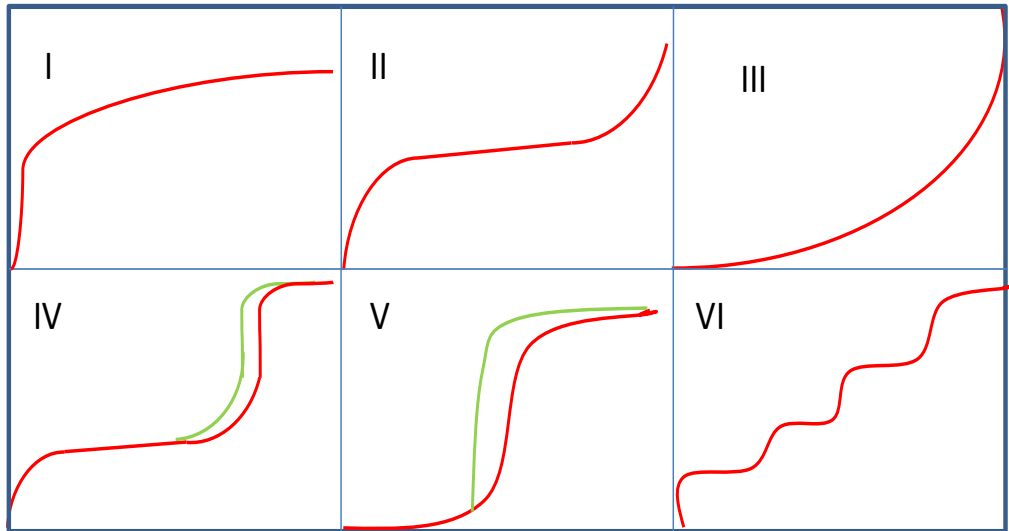
Figure 2: The six different BET isotherm classifications adapted from [iii].

If a pore is fully occupied with a sorbate, the adsorption process can be reversed by withdrawing known amounts of gas from the system in steps. This generates a desorption isotherm. These isotherms rarely overlay each other and produce what is known as a hysteresis. This adsorption-desorption hysteresis loop is helpful in understanding the geometric shape of the pores.

Additionally, the pore size distribution can also be calculated using the Kelvin equation, which quantifies the proportionality between equilibrium gas pressure and the size of capillaries capable of condensing gas within them. Computational methods such as the one by Barrett, Joyner and Halenda (BJH) can convert the equilibrium gas pressures into pore size distributions. This is, however, restricted to pore sizes in the mesoporous range[iv].

$$\ln\left(\frac{p}{p_0}\right) = \frac{2\gamma V_m}{rRT}$$

P=vapour pressure (Pa)
p_0=saturated vapour pressure (Pa)
γ=surface tension (N/m)
V_m=molar volume (m^3/mol)
r=radius (m)
R=universal gas constant (J.mol^{-1}K^{-1})
T=temperature (K)

Equation 1: The Kelvin Equation.

Nevertheless, it is possible to characterise larger pore sizes with mercury porosimetry.

II   Mercury Porosimetry[v]

Mercury porosimetry characterises porosity by applying various levels of pressure to a sample. The sample is immersed in mercury. Pores between 500μm and 3.5nm can be investigated. Since mercury is a non-wetting liquid, it does not spontaneously penetrate into pores by capillary action, it needs to be forced in (see Figure 3). This external pressure is measured and after applying the modified version of the Young-Laplace equation (the Washburn equation) shown below, the size of the pores can be estimated:

$$D = \frac{1}{P} 4\gamma \cos \theta$$

D: pore diameter (m)
P: applied pressure (Pa)
γ: surface tension of mercury (N/m)
θ: contact angle between mercury and the sample (rad)

Equation 2: The Washburn equation.
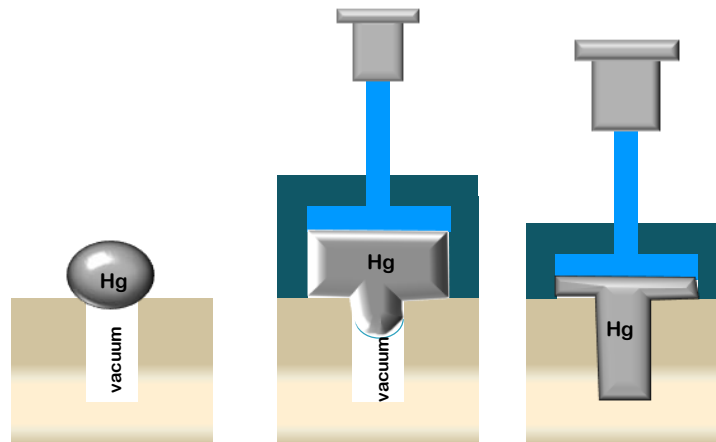
Figure 3: Scheme representing the principle of mercury porosimetry by intrusion adapted from[vi] (taken without permission). Mercury is a non-wetting liquid which does not readily penetrate into pores by capillary action. Pressure, therefore needs to be applied when the sample is under vacuum. The pressure to fully intrude mercury into a pore is related to the pore size.

This equation implies that higher pressures are required to fill smaller pores. The assumption made is that all pores are cylindrical. Although pores are rarely cylindrical in reality, this equation provides a practical representation of pore distributions, yielding very useful results for most applications. As pressure increases during an analysis, pore

size is calculated for each pressure point and the corresponding volume of mercury required to fill these pores is measured. These measurements, taken over a range of pressures, give the pore volume versus pore size distribution for the sample material. A trace called cumulative intrusion trace shows the cumulative amount of mercury intruded for each interval of pressure and the differential intrusion trace, given as a log scale, determines the amount of mercury intruded for each interval of pressure.

However mercury porosimetry also has its own limitations:

(i)   Closed pores are not accessible by mercury intrusion

(ii)   Only external pore dimensions (entrances) can be accessed

(iii)   Materials under study require good mechanical property to sustain applied pressures

(iv)   Small pores (microporosity) would require too large pressures to be accessed. Other techniques, such as scattering methods (x-ray, neutrons) or electron microscopy, are necessary to validate results from mercury intrusion.
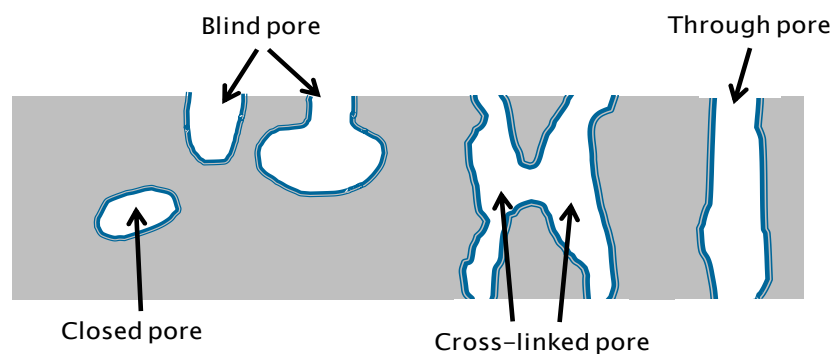
Figure 4: Different types of pores that could be encountered in a material, which illustrates the complexity of structural investigations (adapted from[v]).

III   Thermal Analysis

Thermal analysis of materials tends to be done using Thermal Gravimetric Analysis (TGA) and Differential Scanning Calorimetry (DSC) measurements. TGA determines the change in weight of a sample as a function of change in temperature. The DSC enables to determine the amount of heat required to increase the temperature of a sample and reference as a function of temperature. More specifically for polymeric materials, the thermal properties are linked to the degree of cross-linking.

For the studies in this work, a simultaneous TGA and DSC was used and the instrumentation measures both heat flow and weight changes in a material in a controlled environment. This enables to determine degradation temperatures and adsorbed solvent residues as well as any chemical changes that may occur within materials.

IV   Scanning Electron Microscopy[vii]

Visual inspection in the nanometre scale can also be used to evaluate the openness of the network and the general texture of a material and can be carried out using Scanning Electron Microscopy (SEM). Although only the two dimensional representation of a three dimensional network is accessible with this technique, many structural features (*e.g.* homogeneity, pore and grain sizes etc) are well accounted for and SEM gives a good insight into the overall structure when used in conjunction with the methods previously described.

A beam of electrons is used to scan the surface of a specimen in a high vacuum chamber. Firstly, it is collimated by two successive lenses. It is then focussed by an objective lens into a beam with a very fine spot size (~5nm). Electrons emitted from the sample therefore vary in intensity and the display of the SEM maps these varying signals thus producing an image.

Materials viewed under an electron microscope generally require processing to produce a suitable sample. This is mainly due to the requirement of a high vacuum chamber to enable the electron beam to travel in straight lines. Samples tend to be mounted on a carbon disk as it is conductive. Once this is done the samples are coated in gold or platinum in order to prevent charging (each point on the specimen the incident electron beam loses some energy, and that lost energy is converted into other forms) of the surface and to promote the emission of secondary electrons. A sputterer is used to form an even layer over the sample on the disc and provides a homogenous surface for analysis and imaging.

Functional characterisation techniques

I   **Infrared Spectroscopy**[viii]

Infrared (IR) spectroscopy is a technique commonly employed in both organic and inorganic chemistry to characterise functional groups present in a sample. The IR studies are carried out in this 4000-400 cm^{-1} range also known as the mid-IR range. In this region, IR bands in spectra occur due to vibrational and rotational modes of transition from the

ground state of molecules (or specific molecular bonds) to their excited states. This spectroscopic method is based on how the atoms in a molecule vibrate when exposed to infrared radiation. Depending on the strength of the bond, each mode is excited at a specific energy level manifesting as a characteristic band in the absorption spectrum.

Figure 5 shows the different components that make up an infrared spectrometer.

Figure 5: The different components of an FT- IR spectrometer, adapted from[v].

An ideal IR source is one that gives a continuous and high radiant energy output over the entire IR region. The two sources in most common use are the Nernst Glower (heated up to 2200 K) and the Globar (heated to about 1500 K). In general, in all IR sources the radiant energy, which depends on the temperature of the source, is low in the far infrared, and to obtain sufficient energy the slit width of the source has to be opened considerably (which corresponds to a decrease in resolution).

Between the source and the detector, a device to analyse the radiation is required so that intensity can be evaluated for each wavelength. This can be either monochromators, used in dispersive instruments, or interferometers used in Fourier transform instruments, which is the instrumentation used here.

The final parts of the spectrometer include the detector which is a device that measures the IR energy of the source that has passed through the spectrometer. A spectrum is recorded on a computer by measuring the amount of light that reaches the

detector, after passing through a sample, allowing to identify the amount of energy absorbed. This energy corresponds to a certain vibrational frequency, which can be calculated using Equation 3.

$$E = h\nu$$

E: energy of photon (J)
h: Plank's constant=6.626×10^{-34} (J.s)
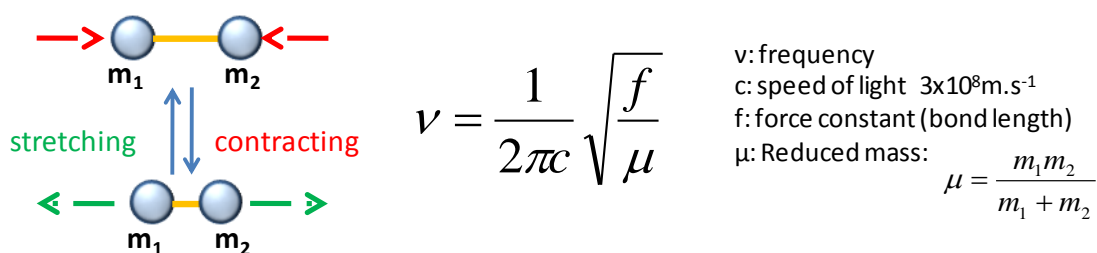v: frequency in (s^{-1})

Equation 3

From this equation the relationship between energy and frequency can be determined. It indicates that the higher the energy absorbed, the higher the vibrational frequency of a bond. There is however a selection rule to observe IR absorption: the molecules must have a change in dipolar moment. When a permanent dipole within a molecule vibrates, it interacts with the oscillating electric field of the incident infrared radiation. This produces an observable infrared band and the greater the change in dipole moment, the more intense this band is.

The two main modes of molecular vibrations that occur in the IR region are stretching and bending, which are motions that occur when atoms within a molecule move relative to one another. In stretching, bond lengths vary and in bending, atoms moves out of a plane causing a change in angle. Figure 6 illustrates the stretching and bending vibrations of the molecule of water.

υ_1 symmetric stretching υ_2 symmetric bending υ_3 asymmetric stretching
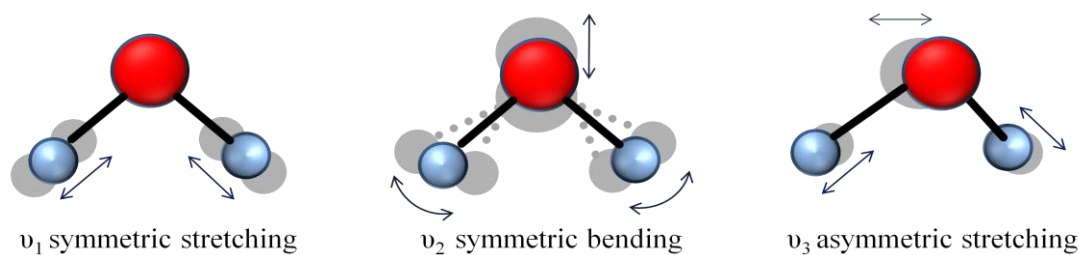
Figure 6: Bending and stretching vibrations for water. υ_1 shows symmetric stretching, υ_2 symmetric bending and υ_3 asymmetric stretching.

The stretching frequency is approximated by applying Hooke's Law (Figure 7):

$$v = \frac{1}{2\pi c}\sqrt{\frac{f}{\mu}}$$

v: frequency
c: speed of light $3\times10^8 m.s^{-1}$
f: force constant (bond length)
μ: Reduced mass: $\mu = \dfrac{m_1 m_2}{m_1 + m_2}$

Figure 7: Hooke's law applied to molecules

The equation outlines two main points. Firstly that light atoms vibrate faster than heavy atoms. This is very clearly shown in Table 1 where one can see that as the mass of the halogen atoms attached to carbon increases, the frequency decreases. Secondly, it shows that stronger (shorter) bonds have higher frequencies (i.e. explaining why C≡C stretching occurs at higher wavenumbers, 2100-2250 cm^{-1}, than C=C, 1680 − 1620 cm^{-1}).

Table 1: Variation in wavenumbers of IR absorptions for a series of CX_4 species (where X is a halogen atom and its mass decreases down the series)

CX_4 species	Wavenumber (cm^{-1}) for IR absorption
CF_4	1280
CCl_4	775
CBr_4	675
CI_4	555

An infrared spectrum can be divided into two regions, one called the functional group region and the other the fingerprint region. The functional group region is generally considered to range from 4000 to 1500 cm^{-1} and all frequencies below 1500 cm^{-1} are considered characteristic of the fingerprint region. The fingerprint region involves molecular vibrations, usually bending motions that are characteristic of the entire molecule or large fragments of the molecule. Thus this region can be used for molecular identification. The functional group region tends to include motions, generally stretching vibrations, which are more localised and characteristic of specific functional groups. While these bands do not confirm identity, they do provide very useful information about the nature of the components that make up the molecule.

Fourier- Transform Infrared Spectroscopy (FT-IR)

As with many other spectral techniques (e.g. NMR spectroscopy, Raman Spectroscopy etc), Fourrier Transform is required to transform the raw data collected into the actual

spectrum. The raw data is collected using a time-based domain which then undergoes computer transformation into the frequency domain thus producing spectra displaying intensity vs. wavenumber.

The essential experiment to record an FT-IR spectrum is to obtain an interferogram with and without a sample in the beam and transforming the interferograms into spectra of (a) the source with sample absorptions and (b) the source without sample absorptions. The ratio of the former and the latter correspond to a double beam dispersive spectrum.

### a) Advantages of using Fourier transform infrared spectroscopy

The method of fast FT-IR overcame the disadvantage of measuring one resolution element at a time. Consequently, FT-IR spectra generally tend to give a good signal to noise ratio by averaging many interferograms. This can generally be done in less time than it would take a dispersive instrument to record one scan.

FT-IR has additional merits such as: higher sensitivity, higher precision (improved frequency, resolution and reproducibility), quickness of measurement and extensive data processing capability (as FTIR is a computer-based technique, it allows storage of spectra and facilities for processing spectra).

b) Attenuated Total Reflectance Spectroscopy (ATR-IR)

There are many different methods for carrying out IR spectrometry. Popular techniques include dispersing the sample into nujol oil and creating a paste that can be spread onto discs that are mid-IR transparent such as KBr or NaCl. Alternatively pellets can be made whereby the sample (solid) is dispersed into KBr powder and pressed under high pressure.

Alternatively a method for analysing solids which requires little sample preparation, and is therefore less "destructive", is ATR (attenuated total reflectance). Thin, small samples can be chipped from the material and analysed. Figure 8 shows the principle of this technique.
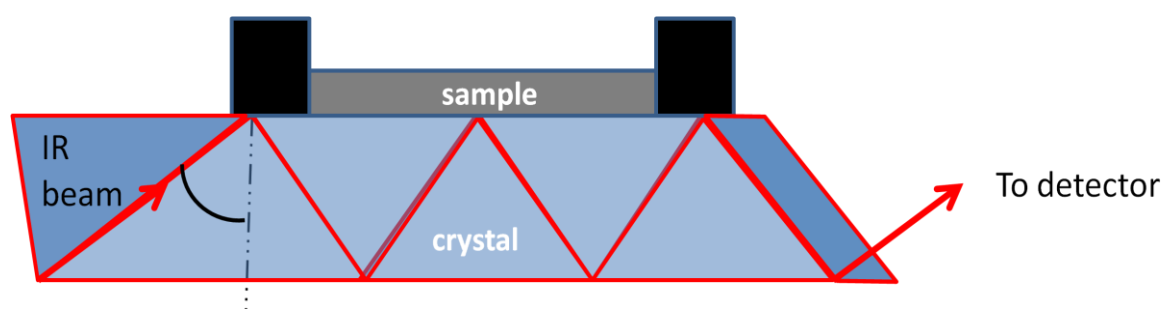
Figure 8: Diagram of the principle of a typical ATR cell

Firstly a beam of radiation enters the crystal and if the angle at which it enters is greater than the critical angle it undergoes total internal reflection i.e. all the radiation is reflected and no refraction occurs. The beam penetrates a fraction of the wavelength beyond the reflecting surface and when it is in close contact with a material that absorbs at this particular wavelength, there is loss of beam energy. The resulting attenuated radiation is measured by a spectrometer and gives rise to the IR spectrum.

The crystals used in ATR cells are usually made from materials with high refractive indices and a low solubility in water.

II   Raman Spectroscopy[ix]

Raman spectroscopy is another vibrational spectroscopic technique based on the inelastic scattering of monochromatic light, usually from a laser source. Photons from the

laser light interact with the molecule and scatter from it. The scattered photons have a frequency that is shifted up or down in comparison with the original monochromatic frequency and this is called the Raman effect. In Raman spectroscopy, this shift helps to obtain information about the vibrational, rotational and other low frequency transitions in molecules. The technique can be used to study solid, liquid and gas samples.

Raman scattering is less widely used than infrared absorption as it can lead to the degradation of the sample and fluorescence intervenes usually producing spectra of low quality. Recent advances however have been made to circumvent this effect and as the presence of water and glass supports do not interfere with the samples spectra, this technique is currently resurging.

The way in which radiation is employed in infrared and Raman spectroscopies is different. IR covers a range of frequencies directed onto the sample whereas Raman spectroscopy uses a single frequency of radiation (monochromatic light) to irradiate the sample and it is the radiation scattered from the incident beam which is detected. The light interacts with the molecule and polarises the cloud of electrons around the nuclei to form a short-lived state, from which the photon is quickly re-radiated. The energy is transferred from the photon to the molecule, or vice-versa, meaning that the frequency of the photon is different to that of the monochromatic light. This is called inelastic scattering. If the energy of the scattered photon is one vibrational unit different to that of the incident photon, it is called Raman scattering.

As with IR there is a basic selection rule to observe Raman scattering. Intense Raman scattering occurs when a change in polarisability of the electron cloud around the molecule occurs which in turn causes vibrations. Therefore symmetric vibrations (as they

are more polarisable) cause the largest change and give the greatest scattering. It is therefore often said that weak bands in IR tend to be stronger in Raman. However, not all vibrations of a molecule can be both infrared and Raman active and the two techniques give different intensity patterns. As a result the two are often complementary and when combined, they give a more solid view of the molecular structure.

Instrumentation

A Raman system consists of four main components, as shown in Figure 9.
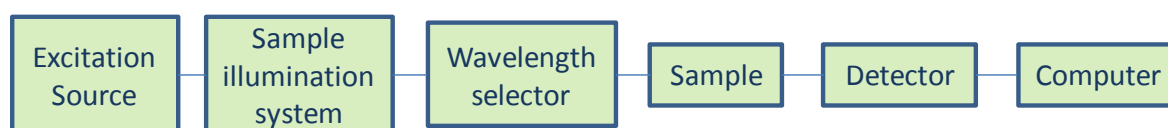
Figure 9: The different components of a Raman spectrometer, adapted from[x].

A sample is normally illuminated with a laser beam in the ultraviolet, visible or near IR range. Scattered light is collected with a lens and is sent through a filter to obtain a Raman spectrum of the sample. Modern multi-channel detectors like Photodiode Arrays (PDA) or Charge-Coupled Devices (CCD) are used to detect the Raman scattered light.

III   Solid-State NMR[x]

NMR spectroscopy is an indispensable tool for chemical structure determination in organic and inorganic compounds. Solid-state NMR is rapidly emerging as a powerful method for the study of solid samples such as catalysts, glasses and polymers.

Both liquid-state and solid-state NMR are based on a physical phenomenon related to the magnetic property of atomic nuclei. Radiowaves are absorbed by the nuclei of certain atoms within a sample which is placed in a magnetic field. The energy associated with this radio frequency ($\sim 10^7$ Hz) is strong enough to affect the nucleon spin property. Nuclei that contain odd numbers of nucleons, spin ½ nuclei, have a magnetic moment and can absorb the radio frequency (RF) radiation. In NMR, the absorption of the frequency by nuclei is measured while applying a strong magnetic field, B_0, created usually using a super conduction solenoid. This changes the direction of their nuclear spinning axis to the higher energy direction. The energy difference ΔE between the two spin states is proportional to the strength of B_0. When the flipped nuclei return to the lower-energy state, they re-emit RF radiation. This is perturbed by the local environment around the nuclei in a molecule and affects the exact transition energy. The NMR records the transitions between the spin states induced by the RF electromagnetic field, B_1.

The most common NMR experiments performed for solid-state samples are those involving the observation of spin ½ nuclei with low abundance, for example ^{13}C, ^{15}N and ^{29}Si. Samples in solution tend to produce very sharp signals in NMR experiments whereas the signals are generally very broad in solid-state NMR. This is due to interactions (mainly heteronuclear and homonuclear dipolar coupling, quadrupolar coupling and chemical-shift anisotropy) that are generally not observable in the liquid-state.

Magic Angle Spinning

When the vector between two nuclei make an angle $\theta = 54.74°$ (the magic angle) with respects to the static magnetic field, the normally broad lines become narrower,

increasing the resolution for better identification and analysis of the spectrum. This is because both the heteronuclear dipolar coupling between magnetic moments of nuclei averages to zero only at the magic angle and the chemical shift anisotropy averages to a non-zero value. This causes the signal to become much narrower with spinning side bands which occur at multiples of the spinning speed.

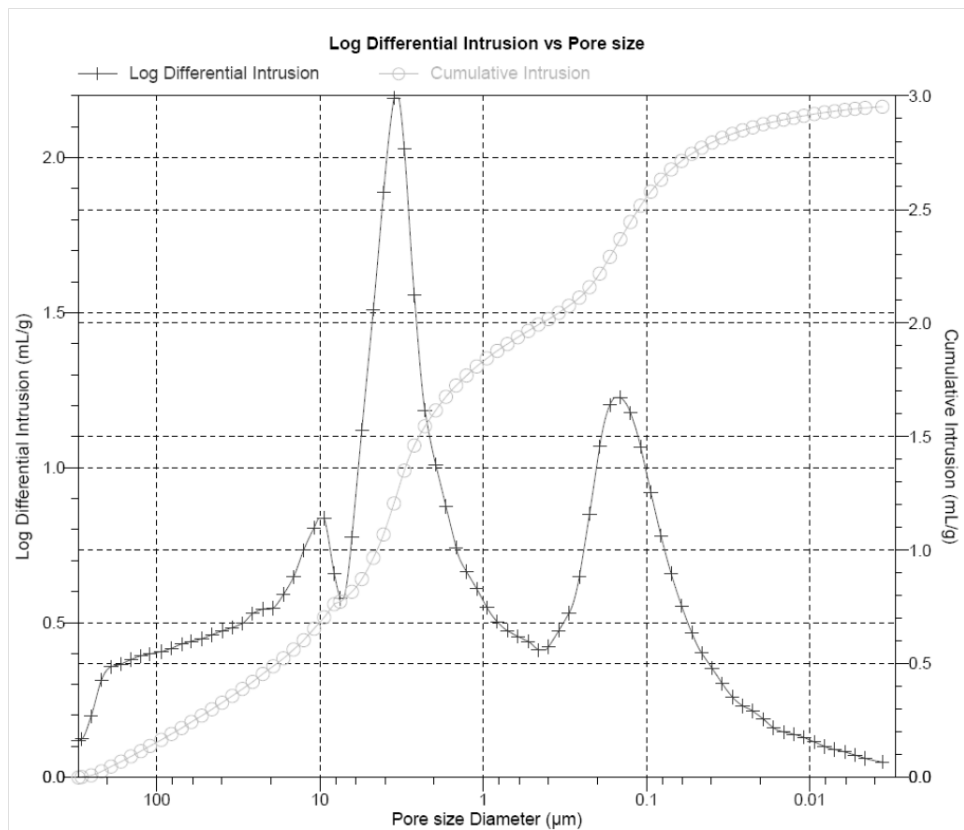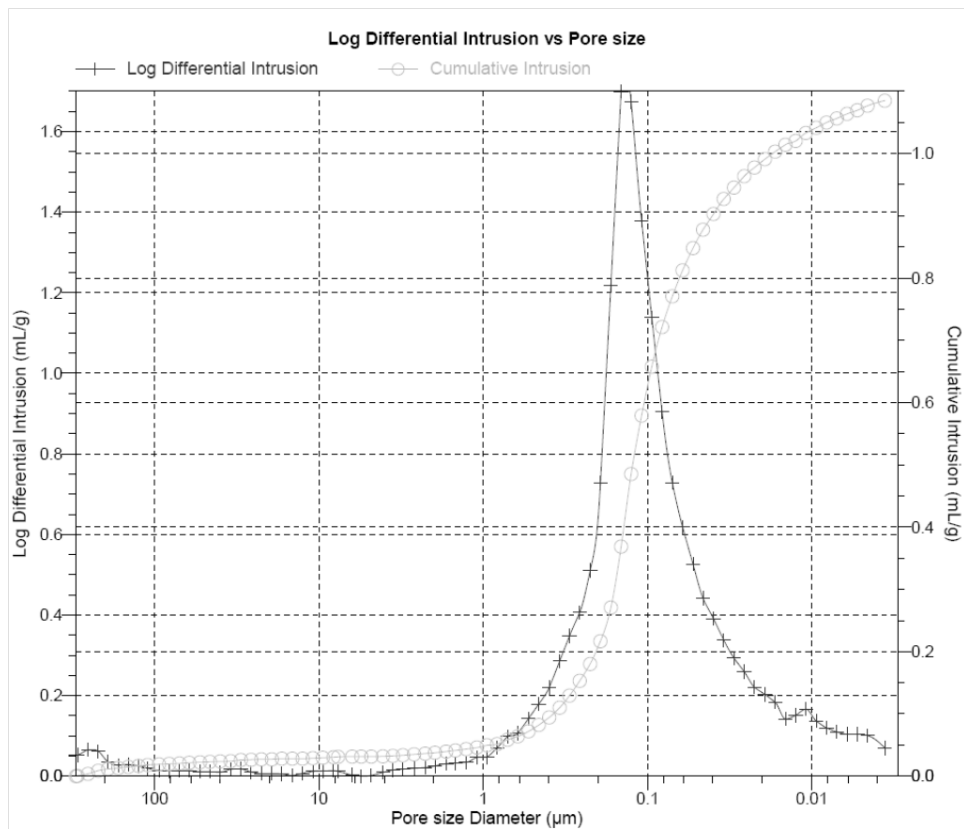# Appendix 3: Mercury porosimetry of bulk and powder MF samples

GSL028PT2 (top-bulk, bottom-powder)
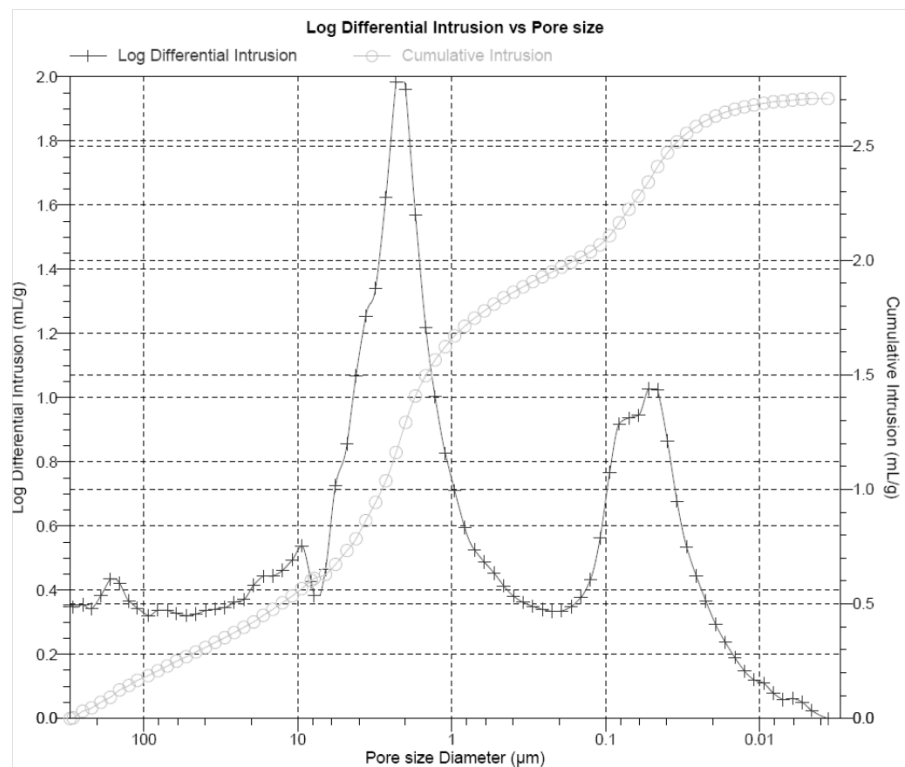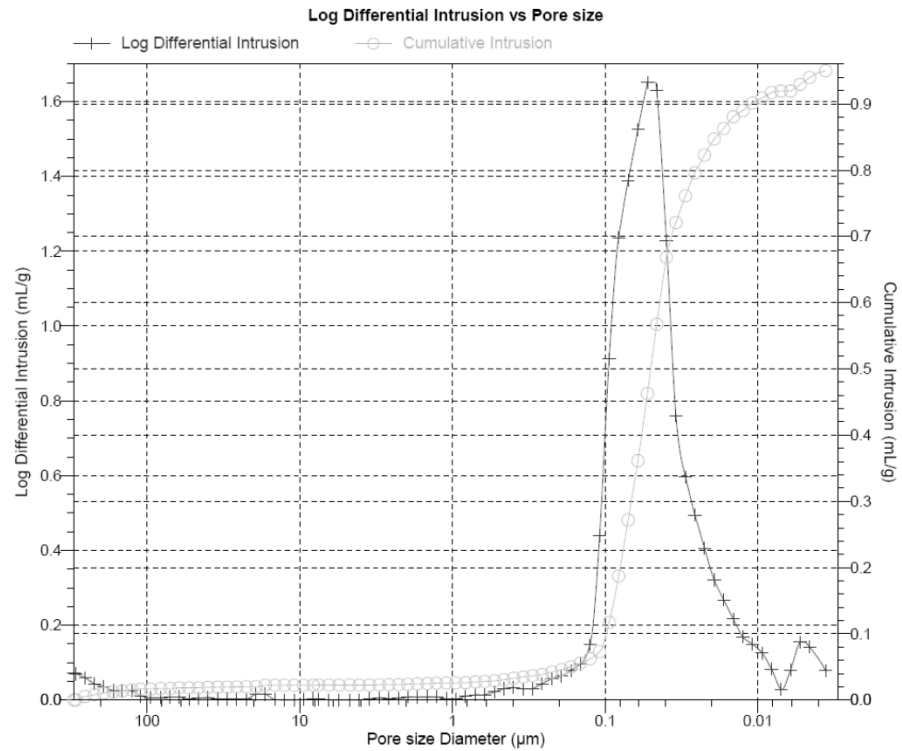
GLMMG1BPT1 (top-bulk, bottom-powder)
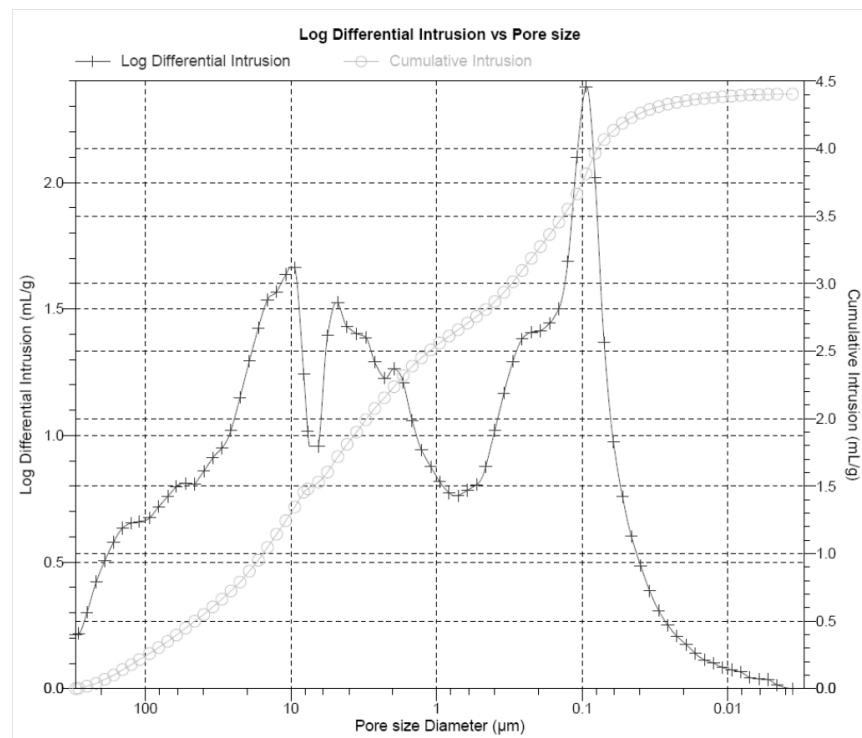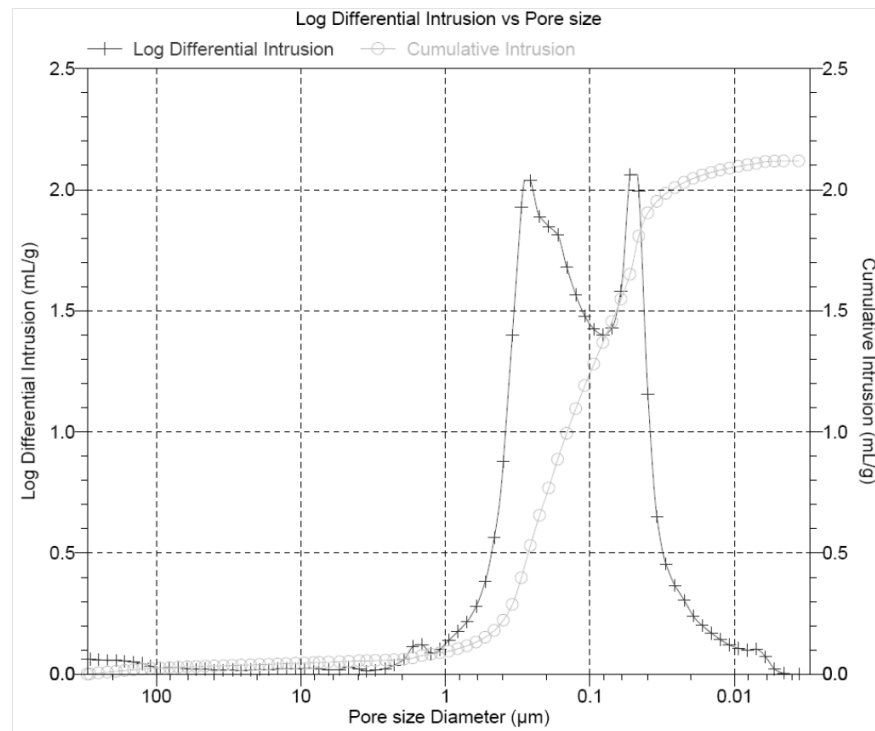
GLM1MF05PT1 (top-bulk, bottom-powder)

References for Appendices

[i] Brunauer, S., P. H. Emmett, et al. (1938). "Adsorption of gases in multimolecular layers." *J. Am. Chem. Soc.* **60**: 309-319.

[ii] http://www.oleinitec.fi/pdf/QC/Autosorb1Bro.pdf   (last accessed 05/07/2011)

[iii] IUPAC Recommendations, *Pure Appl. Chem*., 57 (1985) 603.

[iv] Rouquerol, J., D. Avnir, et al. (1994). "Recommendations for the Characterization of Porous Solids." *Pure Appl. Chem*., **66**(8): 1739-1758.

[v] Giesche, H. (2006). "Mercury porosimetry: A general (practical) overview*." Part. Part. Syst. Char.* **23**(1): 9-19.

[vi]http://www.micromeritics.com/Repository/Files/Mercury_Porosemitry_Theory_poster_.pdf   (last accessed 05/07/2011)

[vii] Michler, G. H. (2008). "Electron Microscopy of Polymers", Springer. Pages 84-120

[viii] Babara Stuart, "Infrared Spectroscopy: Fundamentals and Applications", Wiley, 2004, First edition

[ix] Smith, E. and. Dent, G. (2005). "Modern Raman spectroscopy; a practical approach."

[x] Laws, D. D., H. M. L. Bitter, et al. (2002). "Solid-state NMR spectroscopic methods in chemistry." *Angew. Chem. Int. Ed.* **41**(17): 3096-3129.